

MONASH UNIVERSITY
THESIS ACCEPTED IN SATISFACTION OF THE
REQUIREMENTS FOR THE DEGREE OF
DOCTOR OF PHILOSOPHY

ON 5 July 2002

Sec. Research Graduate School Committee

Under the copyright Act 1968, this thesis must be used only under the normal conditions of scholarly fair dealing for the purposes of research, criticism or review. In particular no results or conclusions should be extracted from it, nor should it be copied or closely paraphrased in whole or in part without the written consent of the author. Proper written acknowledgement should be made for any assistance obtained from this thesis.

Addendum

- Page iv line 12: "[Cu(tacn)₂](BNPP)₂" for "[Cu(tacn)₂](BNPP)"
- Page xii line 20: "OH" for "·OH"
- Page 89 line 6: "log K for the formation of [Cu(tacn)(OH₂)₂]²⁺" for "log K"
- Page 111 line 6: "[Cu(tacn)₂](BNPP)₂" for "[Cu(tacn)₂](BNPP)"
- Page 111 line 10: "[Cu(tacn)₂](BNPP)₂" for "[Cu(tacn)₂](BNPP)"
- Page 111 line 11: "[Cu(tacn)₂](BNPP)₂" for "[Cu(tacn)₂](BNPP)"
- Page 112 line 1: "[Cu(tacn)₂](BNPP)₂" for "[Cu(tacn)₂](BNPP)"
- Page 112 line 2: "[Cu(tacn)₂](BNPP)₂" for "[Cu(tacn)₂](BNPP)"
- Page 136 line 19: "650" should be in the previous column
- Page 165 line 1: "[Cu(tacn)₂](BNPP)₂" for "[Cu(tacn)₂](BNPP)"
- Page 293 line 5: Delete "of" and read "Release of the second mole is achieved by a second catalytic cycle."
-
- Chapter 2: Reference 12 is Chaudhuri, P., Ventur, D., Wieghardt, K., Peters, E. M., Peters, K., Simon, A. *Angew. Chem.* 1985, 97, 55. All subsequent numbers in the reference list should be increased by one.

**METAL COMPLEXES BASED ON
MACROCYCLIC LIGANDS
AND THEIR ABILITY TO
HYDROLYSE PHOSPHATE ESTERS**

A Thesis Submitted for the Degree of Doctor of Philosophy

by

Fiona Helen Fry

B.Sc. (Hons)

School of Chemistry

Monash University

Victoria, Australia

2002

Table of Contents

Summary	ix
Declaration	xiv
Acknowledgements	xv
Abbreviations	xvi
Numbering Scheme for Metal Complexes	xviii

Chapter One Introduction to Phosphate Ester Hydrolysis

1.1	General Introduction	1
1.2	Metalloenzymes	1
1.3	Phosphatase Enzymes	4
	1.3.1 Alkaline Phosphatase	4
	1.3.2 Purple Acid Phosphatases	8
	1.3.3 Protein Phosphatases (PPs)	13
	1.3.3.1 Phosphoserine/Threonine Phosphatases (P-S/T-P)	13
	1.3.4 Phospholipase C	16
	1.3.5 Nuclease P1	20
1.4	The Role of Zinc(II) in Phosphatase Enzymes	21
1.5	Modelling of Phosphatases	22
	1.5.1 Mononuclear Models	23
	1.5.2 Binuclear Models	34
	1.5.3 Trinuclear Models	37

1.6	The Present Study	42
1.7	References	44

Chapter Two Synthesis of Ligands

2.1	Introduction	48
2.2	Synthesis of Unfunctionalised Bis(tacn) Ligands	56
2.2.1	Synthesis of 1,2-, 1,3-, and 1,4-bis(1,4,7-triazacyclonon-1-ylmethyl)benzene hexahydrochloride ($T_2-o-X.6HCl$, $T_2-m-X.6HCl$, $T_2-p-X.6HCl$)	58
2.2.2	Synthesis of 1,2-Bis[<i>N,N'</i> -bis(<i>p</i> -tolylsulphonyl)-1,4,7-triazacyclonon-1-yl]propan-2-ol (T_2PrOHT_{54})	62
2.2.3	Synthesis of 1,2-Bis[1,4,7-triazacyclonon-1-yl]propan-2-ol hexahydrobromide ($T_2PrOH.6HBr$)	64
2.3	Synthesis of Bis(tacn) Ligands Bearing Pendant Arms	66
2.3.1	Synthesis of 1,2- and 1,3-bis(4-(carboxymethyl)-1,4,7-triazacyclonon-1-ylmethyl)benzene hexahydrochloride ($T_2-o-X Ac_2.6HCl$, $T_2-m-X Ac_2.6HCl$)	67
2.4	Synthesis of the Tris(tacn) Ligand	72
2.4.1	Synthesis of 1,3,5-tribromomethylbenzene (Br_3mes)	72
2.4.2	Synthesis of the Tris(tacn) ligand 1,3,5-tris(1,4,7-triazacyclonon-1-ylmethyl)benzene nonahydrochloride ($T_3mes.9HCl$)	73
2.5	Experimental	76
2.6	References	84

**Chapter Three Synthesis and Characterisation of Copper(II) Complexes of
1,4,7-triazacyclononane derivatives**

3.1	Introduction	88
3.2	Complexes of bis(tacn) ligands	96
3.2.1	Preparation of Complexes	96
3.2.2	Crystal Structure of $[\text{Cu}_2(\text{T}_2\text{-}p\text{-X})\text{Cl}_4]$ (3)	98
3.2.3	Crystal Structure of $[\text{Cu}_2(\text{T}_2\text{-PrO})\text{Br}_2]\text{Br}\cdot 2\text{H}_2\text{O}$ (4)	103
3.3	Complexes of bis(tacn) ligands bearing acetate pendant arms	107
3.3.1	Preparation of Complexes	107
3.4	Copper complex of tris(tacn) ligand; $[\text{Cu}_6(\text{T}_3\text{mes})_2(\mu\text{-OH})_6](\text{ClO}_4)_6\cdot 6\text{H}_2\text{O}$ (7)	109
3.5	Copper Complexes Incorporating Phosphate Esters	110
3.5.1	Preparation of $[\text{Cu}(\text{tacn})_2](\text{BNPP})$ (8)	111
3.5.2	Crystal Structure of $[\text{Cu}(\text{tacn})_2](\text{BNPP})$ (8)	111
3.5.3	Preparation of $[\text{Cu}_3(\text{Me}_3\text{tacn})_3(\text{PhP})_2](\text{ClO}_4)_2\cdot \frac{1}{2}\text{H}_2\text{O}$ (9)	114
3.5.4	Crystal Structure of $[\text{Cu}_3(\text{Me}_3\text{tacn})_3(\text{PhP})_2](\text{ClO}_4)_2\cdot \frac{1}{2}\text{H}_2\text{O}$ (9)	116
3.5.5	Synthesis of $[\text{Cu}_2(\text{T}_2\text{-}m\text{-X})(\text{NPP})(\mu\text{-OH})](\text{ClO}_4)\cdot \text{H}_2\text{O}$ (10)	123
3.5.6	Crystal Structure of $[\text{Cu}_2(\text{T}_2\text{-}m\text{-X})(\text{NPP})(\mu\text{-OH})](\text{ClO}_4)\cdot \text{H}_2\text{O}$ (10)	124
3.6	Preparation of the Mononuclear Complex $[\text{Cu}(\text{Me}_3\text{tacn})(\text{H}_2\text{O})_2](\text{ClO}_4)_2$ (11)	133
3.7	Physicochemical Properties of Copper(II) Complexes	134
3.7.1	Electronic Spectra	134
3.7.2	Magnetic and ESR Properties	138
3.7.2.1	Non-bridged Complexes	138

3.7.2.2	Bridged Complexes	144
3.7.2.2.1	Magnetism and ESR Data for $[\text{Cu}_2(\text{T}_2\text{PrO})\text{Br}_2]\text{Br}$ $\cdot 2\text{H}_2\text{O}$ (4)	144
3.7.2.2.2	ESR Data for $[\text{Cu}_6(\text{T}_3\text{mes})_2(\mu\text{-OH})_6]$ $(\text{ClO}_4)_6 \cdot 6\text{H}_2\text{O}$ (7)	148
3.7.2.2.3	Magnetism and ESR Data for $[\text{Cu}_3(\text{Me}_3\text{tacn})(\text{PhP})_2](\text{ClO}_4)_2 \cdot \frac{1}{2}\text{H}_2\text{O}$ (9)	149
3.7.2.2.4	Magnetism and ESR Data for $[\text{Cu}_2(\text{T}_2\text{-}m\text{-X})(\text{NPP})(\mu\text{-OH})](\text{ClO}_4) \cdot \text{H}_2\text{O}$ (10)	154
3.8	Concluding Remarks	156
3.9	Experimental	158
3.10	References	168

Chapter Four Synthesis and Characterisation of Zinc(II) Complexes of 1,4,7-triazacyclononane derivatives

4.1	Introduction	174
4.2	Zinc(II) complexes of bis(tacn) ligands	181
4.2.1	Preparation of Complexes	181
4.2.2	Crystal Structure of $[\text{Zn}(\text{T}_2\text{-}o\text{-X})](\text{ClO}_4)_2 \cdot \text{H}_2\text{O}$ (12)	186
4.2.3	Crystal Structure of $[\text{Zn}_2(\text{T}_2\text{-}p\text{-X})(\text{H}_2\text{O})_4(\text{DMF})_2][\text{ZnCl}_4]$ (14)	189
4.2.4	Solution NMR Spectroscopic Analysis of $[\text{Zn}(\text{T}_2\text{-}o\text{-X})](\text{ClO}_4)_2$ (12), $[\text{Zn}_2(\text{T}_2\text{-}m\text{-X})(\mu\text{-OH})_2]\text{Br}_2 \cdot 3\text{H}_2\text{O}$ (13), $[\text{Zn}_2(\text{T}_2\text{-}p\text{-X})(\text{H}_2\text{O})_4(\text{DMF})_2]$ $[\text{ZnCl}_4]$ (14) and $[\text{Zn}_2(\text{T}_2\text{-PrO})(\text{H}_2\text{O})_2\text{Br}]\text{Br}_2 \cdot \text{H}_2\text{O}$ (15)	193

4.3	Complexes of bis(tacn) ligands with acetate pendant arms	199
4.3.1	Preparation of Complexes	199
4.3.2	Solution NMR Spectroscopy of $[\text{Zn}_2(\text{T}_2\text{-}o\text{-X Ac}_2)(\text{H}_2\text{O})_4](\text{ClO}_4)_2 \cdot 2\text{H}_2\text{O}$ (16) and $[\text{Zn}_2(\text{T}_2\text{-}m\text{-X Ac}_2)(\text{H}_2\text{O})_4](\text{ClO}_4)_2 \cdot 2\text{H}_2\text{O}$ (17)	201
4.4	Complex of a tris(tacn) ligand (18)	206
4.4.1	Preparation of the Complex	206
4.4.2	Solution NMR Spectroscopic Analysis of $[\text{Zn}_6(\text{T}_3\text{mes})_2(\mu\text{-OH})_6(\text{H}_2\text{O})_6](\text{ClO}_4)_6 \cdot \text{H}_2\text{O}$ (18)	207
4.5	Zinc(II) Complex Incorporating Phosphate	212
4.5.1	Preparation of $[(\text{Zn}_2(\text{Me}_3\text{tacn})_2(\text{H}_2\text{O})_4\text{PhP})(\text{ClO}_4)_2 \cdot \text{H}_2\text{O}$ (19)	212
4.5.2	Crystal Structure of $[(\text{Zn}_2(\text{Me}_3\text{tacn})_2(\text{H}_2\text{O})_4\text{PhP})(\text{ClO}_4)_2 \cdot \text{H}_2\text{O}$ (19)	213
4.5.3	Solution NMR Spectroscopic Analysis of $[(\text{Zn}_2(\text{Me}_3\text{tacn})_2(\text{H}_2\text{O})_4\text{PhP})(\text{ClO}_4)_2 \cdot \text{H}_2\text{O}$ (19)	221
4.6	Concluding Remarks	223
4.7	Experimental	224
4.8	References	233

Chapter Five Kinetics of the Hydrolysis of Phosphate Esters

5.1	Introduction	236
5.2	Hydrolytic Studies: Preliminary Screening of Complexes	241
5.3	Kinetic Study of $[\text{Cu}(\text{Me}_3\text{tacn})(\text{H}_2\text{O})_2](\text{ClO}_4)_2$ (11)	245
5.3.1	Reaction Conditions	245
5.3.2	Determination of the Observed Rate Constants	248

5.3.2	Release of the first 4-nitrophenylate anion, k_{obs1}	
	250	
5.3.3	Release of the second 4-nitrophenylate anion, k_{obs2}	251
5.3.4	Determination of the Equilibrium Constants, K_a and K_{dim}	253
5.3.5	Determination of Second Order Rate Constants	260
5.3.6	Attempt at Determining the Equilibrium Constant for Attachment of BNPP to the Complex	270
5.3.7	Thermodynamic Parameters	272
5.3.8	Activation Parameters	274
5.3.9	Catalytic Turnover	277
5.4	Discussion of Results	280
5.4.1	General Observations	280
5.4.2	First Order Rate Constants	282
5.4.3	Second Order Rate Constants	292
5.4.4	Catalytic Turnover Experiment	
	298	
5.5	Concluding Remarks and Future Directions	299
5.6	Experimental	301
5.7	References	307

Appendix One Crystallographic Data

1.1	$[\text{Cu}_2(\text{T}_2\text{-}p\text{-X})\text{Cl}_4]$ (3)	313
-----	--	-----

1.2	[Cu ₂ (T ₂ -PrO)Br ₂]Br·2H ₂ O (4)	314
1.3	[Cu(tacn) ₂](BNPP) (8)	315
1.4	[Cu ₃ (Me ₃ tacn) ₃ (PhP) ₂](ClO ₄) ₂ ·½H ₂ O (9)	316
1.5	[Cu ₂ (T ₂ - <i>m</i> -X)(NPP)(μ-OH)](ClO ₄) ₂ ·½H ₂ O (10)	317
1.6	[Zn(T ₂ - <i>o</i> -X)](ClO ₄) ₂ ·H ₂ O (12)	318
1.7	[Zn ₂ (T ₂ - <i>p</i> -X)(H ₂ O) ₄ (DMF) ₂][ZnCl ₄] (14)	319
1.8	[Zn ₂ (Me ₃ tacn) ₂ (H ₂ O) ₄ (PhP)](ClO ₄) ₂ ·H ₂ O (19)	320
1.9	[Ni(Me ₃ tacn)(H ₂ O) ₃](ClO ₄) ₂	321

Appendix Two Kinetic Data

2.1	Calculated k_{obs} Values	324
2.2	Residual Maps for k_2K_2 , K_a and K_{dim} determined at 42°C using MATLAB	332
2.3	Residual Maps for k_2K_2 , K_a and K_{dim} determined at 50°C using MATLAB	333
2.4	Residual Maps for k_2K_2 , K_a and K_{dim} determined at 57.5°C using MATLAB	334
2.5	Residual Maps for k_2K_2 , K_a and K_{dim} determined at 65°C using MATLAB	335
2.6	Derivation of Equation used in the MATLAB fitting procedure	336

Summary

This thesis describes the synthesis of copper(II) and zinc(II) complexes of 1,4,7-triazacyclononane (tacn) derivatised ligands, and the study of their hydrolytic reactivity with the phosphodiester, bis(4-nitrophenyl)phosphate (BNPP). It was anticipated that by linking a number of M^{2+} -tacn units together, more metal centres would be located in close proximity and as such would act in concert in increasing the rate of hydrolysis of the phosphodiester. Although copper(II) complexes of the unfunctionalised bis(tacn) ligands, especially the tris(tacn) ligand, did increase the rate of hydrolysis compared with that of $[Cu(tacn)(H_2O)_2]^{2+}$, the complex with the fastest rate of hydrolysis was the mononuclear complex, $[Cu(Me_3tacn)(H_2O)_2](ClO_4)_2$ ($Me_3tacn = 1,4,7$ -trimethyl-1,4,7-triazacyclononane). The alkylation of the tacn ligand produced rate enhancements of 60 fold over that of the unalkylated tacn copper(II) complex.

A series of polynucleating ligands was synthesised by reacting bis- or tris-electrophiles with the protected tacn derivative, 1,4,7-triazacyclo[5.2.1.0^{4,10}]decane to form the amidium salts of the ligands. The salts were then hydrolysed in water to produce the formyl derivatives, and these products were treated in one of two ways. In the first, acid hydrolysis of the ligands cleaved the formyl group and the hydrochloride salts of *ortho*, *meta* and *para*-xylyl bridged bis(tacn) ligands, $T_{2-o-X}.6HCl$, $T_{2-m-X}.6HCl$ and $T_{2-p-X}.6HCl$, and the mesitylene linked tris(tacn) ligand, T_{3mes} , were isolated. The second process involved treating the formyl derivatives of the *ortho* and *meta* bridged bis(tacn) ligands with bromoethyl acetate, followed by acid hydrolysis to form bis(tacn) ligands *N*-functionalised with two acetate pendant arms, $T_{2-o-X}Ac_2$ and $T_{2-m-X}Ac_2$. The latter

ligands were not isolated in a pure state and were used directly in the synthesis of metal complexes. An additional bis(tacn) ligand, linked by a propan-2-ol bridge, was synthesised by reacting the doubly protected tacn, *N,N'*-bis(*p*-tolylsulfonyl)-1,4,7-triazacyclononane (tacnTs₂) with the bis(electrophile), 1,3-dibromopropan-2-ol, to form the tetratosyl derivative of the propanol bridged bis(tacn), followed by acid hydrolysis to yield the hydrobromide salt, T₂-PrOH.6HBr.

Copper(II) complexes of the ligands were synthesised by addition of an excess of Cu²⁺ to the ligands. The pH of the solutions of the bis(tacn) ligands and Cu²⁺ were adjusted to *ca.* 5, producing binuclear complexes. A crystal structure of [Cu₂(T₂-*p*-X)Cl₄] confirmed that each macrocyclic compartment bound a Cu(II) centre and that the geometry adopted by the complex was square pyramidal, with each tacn macrocycle bound to one of the four triangular faces of the square pyramid. The acetate functionalised bis(tacn) ligands also formed binuclear complexes with copper(II), with the square pyramidal geometry, as indicated by electronic spectra. The copper(II) complex of the propanol bridged bis(tacn) ligand showed an alkoxo bridge between the two copper(II) centres, with the bridging oxygen shifting the geometry about the copper centres slightly more towards trigonal bipyramidal *cf.* the other copper complexes. The alkoxo bridge was found to facilitate medium strength antiferromagnetic coupling between the copper(II) centres. Each copper(II) bis(tacn) complex has a free coordination site, which is an important feature when designing biomimetic model compounds for the hydrolysis of phosphate esters.

Several copper complexes which incorporated phosphate within the structure were also synthesised. A sandwich-type structure of copper(II) with tacn which has a BNPP moiety

as the anion, $[\text{Cu}(\text{tacn})_2](\text{BNPP})$, was isolated. This has possible implications in hydrolytic studies, as the sandwich structure has no vacant coordination sites, and therefore will be inactive in the hydrolysis of phosphate esters. Reaction of Cu^{2+} with Me_3tacn and phenyl phosphate (PhP) yielded a trinuclear complex with two phosphate bridges between each of the three copper(II) centres, $[\text{Cu}_3(\text{Me}_3\text{tacn})_3(\text{PhP})_2](\text{ClO}_4)_2 \cdot \frac{1}{2}\text{H}_2\text{O}$. A third product isolated consisted of the $\{\text{Cu}_2(\text{T}_2\text{-}m\text{-X})\}$ moiety bridged by both a 4-nitrophenyl phosphate bridge and a hydroxo bridge. This complex exhibits strong antiferromagnetic coupling between the copper(II) centres, facilitated by the hydroxo bridge rather than the phosphate bridge. The latter two complexes have the potential to exhibit cooperative effects of two or three Cu-tacn moieties for the hydrolysis of phosphate esters.

Reactions of zinc(II) salts with the aforementioned ligands resulted in the formation of complexes with different types of structures. The *ortho* bridged ligand formed a mononuclear sandwich type complex, $[\text{Zn}(\text{T}_2\text{-}o\text{-X})](\text{ClO}_4)_2 \cdot \text{H}_2\text{O}$, while the zinc complex of $\text{T}_2\text{-}m\text{-X}$ formed a binuclear complex with hydroxide bridges between the zinc(II) centres. The *para*-xylene bridged ligand formed a binuclear complex with each of the zinc(II) centres bind independently to each tacn macrocycle, with no interactions between the metal centres. The complex of propan-2-ol ligand again formed a bridge between the zinc centres in a similar manner to that of the analogous copper complex. The ligands with the acetate pendant arms formed binuclear complexes, as for the copper(II). Reaction of zinc(II) with T_3mes formed a hexanuclear complex, $[\text{Zn}_6(\text{T}_3\text{mes})_2(\mu\text{-OH})_6(\text{H}_2\text{O})_6](\text{ClO}_4)_6 \cdot \text{H}_2\text{O}$

A phosphate bridged dinuclear zinc complex was isolated from solutions containing Zn^{2+} , Me_3tacn and phenyl phosphate, $[(Zn_2(Me_3tacn)_2(H_2O)_4PhP)(ClO_4)_2.H_2O]$. This complex is of interest in hydrolytic studies as it shows two $Zn-Me_3tacn$ units binding to a single phosphate ester moiety, while still having coordination sites occupied by water ligands. These water molecules are an important feature in designing phosphate ester hydrolytic mimics as they can form an internal nucleophile to hydrolyse the phosphate ester.

The complexes were tested for their hydrolytic activity with BNPP by monitoring the release of 4-nitrophenol spectrophotometrically. It was found that increasing the nuclearity of the complex resulted in an increase in the rate amongst analogous complexes. The $Cu(II)$ complexes of the ligands T_2-o-X and T_2-m-X showed a faster rate than the $Cu(II)$ complex of $tacn$. In addition, the trinuclear $Cu(II)$ complex of the ligand T_3mes exhibited a substantial increase in the rate of hydrolysis of the phosphate diester and needs further investigation. The binuclear $Cu(II)$ copper complexes of the ligands $T_2-o-X Ac_2$ and $T_2-mX Ac_2$ showed that the rate increase was not as great as for the non-pendant arm ligands, indicating the requirement of two sites for hydrolysis to occur.

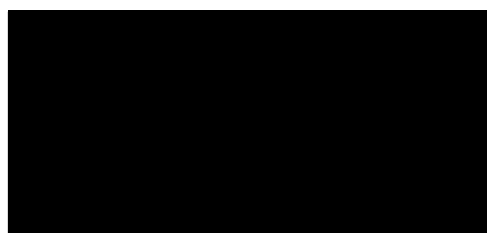
The mononuclear complex $[Cu(Me_3tacn)(H_2O)_2]^{2+}$ was the most active complex tested this study. A detailed kinetic study was carried out on this complex at four temperatures, eight pH values and eleven concentrations. The rate increase for this complex was higher than for other $Cu(II)$ complexes tested. The active precursor to hydrolysis is $[Cu(Me_3tacn)(H_2O)(OH)]^+$, which has the internal $-OH$ nucleophile essential for reactivity for hydrolytic cleavage of the phosphate ester bond. It was also found that an inactive

species, $[(\text{Me}_3\text{tacn})\text{Cu}(\mu\text{-OH})_2\text{Cu}(\text{Me}_3\text{tacn})]^{2+}$, forms in solution. The second order rate constant was determined to be $0.15 \text{ M}^{-1}\text{s}^{-1}$ at 50°C , which is larger than for any other mononuclear complex of a divalent metal ion reported in the literature to date. Activation parameters for both the first order and the second order rate constants were calculated according to the Eyring equation. Catalytic activity was confirmed by a greater than stoichiometric production of the 4-nitrophenylate anion relative to the complex.

The copper(II) complex of the alkylated tacn macrocycle produces an increase in the rate of hydrolysis of BNPP when compared to the copper(II) complex of tacn. Modification of the ligand in such a way as to prevent the formation of the dimeric complex which is inactive in the hydrolysis of phosphate esters, would be expected to produce even greater rate enhancements.

Declaration

I declare that, to the best of my knowledge, that the work presented in this thesis is original. It contains no material that has been published elsewhere or used for the award of any degree or diploma in another university or College, except where due reference is made in the text.



Fiona Fry

February 2002

Acknowledgements

I would like to extend my deepest gratitude to my supervisor, Dr Leone Spiccia, for support and encouragement throughout the course of my PhD.

I would like to thank the following people for their expertise and assistance in the given areas: Drs Gary Fallon, Edward Teikink, Alan White and Christopher Kepert, and to Paul Jensen and Andrew Warden for crystallography; Prof. Keith Murray and Dr Boujemaa Mourabaki for the variable temperature magnetic studies; Dr Peter Nichols and Kevin Lu for help with the molecular modelling program Insight II; Drs Jo Cosgriff and Roger Mulder for the NMR experiments on the 500 MHz spectrometer; Dr Jo Weigold for 2D NMR experiments; Susan Turland for the ^{31}P NMR experiment; Ms Sally Duck for electrospray mass spectrometry; Adrian van der Bergen for microprobe analyses, Simon Drew and Jack Smith for ESR spectra and Dr Joël Brugger for the spectrophotometric modelling studies. I appreciate the computer support given by Jay Black for programming MATLAB, and by Andrew Conn for SigmaPlot calculations. I would like to thank Ms Nicola Williams for the use of her laboratory and for proof-reading this thesis.

I would also like to thank the various students and post-docs that have shared the lab with me over the years I have been at Monash, making it an interesting and an enjoyable place to work: Bim, Chris, Kevin, Andrew, Julianne, Jay, Don, Tiffany, Paul J., Paul A., Jason, Nino, Anna, Vita, Pauline, Glenn, Martin, Sue, Alex, Richard, Ken and Scott.

Thank-you to Miranda, Jo and Tim for the "First Year Experience". I would also like to thank Jo and Michael for proof-reading this thesis.

I greatly appreciate the support from my friends and family, with special mention to Andrew "Chucky" Dorkins, who is a wonderful partner and a good friend.

Finally, I would like to thank the Australian Government for the financial assistance provided the form an Australian Postgraduate Award.

Abbreviations

AP	Alkaline phosphatase
BNPP	bis(4-nitrophenylphosphate)
bpy	2,2'-bipyridine
CHES	2-(<i>N</i> -cyclohexylamino)ethanesulfonic acid
cyclen	1,4,7,10-tetraazacyclododecane
DMF	<i>N, N'</i> -Dimethylformamide
en	ethylenediamine
ENPP	ethyl 4-nitrophenylphosphate
ESR	Electron Spin Resonance
HEPES	<i>N</i> -(2-hydroxyethyl)piperzine- <i>N'</i> -ethanesulfonic acid
IR	Infrared
Me₃tacn	1,4,7-trimethyl-1,4,7-triazacyclononane
MES	2-(<i>N</i> -morpholino)ethanesulfonic acid
MOPS	3-(<i>N</i> -morpholino)propanesulfonic acid
NMR	Nuclear Magnetic Resonance
NP	4-nitrophenylate
NPP	4-nitrophenyl phosphate
PAP	Purple acid phosphatase
PLC	Phospholipase C
SP	Square pyramid(al)
T_{2-m-X}	1,3-[Bis-(1,4,7-triazacyclononan-1-ylmethyl)]benzene
T_{2-m-X} Ac₂	1,3-bis(4-(carboxymethyl)-1,4,7-triazacyclonon-1-ylmethyl)benzene
T_{2-o-X}	1,2-[Bis-(1,4,7-triazacyclononan-1-ylmethyl)]benzene
T_{2-o-X} Ac₂	1,2-bis(4-(carboxymethyl)-1,4,7-triazacyclonon-1-ylmethyl)benzene

T₂PrOH	1,3-[Bis-(1,4,7-triazacyclononan-1-yl)]propan-2-ol
T₂-<i>p</i>-X	1,4-[Bis-(1,4,7-triazacyclononan-1-ylmethyl)]benzene
T₃mes	1,3,5-[Tris(1,4,7-triazacyclononan-1-ylmethyl)]benzene
Tacn	1,4,7-triazacyclononane
TAPS	N-tris(hydroxymethyl)methyl-3-aminopropanesulfonic acid
TBP	Trigonal bipyramid(al)
UV	Ultraviolet
Vis	Visible

Numbering Scheme for Metal Complexes

1	$[\text{Cu}_2(\text{T}_2\text{-}o\text{-X})\text{Cl}_4]$
2	$[\text{Cu}_2(\text{T}_2\text{-}m\text{-X})(\text{H}_2\text{O})_4](\text{ClO}_4)_4 \cdot 3\text{H}_2\text{O} \cdot \text{NaClO}_4$
3	$[\text{Cu}_2(\text{T}_2\text{-}p\text{-X})\text{Cl}_4]$
4	$[\text{Cu}_2(\text{T}_2\text{-PrO})\text{Br}_2]\text{Br} \cdot 2\text{H}_2\text{O}$
5	$[\text{Cu}_2(\text{T}_2\text{-}o\text{-X Ac}_2)(\text{H}_2\text{O})_2](\text{ClO}_4)_2 \cdot 6\text{H}_2\text{O}$
6	$[\text{Cu}_2(\text{T}_2\text{-}m\text{-X Ac}_2)(\text{H}_2\text{O})_2](\text{ClO}_4)_2 \cdot 4\text{H}_2\text{O}$
7	$[\text{Cu}_6(\text{T}_3\text{mes})_2(\mu\text{-OH})_6](\text{ClO}_4)_6 \cdot 6\text{H}_2\text{O}$
8	$[\text{Cu}(\text{tacn})_2](\text{BNPP})$
9	$[\text{Cu}_3(\text{Me}_3\text{tacn})_3(\text{PhP})_2](\text{ClO}_4)_2 \cdot \frac{1}{2}\text{H}_2\text{O}$
10	$[\text{Cu}_2(\text{T}_2\text{-}m\text{-X})(\text{NPP})(\mu\text{-OH})](\text{ClO}_4) \cdot \text{H}_2\text{O}$
11	$[\text{Cu}(\text{Me}_3\text{tacn})(\text{H}_2\text{O})_2](\text{ClO}_4)_2$
12	$[\text{Zn}(\text{T}_2\text{-}o\text{-X})](\text{ClO}_4)_2 \cdot \text{H}_2\text{O}$
13	$[\text{Zn}_2(\text{T}_2\text{-}m\text{-X})(\mu\text{-OH})_2(\text{H}_2\text{O})_2]\text{Br}_2 \cdot \text{H}_2\text{O}$
14	$[\text{Zn}_2(\text{T}_2\text{-}p\text{-X})(\text{H}_2\text{O})_4(\text{DMF})_2][\text{ZnCl}_4]_2$
15	$[\text{Zn}_2(\text{T}_2\text{-PrO})(\text{H}_2\text{O})_2\text{Br}]\text{Br}_2 \cdot \text{H}_2\text{O}$
16	$[\text{Zn}_2(\text{T}_2\text{-}o\text{-X Ac}_2)(\text{H}_2\text{O})_2](\text{ClO}_4)_2 \cdot 2\text{H}_2\text{O}$
17	$[\text{Zn}_2(\text{T}_2\text{-}m\text{-X Ac}_2)(\text{H}_2\text{O})_2](\text{ClO}_4)_2 \cdot 2\text{H}_2\text{O}$
18	$[\text{Zn}_6(\text{T}_3\text{mes})_2(\mu\text{-OH})_6(\text{H}_2\text{O})_6](\text{ClO}_4)_6 \cdot \text{H}_2\text{O}$
19	$[(\text{Zn}(\text{Me}_3\text{tacn})(\text{H}_2\text{O})_2)_2\text{PhP}](\text{ClO}_4)_2 \cdot (\text{H}_2\text{O})$

Chapter One

Introduction to Phosphate Ester Hydrolysis

1.1 General Introduction

Enzymes are important participants in the chemistry of life. Many of the reactions occurring in biological systems would proceed far too slowly on their own to sustain life. Enzymes are biological catalysts which lower the activation energies of these reactions enabling them to proceed at rates that are many orders of magnitude faster than the uncatalysed reactions. In some cases, rate enhancements by a factor of 10^{17} have been observed.¹ Biological systems utilise enzymes to make specific reactions occur, avoiding or minimising wasteful competing reactions. Although much has been discovered about enzymes, fundamental questions remain regarding their reaction mechanisms and the structural features necessary for them to operate.

1.2 Metalloenzymes

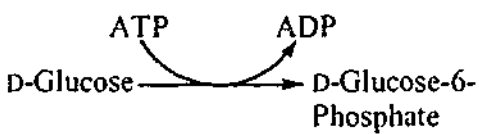
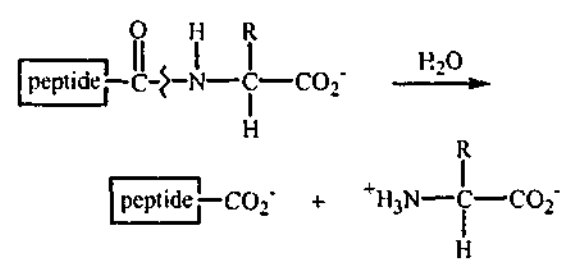
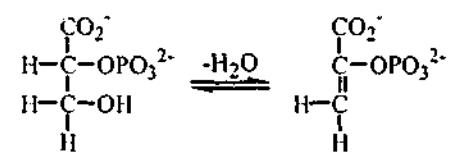
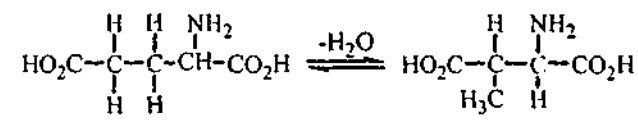
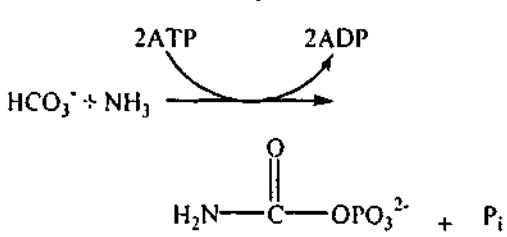
Around 40% of enzymes contain one or more metal centres in their structure.² These metal ions may play one of two roles. In the first instance, the metal ion plays a structural role being involved in the stabilisation of the protein molecule, forming bonds to acid side chains. This controls the local protein folding and conformation, and therefore the metal ion plays a key role in the formation of the tertiary structure of the enzyme. The second role of the metal ion is functional; it is located within the active site of the enzyme, and is an essential component of the catalytic activity.³ It is this latter involvement of the metal ions which gives rise to the subclass of enzymes, known as metalloenzymes.

There are six major classes of enzymes and are as follows:⁴

1. Oxidoreductases – catalyse oxidation-reduction reactions.
2. Transferases – catalyse the transfer of a functional group from one molecule to another.
3. Hydrolases – catalyse hydrolytic cleavage.
4. Lyases – catalyse the addition or removal of a group to a double bond, or other cleavages involving electron rearrangement.
5. Isomerases – catalyse intramolecular rearrangement.
6. Ligases – catalyse reactions in which two molecules are joined.

Metalloenzymes are found in each of the above classes.² Examples and functions of various metalloenzymes are shown in Table 1.1. Metal centres frequently found in biological systems are the alkali- and alkaline earths, sodium, potassium, magnesium and calcium and many of the first row transition metal ions, especially iron, copper and zinc. Others less frequently encountered metal ions are vanadium, manganese, cobalt, nickel, molybdenum and, even less commonly, tungsten.

Table 1.1 Selected metalloenzymes

Enzyme	Class ⁶	Metal Present	Function
Nitrate Reductase ⁵	1	Mo(IV/VI)	Reduction of nitrate to nitrite, a key step of the nitrate assimilation in green plants. $\text{NO}_3^- + 2\text{H}^+ + 2\text{e}^- \rightarrow \text{NO}_2^- + \text{H}_2\text{O}$
Hexokinase ⁶	2	Mg(II)	Converts D-glucose to D-glucose-6-phosphate 
Carboxy-peptidase A ⁶	3	Zn(II)	Hydrolyses peptide bonds 
Enolase ²	4	Mg(II)	Aids removal of OH ⁻ 
Coenzyme B ₁₂ ⁶	5	Co(II)	Coenzyme for several reactions. e.g. reaction catalysed by glutamate mutase. 
Carbamoyl Phosphate Synthetase ⁷	6	Mn(II)	Involved in the urea cycle 

1.3 Phosphatase Enzymes

The metabolism of phosphate plays a key role in the function of living organisms. Indeed, the transfer of phosphoryl groups is the most important mechanism by which cellular processes occur. Hundreds of metabolic pathways are controlled by the phosphorylation reactions catalysed by kinases and the dephosphorylation reactions catalysed by phosphatases. Some examples of these pathways include the oxidation of glucose to provide the cell with energy, the storage of glucose as glycogen (and its reverse), the activation of nucleosides to produce the building blocks for DNA and RNA and the biosynthesis of amino acids and aminoacyl t-RNA molecules to provide the building blocks for proteins and the signal transduction pathways.⁸ Phosphatases are enzymes that catalyse the hydrolytic cleavage of the phosphate ester bond (P-OR), which is found in biological molecules such as DNA, RNA adenosine triphosphate (ATP) and phosphorylated amino acids. Several examples of this type of metalloenzyme are described in the following sections.

1.3.1 Alkaline Phosphatase

Alkaline phosphatases (APs) represent one of the most widely studied classes of enzyme and their function is better understood than many other types of phosphatase enzymes. APs are found in both prokaryotes and eukaryotes, and exhibit optimum activity in slightly basic solution (ca. pH 8.0), a property which is reflected in their name. A common feature of all of the different forms of AP, is that zinc is essential for activity. Although much work has been directed towards the study of these enzymes, the function is still poorly defined. It is generally assumed that AP are non-specific phosphomonoesterases, with the ability to cleave phosphate from phosphomonoesters to

produce free inorganic phosphate, as well as transfer the phosphoryl group to other alcohols.

The crystal structure of an AP isolated from *E. coli* with coordinated inorganic phosphate was determined by Wycoff and coworkers⁹ and shows it to have a dimeric structure with three metal centres, two Zn²⁺ ions and one Mg²⁺ present in the active site of each subunit. A view of the active site of the enzyme is shown in Figure 1.1.

The two zinc ions (Zn1 and Zn2) are 3.94 Å apart, and the magnesium ion is closer to Zn2 (4.88 Å), than Zn1 (7.09 Å). In the second subunit, slightly different intermetallic separations are found: (Zn1-Zn2) 4.18, (Zn2-Mg) 4.66 and (Zn1-Mg) 7.08 Å. Although the Mg ion is located close to Zn(2), it is not directly involved in the catalytic steps.¹⁰ The Zn1 ion resides in a five-coordinate environment, bound to His331, His412, both oxygens from the carboxyl group of Asp327 and an oxygen from the bound phosphate ion. The coordination geometry is described by the authors as pseudotetrahedral, with both oxygens from the chelating Asp327 occupying one apex of the polyhedron.³ Zn2 is bound by four monodentate ligands, His370, Asp51, Asp369 and a phosphate oxygen, giving rise to a distorted tetrahedral coordination sphere. The magnesium ion resides in a slightly distorted octahedral coordination environment, bound by Asp51, Glu322, Thr155 and three water molecules. The phosphate group present in the crystal structure bridges both zinc ions, with two of the phosphate oxygens held in place by hydrogen bonding interactions with the guanine side-chain of Arg166. One of the oxygens is further hydrogen bonded to a water molecule, which forms additional hydrogen bond contacts to Asp153 and possibly Tyr169. The remaining phosphate oxygen is held in place through hydrogen bonding to Ser102 and a magnesium-bound water molecule.

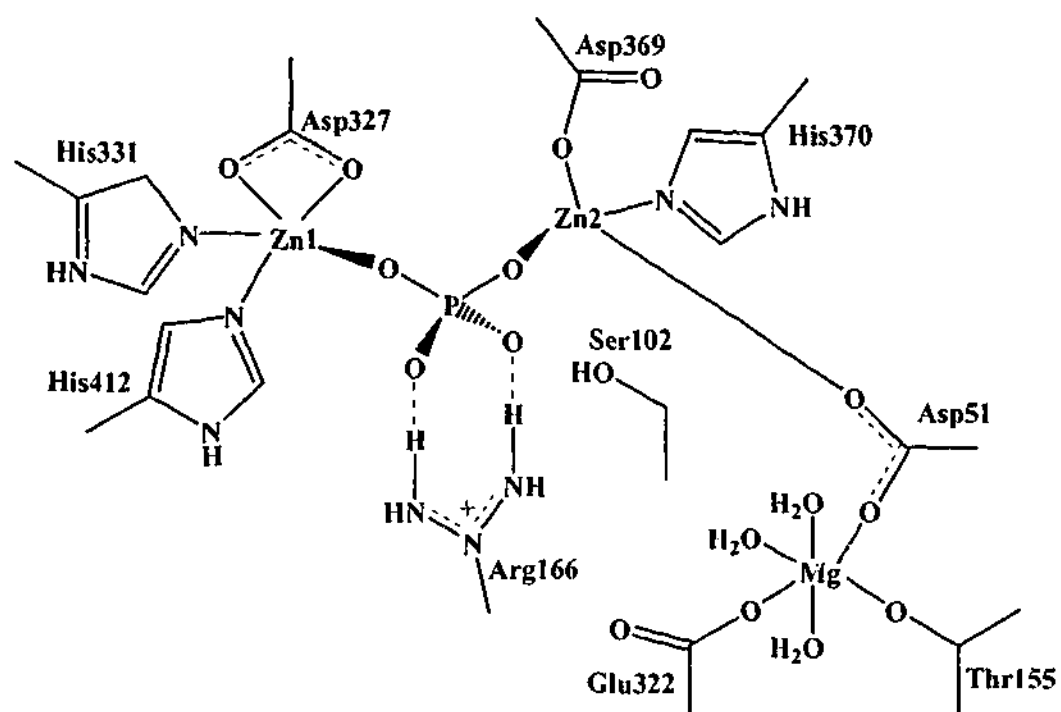
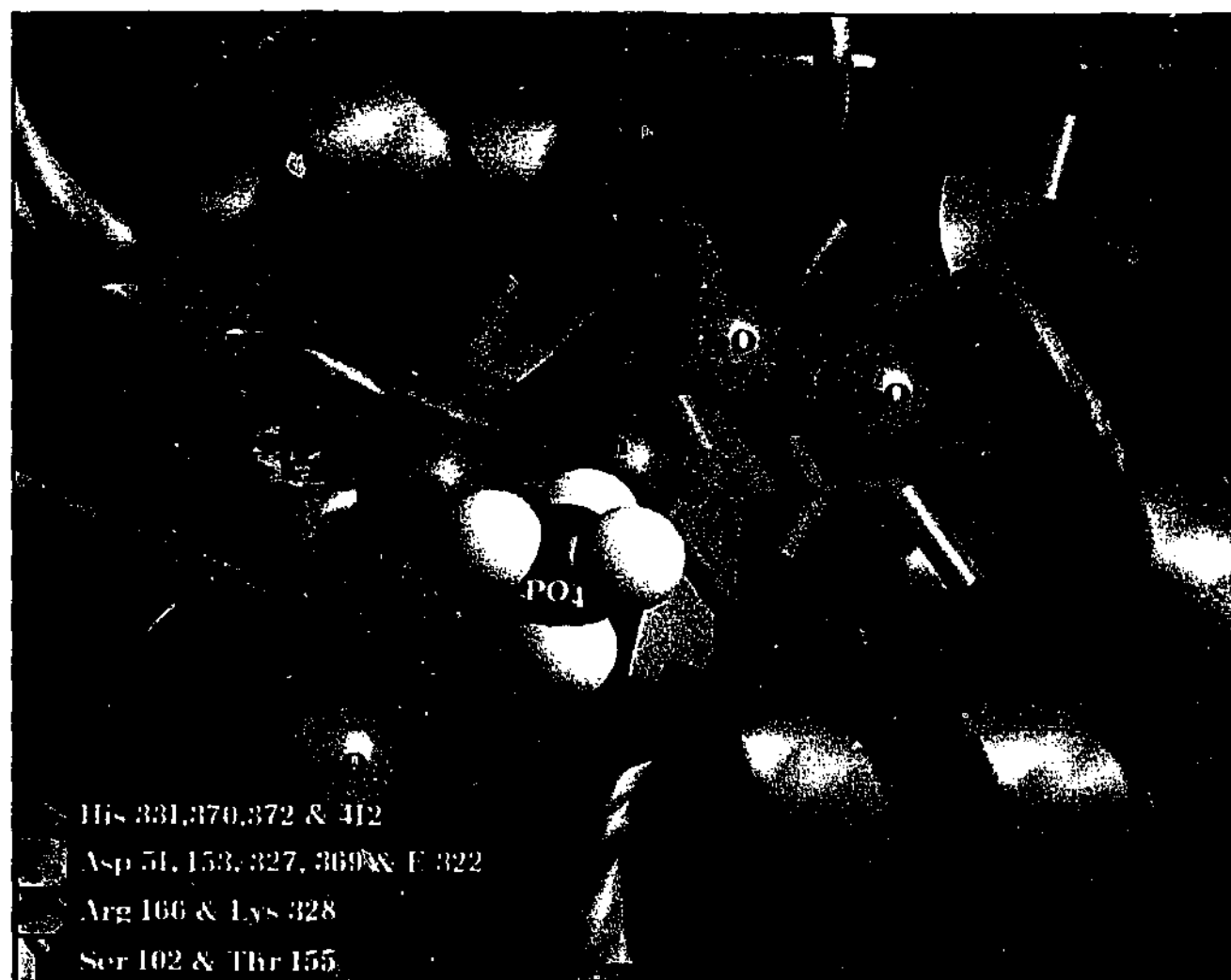
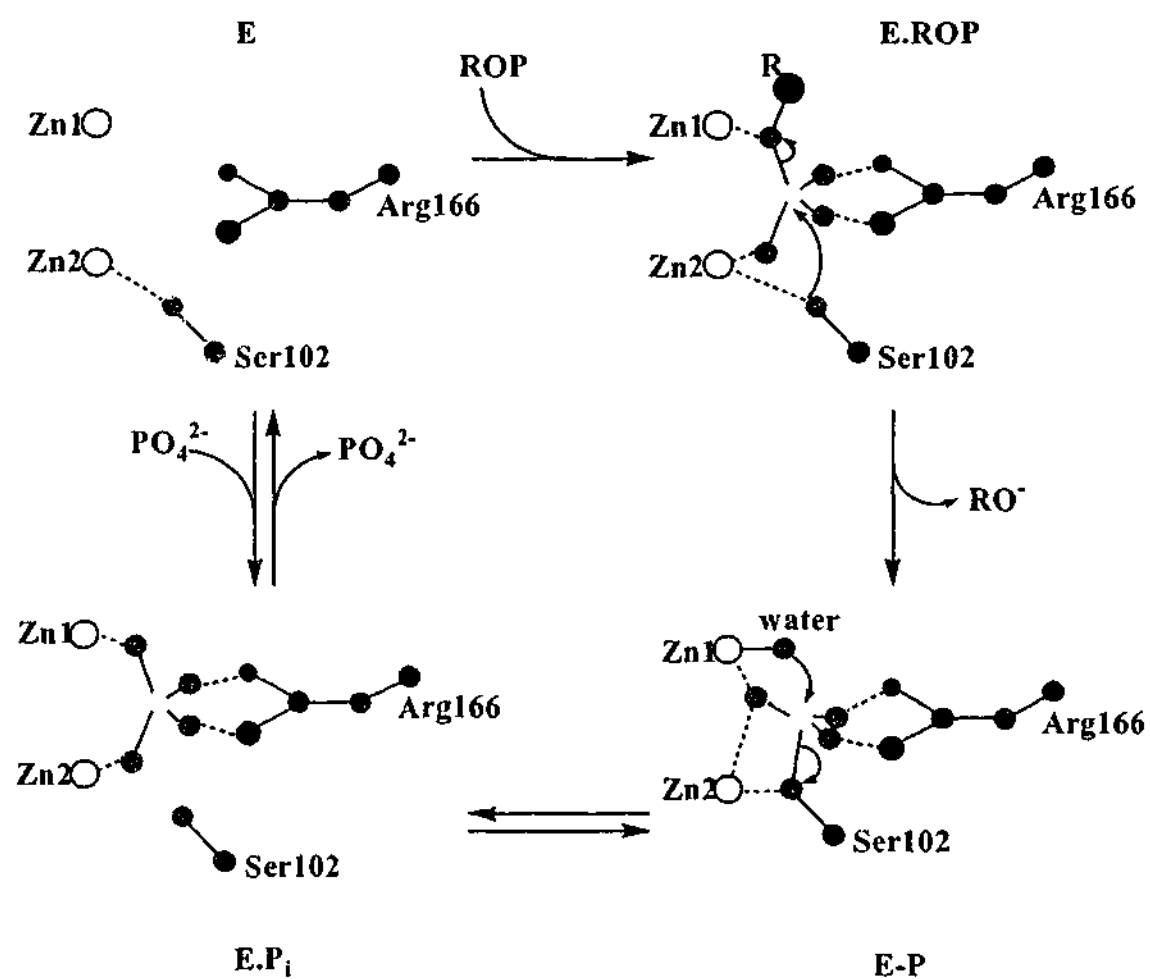


Figure 1.1 Crystal structure (top) and a structural representation (bottom) of the active site of AP bound phosphate

Knowledge of the structure of the AP active site has led to a number of proposals for the mechanisms of action of these enzymes. One proposed reaction pathway for the hydrolysis of phosphate esters by AP is shown in Scheme 1.1. In this case the enzyme is believed to function through the coordination of a terminal oxygen from a phosphate ester group to each of Zn1 and Zn2, as well as interactions to the guanidinium group of Arg166. Ser102 occupies the site opposite the leaving group (RO^-). Formation of the covalent phosphoryl intermediate (E-P) involves the phosphate group moving slightly to maintain the interactions with Arg166 and both Zn1 and Zn2. Nucleophilic attack by the water or hydroxide (coordinated to Zn1) on the covalent intermediate forms the non-covalent phosphate species (E.P_i). The release of the inorganic phosphate is the rate limiting step and results in the regeneration of the free enzyme.¹¹



Scheme 1.1 Hydrolysis of a phosphate monoester by AP¹¹

1.3.2 Purple Acid Phosphatases

Purple acid phosphatases (PAPs) cleave phosphate ester bonds under acidic conditions, with the optimal pH range of 4 to 7. They are characterised by the intense purple colour of their inactive oxidised forms, resulting from a tyrosine-to-Fe^{III} charge transfer transition ($\lambda_{\text{max}} \sim 550$ nm), and the pink colour of the active reduced form ($\lambda_{\text{max}} \sim 510$ nm). Another characteristic feature distinguishing them from other phosphatases is their resistance to inhibition by tartrate, leading to the alternative name “tartrate-resistant acid phosphatases” or TRAPs. They are found in a variety of animal and plant tissues, but were first isolated from porcine uterine fluid and bovine spleen. Mammalian enzymes isolated so far have been found to contain a diiron core at their active site, while PAPs purified from plants such as kidney bean and sweet potato have an iron-zinc or an iron-manganese pair present at their active site.

The crystal structure of kidney bean purple acid phosphatase (KBPAP) was reported by Krebs and coworkers in 1995.¹² The active site contains Fe³⁺ and Zn²⁺ ions which are bridged by a single oxygen atom of the carboxylate group of Asp164, resulting in a short metal-metal separation of 3.1 Å. The Fe³⁺ ion is also coordinated by Tyr167, His325 and Asp135, while the Zn²⁺ ion is coordinated by His286, His323 and Asn201. Due to the moderate resolution of the structure, the positions of the oxygen atoms could not be accurately determined, however, the authors place a μ -hydroxo bridging group between the two metal centres, a coordinated hydroxide on the Fe³⁺ centre and a coordinated water on the Zn²⁺ centre (Figure 1.2). These assignments were made based on the stereochemical preferences of the metals and additional biochemical data. The Fe³⁺ is then in an almost perfectly octahedral environment, while the Zn²⁺ resides in a distorted octahedral environment.

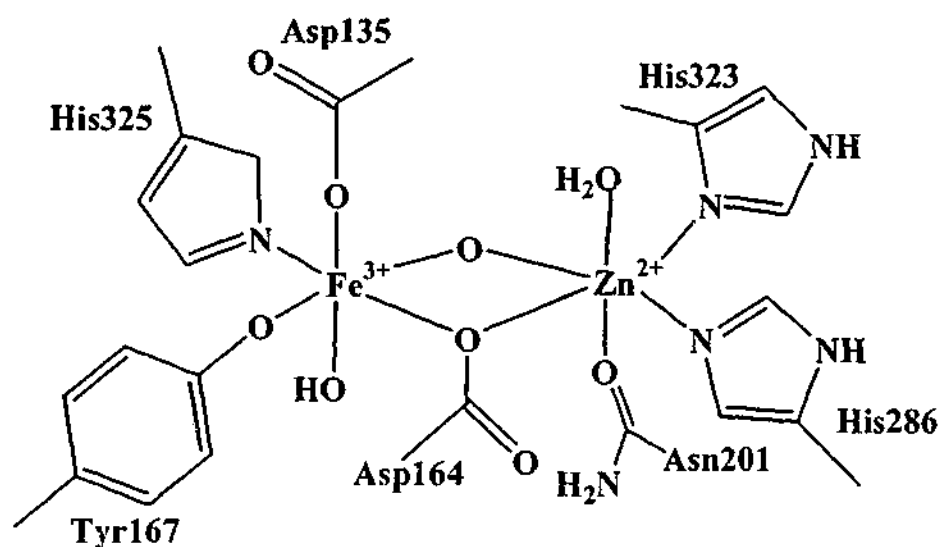


Figure 1.2 Schematic diagram of the binuclear site of KBPAP¹³

The crystal structure of KBPAP with bound phosphate shows the phosphate bridging between the two metal centres in a bidentate fashion, displacing two water ligands found in the phosphate free enzyme. The remaining uncoordinated phosphate oxygen atoms are hydrogen bonded to His202 and His296. These two residues are displaced by ~1 Å relative to their position in the phosphate-free enzyme (Figure 1.3).

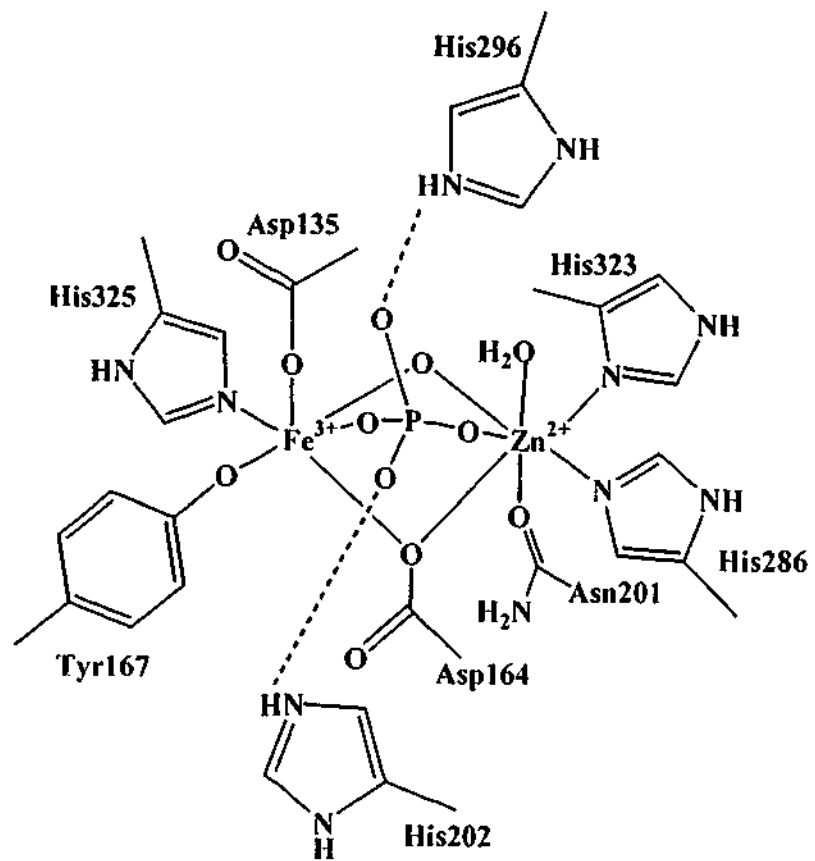
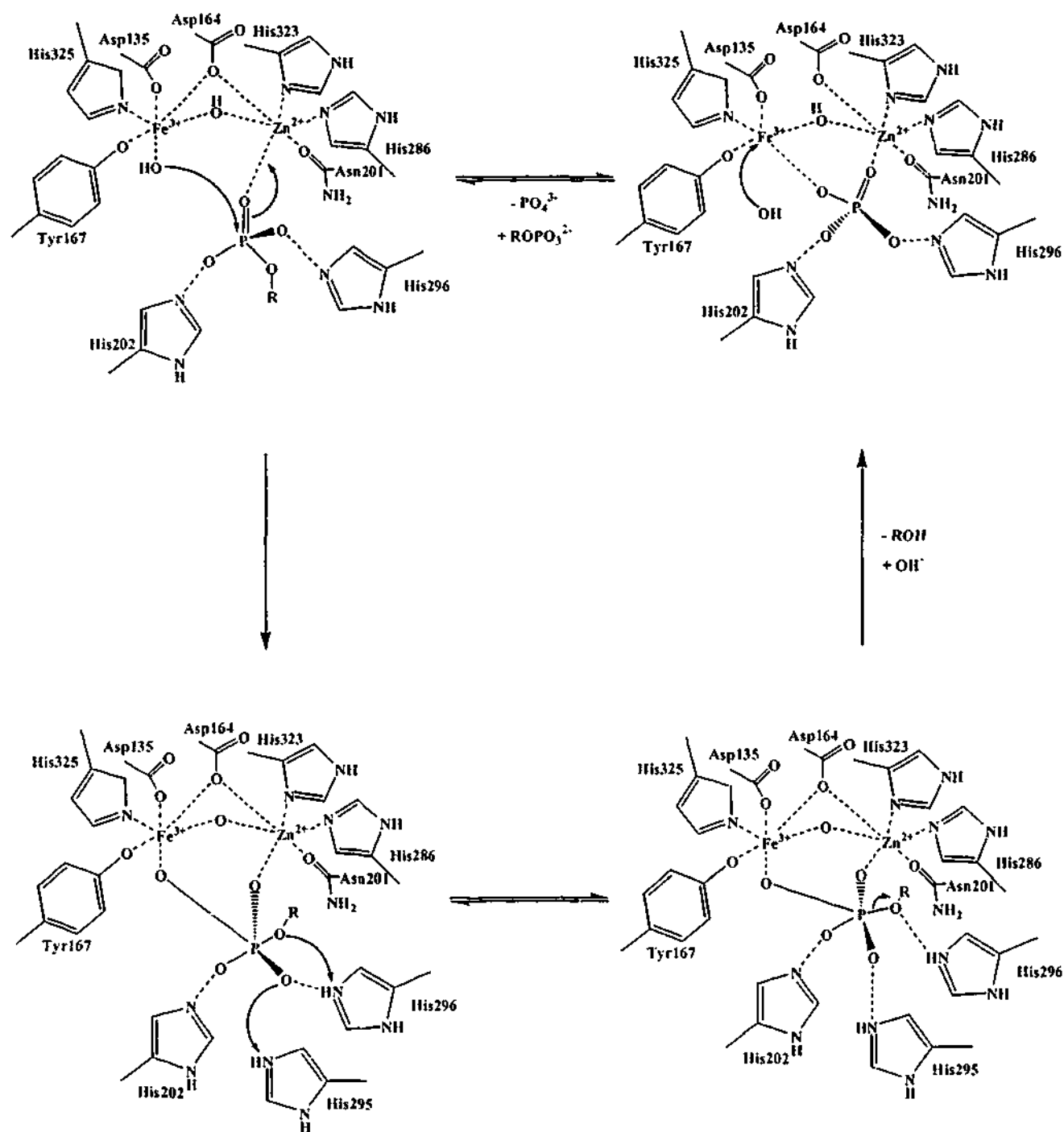


Figure 1.3 Crystal structure of the active site of KBPAP with bound phosphate¹⁴

A mechanism for the binding and hydrolysis of phosphate esters by KBPAP has been proposed by Krebs *et al.*¹⁵ and is shown in Scheme 1.2. It has been observed that an inversion of the stereochemistry of the phosphate occurs during the catalysis, making the possibility of a phosphorylated enzyme intermediate extremely unlikely. The reaction is then likely to proceed via an in-line mechanism, with the formation of a pentacoordinate intermediate in the transition state. The energy of the transition state is lowered not only by the Lewis acidity of the zinc centre, but also by the interactions with His202 and His296 (shown in Figure 1.3), by withdrawing the negative charge from the phosphorous centre.

In binding to the Zn(II) centre, a non-esterified oxygen atom from the phosphate group displaces a bound water molecule. Interactions with the aforementioned His202, His296 and the Zn(II) centre then orientate the substrate for an in-line attack. Transfer of the phosphoryl group from the leaving alcohol directly to the water ligand generates a phosphate bridge between the two metal centres. Attack of the Fe(III) centre by a water molecule releases the product, which retains the "inverted" stereochemistry, as observed experimentally.



Scheme 1.2 Proposed mechanism for phosphate ester hydrolysis by KBPAP15

1.3.3 Protein Phosphatases (PPs)

The phosphorylation of proteins by kinases and dephosphorylation of proteins by phosphatases is a fundamental mechanism that a cell utilises to control its biological processes.¹⁶ This reversible phosphorylation is the key component of the signal transduction pathways by which extracellular signals regulate such things as cell growth¹⁷ and the cell cycle.¹⁸ Protein phosphatases are a class of enzyme which catalyse the cleavage of phosphate groups from specific amino acid residues in proteins. They catalyse the hydrolysis of phosphoserine, phosphothreonine, phosphotyrosine, phosphohistidine or phosphoaspartate, although the most thoroughly characterised enzymes are phosphoserine/threonine and phosphotyrosine phosphatases.¹⁹

1.3.3.1 Phosphoserine/Threonine Phosphatases (P-S/T-P)

The majority of phosphorylated residues in proteins are phosphorylated serine and threonine residues.¹⁶ The P-S/T-Ps can be divided into two groups (PP1 and PP2) based on their substrate specificity, inhibitor behaviour, subunit structure and mechanisms of activation.^{18,19} Of the two groups, the second (PP2) can be further divided into three groups, PP2A, PP2B (also known as calcineurin) and PP2C, based on the particular metal cations at the active site or cofactors required for activity.

The first three dimensional structure of a PP was reported by Goldberg *et al.*,²⁰ who isolated the PP1 protein from rabbit muscle. The protein was isolated with the toxin microcystin attached. The structure revealed a binuclear core at the active site (Figure 1.4), although the authors were not able to determine the identity of the metal centres, and simply referred to them as M1 and M2. Each of the metals were found to be in a five coordinate environment, M1 in a square pyramidal environment and M2 in a

distorted trigonal bipyramidal geometry. The metal centres are bridged by a carboxylate oxygen of Asp92 and also an oxygen from either a water or a hydroxy group and, as a result, the M1...M2 separation of 3.3 Å is quite short. Coordinated to M1 are a nitrogen from His66, an oxygen from Asp64, a terminal water molecule and an oxygen from the coordinated phosphate. The second metal centre is also bound to the phosphate group, as well as two nitrogens from His248 and His173 and an oxygen from Asn124 (Figure 1.4).

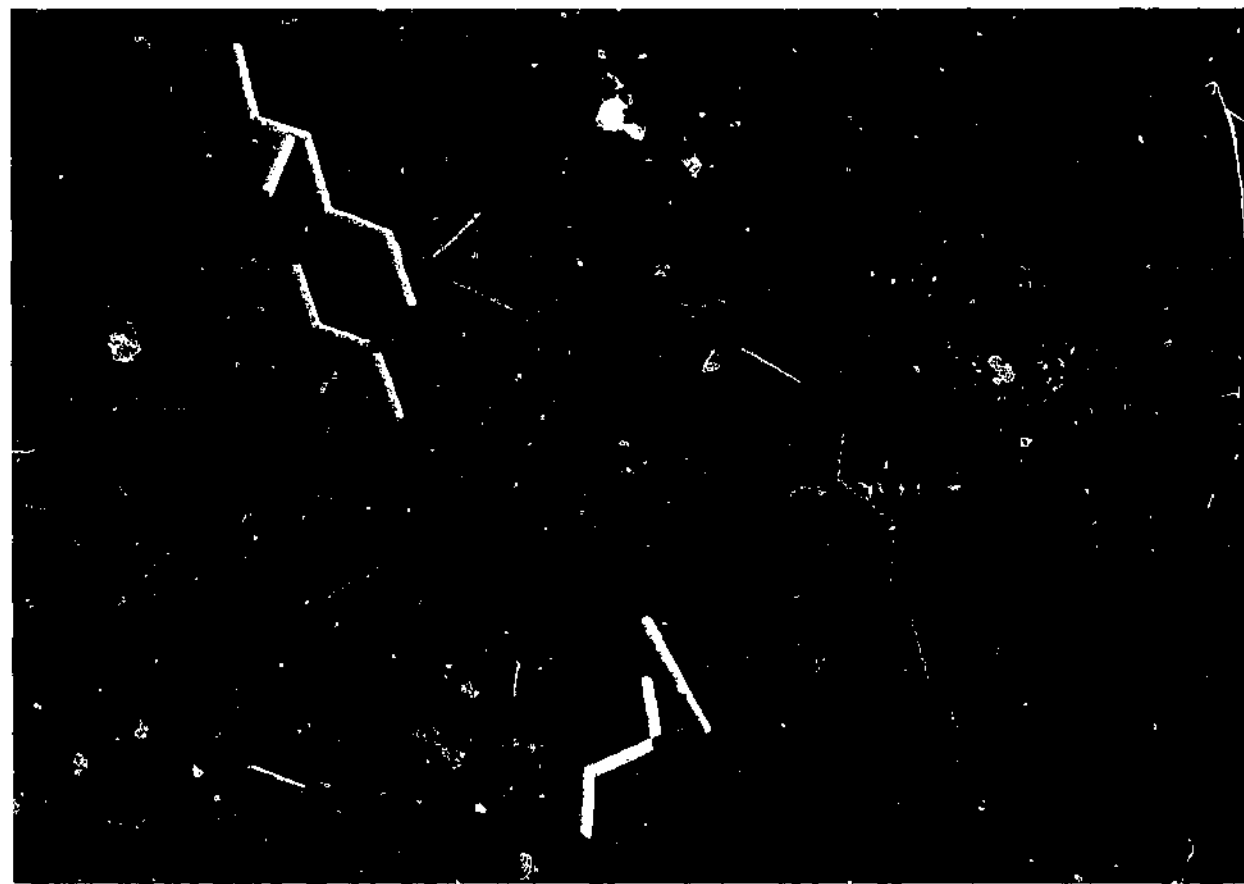
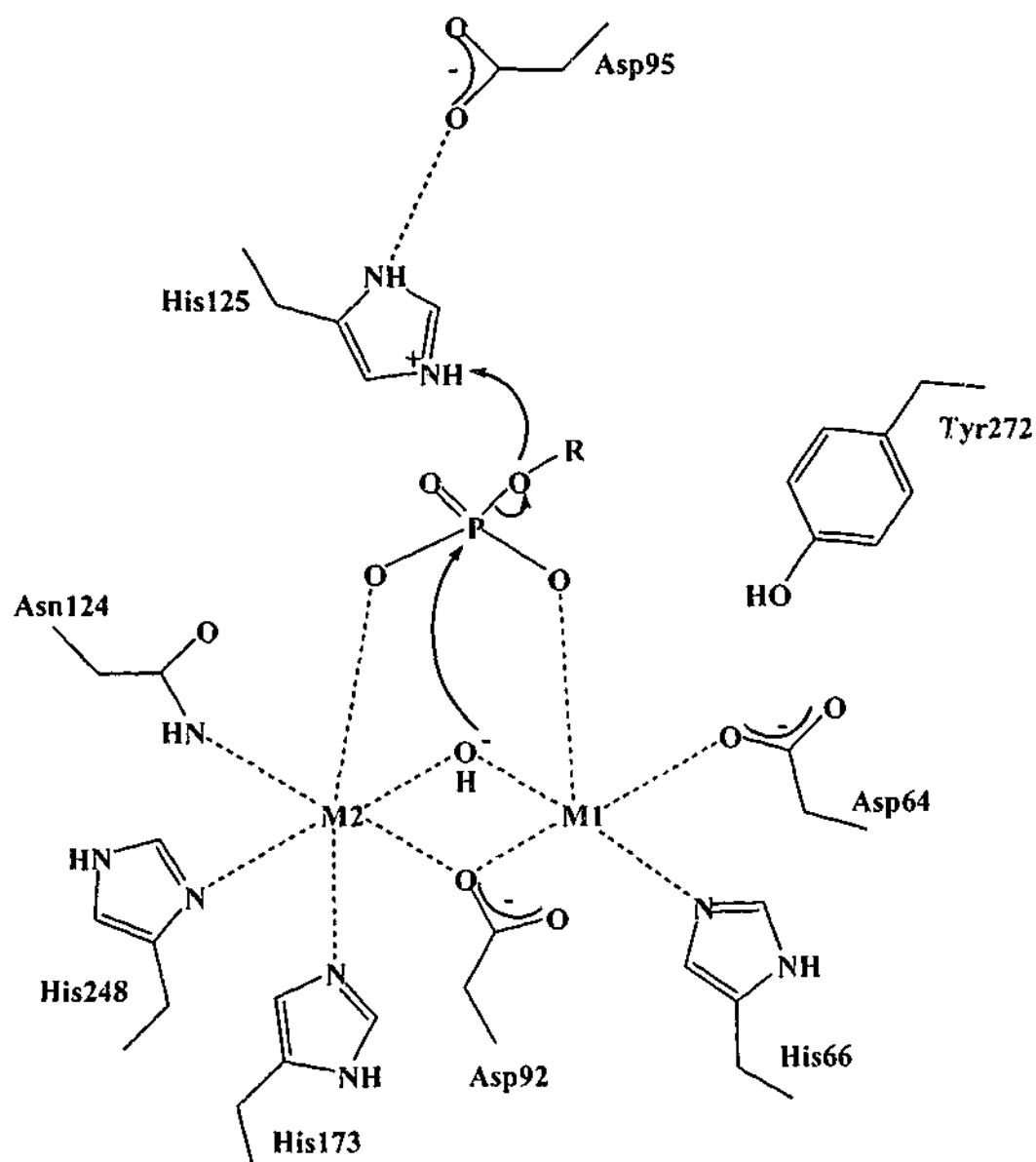


Figure 1.4 Structure of the active site of PP1 from rabbit muscle²⁰

Another group in the same year reported the crystal structure of the catalytic subunit of human PP1²¹, complexed with tungstate, an analogue of phosphate. Egloff *et al.* assigned the metal ions M1 as Fe²⁺ and M2 as Mn²⁺ based on results from proton-

induced X-ray emission spectroscopy on both the native protein and the tungstate derivative. The metals were found to be 3.5 Å apart. A possible mechanism for the reaction catalysed by PP1 is shown in Scheme 1.3.



Scheme 1.3 Proposed reaction mechanism catalysed by PP1²¹

One of the more extensively studied protein phosphatases is PP2B, also known as calcineurin. In 1995, Yu *et al.* reported evidence that the active site of calcineurin isolated from bovine brain contained one iron centre and one zinc centre.²² The crystal

structures of calcineurin from both bovine brain and human²³ were reported in 1995. Human calcineurin also shows an iron and a zinc in the active site. The iron is in an octahedral environment and is coordinated by oxygens from Asp90, Asp118, three water molecules and a nitrogen from His92. The zinc is in a distorted trigonal bipyramidal geometry and is coordinated to oxygens from Asp150, Asp118 and a water molecule, and two nitrogen donors from His281 and His199 (Figure 1.5).



Figure 1.5 Crystal structure of human calcineurin

1.3.4 Phospholipase C

Phospholipase C (PLC) is a class of enzyme involved in the hydrolysis of the phospholipids phosphatidylinositol and phosphatidylcholine (Figure 1.6), and

participates in the generation of second messengers in cells. A second messenger is an intracellular substance that relays a signal from outside the cell, from the cell membrane to the effector protein within the cell.⁴

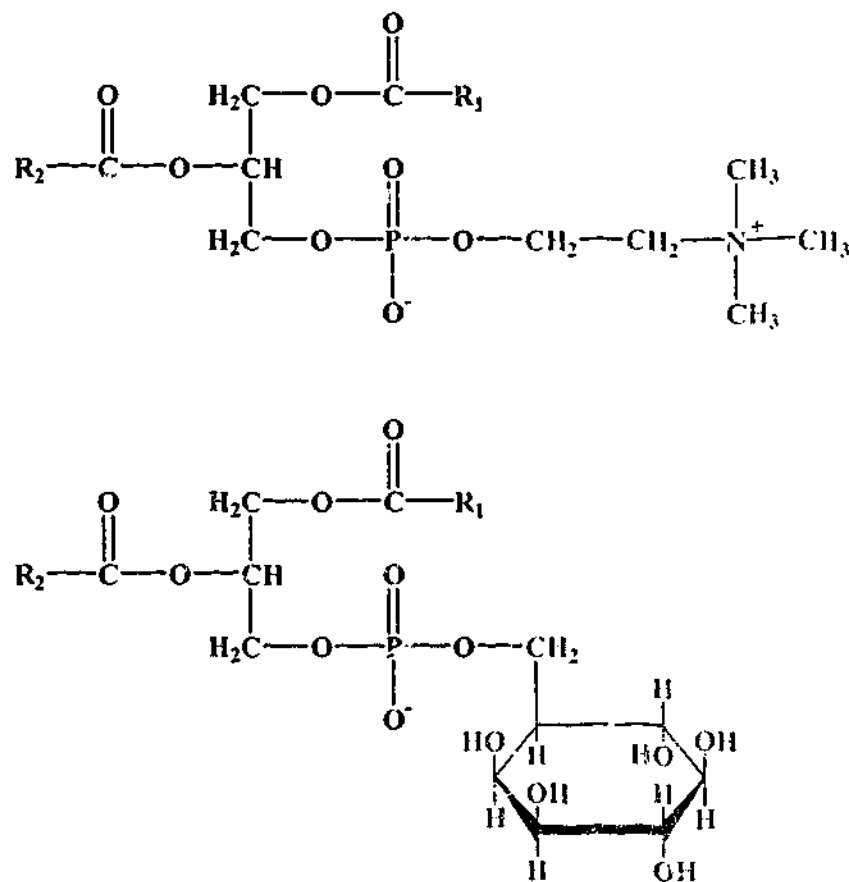


Figure 1.6 The phospholipids phosphatidylcholine (lecithin) (top) and phosphatidylinositol (bottom)⁷

The structure of phospholipase C isolated from the soil bacterium *Bacillus cereus* was reported by Hough *et al.* in 1989.²⁴ It showed the presence of three zinc ions in the active site, two tightly bound and the third bound more weakly (Figure 1.7).

ions are Zn1 – Zn2 3.3 Å, Zn2 – Zn3 6.0 Å and Zn2 – Zn3 4.3 Å. Zn1 is coordinated to His69, His118 and Asp55, and two ligands that bridge between Zn1 and Zn3, *viz.* a bidentate Asp122 and a water/hydroxide molecule. The Zn3 coordination sphere is completed by His14 and Trp1, which coordinates through both the terminal amino group and the carbonyl group from the side chain of the amino acid. Zn2 is bound to three amino acid residues, Glu146, His142, His128, as well as two water molecules (Figure 1.7).

In addition to the structure of native PLC, the structures of the native enzyme with various phosphate analogues have also been solved. The structure of the enzyme with bound phosphate was solved and the phosphate was found to bind to all three zinc ions, displacing the water bound to Zn2 and the water bridging between Zn1 and Zn3, with a phosphate oxygen bridging between the two metal centres (Figure 1.8).^{25,26}

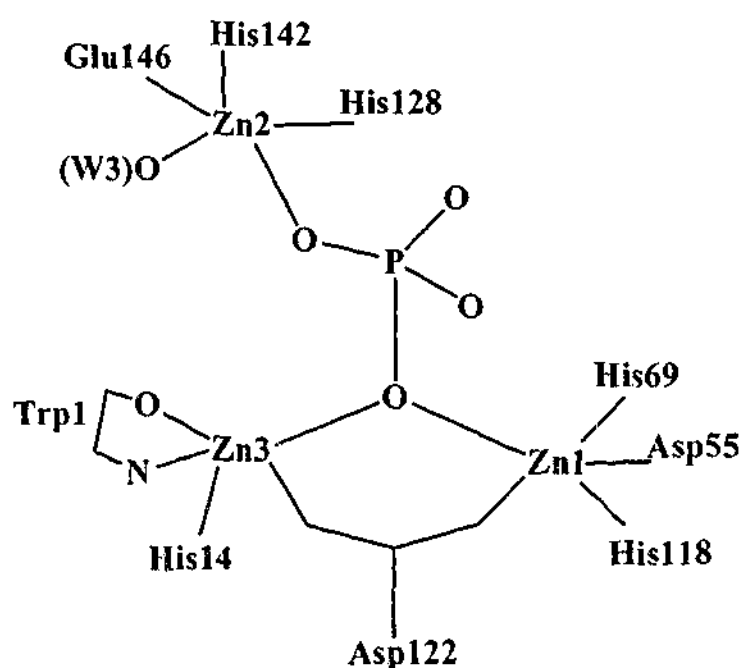


Figure 1.8 Structure of the active site of PLC with coordinated inorganic phosphate

1.3.5 Nuclease P1

Nuclease P1 is a phosphodiesterase that catalyses the hydrolysis of the bond between 3'-hydroxyl and the 5'-phosphate group in single stranded DNA and RNA, causing an inversion of stereochemistry at the phosphate group. The enzyme can then act as a phosphomonoesterase on the 3'-terminal phosphate group giving 5'-mononucleotides as the final cleavage products of single stranded DNA/RNA.

The structure of the enzyme, reported by Volbeda *et al.* in 1991, isolated from *Penicillium citrinum* shows a cluster of three zinc ions in the active site, with an arrangement very similar to that found in PLC.²⁷ The spatial arrangement of the three zinc ions can be described as consisting of a binuclear site, containing Zn1 and Zn3, and a single site containing Zn2. The distances between the zinc ions are 3.2 Å for Zn1 – Zn3, 5.8 Å for Zn1 – Zn2 and 4.7 Å for Zn2 – Zn3. The metal ions are in a trigonal bipyramidal coordination environment, with Zn1 and Zn3 bridged by a water/hydroxide, and a bidentate Asp120, while His116, His50 and Asp45 fill the coordination sphere of Zn1, and Trp1 and His6 complete the coordination geometry of Zn3. Zn2 is coordinated to two terminal water molecules as well as Asp153, His126 and His149. Each of the zinc centres is coordinated to two nitrogen and three oxygen donor atoms (Figure 1.9).

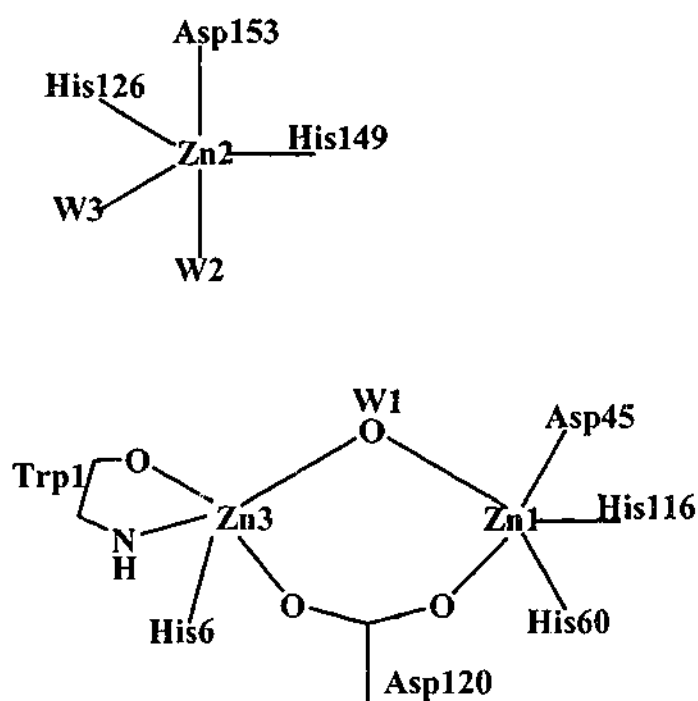


Figure 1.9 Crystal structure of the active site of Nuclease P1

Removal of the zinc ions from the enzyme causes a loss of catalytic activity, and when the zinc is returned to the enzyme, the activity is only partially restored. This suggested that the zinc ions play both a catalytic role as well as a structural role in the enzyme.²⁷

The phosphate binds to the active site by coordinating all three zinc ions in a similar manner to PLC (Section 1.3.4) and shows no phosphorylated intermediate.

1.4 The Role of Zinc(II) in Phosphatase Enzymes

Zinc(II) is a biologically essential ion and is the second most abundant transition metal, after iron, in biological systems.¹⁰ It can be seen from the preceding sections describing hydrolytic enzymes that zinc is present in the active sites of many hydrolytic enzymes, including phosphatase enzymes. The importance of zinc(II) over other divalent transition metal ions can be attributed to several important properties:¹⁰

-
- (i) Zinc can vary its coordination geometry by having the ability to form 4, 5 and 6-coordinate complexes.
 - (ii) Zinc can act as a Lewis acid.
 - (iii) Zinc binds strongly to suitable functional groups in the protein.
 - (iv) The rate of ligand exchange on zinc centres is fast.
 - (v) Zinc does not readily undergo oxidation or reduction (no generation of reactive radicals).
 - (vi) Zinc(II) centres facilitate the generation of nucleophiles under physiological conditions (i.e. at neutral pH), such as the formation of coordinated hydroxide to attack the electrophilic centre of the phosphate group.

Studies of Zn(II) active sites show that the Zn centres do not act alone in promoting the hydrolysis process. Functional groups such as carboxyl groups from Asp, imidazole from His or alcohol from Ser or Thr are located in close proximity to each other and the active site, and to act in concert with the zinc centres to promote the electrophilic reactions at the phosphate groups.²⁸ It has also been found in many cases that replacement of the zinc by another metal centre results in the loss of activity of the enzyme.¹⁴

1.5 Modelling of Phosphatases

An approach to the investigation of enzymes has been to develop low molecular weight model complexes in an attempt to reproduce the function, structure and/or reactivity of the active site. In principle, model complexes have the potential to provide valuable information about the enzyme which can be difficult to obtain through the direct study

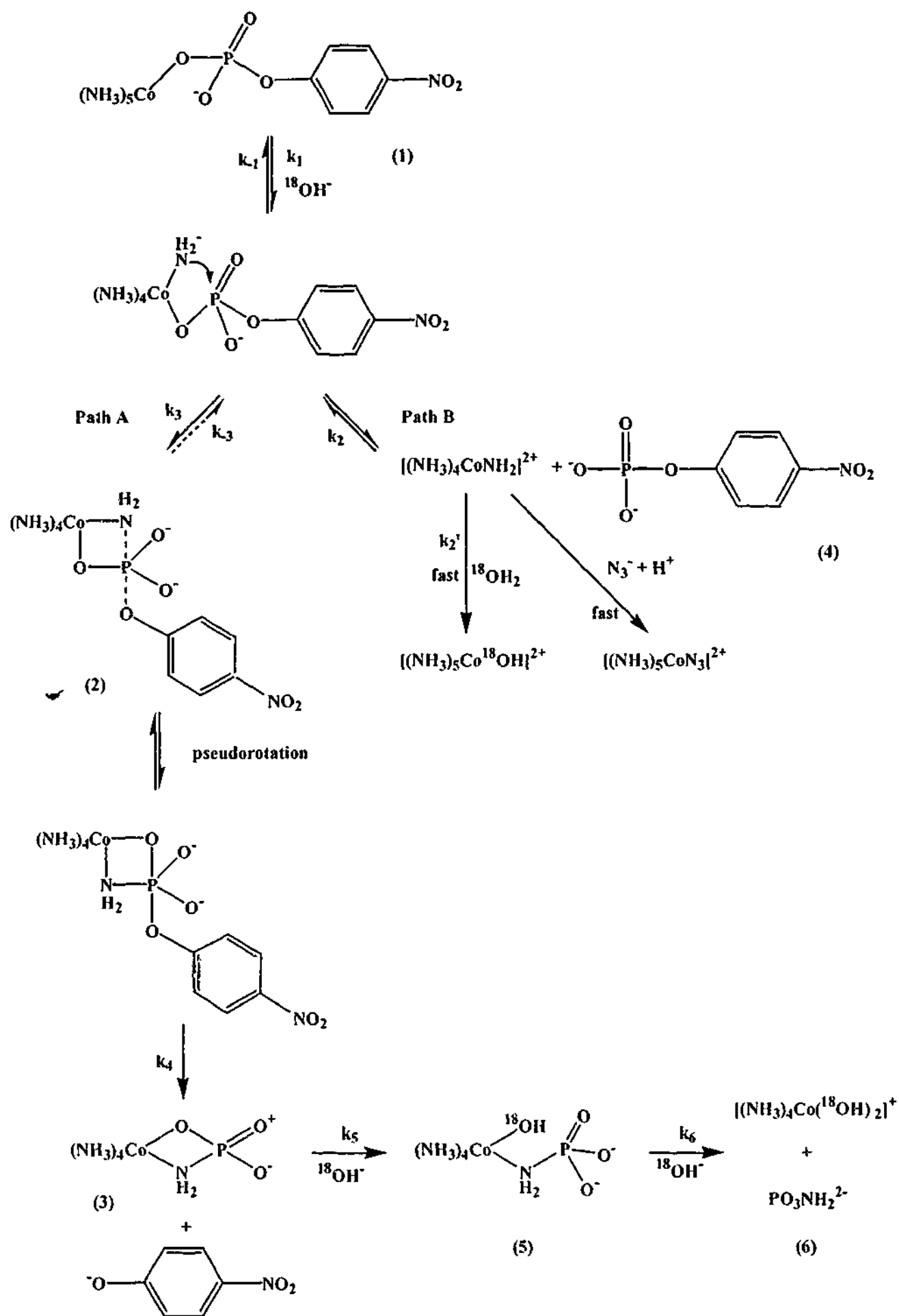
of the protein alone. Systematic variation of ligands and the coordination environment in these biological analogues has in the past provided a valuable insight into the structure and function of enzymes.

Many research groups are involved in the development of new complexes to mimic phosphatase enzymes. Ideally, the ligands designed to coordinate to metals to mimic the enzymes should exhibit some of the following properties: they should form stable and discrete complexes with the metal ions(s) at physiological pH, leave catalytic sites open on the metal centre for the binding of the substrate and offer similar structural and/or functional environments around the metal centre. Since many of these enzymes have been found to contain two or more coordinatively unsaturated metal centres in the active sites, the development of low molecular weight metal complexes which mimic the properties of these metalloenzymes has been a growing area of research over recent years. Some of these complexes simply bind phosphate groups, while others enhance the rate of hydrolysis of a phosphate ester bond. The models range from mononuclear to trinuclear, each with varying number of coordination sites available on the metal, and with a variety of metals, including lanthanides²⁹⁻³⁸ and d-block transition metals.³⁹⁻⁴² Some of the more recently developed models and their properties are discussed in the following sections. The discussion is mainly concerned with models which mimic the function of the enzyme, i.e. the cleavage of the phosphate ester bond.

1.5.1 Mononuclear Models

Sargeson and coworkers were one of the first groups to report a noteworthy enhancement in the rate of phosphate ester hydrolysis by metal complexes. Initially the group studied hydrolysis of nitrophenyl phosphate by a known cobalt(III) complex. The

first example, reported in 1980,⁴³ showed the production of the *p*-nitrophenylate ion, as well as the release of the *p*-nitrophenyl phosphate ligand from $[\text{Co}(\text{NH}_3)_5(\text{O}_3\text{POC}_6\text{H}_4\text{NO}_2)]^+$. Taking advantage of the kinetic inertness of cobalt(III), the workers were able to show that the hydrolysis of the coordinated ester by ammonia and NaOH is accelerated at least 10^8 times over that of the hydrolysis of the uncoordinated ester. The reaction pathway presented in Scheme 1.4 shows the production of both species.



Scheme 1.4 Reaction pathway for hydrolysis of a phosphate ester as presented by

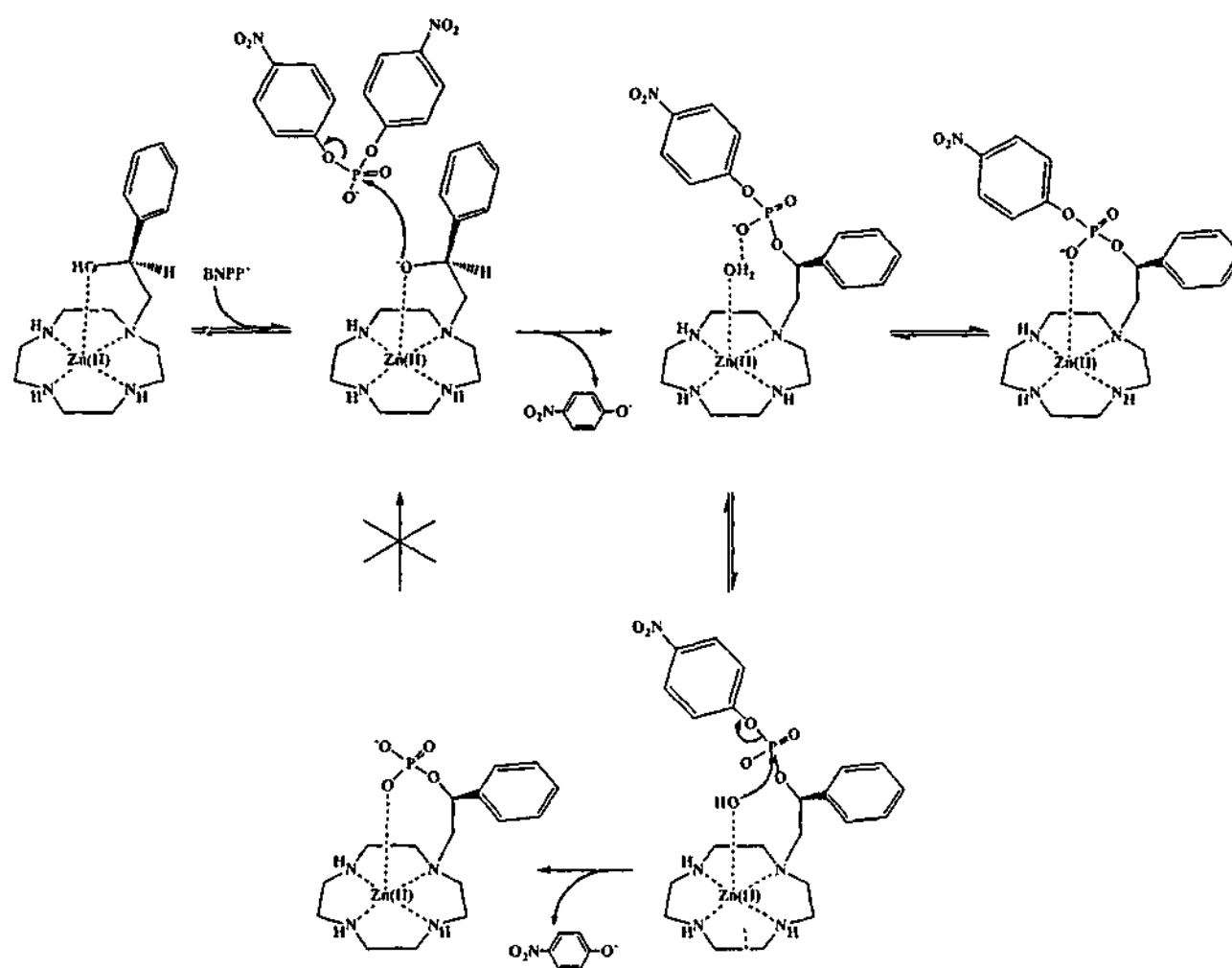
Sargeson and coworkers⁴³

The mechanism for the base hydrolysis of the initial complex accommodates the formation of a phosphoramidate complex (Path A) as well as the release of unreacted nitrophenyl phosphate (Path B). The formation of the phosphoramidate complex requires deprotonation of an ammonia in a *cis* position relative to the coordinated ester. The resulting aminophosphorane species (2) can undergo further reaction and eliminate nitrophenol presumably to give a chelated phosphoramidate ion (3). Path B shows the route for the production of nitrophenyl phosphate. This conjugated dissociative mechanism is frequently found in cobalt(III)ammine chemistry.⁴³ It is characterised by the formation of a presumed five-coordinate species which is able to compete for a variety of nucleophiles in aqueous solution. Two examples are shown in the scheme with the reaction with H₂O and N₃⁻. This conjugated base mechanism is also supported by the ¹⁸O tracer experiments reported by the Sargeson group.⁴³ The product of *p*-nitrophenyl phosphate from Path B (Scheme 1.4) shows no incorporation of ¹⁸O, eliminating the alternative mechanism where by ¹⁸OH⁻ adds to the phosphorus centre and decomposition of the resulting phosphorane leads to [(NH₃)₅CoOH]²⁺ as well as nitrophenyl phosphate. This process would involve the incorporation of ¹⁸O in the cleaved phosphate ester. The rate determining step (*k*₂) is presumed to involve rupture of the Co-O bond and is thought to occur at the same rate as the formation and decomposition of the aminophosphorane. This is indicated by the constant ratio of the nitrophenyl phosphate ion to nitrophenol over the range of OH⁻ concentrations studied by the group.

Several other papers have been published by the group regarding phosphate ester hydrolysis and describe hydrolysis of coordinated *p*-nitrophenyl phosphate in *cis*-[Co(en)₂(OH)O₃POC₆H₄NO₂]⁴⁴ with a rate enhancement of 10⁵ relative to that of the

uncoordinated ester, and also hydrolysis of a dimeric species, bis(μ -4-nitrophenylphosphato)bis[bis(1,2-ethylenediamine) cobalt(III)]²⁺ which also showed a rate enhancement of $\sim 10^5$.⁴⁵

In 1995, Kinura *et al.* reported the synthesis of a mononuclear zinc(II) complex to mimic the active site of alkaline phosphatase.⁴⁶ The zinc centre was coordinated to four nitrogens from a cyclen ring and an oxygen from a pendant phenolate group. This complex was found to mimic the two-step mechanism of phosphate ester hydrolysis performed by alkaline phosphatase. According to these workers, binding of the phosphodiester, bis(4-nitrophenyl)phosphate (BNPP) to the complex initially involved attack by the activated hydroxyl group (from the pendant phenolate arm) at the phosphorus and the formation of a phosphoryl intermediate. The second step involves the hydrolysis of the phosphoryl intermediate by the intramolecular Zn^{II}-OH⁻ moiety (Scheme 1.5). In the enzyme, this two step procedure is performed by the two different zinc centres, with one involved in the activation of Ser102 to produce the phosphoryl intermediate, and the other in the activation of a water molecule to attack the phosphoryl intermediate and cleave the phosphate group. This complex, however, was found to be totally unreactive towards the hydrolysis of the phosphomonoester that was formed in this reaction.



Scheme 1.5 Reaction mechanism of P-O bond cleavage of the phosphodiester proposed

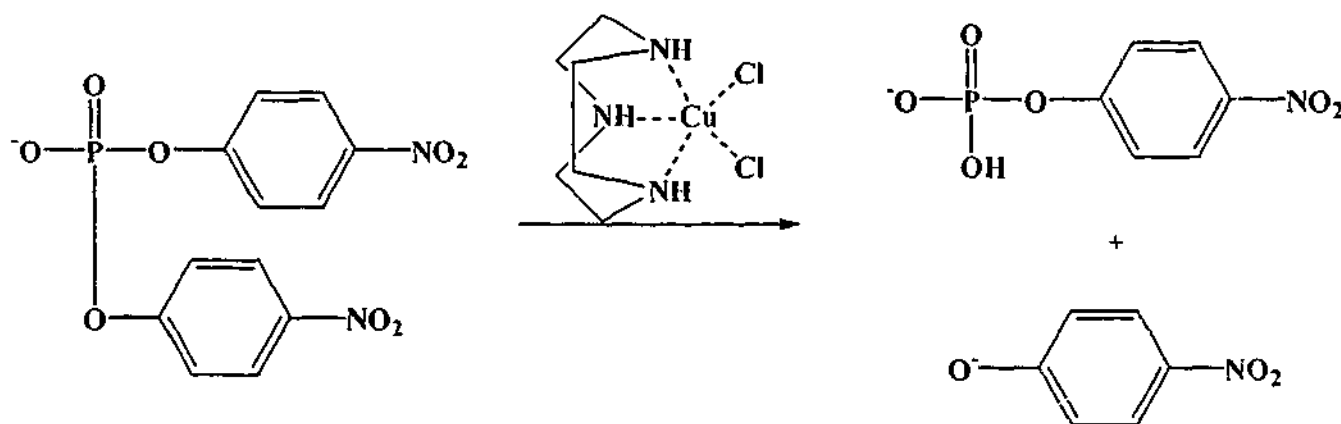
by Kimura *et al.*⁴⁶

Burstyn *et al.* have studied the ability of a mononuclear Cu(II) complex to hydrolyse a phosphate ester. The copper complex of 1,4,7-triazacyclononane, [Cu(tacn)Cl₂], was found to increase the rate of hydrolysis of a phosphodiester compared with the uncatalysed reaction by a 1000-fold (Scheme 1.6).⁴⁷ The complex was also found to be specific for the hydrolysis of the phosphodiester, with the hydrolysis of the monoester 50 times slower than that of the diester.⁴⁸ The first order rate constants for both the mono- and the diester are shown in Table 1.2.

Table 1.2 Observed first-order rate constants for the hydrolysis of phosphate esters by
[Cu(tacn)Cl₂]

Phosphate Ester	k_{obs} (s ⁻¹)
Bis(<i>p</i> -nitrophenyl) phosphate	1.3×10^{-6}
<i>p</i> -nitrophenyl phosphate	2.6×10^{-8}

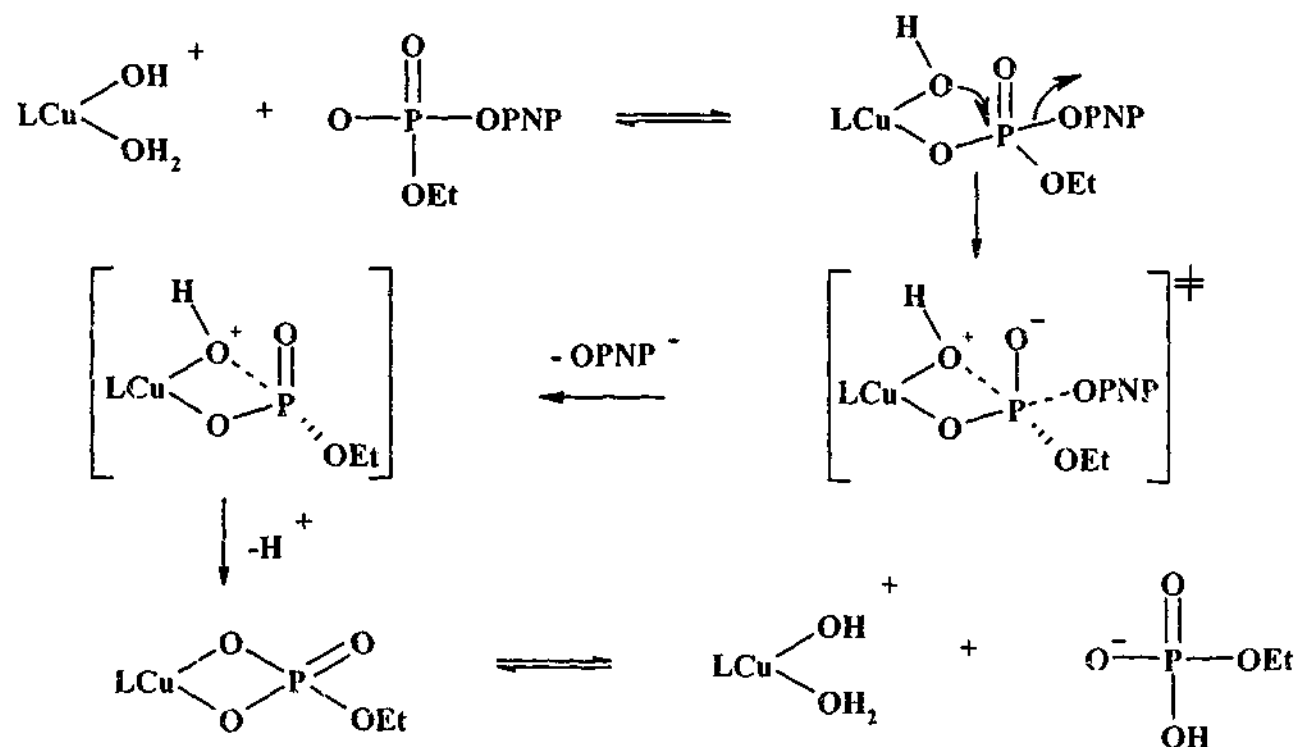
[†]Conditions: [Cu(tacn)Cl₂] = 1 mM; [Phosphate Ester] = 5 mM; pH 7.24, T = 50°C



Scheme 1.6 Hydrolysis of the phosphodiester by [Cu(tacn)Cl₂]

In 1996 Burstyn *et al.* proposed a mechanism for the hydrolysis, which is shown in Scheme 1.7.⁴⁹ Displacement of the chloride ligands by water followed by deprotonation gives the hydroxo aqua species shown. This catalytically active species binds the diester and a hydroxide attached to the same metal centre attacks the phosphate centre via an intramolecular nucleophilic attack, resulting in the departure of the leaving group through a concerted mechanism. Following this, rapid deprotonation gives a

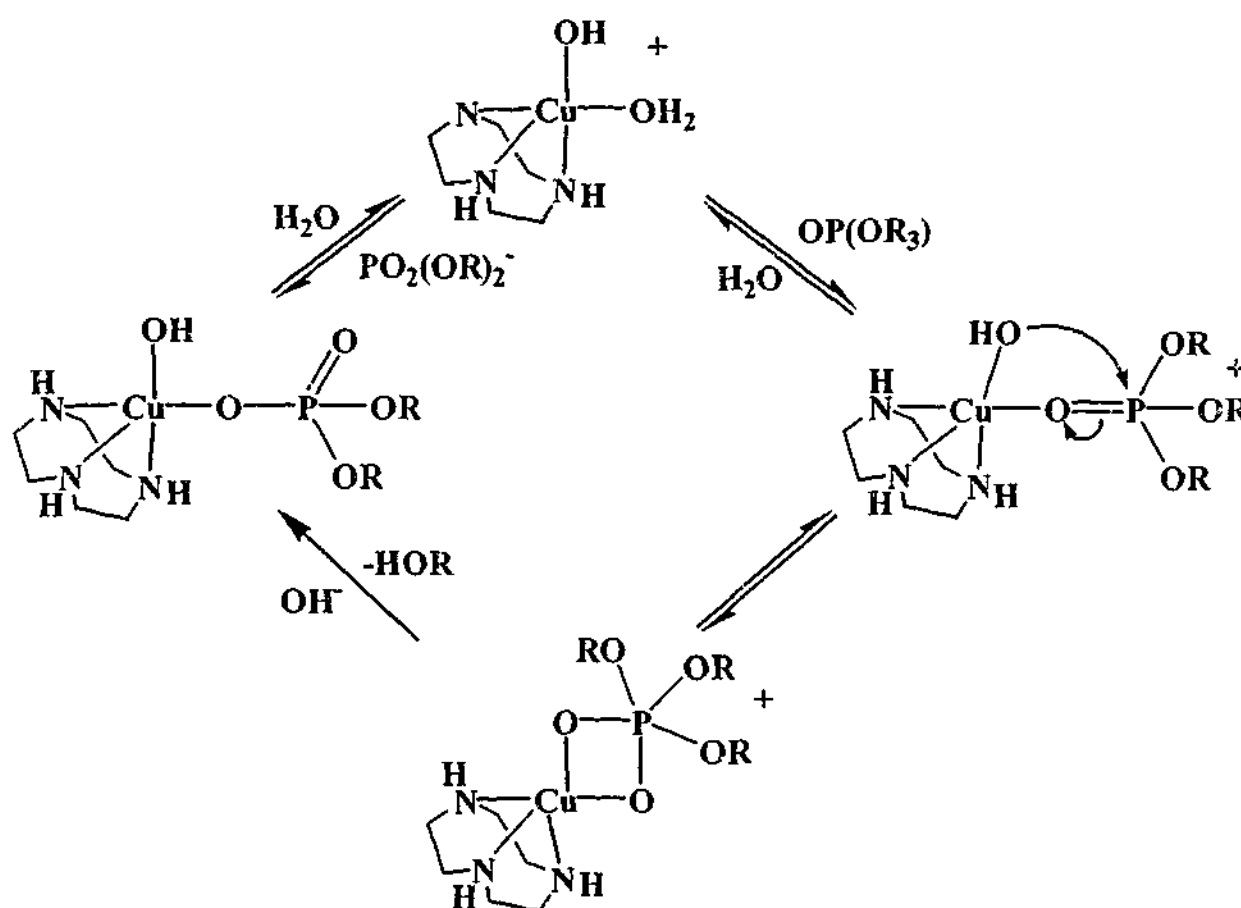
phosphomonoester complex which dissociates to the original complex and the phosphomonoester.



Scheme 1.7 Mechanism for the hydrolysis of a phosphodiester
by $[\text{Cu}(\text{tacn})\text{Cl}_2]^{49}$

The same year Burstyn and coworkers reported the ability of the complex to cleave both single and double stranded DNA. After incubation of DNA with the complex, the single stranded DNA was completely degraded, with many fragments detected, while the double stranded DNA was found to have only two cuts in the strand. The first cut degraded the supercoiled DNA (Form I) to the relaxed circular DNA (Form II) and the second cut produced linear the form (Form III).⁵⁰

Hay and Govan have reported a study of the kinetics of hydrolysis of the phosphate triester 2,4-dinitrophenyldiethylphosphate, by $[\text{Cu}(\text{tacn})\text{Cl}_2]$,⁵¹ together with experiments to show that the complex was able to catalyse the hydrolysis. Rates of 2.2 turnovers per hour could be achieved at 25°C when the ester was in a 15-fold excess. An explanation was offered for the high catalytic activity of the tacn complex and other copper(II) hydroxoquo complexes. Firstly, the value of k_{cat}/α for the complex was about 40 times greater than that of the hydroxide ion. Since the free hydroxide ion is greater than 10^6 times a stronger base than when it is bound to a metal centre, the possibility that the complex was acting simply as a base catalyst was discounted. Previous accounts^{52,53} showed that all the reactions appeared to involve intramolecular attack of the coordinated hydroxide to give a phosphorane intermediate (Scheme 1.8), which then decays to the products. A mechanism in which the metal ion polarises the P=O bond by its Lewis acid effect, and also delivers a coordinated hydroxide in an intramolecular reaction, is the most likely explanation for the efficiency of the complex to hydrolyse the phosphate ester bond.



Scheme 1.8 Mechanism involving a phosphorane intermediate
as presented by Hay and coworkers⁵¹

A recently reported compound⁵⁴ has been studied for the ability to hydrolyse the phosphate diester BNPP. Deal *et al.*⁵⁵ have reported the copper(II) complex of *N,N',N''*-trimethyl-*cis-cis*-1,3,5-triaminocyclohexane ($\text{Cu}(\text{tach-Me}_3)^{2+}$) (Figure 1.10) selectively cleaves BNPP, with the hydrolysis of the monoester being 1000 times slower. The observed first order rate constants are shown in Table 1.3.

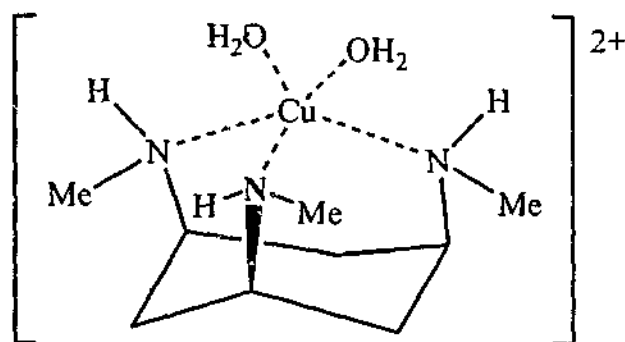


Figure 1.10 Copper(II) *N,N',N''*-trimethyl-*cis-cis*-1,3,5-triaminocyclohexane

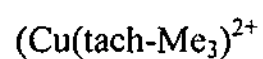
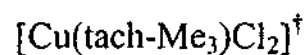


Table 1.3 Observed first-order rate constants for the hydrolysis of phosphate esters by



Phosphate Ester	$k_{\text{obs}} (\text{s}^{-1})^\ddagger$
Bis(<i>p</i> -nitrophenyl) phosphate	$(1.12 \pm 0.02) \times 10^{-5}$
<i>p</i> -Nitrophenyl phosphate	$(1.12 \pm 0.06) \times 10^{-8}$

[†]Conditions: $[\text{Cu}(\text{tach-Me}_3)\text{Cl}_2] = 1 \text{ mM}$; $[\text{Phosphate Ester}] = 5 \text{ mM}$; pH 7.2; $T = 50^\circ\text{C}$

[‡] $k_{\text{obs}} = \text{initial rate}/[\text{phosphate ester}]$

The group have postulated a binuclear intermediate, with the phosphate ester bridging between two Cu(II) centres in one of the three ways shown in Figure 1.11. Further study of the mechanistic features as well as potential biological applications of this complex are still underway.

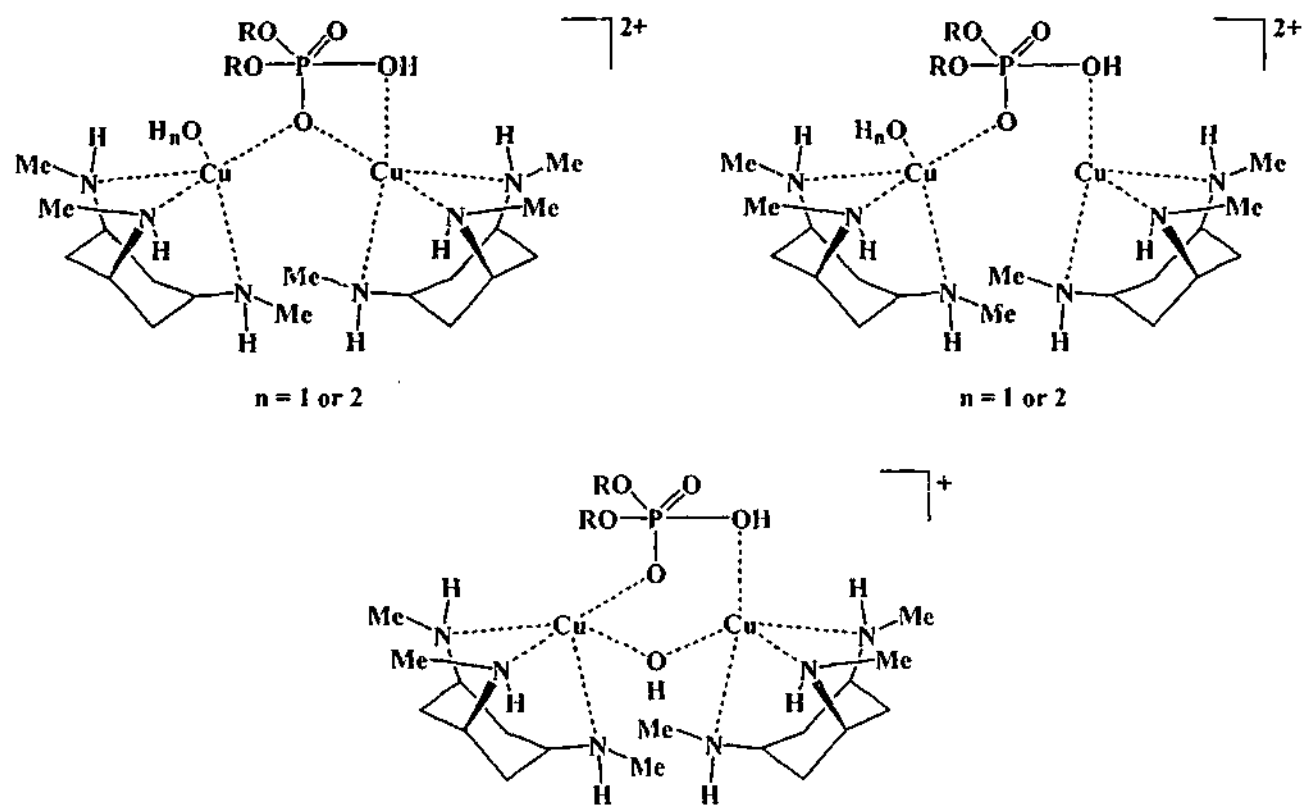


Figure 1.11 Postulated structures of the intermediate for phosphate ester hydrolysis by $[\text{Cu}(\text{tach})\text{Cl}_2]^{55}$

1.5.2 Binuclear Models

Young *et al.* have investigated the ability of the copper(II) complex of a naphthalene bridged bis(1,4,7-triazacyclononane) (Figure 1.12) to hydrolyse phosphate esters.⁵⁶

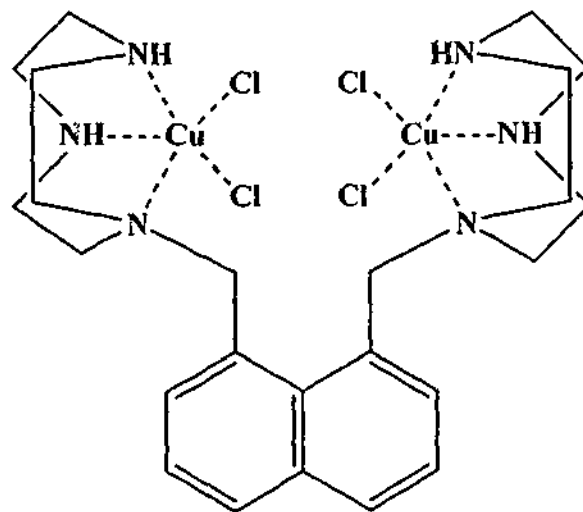
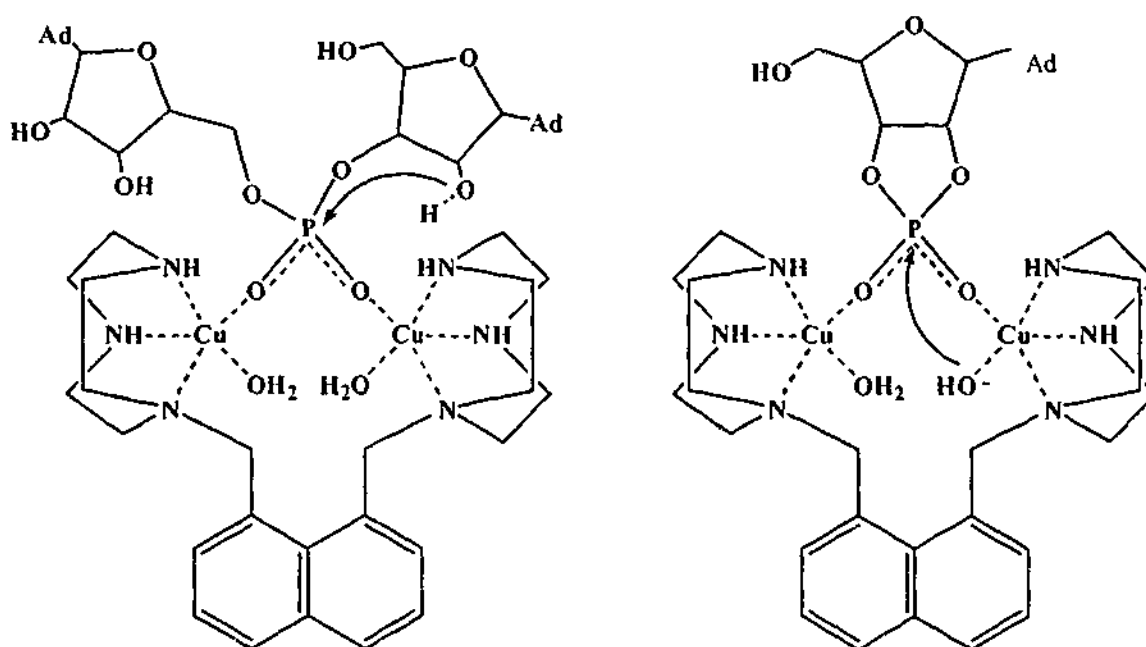


Figure 1.12 Binuclear copper complex with naphthalene bridged bis(tacn)

The complex efficiently hydrolyses ApA to adenosine, 2'-AMP and 3'-AMP, as well as cleavage of 2',3'-cAMP to 2'-AMP and 3'-AMP. It represents the first simple binuclear complex whose metal centres act in concert to cleave the phosphate diester bonds in RNA and 2', 3'-cAMP. Young *et al.*⁵⁶ proposed the mechanism for the cleavage of the phosphate ester bond involving the bridging of the phosphate esters between the two metal centres (Scheme 1.9). These workers also report that the complex cleaves ApA and 2',3'-cAMP at 300-500 times the rate of [Cu(tacn)Cl₂] (see Section 1.5.1).



Scheme 1.9 Mechanism of phosphate ester bond cleavage as proposed by Young *et al.*⁵⁶

In 1997, Lui *et al.*⁵⁷ reported a detailed study of the rate of transesterification of cyclic diribonucleotides (Scheme 1.10) by complexes 1-4 (Figure 1.13) and compared the rate of mononuclear complexes with closely related binuclear complexes.

Complex 1 showed 500 times more activity than complex 3 in the hydrolysis of the adenine derivative of the diribonucleotide. Although not as remarkable, complex 2 shows 35 times more activity than complex 3, and 22 times more than 4. This study clearly demonstrates that two Cu(II) ions (as in 1 and 2) can have highly cooperative effects in promoting the hydrolysis of the cyclic diribonucleotides.

1.5.3 Trinuclear Models

In 1997, Yashiro and coworkers⁵⁸ reported a trinuclear zinc complex which efficiently hydrolysed various diribonucleotides at pH 7 and 50°C. The complex consisted of a tris(2-aminoethyl)amine (tren) backbone with each of the secondary amines functionalised with two pyridine moieties (Figure 1.14). The complex was not isolated, however the ¹H NMR spectrum of the complex and Zn(NO₃)₂ in a 1:3 ratio showed a simple spectrum, indicating that the three di(pyridylmethyl)amine binding sites are equivalent and that three zinc ions had in fact bound to the ligand.

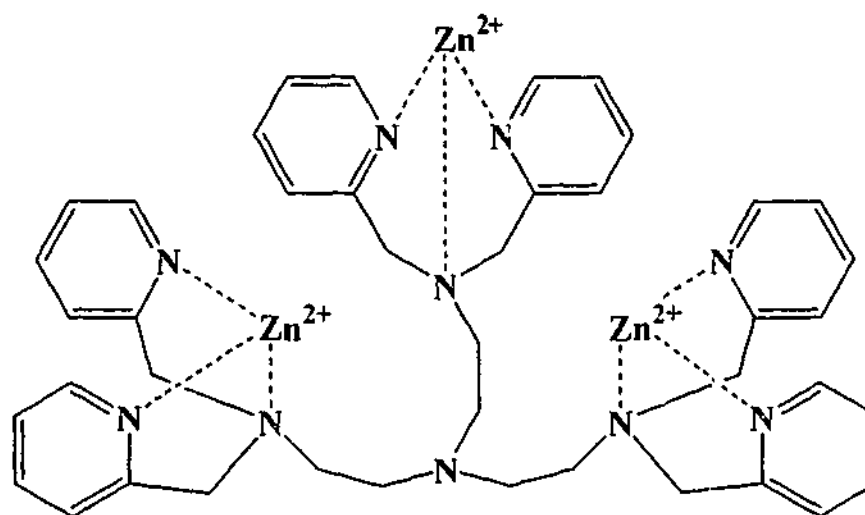


Figure 1.14 Proposed coordination of the trinucleating ligand.

Additional coordination sites on Zn²⁺ were not specified⁵⁸

The complex showed much greater activity than the analogous binuclear complex illustrated in Figure 1.15. The complex selectively hydrolyses the diribonucleotide to produce 3'-NMP over the other possible cleavage product of 2'-NMP. For the diribonucleotides CpA, ApA, GpA and CpA (Figure 1.16), the ratio of 3'-NMP : 2'-NMP is greater than 90%. These results were concluded to be highly significant since the selectivity shown by the binuclear complex was low.

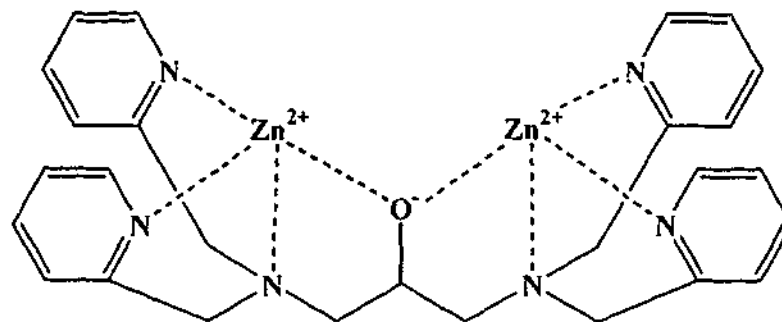


Figure 1.15 Binuclear analogue of Yashiro's trinuclear complex⁵⁸

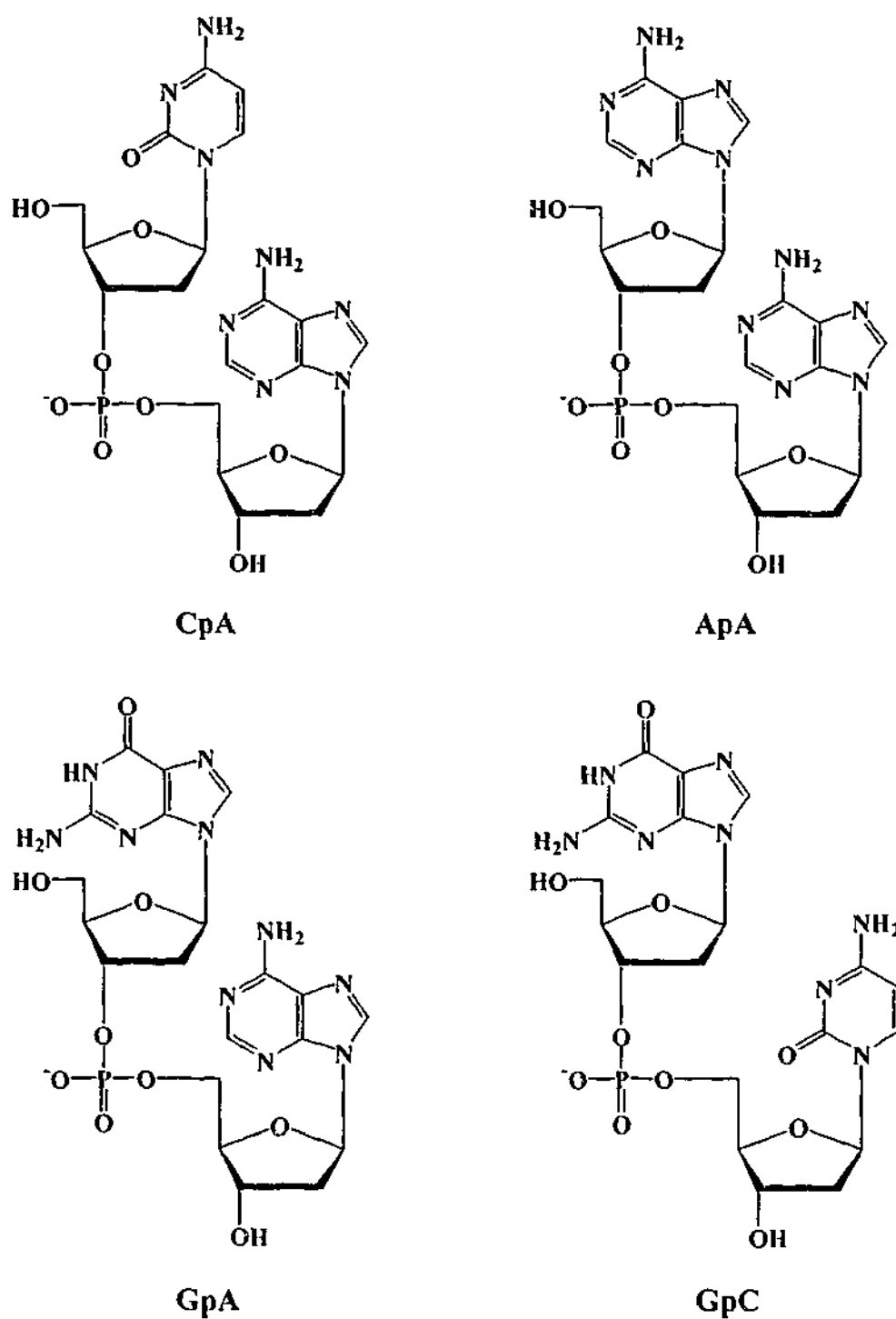


Figure 1.16 Diribonucleotides used in Yashiro's study

Another interesting trinuclear complex has been reported by Spiccia and coworkers in 1997.⁵⁹ The formation of the complex was facilitated through the use of a trinucleating ligand containing three tacn moieties linked together by 1,3,5-trimethylbenzene. The complex consisted of trinuclear copper(II) units which are connected by a bridging phosphate group thereby generating a polymeric chain (Figure 1.17). In the complex,

the Cu^{III}-Cu distances are inequivalent, viz. 3.56 Å, 4.56 Å and 5.47 Å, as is the case for active sites of several enzymes exhibiting trinuclear metal active sites. Thus, the complex is a good model for the zinc enzymes phospholipase C, phosphate modified phospholipase C and P1 nuclease.

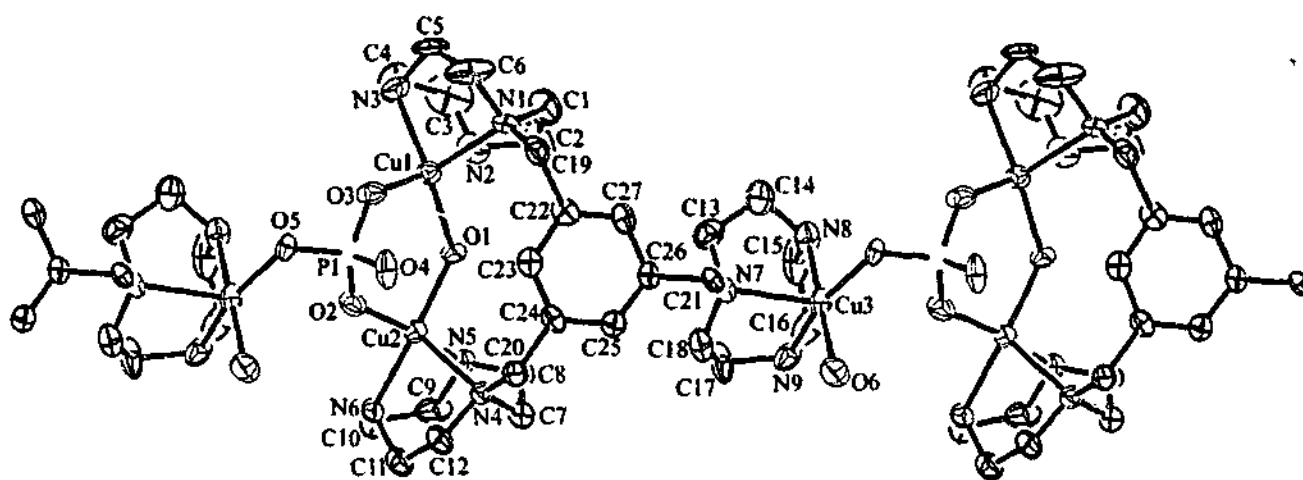


Figure 1.17 Crystal structure of the trinuclear complex with bound phosphate, $\{[\text{Cu}_3\text{L}(\mu\text{-OH})(\mu_3\text{-HPO}_4)][\text{PF}_4]_3 \cdot 3\text{H}_2\text{O}\}_n$ synthesised by Spiccia and coworkers⁵⁹

Kimura *et al.*⁶⁰ reported the synthesis of a 1:3 phosphate to zinc complex. The complex consisted of three [Zn (1,4,7,10-tetraazacyclododecane)] ([Zn(cyclen)]) units linked by the phosphate oxygens from a nitrophenyl phosphate (Figure 1.18).

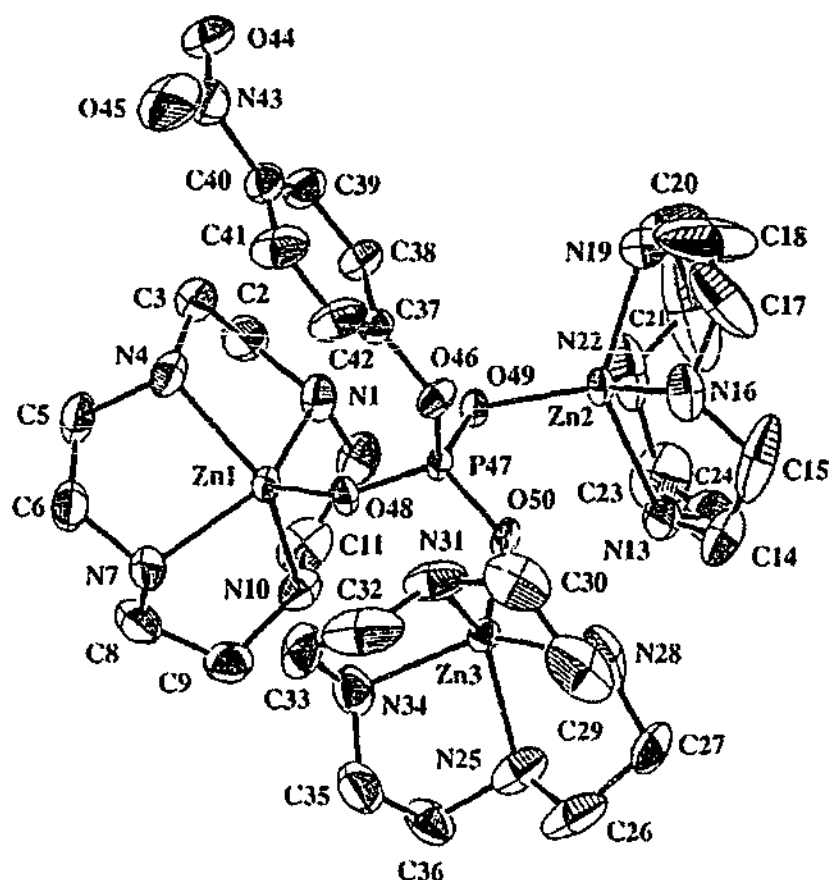


Figure 1.18 Trinuclear zinc(II) – NPP^{2-} complex⁶⁰

This result led Kimura and coworkers⁶⁰ to prepare a trinuclear zinc(II) complex, consisting of three [Zn (cyclen)] units linked by 1,3,5-trimethylbenzene group (Figure 1.19). ^{31}P NMR titration experiments provided evidence that the complex formed a 1:1 complex with the phenylphosphate dianion (PP^{2-}). Potentiometric pH titrations were conducted to determine the affinity constant of the complex with various phosphates in a ratio of 1:1. The results of this experiment show that the trinuclear zinc species has an affinity constant of about 300 times greater than that of the mononuclear cyclen species, and about 60 times greater than that for the binuclear zinc complex of cyclen linked by a *m*-xylene bridge. The high affinity constants of the 1:1 species were attributed to the cooperative effect of all three zinc ions.

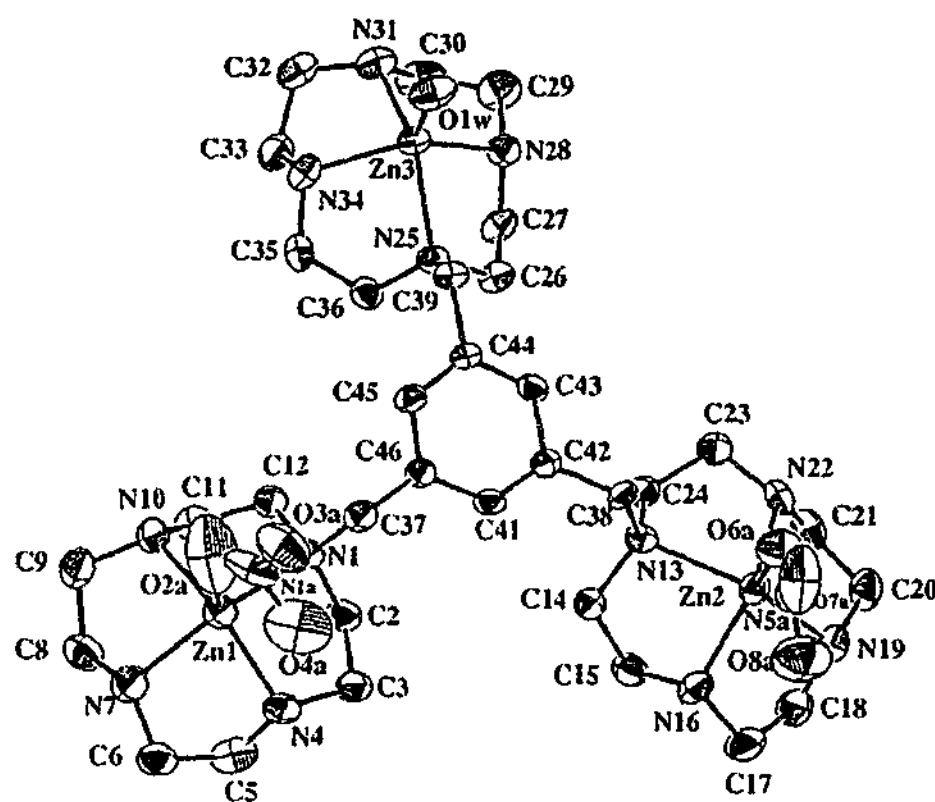


Figure 1.19 Kimura's trinuclear Zn(II) cyclen complex⁶⁰

1.6 The Present Study

Previous studies, some of which have been detailed in the preceding sections, have demonstrated that positive contributions for the understanding of the behaviour and function of phosphatase enzymes can be made through the use of low molecular weight mimics. One important finding to emerge from these studies is that the rate of hydrolysis of phosphate ester bond increases as the number of metal centres in the model compound increases. The objective of the work reported in this thesis was to further explore some of these findings through the study of a variety of metal complexes.

The aim of this research project was, therefore, to:

- design a variety of ligands able to complex a number of metal centres. This was achieved by linking two or three tacn rings together by various linker groups.
- complex these ligands with copper(II), nickel(II) and zinc(II) and study their physicochemical properties.
- test these complexes for their ability to promote the hydrolysis of phosphate esters.

1.7 References

- (1) Radzicka, A., Wolfenden, R. *Science* **1995**, *267*, 90.
- (2) Wilkins, P. C., Wilkins, R. G. *Inorganic Chemistry in Biology*; Oxford University Press: New York, 1997.
- (3) Fenton, D. E. *Biocoordination Chemistry*; Oxford University Press: New York, 1995.
- (4) Mathews, C. K., Van Holde, K. E., Ahern, K. G. *Biochemistry*; Third ed.; Addison Wesley Longman, 2000.
- (5) Pilato, R. S., Stiefel, E. I. In *Bioinorganic Catalysis*; Second ed.; Reedijk, J., Bouwman, E., Ed.; Marcel Dekker: New York, 1999.
- (6) Lippard, S. J., Berg, J. M. *Principals of Bioinorganic Chemistry*; University Science Books: Mill Valley, 1994.
- (7) Voet, D., Voet, J. G., Pratt, C. W. *Fundamentals of Biochemistry*; John Wiley & Sons: New York, 1999.
- (8) Gani, D., Wilkie, J. *Structure and Bonding* **1997**, *89*, 133.
- (9) Kim, E. E., Wyckoff, H. W. *J. Mol. Biol.* **1991**, *218*, 449.
- (10) Lipscomb, W. N., Strater, N. *Chem. Rev.* **1996**, *96*, 2375.
- (11) Holtz, K. M., Krantowitz, E. R. *FEBS Letters* **1999**, *462*, 7.
- (12) Strater, N., Klabunde, T., Tucker, P., Witzel, H., Krebs, B. *Science* **1995**, 1489.
- (13) Klabunde, T., Strater, N., Krebs, B., Witzel, H. *FEBS Letters* **1995**, *367*, 56.
- (14) Strater, N., Lipscomb, W. N., Klabunde, T., Krebs, B. *Angew. Chem. Int. Ed. Eng.* **1996**, *35*, 2024.
- (15) Klabunde, T., Strater, N., Frohlich, R., Witzel, H., Krebs, B. *J. Mol. Biol.* **1996**, *259*, 737.
- (16) Zhang, Z.-Y. *Crit. Rev. Biochem. Mol. Biol.* **1998**, *33*, 1.

-
- (17) Barford, D. *TIBS* **1996**, *21*, 407.
- (18) Faux, M. C., Scott, J. D. *TIBS* **1996**, *21*, 312.
- (19) Vincent, J. B., Crowder, M. W. *Phosphatases in Cell Metabolism and Signal Transduction: Structure, Function and Mechanism of Action*; R.G. Landes: Austin, 1995.
- (20) Goldberg, J., Huang, H-B., Kwon, Y-G., Greengard, P., Nairn, A. C., Kuriyan, J. *Nature* **1995**, *376*, 745.
- (21) Egloff, M.-P., Cohen, P. T. W., Reinemer, P., Barford, D. *J. Mol. Biol.* **1995**, *254*, 942.
- (22) Yu, L., Haddy, A., Rusnak, F. *J. Am. Chem. Soc.* **1995**, *117*, 10147.
- (23) Kissinger, C. R., Parge, H. E., Knighton, D. R., Lewis, C. T., Pelletier, L. A., Tenpczyk, A., Kalish, V. J., Tucker, K. D., Showalter, R. E., Moomaw, E. W., Gastinel, L. N., Habuka, N., Chen, X., Maldonado, F., Barker, J. E., Bacquet, R., Villafranca, J. E. *Nature* **1995**, *378*, 641.
- (24) Hough, E., Hansen, L. K., Birknes, B., Jynge, K., Hansen, S., Hordvik, A., Little, C., Dodson, E., Derewenda, Z. *Nature* **1989**, *338*, 357.
- (25) Hansen, S., Hough, E., Svensson, L. A., Wong, Y-L., Martin, S. F. *J. Mol. Biol.* **1993**, *234*, 179.
- (26) Hansen, S., Hansen, L. K., Hough, E. *J. Mol. Biol.* **1992**, *225*, 543.
- (27) Volbeda, A., Lahm, A., Sakiyama, F., Such, D. *The EMBO Journal* **1991**, *10*, 1607.
- (28) Kimura, E. *Prog. Inorg. Chem* **1991**, 443.
- (29) Irisawa, M., Takeda, N., Komiyama, M. *J. Chem. Soc., Chem. Commun.* **1995**, 1221.
- (30) Chin, K. O. A., Morrow, J. R. *Inorg. Chem.* **1994**, *33*, 5036.

-
- (31) Haner, R., Hall, J. *Helv. Chim. Acta* **1997**, *80*, 487.
- (32) Oh, S. J., Song, K. H., Whang, D., Kim, K., Yoon, T. H., Moon, H., Park, J. W. *Inorg. Chem.* **1996**, *35*, 3780.
- (33) Takeda, N., Irisawa, M., Komiyama, M. *J. Chem. Soc., Chem. Commun.* **1994**, 2773.
- (34) Hettich, R., Schneider, H.-J. *J. Chem. Soc., Perkin Trans.* **1997**, 2069.
- (35) Jurek, P. E., Jurek, A. M., Martelli, A. E. *Inorg. Chem.* **2000**, *39*, 1016.
- (36) Miyama, S., Asanuma, H., Komiyama, M. *J. Chem. Soc., Perkins Trans. 2* **1997**, 1685.
- (37) Ragunathan, K. G., Schneider, H.-J. *Angew. Chem. Int. Ed. Engl.* **1996**, *35*, 1219.
- (38) Gómez-Tagle, P., Yatsimirsky, A. K. *J. Chem. Soc., Dalton Trans.* **2001**, 2663.
- (39) Silver, G. C., Trogler, W. C. *J. Am. Chem. Soc.* **1995**, *117*, 3983.
- (40) Itoh, T., Hisada, H., Sumiya, T., Masono, M., Usui, Y., Fujii, Y. *Chem. Commun.* **1997**, 677.
- (41) Yan, S., Pan, X., Taylor, L. F., Zhang, J. H., O'Connor, C. J., Britton, D., Anderson, O. P., Que, L. *Inorg. Chim. Acta* **1996**, *243*, 1.
- (42) Srivatsan, S. G., Verma, S. *Chem. Commun.* **2000**, 515.
- (43) Harrowfield, J. M., Jones, D. R., Lindoy, L. F., Sargeson, A. M. *J. Am. Chem. Soc.* **1980**, *102*, 7733.
- (44) Jones, D. R., Lindoy, L. F., Sargeson, A. M. *J. Am. Chem. Soc.* **1983**, *105*, 7327.
- (45) Jones, D. R., Lindoy, L. F., Sargeson, A. M. *J. Am. Chem. Soc.* **1984**, *106*, 7807.
- (46) Kimura, E., Kodama, Y., Koike, T., Shiro, M. *J. Am. Chem. Soc.* **1995**, *117*, 8304.
- (47) Burstyn, J., Deal, K. *Inorg. Chem.* **1993**, *32*, 3585.
- (48) Deal, K., Burstyn, J. *Inorg. Chem.* **1996**, *35*, 2792.

-
- (49) Deal, K., Hengge, A. C., Burstyn, J. N. *J. Am. Chem. Soc.* **1996**, *118*, 1713.
- (50) Hegg, E. L., Burstyn, J. N. *Inorg. Chem.* **1996**, *35*, 7474.
- (51) Hay, R. W., Govan, N. *Polyhedron* **1998**, *17*, 463.
- (52) Morrow, J., Trogler, W. C. *Inorg. Chem.* **1989**, *28*, 2330.
- (53) Gellman, S. H., Petter, R., Breslow, R. *J. Am. Chem. Soc.* **1986**, *108*, 2388.
- (54) Park, G., Shao, J., Lu, F. H., Rogers, R. D., Chasteen, N. D., Brechbiel, M. W., Planalp, R. P. *Inorg. Chem.* **2001**, *40*, 4167.
- (55) Deal, K. A., Park, G., Shao, J., Chasteen, N. D., Brechbiel, M. W., Planalp, R. P. *Inorg. Chem.* **2001**, *40*, 4176.
- (56) Young, M. J., Chin, J. *J. Am. Chem. Soc.* **1995**, *117*, 10577.
- (57) Lui, S., Luo, Z., Hamilton, A. D. *Angew. Chem. Int. Ed. Engl.* **1997**, *36*, 2678.
- (58) Yashiro, M., Ishikubo, A., Komiyama, M. *Chem. Commun.* **1997**, 83.
- (59) Spiccia, L., Graham, B., Hearn, M. T. W., Lazarev, G., Moubaraki, B., Murray, K. S., Tiekink, E. R. T. *J. Chem. Soc., Dalton Trans.* **1997**, 4089.
- (60) Kimura, E., Aoki, S., Koike, T., Shiro, M. *J. Am. Chem. Soc.* **1997**, *119*, 3068.

Chapter Two

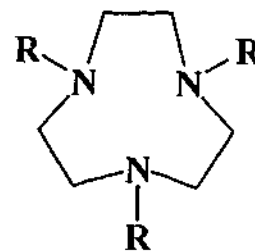
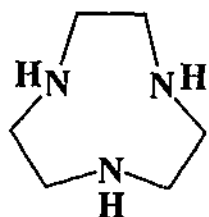
Synthesis of Ligands

2.1 Introduction

Ligands binding two or more metals are of interest in the modelling of phosphatase active sites since many such enzymes contain two or more metal centres at the active site. The metal ions generally coordinate to nitrogen atoms (*e.g.* from the imidazole ring in histidine) and oxygen donor atoms (*e.g.* from carboxylate in aspartate and glutamate residues). In general, the design of ligands for use in the development of mimics for phosphatases has been concentrated on nitrogen donors, but in some cases, oxygen donors have been introduced. The ligands of choice bind strongly to the metal centres but also allow for the presence of weakly coordinating ligands, which can be displaced by a substrate (in this case phosphate esters of various types) and for ligands which can be deprotonated to generate coordinated nucleophiles which can intramolecularly attack the coordinated substrate.

The facially coordinating 1,4,7-triazacyclononane (tacn) macrocycle was chosen as the building block for the development of a series of ligands since it has the ability to bind strongly to metal ions, and also fulfils the requirements for substrate coordination and for the generation of a suitable nucleophile for attacking the substrate. Previous studies on tacn derivatives have focussed mainly on mononuclear¹⁻⁵ and binuclear complexes^{6,7} and only very recently has attention been devoted to tri- and tetranuclear complexes.^{8,9} It should be noted, however, that other acyclic and macrocyclic ligands have also found application in this field.¹⁰

The synthesis of the tacn macrocycle was first reported by Koyama *et al.* in 1972.¹¹ Since then numerous examples of tacn derivatised with pendant arms have appeared in the literature. Figure 2.1 shows a selection of such ligands.



R =	Reference
	12
	13
	14
	15
	16, 17
	18
	19

Figure 2.1 Tacn and a selection of derivatised tacn ligands

The first bis(tacn) ligand was reported by Takamoto *et al.*²⁰ in 1977 and consisted of two tacn moieties linked by an ethane bridge. The binucleating potential of the ligand was not recognised at the time and only a sandwich-type structure was reported. Subsequently, Wieghardt *et al.*²¹ reported a number of binuclear complexes incorporating the bis(tacn) unit, and since this time a variety of bis(tacn) ligands have been prepared, with bridges that include polymethylene,²¹⁻²⁴ propanol,²⁵ xylene,^{7,26} naphthalene,²⁷ phenol²⁸ pyrazole²⁹ and ether.³⁰

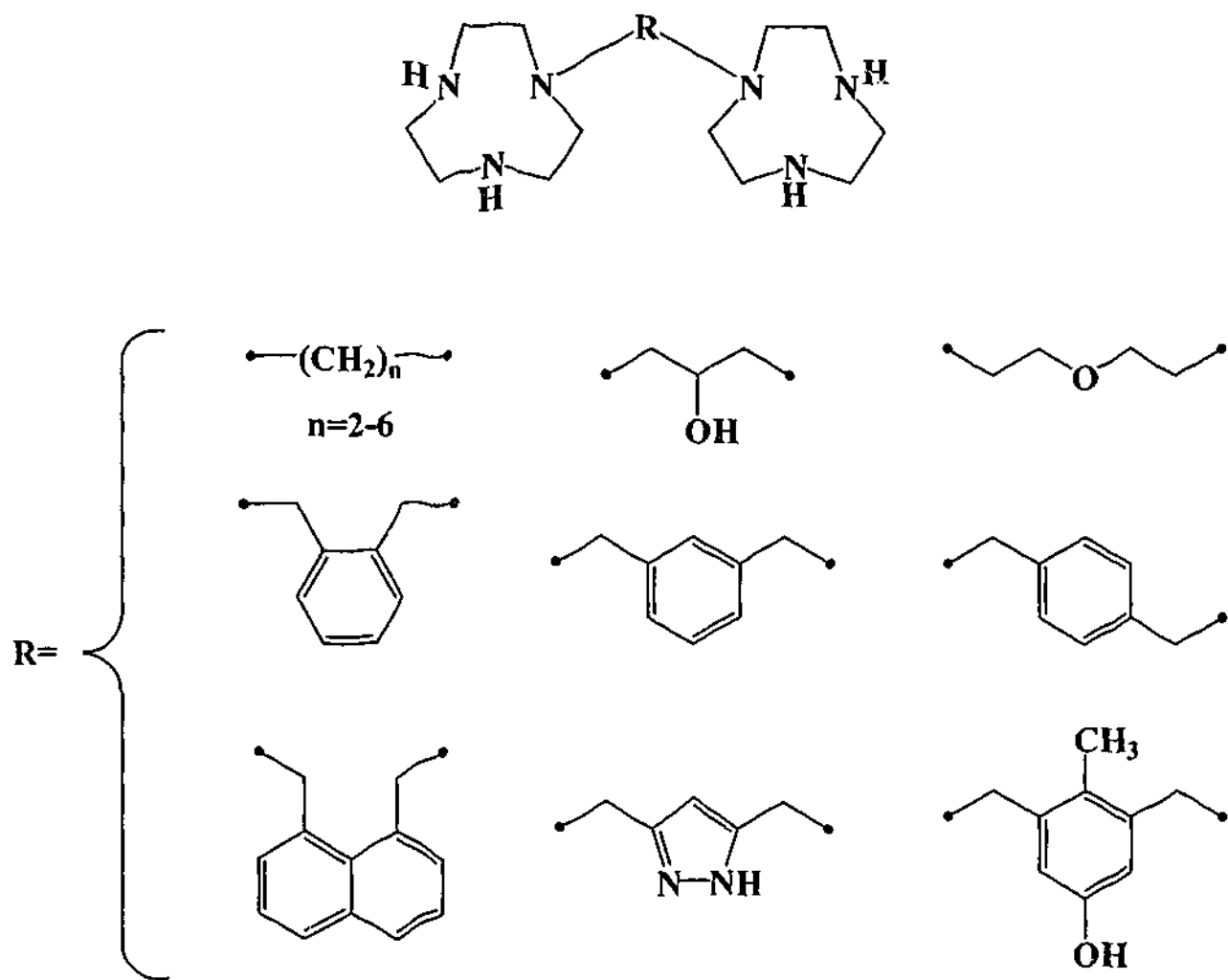


Figure 2.2 Previously reported bis(tacn) ligands

Several bis(tacn) ligands have been further functionalised by the addition of pendant arms, at each of the secondary nitrogens in the macrocyclic ring. The pendant arms may either be non-coordinating, such as methyl,^{31,32} isopropyl,³³ or they may be coordinating, such as pyridylmethyl,³⁴ alcohols,³⁵ carboxylate,³⁶ methylimidazole³⁷ or aminopropyl.³⁸

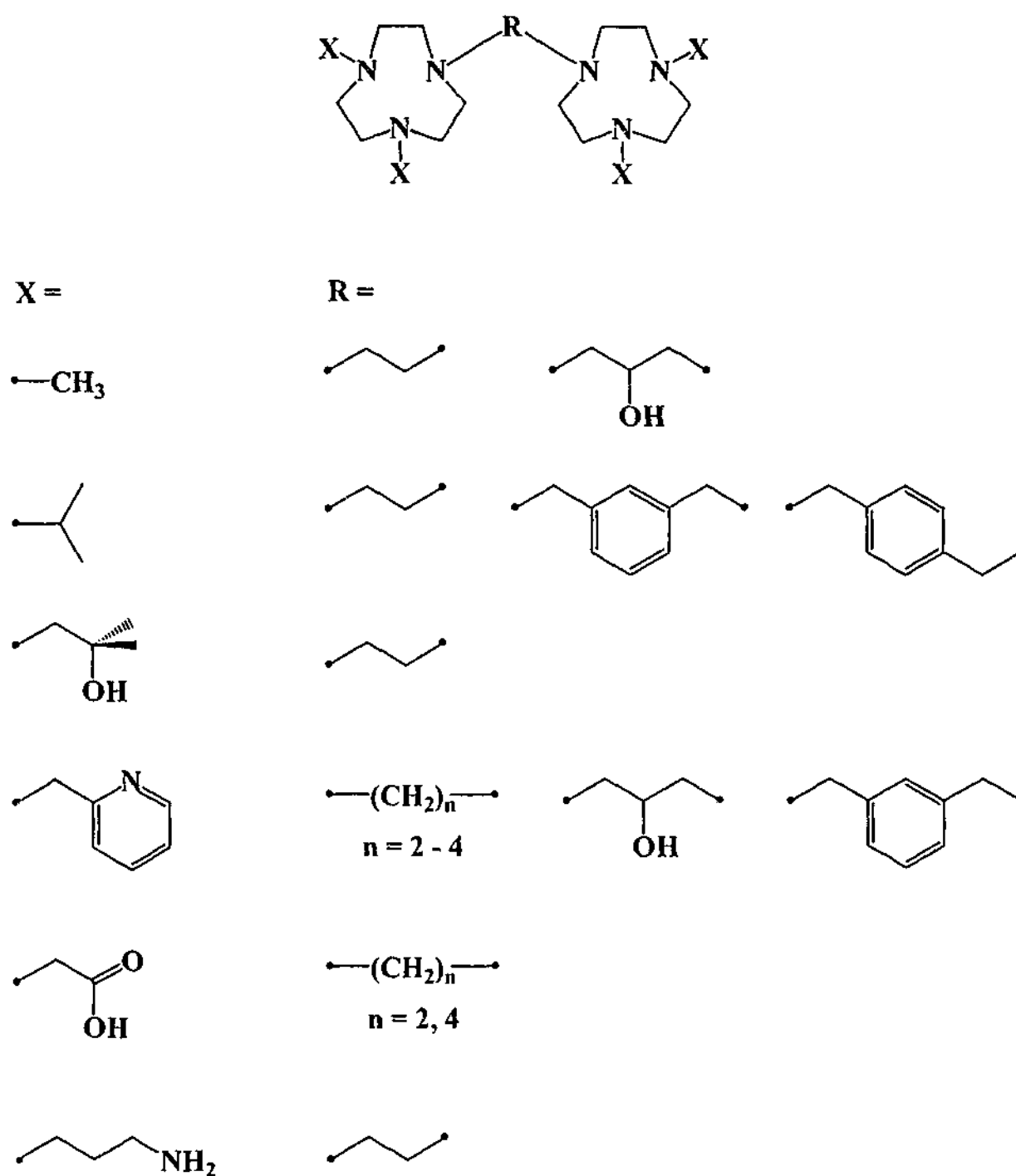


Figure 2.3 *N*-functionalised bis(tacn) ligands with pendant arms

In addition to the complete functionalisation of the nitrogens of tacn, there have been several cases where partial functionalisation of the tacn ring has been reported. Most of these examples relate to tacn itself and very few examples relate to polymacrocyclic derivatives of tacn.³⁹ A selection of partially *N*-functionalised tacn molecules are shown in Figure 2.4 and include mono-2-hydroxybenzyl (a),⁴⁰ bis-pyridylmethyl (b),³⁴ mono-(c)⁴¹ and bis-acetate (d),⁴² mono- (e) and bis-aminopropyl (f),⁴³ mono-3-propene (g)⁴⁴ bis-tert-alcohol groups (h),⁴⁵ and mono- (i) and bis-phosphate (j)⁴² derivatives.

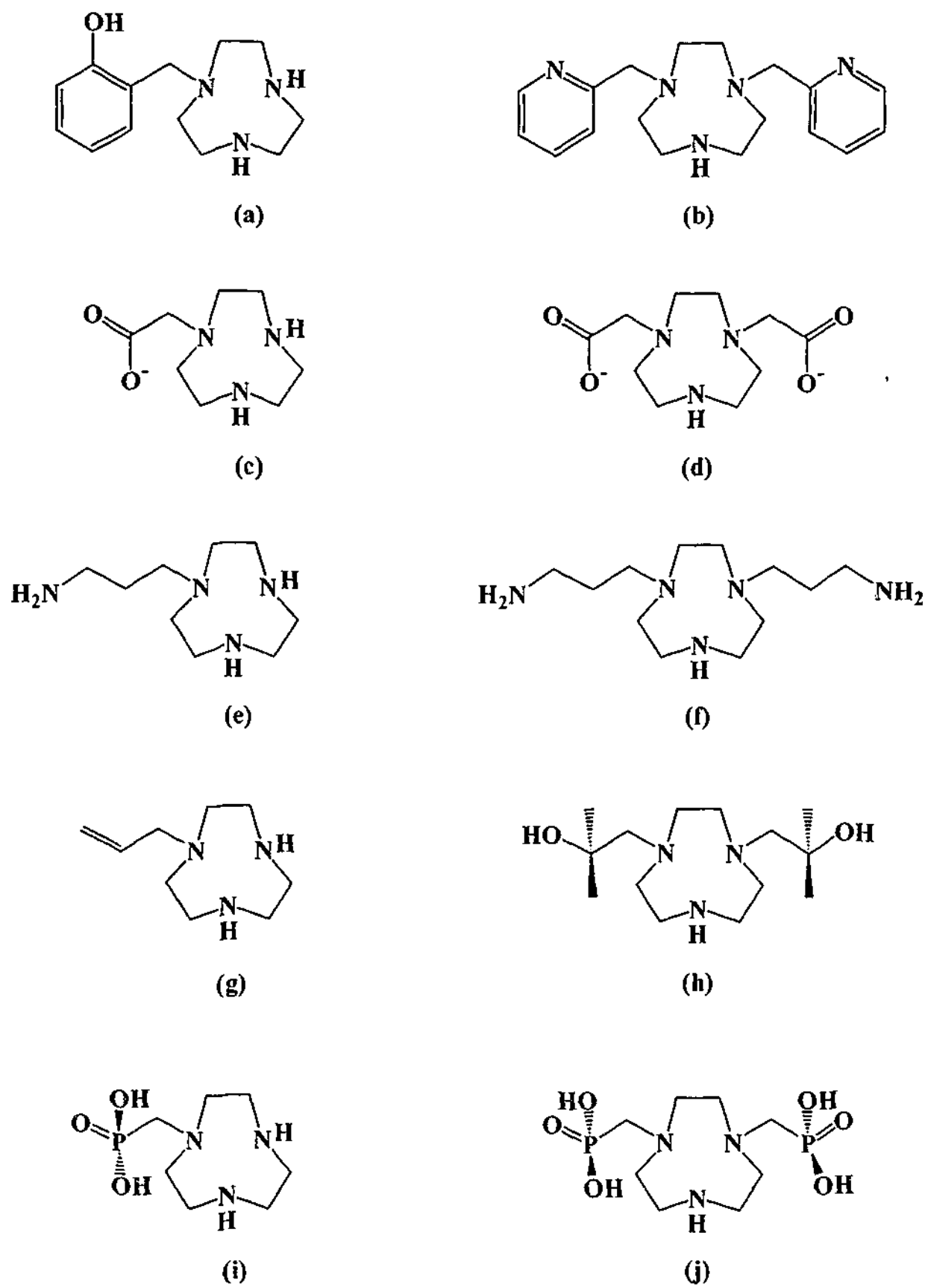


Figure 2.4 Examples of partially *N*-functionalised derivatives of tacn

The ligands developed in this investigation, for application in phosphate ester hydrolysis studies, were primarily bis- and tris(tacn) ligands, with and without added coordinating pendant arms. Some of these ligands such as the xylene and the mesitylene bridged tacn, have been reported^{7,9,26,46} since the commencement of this research. The bis(tacn) ligands with a single pendant arm on each macrocycle are the first examples of the partial functionalisation of a bis(tacn) ligand. The ligands are illustrated in Figure 2.5.

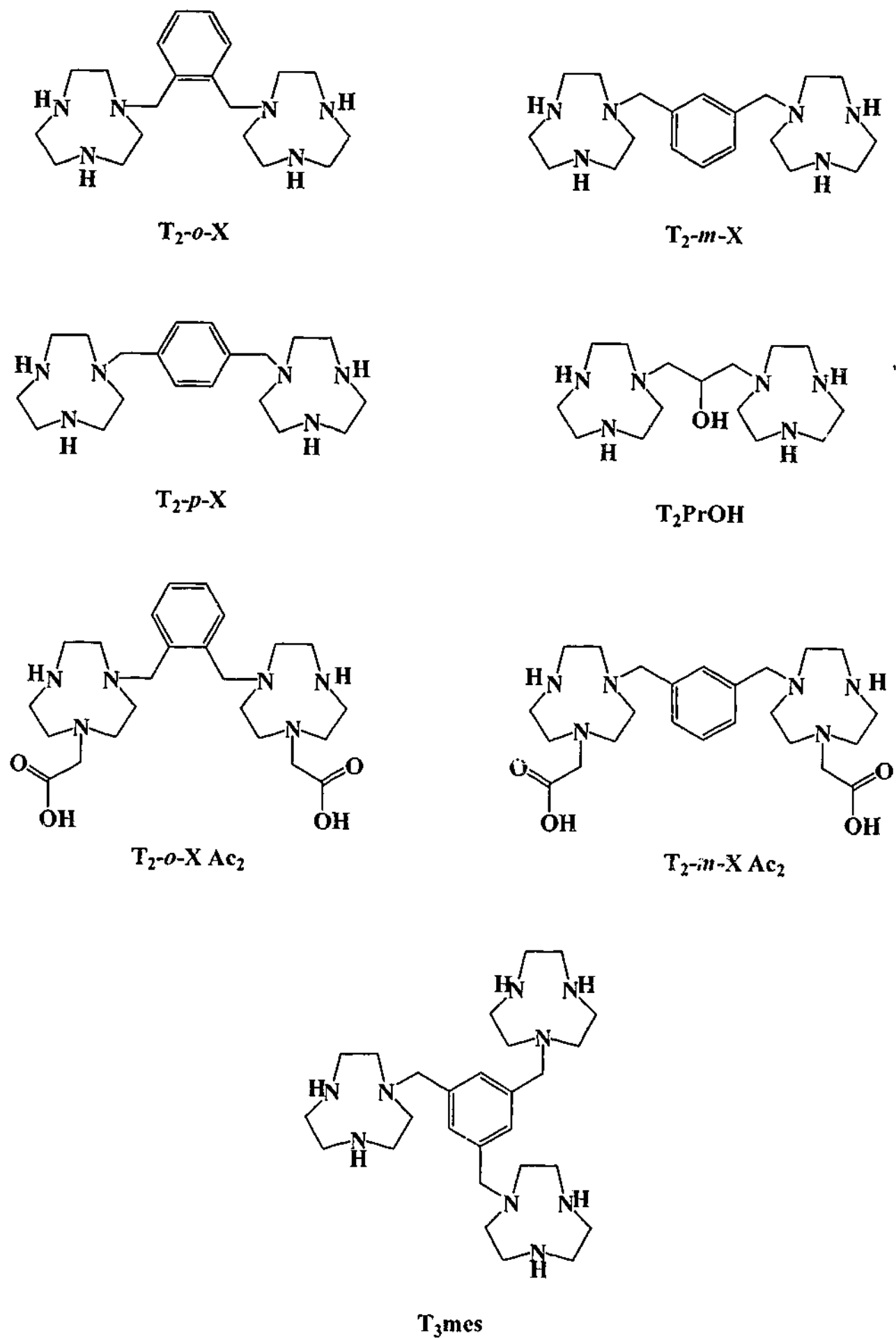
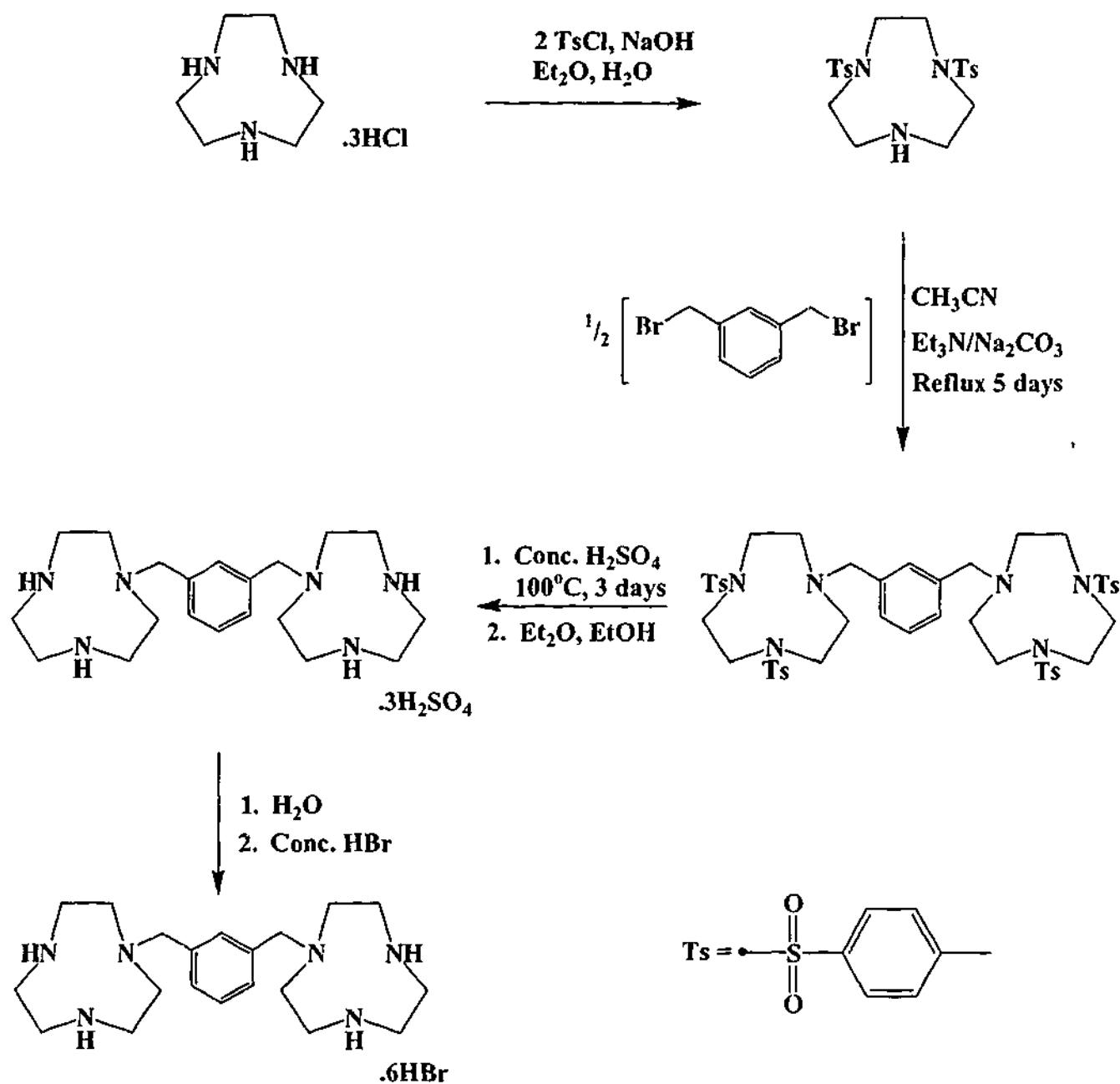


Figure 2.5 Ligands prepared in this study

2.2 Synthesis of Unfunctionalised Bis(tacn) Ligands

Synthetic routes to bis(tacn) ligands were originally based on the coupling of two doubly protected tacn units with a bis(electrophile),^{21,22,29} or more simply coupling the unprotected tacn.²⁸ This method involved a several step synthesis which took several days, and in some cases decomposition of the ligand occurred during the hydrolysis of the tosyl groups in acid (Scheme 2.1). A more versatile and reliable synthesis of bis(tacn) derivatives has been through the use of 1,4,7-triazatricyclo[5.2.1.0^{4,10}]decane (tacn orthoamide).⁴⁷ This method has been employed by Zompa and coworkers for the synthesis of propane and butane bridged bis(tacn).²⁴ The method, however, proved unsuccessful for the synthesis of T₂PrOH, which had to be synthesised via the doubly protected *N,N'*-bis(*p*-tolylsulphonyl)-1,4,7-triazacyclononane (TacnTs₂).

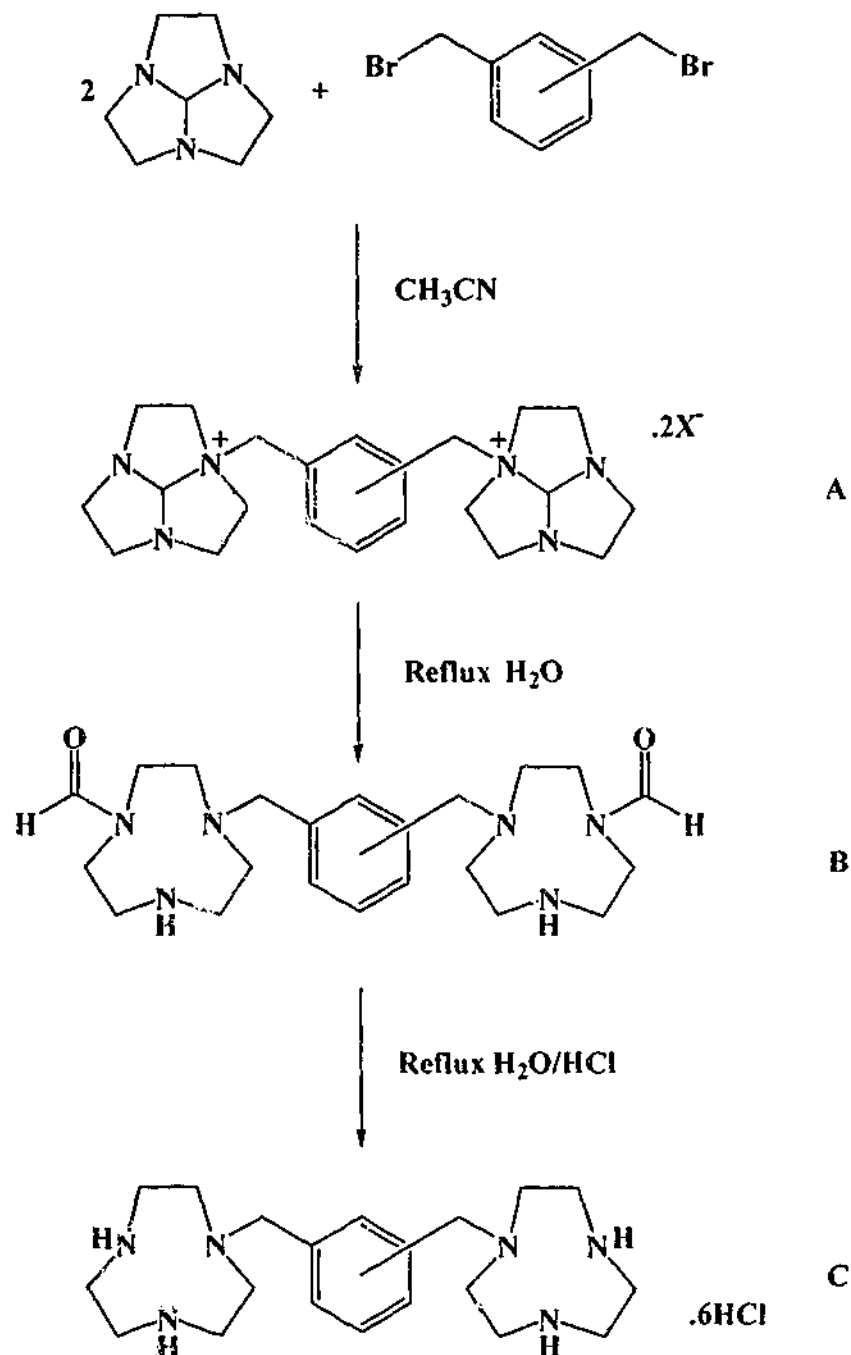


Scheme 2.1 Synthetic route to $\text{T}_2\text{-}m\text{-X.6HBr}$ via a doubly protected tacn

The synthesis of 1,4,7-triazatricyclo[5.2.1.0^{4,10}]decane was undertaken as described by Weisman *et al.*³⁰ and later by Zompa and coworkers.²⁴ The product was isolated in good yields as a colourless oil. The product was characterised by ^1H and ^{13}C NMR spectroscopy and are in agreement with literature values.

2.2.1 Synthesis of 1,2-, 1,3-, and 1,4-bis(1,4,7-triazacyclonon-1-ylmethyl)benzene hexahydrochloride ($T_2-o-X.6HCl$, $T_2-m-X.6HCl$, $T_2-p-X.6HCl$)

Three bis(tacn) ligands in which the two macrocyclic rings are linked by *ortho*, *meta* and *para*-xylene groups, were synthesised as outlined in Scheme 2.2. The synthesis involved reacting two molar equivalents of 1,4,7-triazatricyclo[5.2.1.0^{4,10}]decane with the appropriate α,α -dibromoxylene in acetonitrile and stirring overnight. The cream coloured precipitate of the bis(amidinium) salt (A) was isolated and then hydrolysed by refluxing in water to form the bis(formyl) derivative (B). Acid hydrolysis of the formyl groups was achieved by refluxing in 4M HCl. The products were isolated as the hexahydrochloride salts (C) by adding excess concentrated HCl. In order to fully precipitate the product, the suspension was allowed to stand at 4°C overnight. The white powder was obtained in a yield of 78%, 65% and 63% (from tacn orthoamide to C) for the *ortho*, *meta* and *para* bridged ligands respectively. Similar synthetic procedures to these ligands were reported during the course of this work and comparable yields obtained.^{7,46}

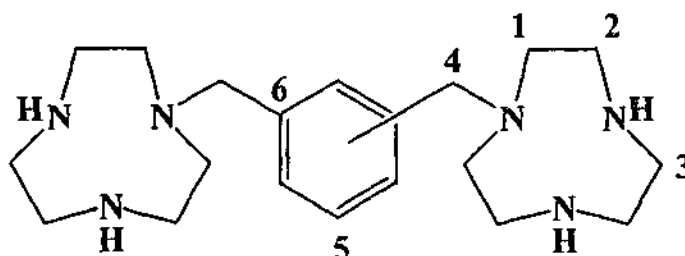


Scheme 2.2 Synthesis of T_2 -(*o*, *m*, *p*)-X ligands as hydrochloride salts

The products were characterised by ^1H NMR and ^{13}C NMR spectroscopy and the results are summarised in Tables 2.1 and 2.2. The ^1H NMR spectrum for the *p*-xylene bridged species shows a simple spectrum, with two triplets at 3.10 and 3.24 ppm for the two inequivalent methylene environments adjacent to the linker and a singlet at 3.67 ppm for the two remaining equivalent methylenes on the tacn ring. The methylene protons in

the bridge give a singlet at 3.99 ppm, while the four equivalent aromatic protons in the bridge give rise to a singlet at 7.51 ppm. In the ^{13}C NMR spectrum, the three furthest upfield signals at 44.50, 45.81 and 49.82 ppm correspond to the three carbon environments in the tacn ring. The signal at 60.98 ppm arises from the methylene carbons in the bridging unit. The aromatic CH carbons give rise to a signal at 133.20 ppm, and the signal at 137.41 ppm is attributed to the quaternary aromatic carbons. In the case of the $\text{T}_2\text{-o-X.6HCl}$ and the $\text{T}_2\text{-m-X.6HCl}$ ligands, the ^1H and ^{13}C signals due to the methylene regions show close correspondence with those of the $\text{T}_2\text{-p-X.6HCl}$ ligand, however, the aromatic regions of the spectra are more complicated. In the ^1H spectra, two multiplets centred at 7.49 and 7.63 ppm, for each of two protons in $\text{T}_2\text{-o-X.6HCl}$, and a multiplet at 7.50 ppm for the four protons for $\text{T}_2\text{-m-X.6HCl}$ were observed. In the ^{13}C spectrum of $\text{T}_2\text{-o-X.6HCl}$, the two signals at 127.78 and 130.67 ppm are attributed to the two different environments in the CH aromatic region, while the expected three signals were seen at 131.78, 132.72 and 134.57 ppm for $\text{T}_2\text{-m-X.6HCl}$.

Table 2.1 ^1H NMR chemical shifts (δ , ppm) for T_2 -(*o,m,p*)-X.6HCl recorded in D_2O



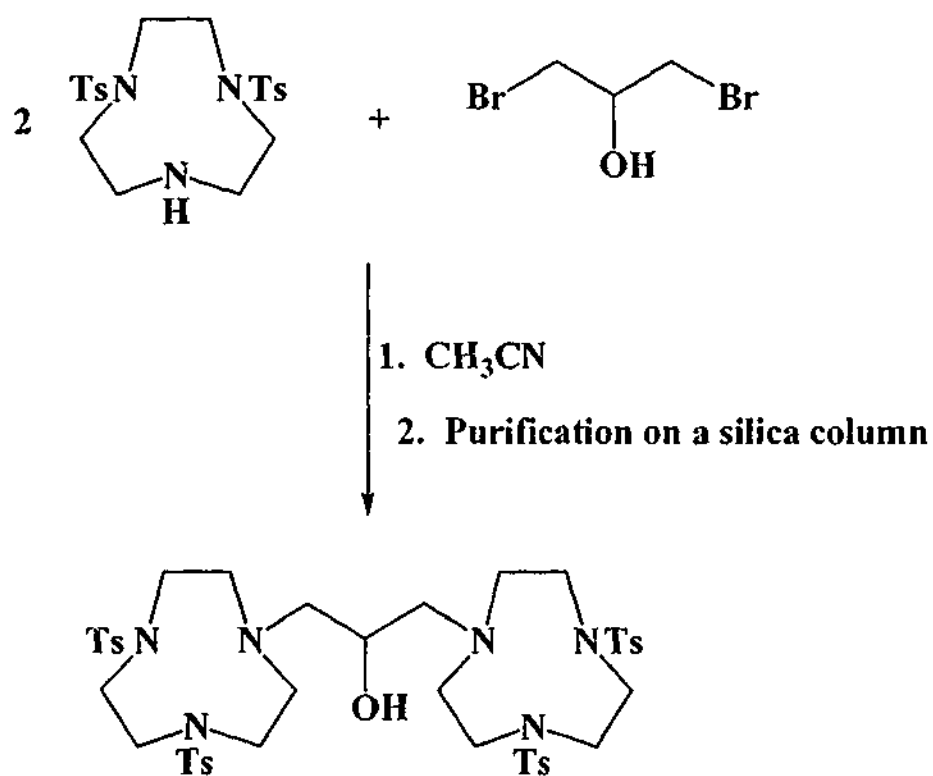
Proton Type	T_2 - <i>o</i> -X δ , ppm	T_2 - <i>m</i> -X δ , ppm	T_2 - <i>p</i> -X δ , ppm
1	3.09, t, 8H	3.07, t, 8H	3.10, t, 8H
2	3.26, t, 8H	3.26, t, 8H	3.24, t, 8H
3	3.72, s, 8H	3.58, s, 8H	3.67, s, 8H
4	4.11, s, 4H	3.96, s, 4H	3.99, s, 4H
5	7.49, m, 2H 7.63, m, 2H	7.50, m, 4H	7.51, s, 4H

Table 2.2 ^{13}C NMR chemical shifts (δ , ppm) for T_2 -(*o, m, p*)-X.6HCl recorded in D_2O

Carbon Type	T_2 - <i>o</i> -X δ , ppm	T_2 - <i>m</i> -X δ , ppm	T_2 - <i>p</i> -X δ , ppm
1	41.71	44.63	44.50
2	43.23	46.07	45.81
3	47.68	49.94	49.82
4	55.22	61.15	60.98
5	127.78 130.67	131.78 132.72 134.57	133.20
6	134.39	138.19	137.41

2.2.2 Synthesis of 1,2-Bis[*N,N'*-bis(*p*-tolylsulphonyl)-1,4,7-triazacyclonon-1-yl]propan-2-ol ($T_2PrOHTs_4$)

Due to the lack of success in obtaining this ligand using the method as described in section 2.2.1, the method described by Weighardt and coworkers²¹ was employed. $TacnTs_2$ was dissolved in acetonitrile and the bis(electrophile), dibromopropan-2-ol, was added. The solution was refluxed under N_2 for 3 days. The product was extracted into CH_2Cl_2 and purified on a silica column. Following removal of the solvent, the product was isolated as a fluffy white solid in a good yield of 80% (Scheme 2.3).



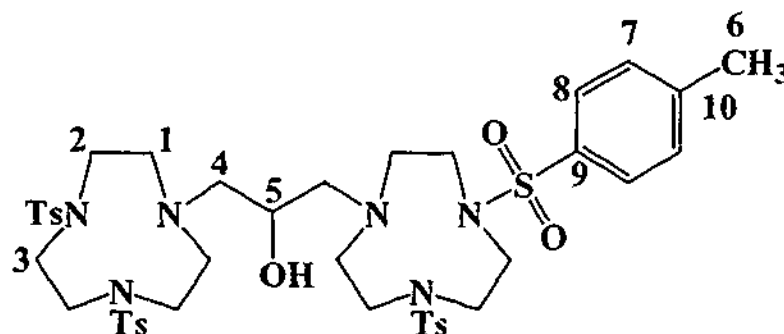
Scheme 2.3 Synthesis of $T_2PrOHTs_4$

The product was characterised by NMR spectroscopy and the results are summarised in Table 2.3. The presence of the tosyl groups can be seen clearly in the 1H NMR spectrum by a singlet at 2.40 ppm arising from the methyl group and two multiplets at

7.27 and 7.65 ppm from the aromatic protons. Three broad singlets at 3.01, 3.24 ppm and a multiplet at 3.45 ppm are attributed to the methylene protons on the tacn ring. The protons in the bridge give a broad unresolved multiplet at 3.79 ppm due to the CH and two doublets of doublets are observed for the methylene protons at 2.56 and 2.76 ppm. Each of the methylene protons in the bridge (see position 4 below) are slightly different and therefore give rise to two signals, two doublets of doublets due to the coupling with the proton on the same carbon, as well as coupling with the proton on the adjacent carbon. In the ^{13}C NMR spectrum the tosyl protecting groups give peaks at 21.47, 127.15, 129.75, 135.07 and 143.45 ppm from the methyl, two aromatic CH and two aromatic quaternary carbons, respectively. For the three different methylene carbons in the macrocyclic ring, signals are observed at 52.24, 52.93 and 56.52 ppm, while those in the bridge are seen at 62.78 ppm. The final signal at 67.61 ppm is attributed to the CH in the bridge.

Table 2.3 ^1H and ^{13}C NMR chemical shifts (δ , ppm) for $\text{T}_2\text{PrOHTs}_4$

recorded in CDCl_3



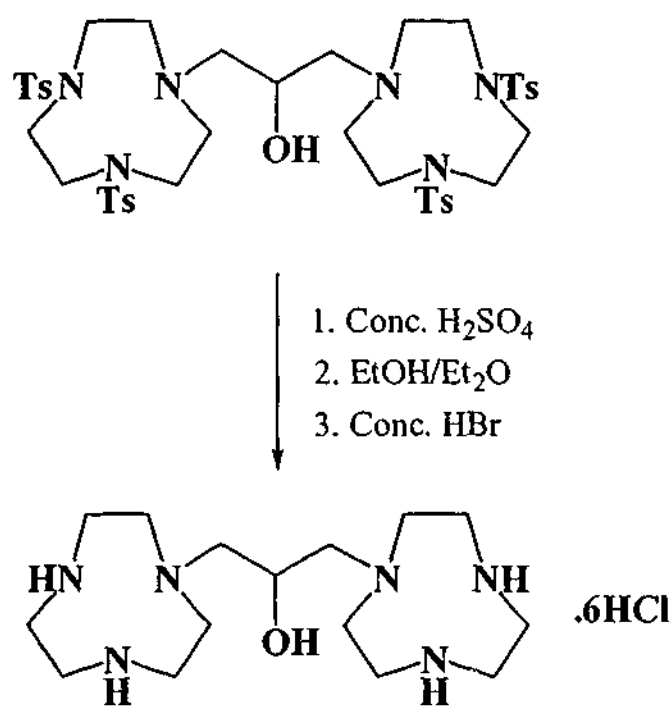
	^1H δ , ppm	^{13}C δ , ppm
1	3.01, br s, 8H	52.24
2	3.24, br s, 8H	52.93
3	3.44, m, 8H	56.52
4	2.56, dd, 2H 2.76, dd, 2H	62.78
5	3.79, br m, 1H	67.61
6	2.40, s, 12H	21.47
7	7.27, m, 8H	127.15
8	7.65, m, 8H	129.75
9	-	135.07
10	-	143.45

2.2.3 Synthesis of 1,2-Bis[1,4,7-triazacyclonon-1-yl]propan-2-ol hexahydrobromide ($\text{T}_2\text{PrOH} \cdot 6\text{HBr}$)

The product described above (Section 2.2.2) was deprotected by acid hydrolysis. This was achieved by stirring $\text{T}_2\text{PrOHTs}_4$ in concentrated H_2SO_4 for 2 days at 90°C . After the dark brown solution had cooled, the solution was added dropwise to a 1:1 mixture of

Chapter Two

cold ethanol:ether. This precipitated the hydrosulphate salt of the ligand as a grey, hygroscopic residue. The product was dissolved in a minimum amount of water and treated with concentrated HBr solution. This procedure precipitated the hexahydrobromide salt of the ligand which was collected as a tan coloured powder in a yield of 78% (Scheme 2.4).

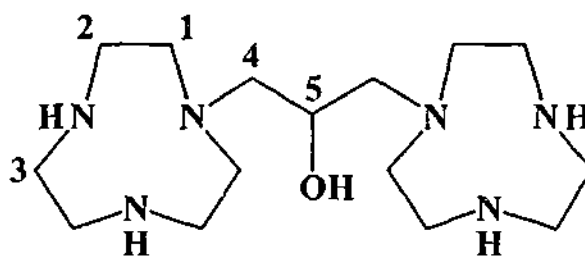


Scheme 2.4 Synthesis of T₂PrOH.6HBr

The product was characterised by ¹H and ¹³C NMR spectroscopy. In the ¹H NMR spectrum, signals were observed at 3.18, 3.42 and 3.70 ppm for the methylene protons in the ring. The bridge protons gave a two multiplets, one at 2.80 ppm for the methylene protons and the other at 4.35 ppm for the remaining proton. In the ¹³C NMR spectrum five signals were also observed. Three attributable to the methylene carbons in the tacn ring were found at 44.51, 46.05 and 50.59 ppm, while the remaining

methylene carbon in the bridge gave a signal at 61.08 ppm, and the methyne carbon gave a peak at 68.27 ppm.

Table 2.4 ^1H and ^{13}C NMR chemical shifts for (δ , ppm) $\text{T}_2\text{PrOH}\cdot 6\text{HBr}$
recorded in D_2O



	^1H δ , ppm	^{13}C δ , ppm
1	3.18, m, 8H	44.51
2	3.42, t, 8H	46.05
3	3.70, s, 8H	50.59
4	2.80, m, 4H	61.01
5	4.35, s, 1H	68.27

2.3 Synthesis of Bis(tacn) Ligands Bearing Pendant Arms

Functionalisation via the secondary nitrogens of bis(tacn) ligands have included a variety of both coordinating and non-coordinating pendant arms (see Figure 2.3). Asymmetric functionalisation of the bis(tacn) ligands is a developing field, and, with

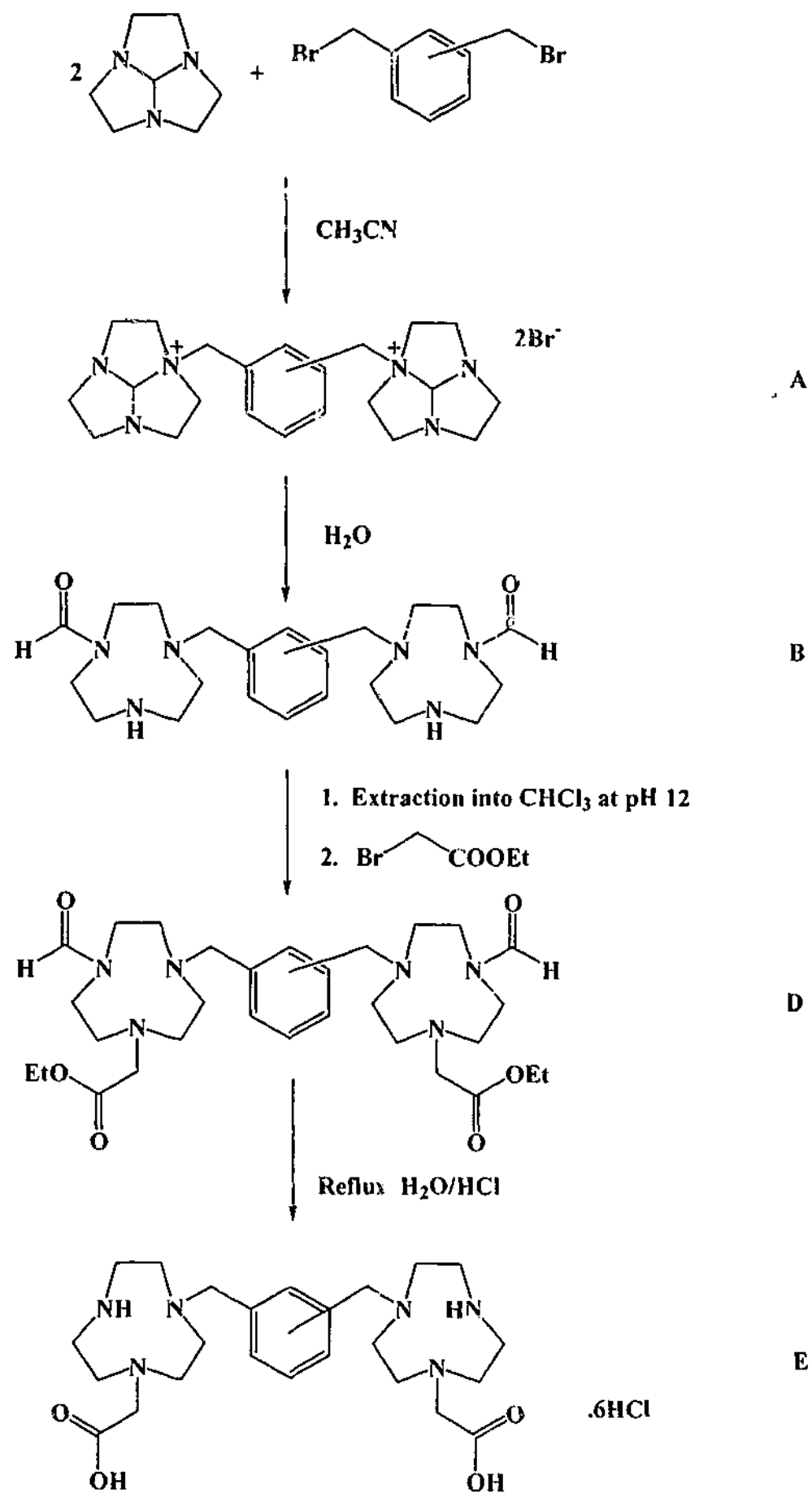
the relatively new synthetic path to the linking of two tacn rings together via the orthoamide route, this has proved relatively straightforward. Hydrolysis of the bis(amidium) salts results in bis(formyl) derivatives which have one nitrogen available for selective functionalisation with pendant groups.

2.3.1 Synthesis of 1,2- and 1,3-bis(4-(carboxymethyl)-1,4,7-triazacyclonon-1-ylmethyl)benzene hexahydrochloride ($T_2\text{-}o\text{-X Ac}_2\cdot 6\text{HCl}$, $T_2\text{-}m\text{-X Ac}_2\cdot 6\text{HCl}$)

The synthesis of the ligands with acetate pendant arms followed that for the unsubstituted bis(tacn) ligands up to the formation of the bis(formyl) derivative (**B**) (Scheme 2.2). At this point, the pH of the aqueous solution containing the bis(formyl) derivatives was increased to *ca.* 12 and the product extracted into chloroform to yield a yellow oil of the bis(formyl) ligand (**B**). The presence of a strong band at *ca.* 1660 cm^{-1} in the IR spectrum of the products, attributable to the amide carbonyl, confirmed the presence of the formyl group. The bis(formyl) derivatives were dissolved in acetonitrile and two molar equivalents of bromoethyl acetate were added in the presence of solid Na_2CO_3 . The mixture was refluxed for 48 hours, filtered, and the solvent removed *in vacuo* leaving a yellow oil of the bis(formyl)-bis(ester) derivative (**D**). The presence of a band at $\sim 1730\text{ cm}^{-1}$ in the IR spectrum of **D** confirmed the presence of the ester functionality while a second band at $\sim 1660\text{ cm}^{-1}$ confirmed that the amide functionality was still present. The yellow oil was refluxed in aqueous acid solution, a procedure which hydrolysed the formyl and ester groups, thereby generating the ligand of interest. The solvent was removed *in vacuo* leaving a pale brown residue of the hydrochloride salt of the bis(acetate) functionalised ligand (**E**). IR spectroscopy of the products showed a $\nu_{\text{asym}}(\text{CO})$ band at $\sim 1720\text{ cm}^{-1}$ and $\nu_{\text{sym}}(\text{CO})$ at $\sim 1450\text{ cm}^{-1}$ attributable to the

Chapter Two

acetate moiety. Attempts were made to crystallise the product in the same manner as for the unfunctionalised bis(tacn) ligands, however no precipitate formed when the compound was treated with concentrated acid. Attempts to extract the free ligand into organic solvents also proved unsuccessful. The product was therefore characterised and used, presuming formation of a hexahydrochloride salt of the ligand.

Scheme 2.5 Synthesis of $\text{T}_2\text{-(}o, m\text{)-X Ac}_2$ ligands

The IR spectra of the products show strong broad OH stretches at 3442 and 3426 cm^{-1} due to water in each of the products, $\text{T}_2\text{-}o\text{-X Ac}_2\cdot 6\text{HCl}$ and $\text{T}_2\text{-}m\text{-X Ac}_2\cdot 6\text{HCl}$ respectively. Due to the broadness of the peaks, the NH stretches of the product were not observed. Peaks at 1721 and 1458 cm^{-1} , and 1722 and 1447 cm^{-1} in each of the compounds (*ortho*- and *meta*- respectively) confirm the presence of the acetate pendant arms.

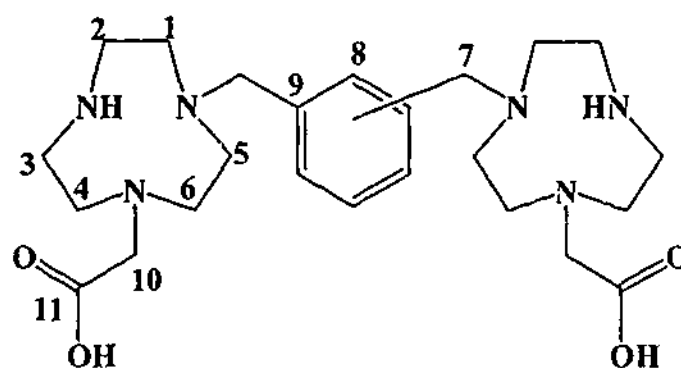
The crude products were characterised by ^1H and ^{13}C NMR spectroscopy. Table 2.5 shows selected signals from the NMR spectra of each compound. The ^1H NMR spectra of the ligands do not give indisputable characterisation of the target compounds, however characteristic patterns which indicate the presence of these compounds can be distinguished. A pair of multiplets in the aromatic region for the *ortho* species and a multiplet present in the same region for the *meta* ligand are observed. A number of peaks in the region of 2.8 – 4.3 ppm are present, which is the region typical of tacn and bridge methylene protons to resonate. The methylene protons in the pendant arm will also give a signal in this region.

The ^{13}C NMR spectra of both compounds provide better characterisation of the compounds. Both of the spectra show eight signals in the region of 40 – 60 ppm. These are due to methylene protons within the tacn ring, in the pendant arms and in the bridge. In the aromatic region, a signal due to the quaternary carbons appears at 128.98 and 128.91 ppm for the *ortho* and *meta*, respectively. The *ortho* ligand shows two signals at 132.53, 133.04 and 133.42 ppm due the CH groups in the aromatic ring. The *meta* species shows three signals for the CH groups in the aromatic ring, at 130.77, 132.23

Chapter Two

and 133.02 ppm. Both ligands show a signal for the carboxylate carbon, at 175.26 ppm for *ortho* ligand and at 174.74 ppm for the *meta* ligand.

Table 2.5 Selected ^1H and ^{13}C NMR chemical shifts (δ , ppm) recorded in D_2O



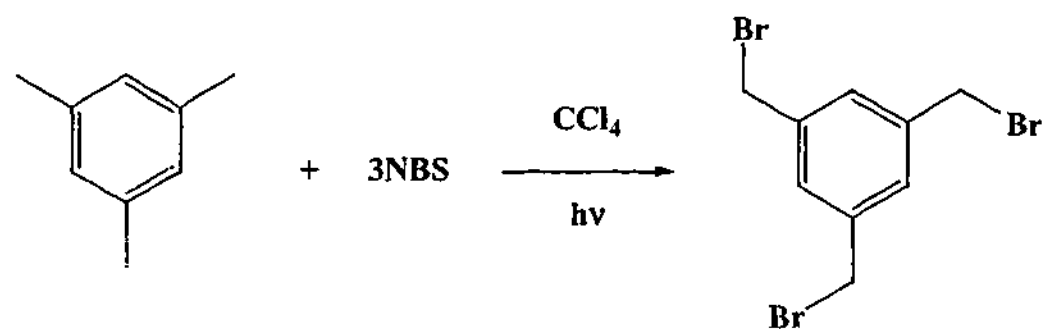
	^1H NMR (δ , ppm)		^{13}C NMR (δ , ppm)	
	<i>ortho</i>	<i>meta</i>	<i>ortho</i>	<i>meta</i>
1-6	3.14, m	3.15, m	40.39	40.58
	3.36, m	3.35, m	42.08	42.83
	3.51, m	3.54, m	42.78	43.55
			46.95	47.23
			48.59	48.80
			50.10	50.34
7	3.92, m	3.90, m	54.64	54.61
8	7.71, 2H, m	7.79 m	132.53	130.78
	7.89, 2H, m		133.14	132.24
			133.42	133.02
9	-	-	128.98	128.91
10	3.58, s	3.61, s	55.83	56.94
11	-	-	175.26	174.72

2.4 Synthesis of Tris(tacn) Ligand

Although not published at the commencement of this work, complexes incorporating the tris(tacn) linked via 1,3,5-trimethyl benzene have since appeared in the literature.⁹ The synthesis of ligands capable of binding a number of metals centres is an expanding area of research. The synthesis of the tris(1,4,7,10-tetraazacyclododecane) ligand was reported by Kimura and coworkers in 1997 and a trinuclear zinc complex of this ligand was used as a phosphate dianion receptor.⁴⁸ Similarly, the complex of the tris(tacn) ligand which has been reported⁹ was also found to bind phosphate (see also section 1.5.3).

2.4.1 Synthesis of 1,3,5-tribromomethylbenzene (Br₃mes)

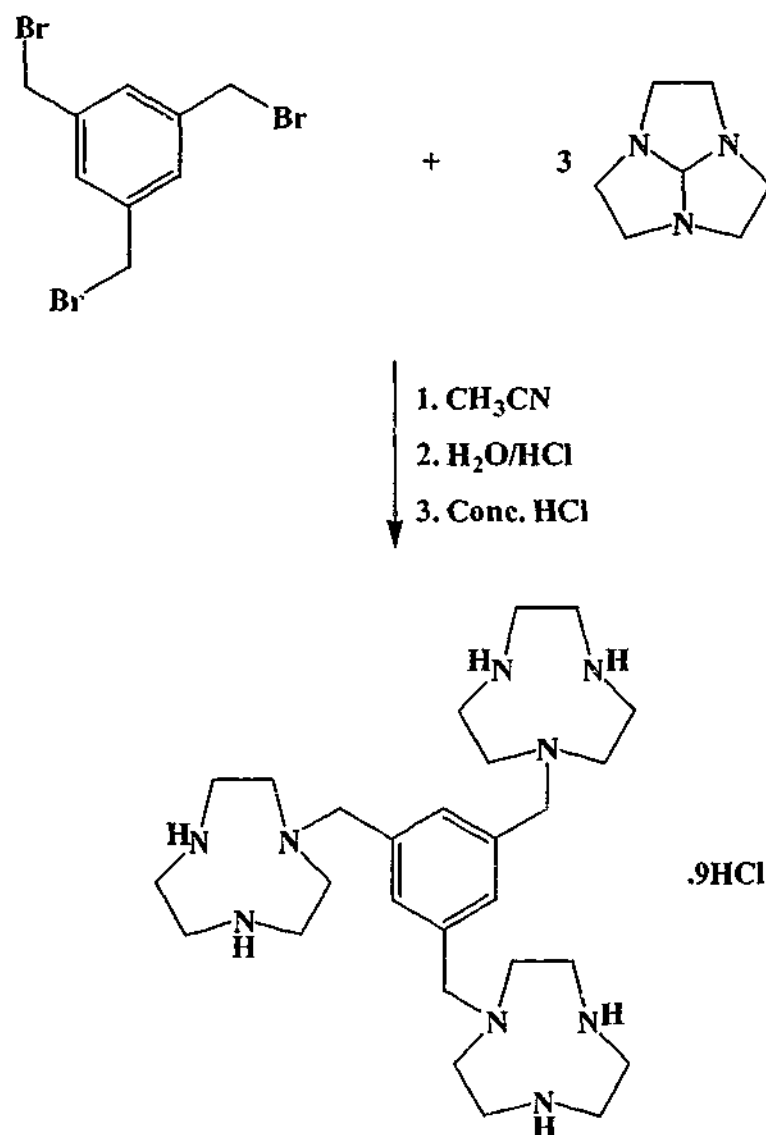
The bromination of 1,3,5-trimethylbenzene (mesitylene) was achieved by refluxing three mole equivalents of *N*-bromosuccinimide with mesitylene in carbon tetrachloride and in the presence of light (Scheme 2.6).⁴⁹ The succinimide which formed as the by-product was removed by filtration and the filtrate was taken to dryness. The residue was dissolved in dichloromethane and crystallisation induced by the addition of petroleum spirit. The white solid was obtained in 41% yield. The ¹H NMR spectrum exhibited only two peaks, one at 4.46 ppm due to the methylene protons and one at 7.36 ppm arising from the aromatic protons. The ¹³C NMR spectrum showed signals at 32.65 ppm from the methylene carbons and signals at 129.79 and 139.22 ppm due to the CH and the quaternary carbons on the aromatic ring.



Scheme 2.6 Synthesis of Br₃mes

2.4.2 Synthesis of the Tris(tacn) ligand 1,3,5-tris(1,4,7-triazacyclonon-1-ylmethyl)benzene nonahydrochloride (T₃mes.9HCl)

The mesityl linked version of the tris(tacn) ligands was prepared in an analogous manner to the bis(tacn) ligands (see Scheme 2.7). The ligand was isolated as the hexahydrochloride salt in 82% yield.

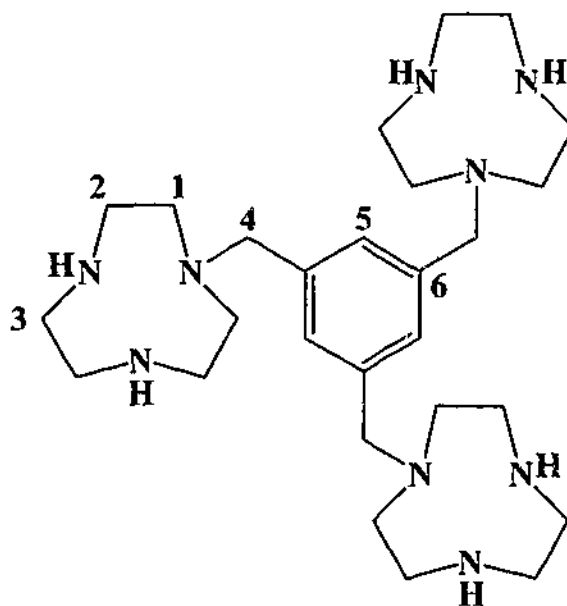


Scheme 2.7 Synthesis of Tris(tacn) Ligands

The product was characterised by ¹H and ¹³C NMR spectroscopy and the results are summarised in Table 2.6. Three peaks were observed at 3.05, 3.34 and 3.70 ppm for the three different methylene environments in the tacn ring. The first two signals were triplets due to coupling with the adjacent CH₂, with the latter observed as a singlet. The bridge methylene protons give rise to a singlet at 4.01 ppm, and the final signal at 7.53 ppm is a singlet arising from the aromatic CH protons in the bridge. The ¹³C NMR spectrum showed six resonances as expected. Three signals at 41.11, 42.62 and 46.22 ppm are due to the three methylene environments in the tacn ring. The bridge gives rise to the remaining three signals, the methylene protons resonating at 57.00 ppm while the

two aromatic signals appear at 130.70 and 135.16 ppm for the CH and the quaternary carbons, respectively.

Table 2.6 ^1H and ^{13}C NMR chemical shifts (δ , ppm) for $\text{T}_3\text{mes.6HCl}$ recorded in D_2O



	^1H	^{13}C
	δ , ppm	δ , ppm
1	3.05, t, 12H	46.22
2	3.34, t, 12H	41.11
3	3.70, s, 12H	42.62
4	4.01, s, 6H	57.00
5	7.53, s, 3H	130.70
6	-	135.16

2.5 Experimental

Reagents and Instruments

Laboratory chemicals, solvents, and nitrogen gas

All reagents were of reagent grade quality, obtained from commercial suppliers and used without further purification. Solvents were used as received or dried over 4A molecular sieves. Water was distilled prior to use. $\text{Tacn}\cdot 3\text{HCl}$ was synthesised according to the published procedure.²¹

^1H and ^{13}C Nuclear Magnetic Resonance (NMR) spectra

^1H and broad band decoupled ^{13}C NMR spectra were recorded on either a Bruker AC200, Bruker DPX300 or Bruker DRX400 spectrometer. Internal standards of tetramethylsilane (TMS) for non-aqueous solvents and sodium(2,2,3,3- d_4 -3-(trimethylsilyl)propionate (TMSP-D) for D_2O were used as the reference, and the chemical shifts (δ) are reported in ppm using the high frequency positive convention. Abbreviations used to describe the resonances are: s (singlet), d (doublet), t (triplet), m (multiplet) and br (broad).

Infrared spectra

Infrared spectra were recorded using KBr disks or nujol mulls on a Perkin-Elmer 1600 series FTIR spectrophotometer at a resolution of 4.0 or 8.0 cm^{-1} . Abbreviations used to describe intensities are: s (strong), m (medium), w (weak) and br (broad).

Melting points

Melting points were recorded using an Electrothermal melting point apparatus (0-360°C).

Synthesis of Ligands

1,4,7-triazatricyclo[5.2.1.0^{4,10}]decane

Tacn.3HCl (22.76 g, 0.095 mol) was dissolved in water (200 ml) and solid NaOH (5.20 g, 0.130 mol) was added. Following dissolution, the solution was taken to dryness *in vacuo*. Toluene (200 ml) was added and the residual water was removed through azeotropic distillation. The solid was extracted three times with toluene (100 ml) and all washings were combined. Dimethylformamide dimethylacetal (11.37 g, 0.0954 mol) was added to the toluene solution and the solution heated on a steam bath with a drying tube fitted to the top of a condenser. After 4 hours the solvent was removed *in vacuo* leaving a yellow oil. The oil was distilled under high vacuum and the fraction at 40-44°C was collected. The product was a colourless oil.

Yield: 9.13 g (69 %). ¹H NMR (D₂O): δ 2.95 (12H, m, 6 x CH₂), 5.03 (1H, s, CH). ¹³C NMR (D₂O): δ 51.49 (CH₂), 103.71 (CH).

N,N'-Bis(*p*-tolylsulphonyl)-1,4,7-triazacyclononane (TacnTs₂)

A solution of *p*-toluenesulphonylchloride (15.25 g, 0.08 mol) in ether (750 ml) was added dropwise over 5 hours to a solution of tacn.3HCl (15.0 g, 0.04 mol) in 7.5 M aqueous NaOH (100 ml). The white precipitate which formed was collected and dissolved in chloroform. The solution was washed with distilled water (2 x 100 ml),

dried over anhydrous MgSO_4 and then filtered. Removal the solvent *in vacuo* gave the product as a white solid.

Yield: 14.71 g (84%). Melting point: 222-223°C (Lit.⁵⁰ 219-224°C). ^1H NMR (CDCl_3): δ 1.61 (1H, br, NH tacn ring), 2.40 (6H, s, 2 x CH_3), 3.18 (8H, m, 2 x $\text{TsNCH}_2\text{CH}_2\text{NH}$), 3.45 (4H, s, 2 x $\text{TsNCH}_2\text{CH}_2\text{NTs}$), 7.30 (4H, m, aromatic CH), 7.68 (4H, m, aromatic CH). ^{13}C NMR (CDCl_3): δ 21.31 (CH_3), 48.90 (CH_2), 52.74 (CH_2), 53.63 (CH_2), 127.04 (aromatic CH), 129.64 (aromatic CH), 135.06 (aromatic CH), 143.42 (aromatic CH).

Synthesis of Bis(tacn) Ligands

1,2-Bis(1,4,7-triazacyclonon-1-ylmethyl)benzene hexahydrochloride ($\text{T}_2\text{-}o\text{-X.6HCl}$)

A solution of α,α -dibromo-*o*-xylene (3.09 g, 0.0130 mol) in acetonitrile (50 ml) was added dropwise to a solution of 1,4,7-triazatricyclo[5.2.1.0^{4,10}]decane (3.42 g, 0.025 mol) in acetonitrile (50 ml) with stirring. A cream coloured precipitate formed almost immediately. The mixture was stirred overnight after which the precipitate was collected by vacuum filtration and dissolved in water (100 ml). The solution was refluxed for 4 hours after which time the solvent was removed. The brown syrupy residue that remained was dissolved in 4 M HCl (100 ml) and refluxed for 6 hours. The acid was removed *in vacuo* leaving a brown residue. This was dissolved in a minimum amount of water, concentrated HCl (40 ml) was added and the solution left at 4°C overnight. The cream coloured precipitate that formed was collected by vacuum filtration, washed with acetone and air dried.

Yield: 5.55 g (78%). ^1H NMR (D_2O): δ 3.09 (8H, t, CH_2 tacn ring), 3.26 (8H, t, CH_2 tacn ring), 3.72 (8H, s, CH_2 tacn ring), 4.11 (4H, s, CH_2 bridge), 7.49 (2H, m, ArCH),

7.63 (2H, m, ArCH). ^{13}C NMR (D_2O): δ 41.71 (CH_2 tacn ring), 43.28 (CH_2 tacn ring), 47.68 (CH_2 tacn ring), 55.22 (CH_2 bridge), 127.78 (ArCH), 130.67 (ArCH), 134.39 (quaternary C)

1,3-Bis(1,4,7-triazacyclonon-1-ylmethyl)benzene hexahydrochloride ($\text{T}_2\text{-}m\text{-X.6HCl}$)

$\text{T}_2\text{-}m\text{-X.6HCl}$ was prepared according to the procedure used for $\text{T}_2\text{-}o\text{-X.6HCl}$ using 1,4,7-triazatricyclo[5.2.1.0^{4,10}]decane (5.75 g, 0.0413 mol) and α,α -dibromo-*m*-xylene (5.45 g, 0.0206 mol).

Yield: 7.76 g (65%). ^1H NMR (D_2O): δ 3.07 (8H, t, CH_2 tacn ring), 3.26 (8H, t, CH_2 tacn ring), 3.58 (8H, s, CH_2 tacn ring), 3.96 (4H, s, CH_2 bridge), 7.50 (4H, m, aromatic CH). ^{13}C NMR (D_2O): δ 44.63 (CH_2 tacn ring), 46.07 (CH_2 tacn ring), 49.94 (CH_2 tacn ring), 61.15 (CH_2 bridge), 131.78 (ArCH), 132.72 (ArCH), 134.57 (ArCH), 138.19 (quaternary C).

1,4-Bis(1,4,7-triazacyclonon-1-ylmethyl)benzene hexahydrochloride ($\text{T}_2\text{-}p\text{-X.6HCl}$)

$\text{T}_2\text{-}p\text{-X.6HCl}$ was prepared following the procedure used for $\text{T}_2\text{-}o\text{-X.6HCl}$, using 1,4,7-triazatricyclo[5.2.1.0^{4,10}]decane (3.62 g, 0.0137 mol) and α,α -dibromo-*p*-xylene (3.83 g, 0.0274 mol).

Yield: 5.00 g (63%). ^1H NMR (D_2O): δ 3.10 (8H, t, CH_2 tacn ring), 3.24 (8H, t, CH_2 tacn ring), 3.67, (8H, s, CH_2 tacn ring), 3.99 (4H, s, CH_2 bridge), 7.51 (4H, s, aromatic CH). ^{13}C NMR (D_2O): δ 44.50 (CH_2 tacn ring), 45.81 (CH_2 tacn ring), 49.82 (CH_2 tacn ring), 60.98 (CH_2 bridge), 133.20 (ArCH), 137.41 (quaternary C).

1,2-Bis[N,N'-bis(*p*-tolylsulphonyl)-1,4,7-triazacyclonon-1-yl]propan-2-ol**(T₂PrOHTs₂)**

TacnTs₂ (10.00 g, 0.0288 mol) was dissolved in dry acetonitrile (125 ml) and 1,3-dibromopropan-2-ol (2.60 g, 0.0114 mol) was added. The solution was refluxed with stirring under nitrogen for 3 days. The orange solution was cooled to room temperature and water (125 ml) and CHCl₃ (250 ml) were added. The organic layer was separated, dried over MgSO₄, filtered and the filtrate taken to dryness *in vacuo*. The resulting orange oil was purified by column chromatography on silica gel using a 2% methanol/chloroform mixture as the eluent.

Yield: 8.40 g (79%). ¹H NMR (CDCl₃): δ 2.40 (12H, s, 4 x CH₃), 2.56 (2H, dd, CH₂ bridge), 2.76 (2H, dd, CH₂ bridge) 3.01 (8H, br s CH₂), 3.24 (8H, br s CH₂ tacn ring), 3.44 (8H, m, CH₂ tacn ring), 3.79 (1H, br m, CH bridge), 7.27 (8H, m, 8 x aromatic CH), 7.65 (8H, d, 8 x aromatic CH). ¹³C NMR (CDCl₃): δ 21.47 (CH₃), 52.24 (CH₂), 52.93 (CH₂), 56.52 (CH₂), 62.78 (CH₂ bridge), 67.61 (CH bridge), 127.15 (ArCH), 129.75 (ArCH), 135.07 (quaternary C), 143.45 (quaternary C).

1,2-Bis[1,4,7-triazacyclonon-1-yl]propan-2-ol hexahydrochloride (T₂PrOH.6HCl)

T₂PrOHTs₄ (8.40 g, 9.02 mmol) was dissolved in concentrated H₂SO₄ (75 ml) and the solution stirred at 90°C for 48 hours. The mixture was cooled to room temperature and then added dropwise to an ice cold solution of ethanol (250 ml) and diethyl ether (250 ml) with stirring. The grey slurry that formed was allowed to stand for one hour and the mixture was filtered to isolate the ligand as a dihydrogen sulphate salt. This grey precipitate was dissolved in a minimum amount of water and concentrated HBr (110

ml) was added slowly. The solution was left at 4°C overnight. The cream coloured precipitate that formed was collected and air dried.

Yield: 6.63 g (78%). ¹H NMR (CDCl₃): δ 2.80 (4H, m, CH₂ bridge), 3.18, (8H, m, CH₂ tacn ring), 3.42 (8H, t, CH₂ tacn ring), 3.70 (8H, s, CH₂ tacn ring), 4.35 (1H, m, CH bridge). ¹³C NMR (CDCl₃): δ 44.51 (CH₂), 46.05 (CH₂), 50.59 (CH₂), 61.01 (CH₂ bridge), 68.27 (CH bridge).

1,2-Bis(4-carboxymethyl-1,4,7-triazacyclonon-1-ylmethyl)benzene (T₂-o-X Ac₂)

A solution of α,α-dibromo-*o*-xylene (0.78 g, 2.95 mmol) in acetonitrile (20 ml) was added dropwise to a solution of 1,4,7-triazatricyclo[5.2.1.0^{4,10}]decane (0.82 g, 5.89 mmol) in acetonitrile (20 ml) with stirring. A cream coloured precipitate started to form almost immediately. After stirring overnight the precipitate was collected by vacuum filtration and dissolved in water (50 ml). The solution was refluxed for 4 hours to generate the bis(formyl) derivative, at which time the solvent was removed. The pH of the yellow solution was adjusted to 12 with 5M NaOH and the product was extracted with CHCl₃ (5 x 50 ml). All the chloroform washings were combined, dried over MgSO₄ and filtered. The solvent was removed *in vacuo* leaving a yellow oil. The oil was dissolved in CH₃CN (50 ml) and bromoethylacetate (0.98 g, 5.89 mmol) and Na₂CO₃ (1 g) were added with stirring. The solution was refluxed for 48 hours. It was cooled to room temperature and following removal of the precipitate, the solvent was removed from the filtrate at reduced pressure leaving a pale brown residue. This was dissolved in 4M HCl (50 ml) and refluxed for 6 hours. The solution was taken to dryness *in vacuo* yielding a pale brown sticky residue. Since attempts to further purify

the product were unsuccessful, the residue was used directly in the synthesis of complexes.

Crude yield: 1.69 g (82%). IR (KBr, ν cm^{-1}): 3442s br, 2966s, 1721s, 1460s, 1209m, 1080m, 749w, 604w. ^1H NMR (D_2O) selected peaks: δ 3.14 (m, CH_2 tacn ring), 3.36 (m, CH_2 tacn ring), 3.51 (m, CH_2 tacn ring), 3.58 (s, CH_2 pendant arm), 3.92 (m, CH_2 bridge), 7.71 (2H, m, ArCH), 7.89 (2H, m, ArCH). ^{13}C NMR (D_2O) selected peaks: δ 40.39 (CH_2), 42.08 (CH_2), 42.78 (CH_2), 46.95 (CH_2), 48.59 (CH_2), 50.10 (CH_2), 54.64 (CH_2), 55.83 (CH_2), 128.98 (quaternary C), 132.53 (ArCH), 133.14 (ArCH), 133.42 (ArCH), 175.26 (CO).

**1,3-Bis(4-(carboxymethyl)-1,4,7-triazacyclonon-1-ylmethyl)benzene
hexahydrochloride (T_2 -*m*-X $\text{Ac}_2 \cdot 6\text{HCl}$)**

T_2 -*m*-X $\text{Ac}_2 \cdot 6\text{HCl}$ was prepared using the same procedure as T_2 -*o*-X $\text{Ac}_2 \cdot 6\text{HCl}$, using 1,4,7-triazatricyclo[5.2.1.0^{4,10}]decane (0.88 g, 6.32 mmol) and α,α -dibromo-*m*-xylene (1.05 g, 3.94 mmol).

Crude yield: 1.64 g (60%). IR (KBr, ν cm^{-1}): 3426s br, 2966s, 1722s, 1447m, 1405s, 1170m, 1078m, 1022m, 750w, 684w, 604w. ^1H NMR (D_2O) selected peaks: δ 3.15, (m, CH_2 tacn ring), 3.35 (m, CH_2 tacn ring), 3.54 (m, CH_2 tacn ring), 3.61 (s, CH_2 pendant arm), 3.90 (m, CH_2 bridge), 7.79 (m, ArCH). ^{13}C NMR (D_2O) selected peaks: δ 40.59 (CH_2), 42.82 (CH_2), 43.55 (CH_2), 47.24 (CH_2), 48.80 (CH_2), 50.34 (CH_2), 54.61 (CH_2), 56.94 (CH_2), 128.91 (quaternary C), 130.78 (ArCH), 132.24 (ArCH), 133.02 (ArCH), 174.72 (CO).

Synthesis of Tris(tacn) Ligand**1,3,5-Tribromomethylbenzene (Br₃mes)**

1,3,5-Trimethylbenzene (13.02 g, 0.11 mol) was dissolved in CCl₄ (100 ml) and *N*-bromosuccinimide (57.84 g, 0.33 mol) was added. The mixture was heated to reflux with stirring and then irradiated with light from a halogen lamp overnight. It was then cooled to room temperature and the succinimide precipitate was removed by vacuum filtration. The solvent was then removed *in vacuo* to yield a yellow solid which was recrystallised from dichloromethane and petroleum spirit giving a cream coloured product.

Yield: 15.82 g (41%). ¹H NMR (CDCl₃): δ 4.46 (6H, s, 3 x CH₂), 7.36 (3H, s, 3 x ArCH). ¹³C NMR (CDCl₃): δ 32.65 (CH₂), 129.79 (ArCH), 139.22 (quaternary C).

1,3,5-Tris(1,4,7-triazacyclonon-1-ylmethyl)benzene nonahydrochloride**(T₃mes.9HCl)**

T₃mes.9HCl was prepared using an analogous procedure as T₂-*o*-X.6HCl, using [5.2.1.0^{4,10}]decane (2.31 g, 16.81 mmol) and Br₃mes (2.00 g, 5.60 mmol).

Yield: 2.30 g (82%). ¹H NMR (D₂O): δ 3.05 (12H, t, bridge-NCH₂CH₂N), 3.34 (12H, t, bridge-NCH₂CH₂N), 3.70 (12H, s, NCH₂CH₂N), 4.01 (6H, s, CH₂ bridge), 7.53 (3H, s, aromatic CH). ¹³C NMR (D₂O): δ 41.11 (CH₂ tacn), 42.62 (CH₂ tacn), 46.22 (CH₂ tacn), 57.00 (CH₂ bridge), 130.70 (ArCH bridge), 135.16 (quaternary C bridge).

2.6 References

- (1) Bereman, R. D., Churchill, M. R., Schaber, P.M., Winkler, M. E. *Inorg. Chem.* **1979**, *18*, 3123.
- (2) Burstyn, J., Deal K. *Inorg. Chem.* **1993**, *32*, 3585.
- (3) Hay, R. W., Govan, N. *Polyhedron* **1998**, *17*, 463.
- (4) Kirk, A. D., Cai, L.-Z. *Inorg. Chem.* **1995**, *34*, 3986.
- (5) Yang, R., Zompa, L. J. *Inorg. Chem.* **1976**, *15*, 1499.
- (6) Koshino, N., Funahashi, S., Takagi, H. D. *J. Chem. Soc., Dalton Trans.* **1997**, 4175.
- (7) Farrugia, L. J., Lovatt, P. A., Peacock, R. D. *J. Chem. Soc., Dalton Trans.* **1997**, 911.
- (8) Graham, B., Grannas, M. J., Hearne, M. T. W., Kepert, C. M., Spiccia, L., Skelton, B. W., White, A. H. *Inorg. Chem.* **2000**, *39*, 1092.
- (9) Spiccia, L., Graham, B., Hearn, M. T. W., Lazarev, G., Moubaraki, B., Murray, K. S., Tiekink, E. R. T. *J. Chem. Soc., Dalton Trans.* **1997**, 4089.
- (10) Kimura, E., Kodama, Y., Koike, T., Shiro, M. *J. Am. Chem. Soc.* **1995**, *117*, 8304.
- (11) Koyama, H., Yoshino, T. *Bull. Chem. Soc. Jpn* **1972**, *45*, 481.
- (12) Di Vaira, M., Mani, F., Stoppioni, P. *J. Chem. Soc., Dalton Trans.* **1994**, 3739.
- (13) Arishima, T., Hamada, K, M., Takamoto, S. *Nippon Kagaku Kaishi* **1973**, 1119.
- (14) Sayer, B. A., Michael, J. P., Hancock, R. D. *Inorg. Chim. Acta* **1983**, *77*, L63.
- (15) Christiansen, L., Hendrickson, D. N., Toftlund, H., Wilson, S. R., Xje, C. L. *Inorg. Chem.* **1986**, *25*, 2813.

-
- (16) Weighardt, K., Schöffmann, E., Nuber, B., Weiss, J. *Inorg. Chem.* **1986**, *25*, 4877.
- (17) Auerbach, U., Eckert, U., Weighardt, K., Nuber, B., Weiss, J. *Inorg. Chem.* **1990**, *29*, 938.
- (18) Biessel, T., Bürger, K. S., Voigt, G., Weighardt, K. *Inorg. Chem.* **1993**, *32*, 124.
- (19) Tanaka, N., Kobayashi, Y., Takamoto, S. *Chem. Lett.* **1977**, 107.
- (20) Weighardt, K., Tolksdorf, I., Herrmann, W. *Inorg. Chem.* **1985**, *24*, 1230.
- (21) Sessler, J. L., Silbert, J. W., Lynch, V. *Inorg. Chem.* **1990**, *29*, 4143.
- (22) Haidar, R., Ipek, M., DasGupta, B., Yousaf, M., Zompa, L. J. *Inorg. Chem.* **1997**, *36*, 3125.
- (23) Zhang, X., Hsieh, W-Y., Margulis, T. N., Zompa, L. J. *Inorg. Chem.* **1995**, *34*, 2883.
- (24) Sessler, J. L., Silbert, J. W., Lynch, V., Markert, J. T., Wooten, C. L. *Inorg. Chem.* **1993**, *32*, 621.
- (25) Graham, B. *PhD Thesis, Department of Chemistry, Monash University.* **1998**.
- (26) Young, M. J., Chin, J. *J. Am. Chem. Soc.* **1995**, *117*, 10577.
- (27) Chang, H., Diril, H., Nilges, M. J., Zhang, X., Potenza, J. A., Schugar, H. J., Hendrickson, D. N., Isied, S. S. *J. Am. Chem. Soc.* **1988**, *110*, 625.
- (28) Behle, L., Neuburger, M., Aehnder, M., Kaden, T. A. *Helv. Chim. Acta* **1995**, *78*, 693.
- (29) Weisman, G. R., Vachon, D. J., Johnson, V. B., Gronbeck, D. A. *J. Chem. Soc., Chem. Commun.* **1987**, 886.
- (30) Beer, P. D., Drew, M. G. B., Leeson, P. B., Lyssenko, K., Ogden, M. I. *J. Chem. Soc., Chem. Commun.* **1995**, 929.

-
- (31) Hanke, D., Weighardt, K., Nuber, B., Lu, R-S., McMullan, R. K., Koetzie, T. F., Bau, R. *Inorg. Chem.* **1993**, *32*, 4300.
- (32) Tolman, W. B. *Acc. Chem. Res.* **1997**, *30*, 227.
- (33) Brudenell, S. J., Spiccia, L., Tiekink, E. R. T. *Inorg. Chem.* **1996**, *35*, 1974.
- (34) Blake, A. J., Donlevy, T. M., Engalnd, P. A., Fallis, I. A., Parsons, S., Ross, S. A., Schröder, M. *J. Chem. Soc., Chem. Commun.* **1994**, 1981.
- (35) Fry, F. H., Graham, B., Spiccia, L., Hockless, D. C. R., Tiekink, E. R. T. *J. Chem. Soc., Dalton Trans.* **1997**, 827.
- (36) Di Vaira, M., Mani, F., Stoppioni, P. *J. Chem. Soc., Dalton Trans.* **1998**, 3209.
- (37) Blake, A. J., Danks, J. P., Li, W-S., Lippolis, V., Schröder, M. *J. Chem. Soc., Dalton Trans.* **2000**, 3034.
- (38) Blake, A. J., Fallis, I. A., Parsons, S., Ross, S. A., Schröder, M. *J. Chem. Soc., Dalton Trans.* **1996**, 525.
- (39) Schultz, D., Weyhermüller, T., Weighardt, K., Nuber, B. *Inorg. Chim. Acta* **1995**, *240*, 217.
- (40) Graham, B., Moubaraki, B., Murray, K. S., Spiccia, L., Cashion, J. D., Hockless, D. C. R. *J. Chem. Soc., Dalton Trans.* **1997**, 887.
- (41) Kovacs, Z., Sherry, D. *Tetrahedron Lett.* **1995**, *36*, 9269.
- (42) Fortier, D. G., McAuley, A. *J. Chem. Soc., Dalton Trans.* **1991**, 101.
- (43) Farrugia, L. J., Lovatt, P. A., Peacock, R. D. *Inorg. Chim. Acta* **1996**, *246*, 343.
- (44) Blake, A. J., Fallis, I. A., Gould, R. O., Parsons, S., Ross, S. A., Schröder J. *J. Chem. Soc., Chem. Commun.* **1994**, 2467.
- (45) Graham, B., Fallon, G. D., Hearn, M. T. W., Hockless, D. C. R., Lazarev, G., Spiccia, L. *Inorg. Chem.* **1997**, *36*, 6366.

-
- (46) Atkins, T. J. *J. Am. Chem. Soc.* **1980**, *102*, 6364.
- (47) Kimura, E., Aoki, S., Koike, T., Shiro, M. *J. Am. Chem. Soc.* **1997**, *119*, 3068.
- (48) Vogtle, F., Zuber, M., Lichtenthaler, R.G. *Chem. Ber.* **1973**, *106*, 717.
- (49) Brudenell, S. L. *Honours Thesis, Department of Chemistry, Monash University*,
1993.

Chapter Three

Synthesis and Characterisation of Copper(II) Complexes of 1,4,7-triazacyclononane Derivatives

3.1 Introduction

Copper complexes are the most extensively studied of all the transition metals. Most research has focussed on the 2+ oxidation state and to a lesser degree, the 1+ and 3+ oxidation states. The coordination number of copper(II) complexes ranges from 4 to 6, with the normally less favoured coordination number of 5 being quite common. Four-coordinate copper(II) complexes form both square planar and distorted tetrahedral complexes, 5-coordinate complexes range from trigonal bipyramidal to square pyramidal geometries, while 6-coordinate complexes form distorted octahedral complexes. The d^9 configuration of copper(II), makes it subject to Jahn-Teller distortion. The distortion is generally elongation along one axis, the result being, in an octahedral environment, four short bonds and two longer transoid bonds.¹

The copper ion is found in 1+, 2+ and 3+ oxidation states in the active site in a number of enzymes, which are involved in cellular transport or catalysing the transfer of dioxygen to various substrates, processes that involves changes in the oxidation states of copper. These include haemocyanin, which has two Cu(I) ions and reversibly binds dioxygen, superoxide dismutase, which contains one copper and one zinc ion and converts superoxide to dioxygen and hydrogen peroxide, ascorbate oxidase, a tricopper enzyme which oxidises ascorbate, galactose oxidase, a mononuclear enzyme which is involved in the oxidation of primary alcohols to aldehydes and cytochrome oxidase, an

Chapter Three

enzyme which has a copper and an iron ion in the active site and which converts O_2 to H_2O .²

The small tridentate macrocycle 1,4,7-triazacyclononane has been used extensively in the synthesis of small model compounds for the active sites of enzymes.³⁻⁹ The very high thermodynamic and kinetic stability that these complexes exhibit (stability constant, $\log K = 15.5$)¹⁰, together with the fact that coordination sites are available on the metal centre for the coordination of substrates and small molecules (e.g. O_2), make such ligands ideal candidates for conducting biomimetic studies.

The isolation of a Cu(II) tacn complex was first reported by Bereman *et al.* in 1979, who reported the structure of $[Cu(tacn)Br_2]$.¹¹ followed shortly after by the analogous chloride complex (Figure 3.1, A).¹² The copper(II) centres were found to be 5-coordinate, adopting a distorted square pyramidal (SP) geometry, with one of the nitrogens occupying the apical site, and the other two lying in the basal plane. This is a feature of all Cu(II) complexes incorporating tacn and its derivatives. The Cu(II) complex with two tacn units, $[Cu(tacn)_2]^{2+}$, was reported shortly afterwards.^{13,14} In this case, the Cu(II) centre is sandwiched between the two tacn rings, residing in a distorted octahedral environment due to Jahn-Teller distortion (Figure 3.1, B). Since then, a multitude of Cu(II) complexes of tacn and its derivatives have appeared in the literature.¹⁵⁻²⁵

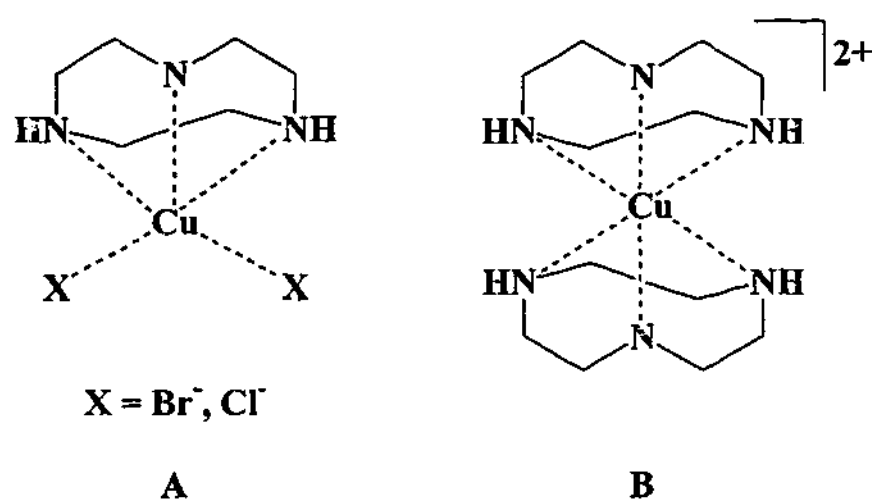


Figure 3.1 Two types of Cu(II) complexes formed by 1,4,7-triazacyclononane (tacn)

Isolation of the first copper(II) complex with a bis(tacn) ligand was achieved by Wieghardt and coworkers, who reported both the mono- and binuclear complex of dtne, a ligand in which two tacn moieties are linked by an ethane bridge (Figure 3.2, A and B, $n=2$).²⁶ Since this report a host of new copper(II) complexes have been synthesised which incorporate ligands with two or more tacn assemblies. Zompa and coworkers extended this work by preparing a series of bis(tacn) copper(II) complexes with polymethylene bridges, with the number of carbons in the chain ranging from $n=2-8$ (Figure 3.2, A and B).^{20,27} Equilibrium measurements (by pH titrations) of the complexes in aqueous solution found that stable 1:1 and 2:1 complexes are formed when $n=3-8$, while $n=2$ forms only the sandwich structure in dilute solution. Those complexes of ligands with $n=4-8$ were more likely to form dimeric (Figure 3.2 C) or oligomeric species in solution. Crystal structures were obtained of $[CuL]SO_4 \cdot 6H_2O$ and $[Cu_2LCl_4] \cdot 2H_2O$ for $n=2$, $[CuL][ZnCl_4] \cdot H_2O$ for $n=3$ and $[Cu_2LCl_4]$ for $n=6$ and 8 .^{20,27,28} Other copper(II) complexes of bis(tacn) have included those of ligands with naphthalene²⁹ (Figure 3.2 D) and xylene bridges, which in one example also contains additional exogenous hydroxyl bridging groups (Figure 3.2 E).^{15,20,30}

Chapter Three

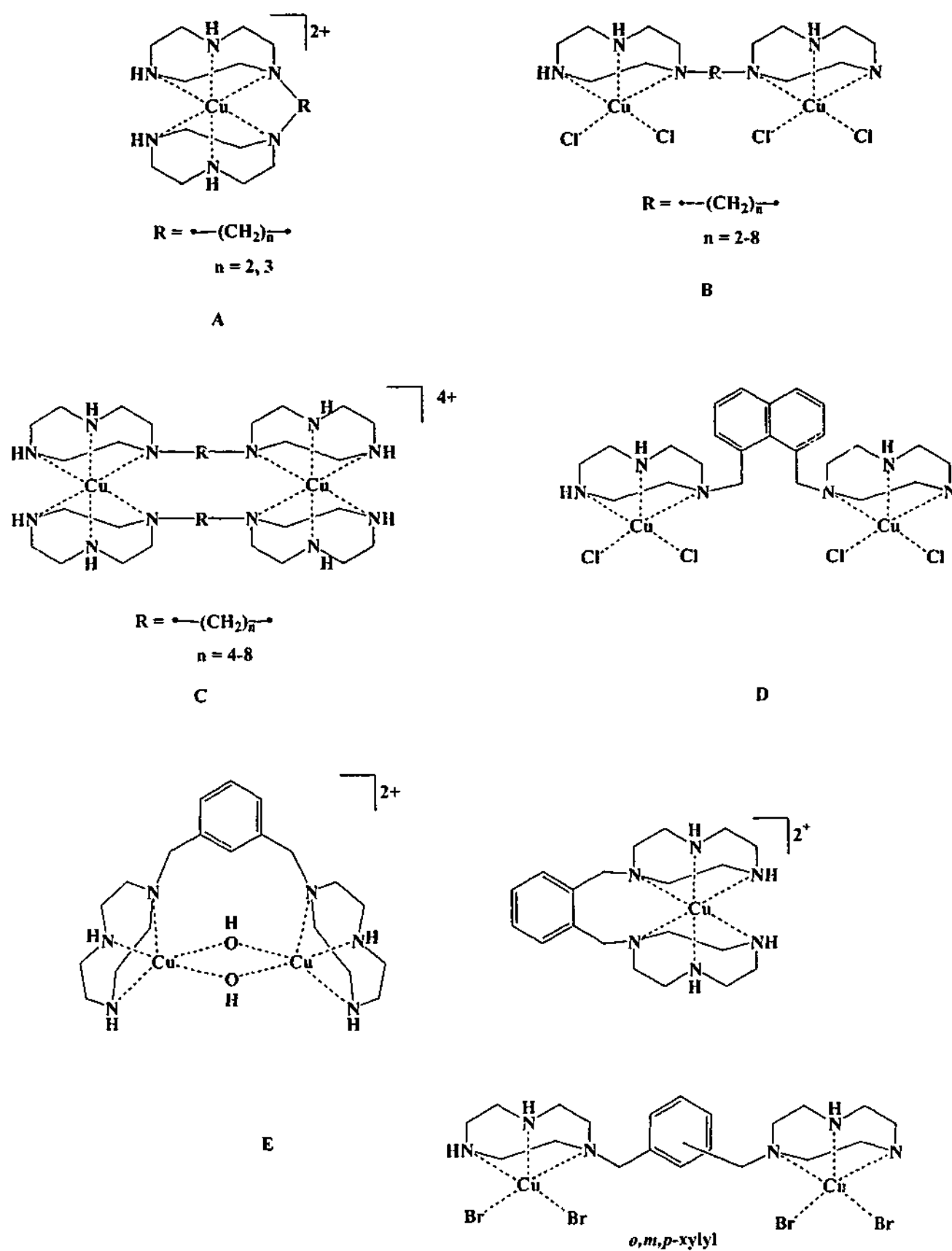


Figure 3.2 Cu(II) complexes of several bis(tacn) ligands^{15,20,26-28,30}

Chapter Three

The study of the copper(II) complexes of *N*-functionalised bis(tacn) ligands is an area that has been expanding in recent years. Such pendant arms have included the non-coordinating isopropyl groups, the complexes of which have been used in studies of the binding of dioxygen (Figure 3.3 A),³¹ and those with coordinating groups such as alcohol³² (Figure 3.3 B), pyridylmethyl,¹⁶ (Figure 3.3 C), acetate³³ (Figure 3.3 D) and amine (Figure 3.3 E).³⁴ In these complexes, the Cu(II) centres are in a five-coordinate, distorted SP environment, with the apical site occupied by the bridgehead nitrogen. In each ligand, the amines in the tacn backbone are functionalised, and in the case of the coordinating pendant arms, the propensity of the Cu(II) centre to form 5-coordinate complexes means that there are no free sites available for coordination and activation of other molecules, such as a substrate.

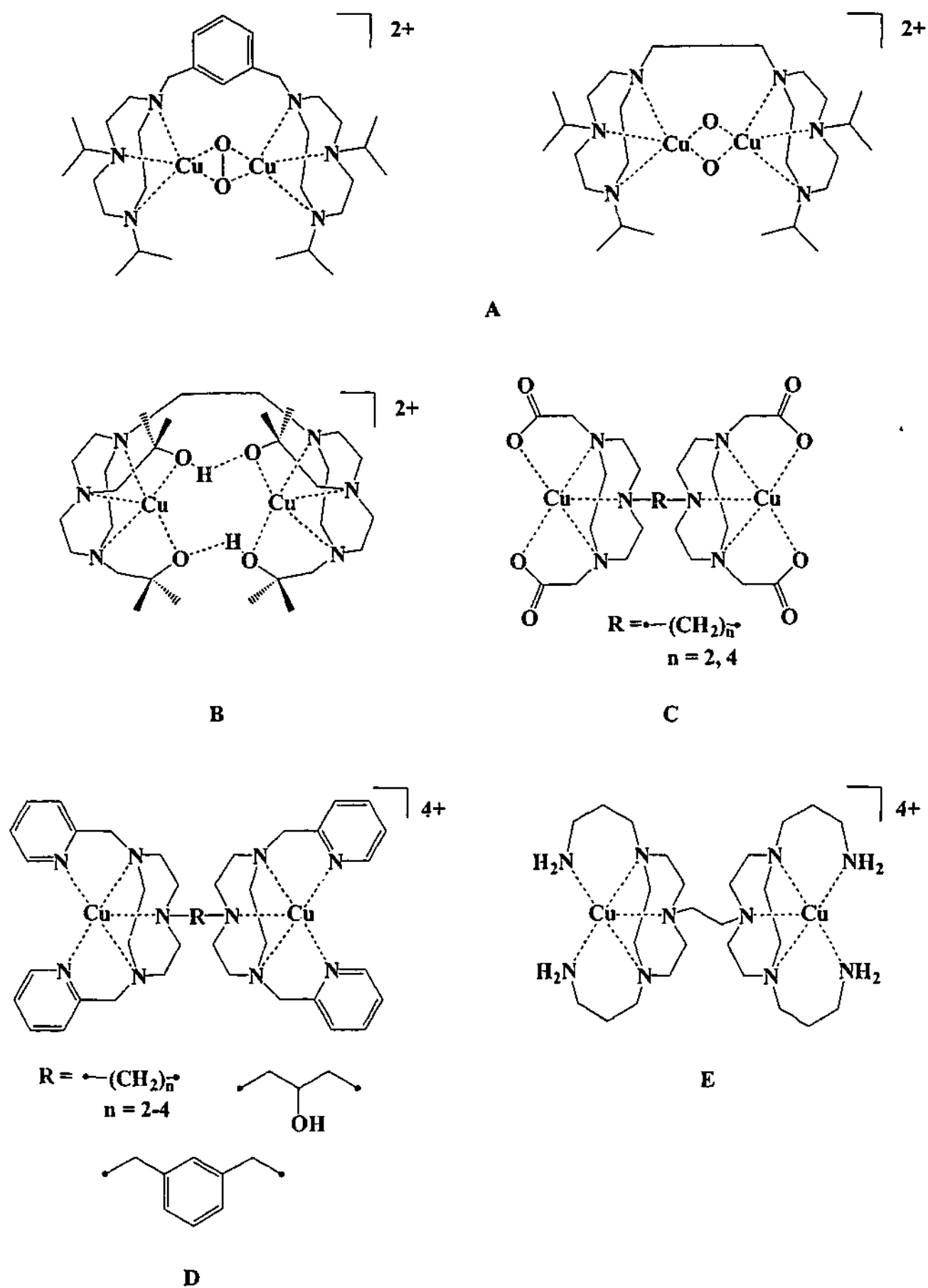


Figure 3.3 Copper(II) complexes of bis(tacn) ligands with pendant arms^{16,31-34}

Chapter Three

Copper(II) complexes of poly(tacn) species are far less common, and have only recently been reported.^{6,35} Copper(II) complexes of a tris(tacn) ligand assembled around a mesitylene bridge and a tetrakis(tacn) ligand coordinated around a durene bridge have been prepared and their properties studied.^{35,36} The tris(tacn) ligand has been used to generate three different metal complexes, two binuclear and one hexanuclear, depending on the pH of the solution from which they were crystallised (Figure 3.4).³⁶ One trinuclear complex (A) has no bridges between the Cu(II) centres, while in the other (B), two Cu(II) centres are linked by two OH⁻ bridges. When two molecules of (B) are linked together by further OH⁻ bridges, a hexanuclear Cu(II) complex forms (C).³⁶ For the tetrakis(tacn) ligand, four complexes have been reported.³⁵ Addition of two moles of Cu(II) to one mole of ligand produces a complex in which one Cu(II) centre is sandwiched between two tacn rings, generating a binuclear structure (Figure 3.4 D). Alternatively, addition of four moles of Cu(II) to one mole of ligand produces a tetranuclear complex with one Cu(II) centre bound to each tacn ring (Figure 3.4 E). Increasing the pH of the latter complex leads to the formation of hydroxo-bridges between the *meta* pairs of Cu-tacn units (Figure 3.4 F). A related compound was made by the addition of N₃⁻ producing a tetranuclear compound in which the *meta* Cu(II)-tacn units are linked by N₃⁻ (Figure 3.4 G).³⁷

Chapter Three

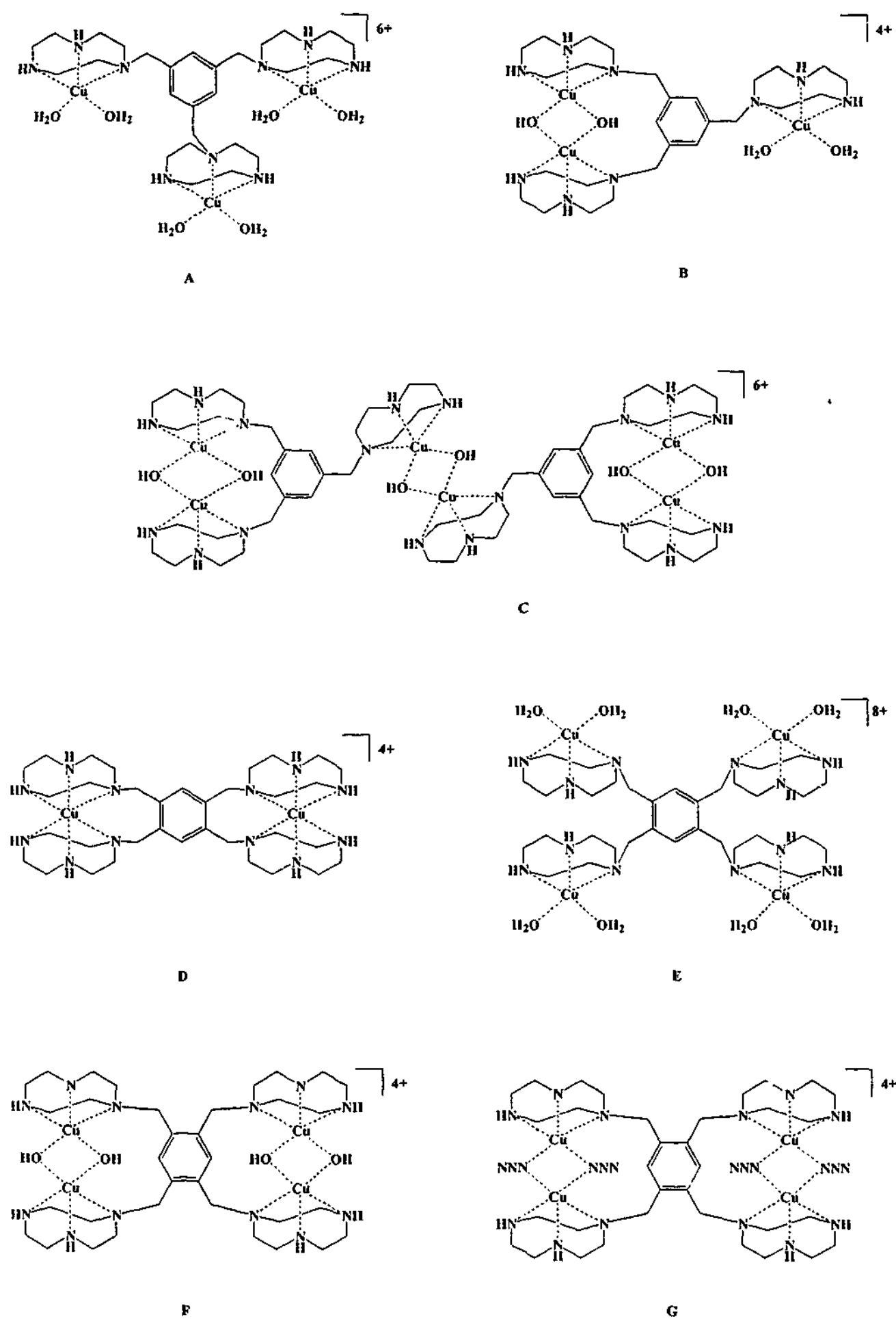


Figure 3.4 Copper(II) complexes of poly(tacn) ligands³⁵⁻³⁷

Chapter Three

In order to further develop the chemistry of polynuclear Cu(II) complexes based on ligands incorporating tacn, copper(II) complexes of the ligands described in Chapter 2 were prepared and characterised. Analysis by single crystal studies, showed the binuclear nature of many of these complexes. Since a major objective of this work was to develop new complexes that catalyse the cleavage of phosphate esters, a number of complexes incorporating phosphate esters were prepared and characterised. These phosphate complexes have been examined by X-ray crystallography to determine the preferred coordination mode of the phosphate ester, and by physicochemical methods to probe whether the phosphato bridges promote electronic interactions between the Cu(II) centres.

3.2 Complexes of bis(tacn) ligands

3.2.1 Preparation of Complexes

Copper(II) complexes of the ligands T_{2-o-X} , T_{2-m-X} and T_{2-p-X} (see Figure 3.5) were synthesised by addition of aqueous solutions of the hexahydrochloride salt of the ligands to two equivalents of either $Cu(ClO_4)_2 \cdot 6H_2O$ or $CuCl_2$ in water and adjusting the pH to *ca.* 5. Dark blue solutions of the complexes resulted. The solution of T_{2-m-X} with copper was purified by cation exchange chromatography using 0.4 M $NaClO_4$ as the eluent. For the case of T_2PrOH , the hexahydrobromide salt of the ligand was used and two molar equivalents of $CuBr_2$ were added. The pH of the solution were adjusted to *ca.* 5 with 1M NaOH and any precipitate of copper hydroxide was removed by filtration, resulting in dark blue solutions of the copper complex. Crystals of $[Cu_2(T_{2-p-X})Cl_4]$ (3) and $[Cu_2(T_2-PrO)Br_2]Br \cdot 2H_2O$ (4) were grown by slow evaporation of the solutions, while all other complexes precipitated as blue powders from the solutions. The yields of the complexes ranged from 27 to 63%.

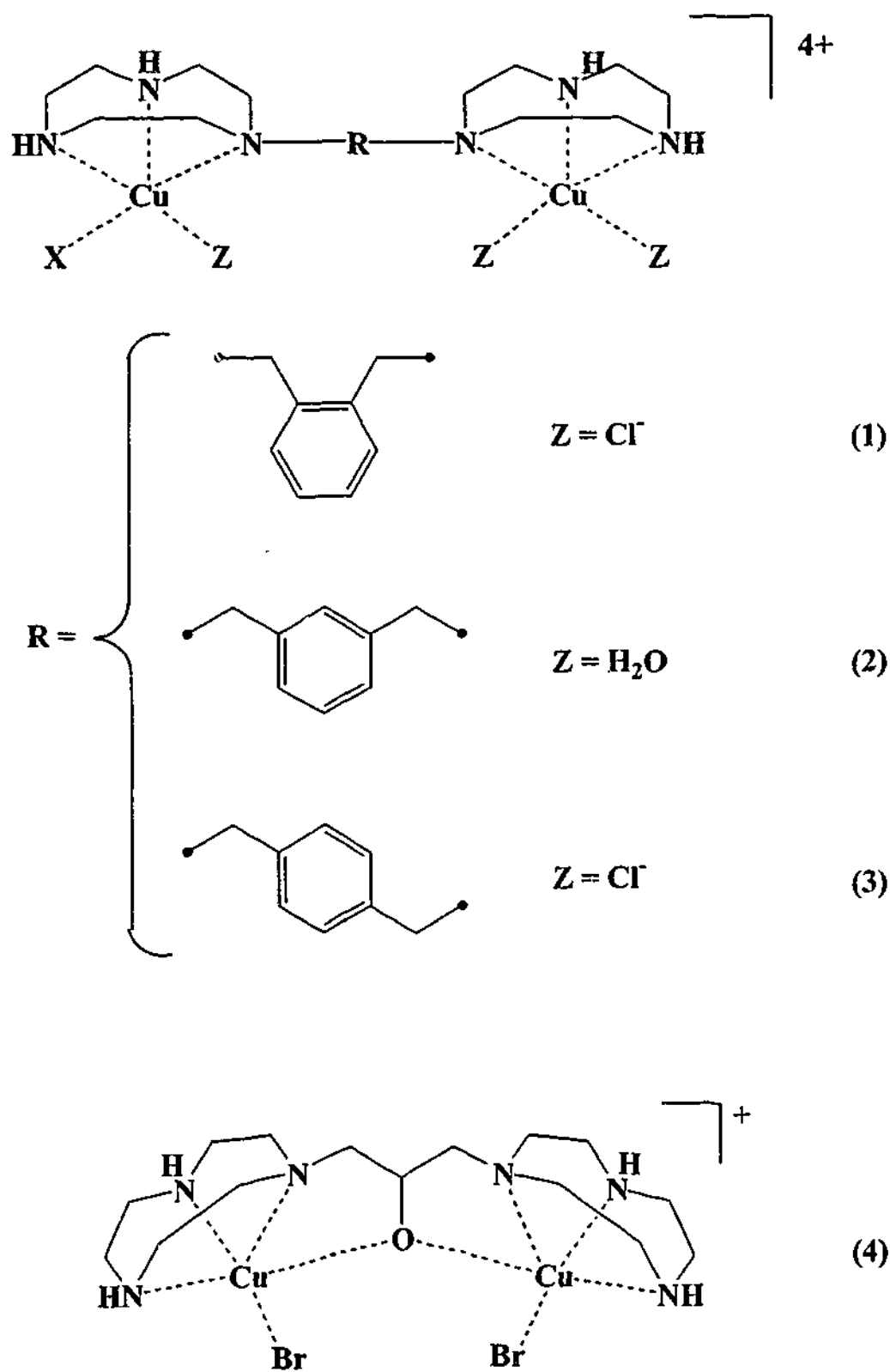


Figure 3.5 Copper (II) complexes of T₂-(*o*, *m*, *p*)-X and T₂-PrOH ligands

The IR spectra of the complexes show sharp absorptions due to the NH stretch of the tacn ring in the region of 3216 - 3335 cm⁻¹ and compound 2 showed bands at 1086 and 625 cm⁻¹ due to the perchlorate counter ions. Compounds 1 - 3 show bands in the

Chapter Three

fingerprint region due to stretching frequencies of the aromatic ring in the bridging group of the ligands. Microanalytical data for the complexes support the formulae displayed in Table 3.1. The molar conductivities are consistent with the proposed structures.

Table 3.1 Elemental data for compounds 1-4

Calculated values are given in parentheses

Complex	C (%)	H (%)	N (%)
1 [Cu ₂ (T _{2-o} -X)Cl ₄]	37.9 (38.2)	5.9 (5.8)	13.2 (13.4)
2 [Cu ₂ (T _{2-m} -X)(H ₂ O) ₄](ClO ₄) ₄ .3H ₂ O.NaClO ₄	21.2 (21.2)	4.3 (4.4)	7.4 (7.4)
3 [Cu ₂ (T _{2-p} -X)Cl ₄]	37.6 (38.2)	5.9 (5.8)	13.4 (13.4)
4 [Cu ₂ (T _{2-Pr} O)Br ₂] ₂ Br.2H ₂ O	25.5 (25.2)	5.1 (5.2)	11.4 (11.7)

3.2.2 Crystal Structure of [Cu₂(T_{2-p}-X)Cl₄] (3)

A crystal structure determination of **3** was undertaken to confirm the binuclear nature of the complex. Cell parameters and details of the data collection are presented in section 1.1 of the Appendix. The crystals consist of discrete [Cu₂(T_{2-p}-X)Cl₄] units. An ORTEP plot of the complex is shown in Figure 3.6, while selected bond lengths and angles are shown in Table 3.2.

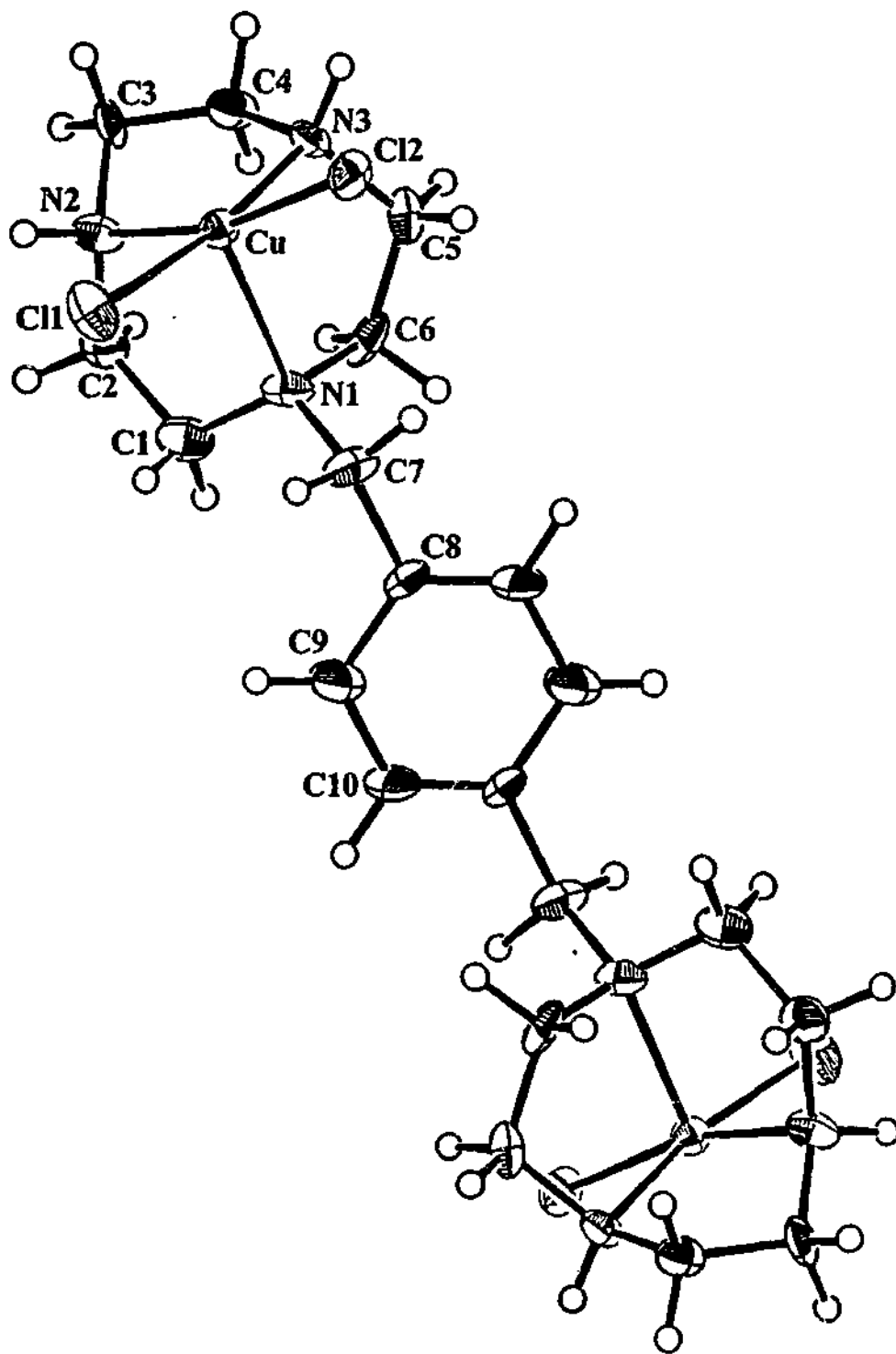


Figure 3.6 ORTEP plot of [Cu₂(T₂-p-X)Cl₄] (3) with atomic labelling scheme

Table 3.2 Selected bond distances (Å) and angles (°) for [Cu₂(T₂-p-X)Cl₄] (3)

Cu-N(1)	2.250(8)	Cu-Cl(1)	2.270(3)
Cu-N(2)	2.02(1)	Cu-Cl(2)	2.284(4)
Cu-N(3)	2.046(8)		
Cl(1)-Cu-Cl(2)	95.3(1)	Cl(2)-Cu-N(2)	166.3(2)
Cl(1)-Cu-N(1)	102.9(3)	Cl(2)-Cu-N(3)	90.2(3)
Cl(1)-Cu-N(2)	89.4(3)	N(1)-Cu-N(2)	82.9(4)
Cl(1)-Cu-N(3)	170.4(3)	N(1)-Cu-N(3)	82.7(3)
Cl(2)-Cu-N(1)	108.4(3)	N(2)-Cu-N(3)	83.5(4)

Complex 3 is centrosymmetric about the centre of the xylene aromatic ring, with the coordinated copper(II) centres lying on opposite sides of the structure, thus exhibiting a *anti*-conformation. As a consequence, the Cu...Cu separation is large at 11.81 Å. The copper(II) centres are in a distorted SP environment, with the basal plane defined by the two Cl atoms, Cl(1) and Cl(2), and the two secondary nitrogens, N(2) and N(3). An effective means of quantifying the degree of distortion in five-coordinate Cu(II) complexes was developed by Addison *et al.*³⁸ The defining parameter, τ , measures the degree of distortion from SP to TBP, where τ is zero for a regular SP and unity for an ideal TPB geometry. The value of τ for 3 was found to be 0.07, indicating there is little distortion towards TBP from the SP geometry. The bridgehead nitrogen, N(1), occupies the apical position. The mean deviation of Cl(1), Cl(2), N(2) and N(3) from their least-squares plane is 0.045 Å and the copper(II) centre lies 0.188(1) Å above this plane, towards N(1). The Cu-Cl distances of 2.270(3) and 2.284(4) Å are typical of such coordinations.³⁹ The Cu-N distances in the basal plane of 2.02(1) and 2.046(8) Å, are shorter than the Cu-N(apical) distance of 2.250 Å. This feature is typical of copper in a SP coordination environment and reflects the Jahn-Teller distortion exhibited by the d⁹ copper(II) atom.³³

Chapter Three

Bond angles reflect the constraints induced by the tacn ring, with N-Cu-N angles all below 90° , N(1)-Cu-N(2), N(1)-Cu-N(3) and N(2)-Cu-N(3) being $82.9(4)^\circ$, $82.7(3)^\circ$ and $83.5(4)^\circ$ respectively. The other two *trans* angles, Cl(1)-Cu-N(2) and Cl(2)-Cu-N(3) ($166.3(2)^\circ$ and $170.4(3)^\circ$ respectively) are below the value of 180° expected for a perfect SP environment; again this is due to the constraints by the tacn ring.

As can be seen from Figure 3.7, there are some associations between the molecules within the crystal. The hydrogen bonded to C(4) is separated from a symmetry related Cu(II) centre (symmetry operation: $x, \frac{3}{2}-y, -\frac{1}{2}+z$) by $3.719(11)$ Å and the angle subtended at H is 175° . These interactions form a zig-zag pattern within the crystal lattice. Each coordination geometry accepts one of these H atoms from a neighbouring molecule, and also donates to another molecule, translated along the *c* axis. Therefore, each molecule (containing two copper(II) centres) is involved in two acceptor and two donor interactions. These associations lead to the formation of a layer structure, stacked along the *a* axis. The zig-zag chains are reinforced by weak N-H...Cl and C-H...Cl. Interactions: N(3)-H...Cl(2) is 2.60 Å, N(3)...Cl(2) is 3.380 Å with the bonds centred about H at 139° (symmetry operation: $x, \frac{3}{2}-y, -\frac{1}{2}+z$). These interactions link the molecules together in the same way as the associations mentioned above. Translationally related molecules are linked together by C-H...Cl interactions (distances: C(2)-H...Cl(1) 2.73 Å, C(2)...Cl(1) $3.705(10)$ Å, and the angle about the H is 176° (symmetry operation: $x, y, 1+z$) and, distances: C(4)-H...Cl(1) 2.78 Å, C(4)...Cl(1) $3.688(14)$ Å, and the angle about the H is 156° (symmetry operation: $x, y, 1+z$)). The links between the layers are provided by interactions between N(2)-H...Cl(2) (distances: N(2)-H...Cl(2) 2.50 Å, N(2)...Cl(2) $3.293(12)$ Å, and the angle about the H is 141° (symmetry operation: $\frac{1}{2}+x, y, \frac{1}{2}-z$)).

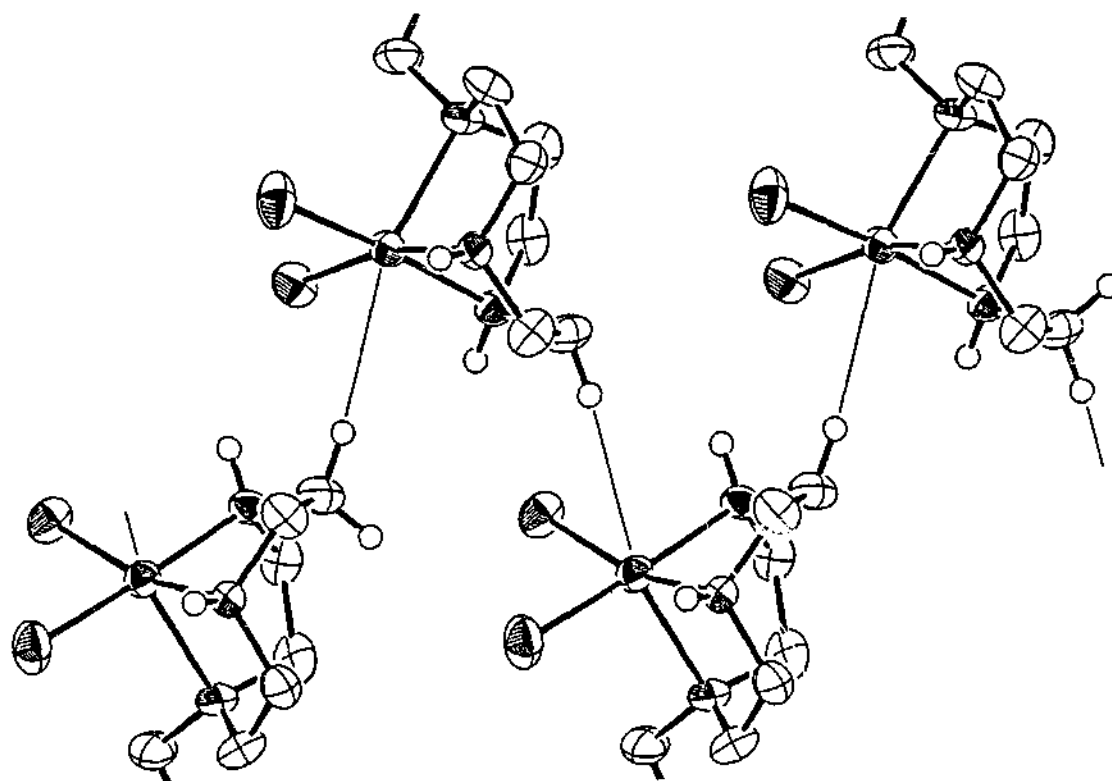


Figure 3.7 Partial molecular packing diagram of $[\text{Cu}_2(\text{T}_2\text{-}p\text{-X})\text{Cl}_4]$ (3) showing interactions between molecules

Comparison between this structure and other Cu-tacn-chloride complexes reveal similar features (see Table 3.3). $[\text{Cu}(\text{tacn})\text{Cl}_2]$ ¹², as well as other polynuclear tacn species such as $[\text{Cu}_2(\text{T}_2\text{-prop})\text{Cl}_4] \cdot 2\text{H}_2\text{O}$ ($\text{T}_2\text{-prop}$ = 1,3-bis(1,4,7-triazacyclonon-1-yl)propane) and $[\text{Cu}_2(\text{T}_2\text{-but})\text{Cl}_4]$ ($\text{T}_2\text{-but}$ = 1,3-bis(1,4,7-triazacyclonon-1-yl)butane)²⁸ all show copper to reside in distorted SP geometry, and in the case of the bis(tacn), the bridgehead nitrogen occupies the apical site, while the chlorides and the secondary nitrogens occupy the sites in the basal plane. The bond distances from the copper centre to the coordinated atoms are virtually identical to the distances quoted for the mononuclear species. This illustrates the propensity of the tacn macrocycle to form complexes with SP rather than TBP geometries.

Chapter Three

Table 3.3 Comparison of **3** with other Cu-tacn-chloride species

Bond Lengths (Å)	3	[Cu(tacn)Cl ₂] ¹²	[Cu ₂ (T ₂ -but)Cl ₄] ²⁸
Cu-N(apical)	2.250(8)	2.246	2.285(3)
Cu-N(basal)	2.02(1)	2.037	2.034(4)
	2.046(8)	2.062	2.061(4)
Cu-Cl	2.270(3)	2.267	2.26(1)
	2.284(4)	2.312	2.301(1)
Bond Angles (°)			
N(apical)-Cu-N(basal)	82.9(4)	82.96	81.9(1)
	82.7(3)	82.62	82.4(1)
N(basal)-Cu-N(basal)	83.5(4)	82.25	82.9(1)
N(apical)-Cu-Cl	102.9(3)	105.88	100.4(1)
	108.4(3)	107.24	113.5(1)
N(basal)-Cu-Cl	89.4(3)	90.50	88.3(1)
	90.2(3)	91.0	91.5(1)
	166.3(2)	167.03	161.1(1)
	170.4(3)	168.21	173.3(1)

3.2.3 Crystal Structure of [Cu₂(T₂-PrO)Br₂].2H₂O (**4**)

X-ray crystallography of **4** was undertaken to confirm the binuclear nature of the complex. Cell parameters and details of the data collection for complex **4** are presented in section 1.2 of the Appendix. The crystal consisted of discrete [Cu₂(T₂-PrO)Br₂] units, a bromide counter ion and waters of crystallisation. A selection of bond lengths and angles are given in Table 3.4, while a plot of the ORTEP diagram is given in Figure 3.8 and the extended packing array is shown in Figure 3.9.

Chapter Three

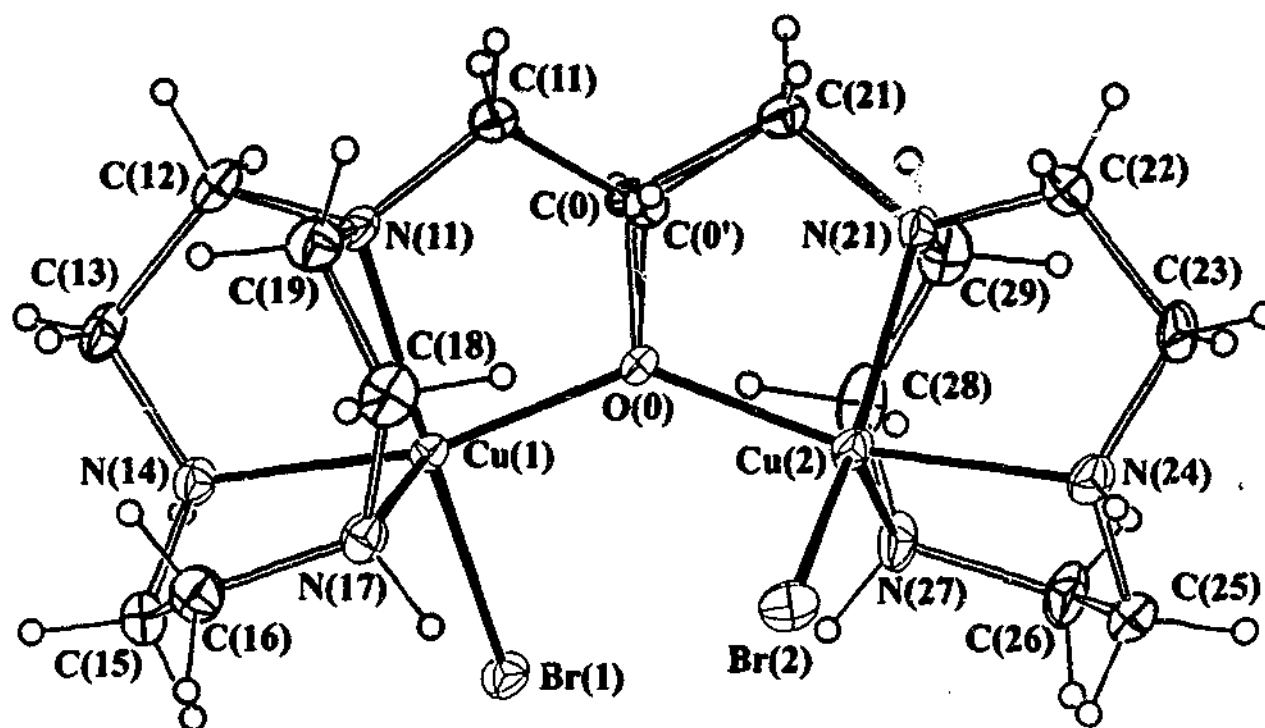


Figure 3.8 ORTEP plot of $[\text{Cu}_2(\text{T}_2\text{-PrO})\text{Br}_2]\cdot\text{Br}\cdot 2\text{H}_2\text{O}$ (4) with atomic labelling scheme

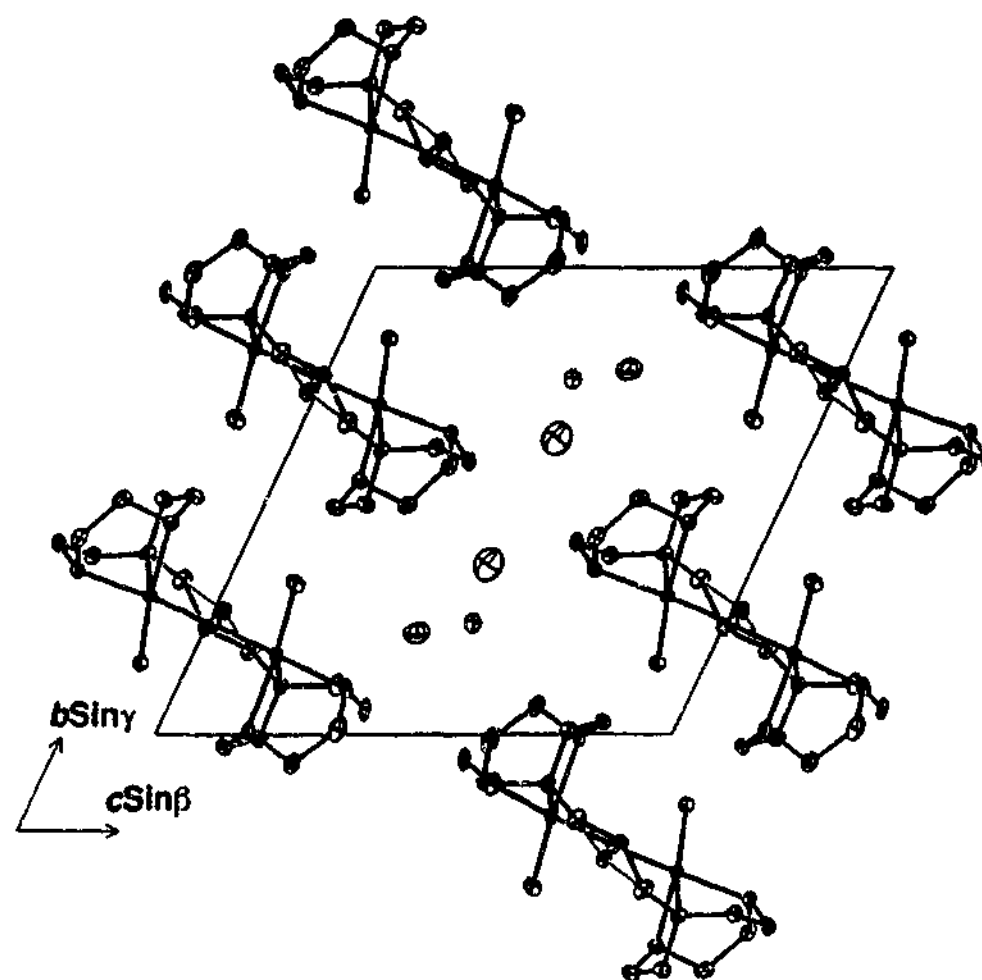


Figure 3.9 Extended packing diagram for $[\text{Cu}_2(\text{T}_2\text{-PrO})\text{Br}_2]\cdot\text{Br}\cdot 2\text{H}_2\text{O}$ (4)

Chapter Three

Table 3.4 Selected bond distances (Å) and angles(°) for [Cu₂(T₂-PrO)Br₂]Br·2H₂O (4)

Cu(1)-N(11)	2.087(5)	Cu(2)-N(21)	2.088(5)
Cu(1)-N(14)	2.015(6)	Cu(2)-N(24)	2.018(6)
Cu(1)-N(17)	2.195(6)	Cu(2)-N(27)	2.175(7)
Cu(1)-Br(1)	2.425(1)	Cu(2)-Br(2)	2.432(1)
Cu(1)-O(0)	2.046(8)	Cu(2)-O(0)	1.930(4)
<hr/>			
N(11)-Cu(1)-N(14)	83.7(2)	N(21)-Cu(2)-N(24)	83.9(2)
N(11)-Cu(1)-N(17)	83.9(2)	N(21)-Cu(2)-N(27)	84.6(2)
N(11)-Cu(1)-Br(1)	164.4(2)	N(21)-Cu(2)-Br(2)	149.1(2)
N(11)-Cu(1)-O(0)	83.9(2)	N(21)-Cu(2)-O(0)	82.4(2)
N(14)-Cu(1)-N(17)	82.8(2)	N(24)-Cu(2)-N(27)	82.7(3)
N(14)-Cu(1)-Br(1)	93.4(2)	N(24)-Cu(2)-Br(2)	94.1(2)
N(14)-Cu(1)-O(0)	164.2(2)	N(24)-Cu(2)-O(0)	165.9(2)
N(17)-Cu(1)-Br(1)	110.0(1)	N(27)-Cu(2)-Br(2)	125.9(2)
N(17)-Cu(1)-O(0)	105.7(2)	N(27)-Cu(2)-O(0)	99.3(2)
Br(1)-Cu(1)-O(0)	96.1(1)	Br(2)-Cu(2)-O(0)	95.9(1)
Cu(1)-O(0)-Cu(2)	136.2(2)		

The crystal structure of **4** confirmed the presence of an endogenous alkoxo bridge between the Cu(II) centres. The copper coordination sphere is completed by three nitrogens from the tacn ring and one bromide ligand. The two Cu(II) centres lie in a slightly different environment. The Cu(1) centre is in a slightly distorted SP environment ($\tau = 0.003$), with the apical site occupied by N(17), a secondary nitrogen. This is strikingly different from the other bis(tacn) species studied thus far, where the apical site has generally been occupied by the bridgehead nitrogen. In **4**, the basal plane is defined by the remaining nitrogens, N(11) and N(14), the bridging oxygen, O(0) and Br(1). The Cu-N distances in the basal plane of 2.015(6) and 2.087(5) Å, as well as the Cu(1)-O(0) distance of 2.046(8) Å are shorter than the Cu-N(apical) distance of 2.195(6) Å due to the Jahn-Teller distortion of Cu(II) centre.³³ The Cu(1)-Br(1) distance is longer at 2.425 Å but is typical of Cu-Br distances.^{11,15} As a consequence of the bridging oxygen between the two Cu(II) centres, the Cu...Cu distance is quite short

(3.57 Å). The same ligand was synthesised by Sessler *et al.* and used to make an oxo-bridged iron cluster.³⁹ Although a more complicated structure, forming a tetramer, with oxo- and hydroxo-bridges between the individual [Fe(III)₂(T₂PrO)] units, the oxygen within the ligand was also found to form an endogenous bridge between two iron centres. The Fe...Fe distances are comparable to **4** with separations of 3.510(2) and 3.513(2) Å. Complexes isolated by Tolman where two [Cu(ⁱPr₃tacn)]²⁺ (ⁱPr₃tacn = 1,4,7-triisopropyl-1,4,7-triazacyclononane) units are linked by endogenous peroxo or bis(μ-oxo) bridges,³¹ have Cu...Cu distances ranging from 2.91 to 3.18 Å, which is shorter than those found for **4** and by Sessler. Another copper(II) complex isolated by Graham *et al.* has two of the Cu(II) centres bridged by hydroxo as well as a phosphato bridge. The distance between the two copper centres in this complex are very similar to that of **4**, being 3.55 Å. Other copper complexes which have been isolated that have exogenous dihydroxo bridges between copper centres have Cu...Cu distances less than that of **4**. Weighardt and coworkers isolated the complex [(Me₃tacn)Cu(μ-OH)₂Cu(Me₃tacn)]²⁺²⁴ which had a Cu...Cu distance of 2.971(1) Å, and a second complex crystallised by Peacock and coworkers, [Cu₂(T₂-*m*-X)(μ-OH)₂]²⁺, had a Cu...Cu distance of 2.95 Å.

The bond angles again reflect the constraints imposed by the tacn ring, with all the angles below the ideal of 90°, being 83.7(2)°, 83.9(2)° and 82.8(2)° for N(11)-Cu(1)-N(14), N(11)-Cu(1)-N(17) and N(14)-Cu(1)-N(17), respectively. Other bond angles are also smaller than the expected values for a perfect SP geometry, with N(11)-Cu(1)-Br(1) and N(14)-Cu(1)-O(0) both below 180°, at 165.4(2)° and 164.2(2)°, respectively.

Chapter Three

The coordination geometry of the second copper ion, Cu(2), is significantly more distorted than that of Cu(1). Again, the apical site is occupied by a secondary nitrogen, N(27) instead of the usual bridgehead nitrogen, and the general Cu(2)-ligand distances are comparable to those about Cu(1), with the exception that the Cu(2)-O(0) distance is shorter at 1.930(4) Å (*cf.* 2.046(8) Å for Cu(1)-O(0)). The other notable difference is the positioning of Br(2). This ligand is shifted significantly out of the basal plane compared with Br(1), away from the apical nitrogen, N(27) and as a consequence of this the Cu(2) centre exhibits greater distortion towards TBP geometry (τ value of 0.28 for Cu(2) *cf.* 0.00 for Cu(1)). The N(apical)-Cu-Br about Cu(2) is 125.9(2)° compared with 110.0(1)° about Cu(1). The other notable difference in the angles is that of N(21)-Cu(2)-Br(2), which is 149.1(2)°, is more acute than the corresponding angle about Cu(1) (164.4(2)°), and it also shows a shift towards the TBP geometry.

3.3 Complexes of bis(tacn) ligands bearing acetate pendant arms

3.3.1 Preparation of Complexes

Addition of two molar equivalents of $\text{Cu}(\text{ClO}_4)_2 \cdot 6\text{H}_2\text{O}$ to an aqueous solution of the crude oil of $\text{T}_2\text{-o-X Ac}_2$ or $\text{T}_2\text{-m-X Ac}_2$ and adjustment of the pH to *ca.* 5, produced dark blue solutions of the copper complexes. The solutions were loaded onto a cation exchange column and the complexes eluted with 0.1 M NaClO_4 solution. After concentration of the eluent *in vacuo*, the solutions were left to slowly evaporate, producing blue powders. Proposed structures are shown in Figure 3.10.

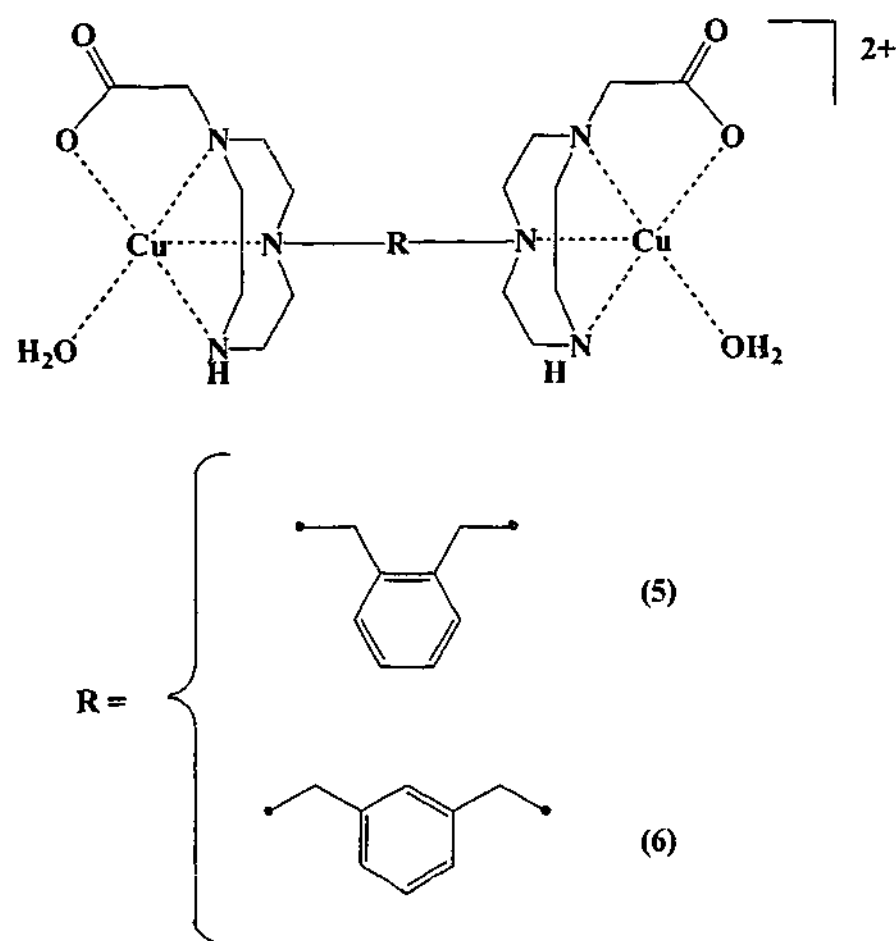


Figure 3.10 Proposed structures of compounds 5 and 6

The IR spectra of complexes 5 and 6 are virtually identical. Sharp bands in the region of 3297 and 3315 cm^{-1} for the complexes of the *ortho* and *meta* bridged species, respectively, are attributed to the NH stretch, while bands around 1100 and 625 cm^{-1} are due to the perchlorate counter ions. Strong bands at 1598 and 1625 cm^{-1} (*ortho* (5) and *meta* (6), respectively) and weaker bands at around 1370 and 1383 cm^{-1} (*ortho* (5) and *meta* (6), respectively) are assigned to the asymmetric and the symmetric stretching modes of the carboxylate group, respectively. The positions of the acetate stretching frequencies and the differences between them suggest that the acetate pendant arm coordinates in a unidentate fashion.⁴⁰ Strong, broad OH stretching bands at 3420 and 3450 cm^{-1} (*ortho* (5) and *meta* (6), respectively) indicate the presence of water. Table

3.5 shows the elemental analyses for these complexes and proposed composition that are in agreement with these analyses.

Table 3.5 Elemental Analyses for complexes 5 and 6

Calculated values are given in parentheses

Complex	C (%)	H (%)	N (%)
5 $[\text{Cu}_2(\text{T}_2\text{-}o\text{-X Ac}_2)(\text{H}_2\text{O})_2](\text{ClO}_4)_2 \cdot 6\text{H}_2\text{O}$	30.6 (30.5)	5.0 (5.8)	8.9 (8.9)
6 $[\text{Cu}_2(\text{T}_2\text{-}m\text{-X Ac}_2)(\text{H}_2\text{O})_2](\text{ClO}_4)_2 \cdot 4\text{H}_2\text{O}$	31.7 (31.7)	4.9 (5.6)	9.4 (9.3)

As expected from the similar empirical formula of the two complexes, the electrospray mass spectra of the two compounds were very similar. In particular both spectra show a peak at m/z 701 which corresponds to the $\{[\text{Cu}_2(\text{T}_2\text{-}(o,m)\text{-X Ac}_2)]\text{ClO}_4\}^+$ ion.

3.4 Copper complex of tris(tacn) ligand; $[\text{Cu}_6(\text{T}_3\text{mes})_2(\mu\text{-OH})_6](\text{ClO}_4)_6 \cdot 6\text{H}_2\text{O}$ (7)

The complex 7 was made by addition of an aqueous solution the free ligand of T_3mes to an excess of $\text{Cu}(\text{ClO}_4)_2 \cdot 6\text{H}_2\text{O}$. After adjustment of the pH to ~ 9 , the solution was diluted and loaded onto a cation exchange chromatography column and eluted with NaClO_4 . Crystals deposited that were suitable for X-ray crystallographic studies. Unit cell analysis of the crystal revealed the unit cell to be the same as a recently reported structure (Figure 3.11).³⁶ All other analyses were consistent with the literature. In this work, the potential of this complex to act as a catalyst for the hydrolysis of phosphate esters is reported. With three Cu(II) centres within the same assembly, it was

anticipated that this complex would exhibit faster rates of phosphate ester hydrolysis than those reported by Burstyn and coworkers for $[\text{Cu}(\text{tacn})\text{Cl}_2]$.⁴¹⁻⁴³

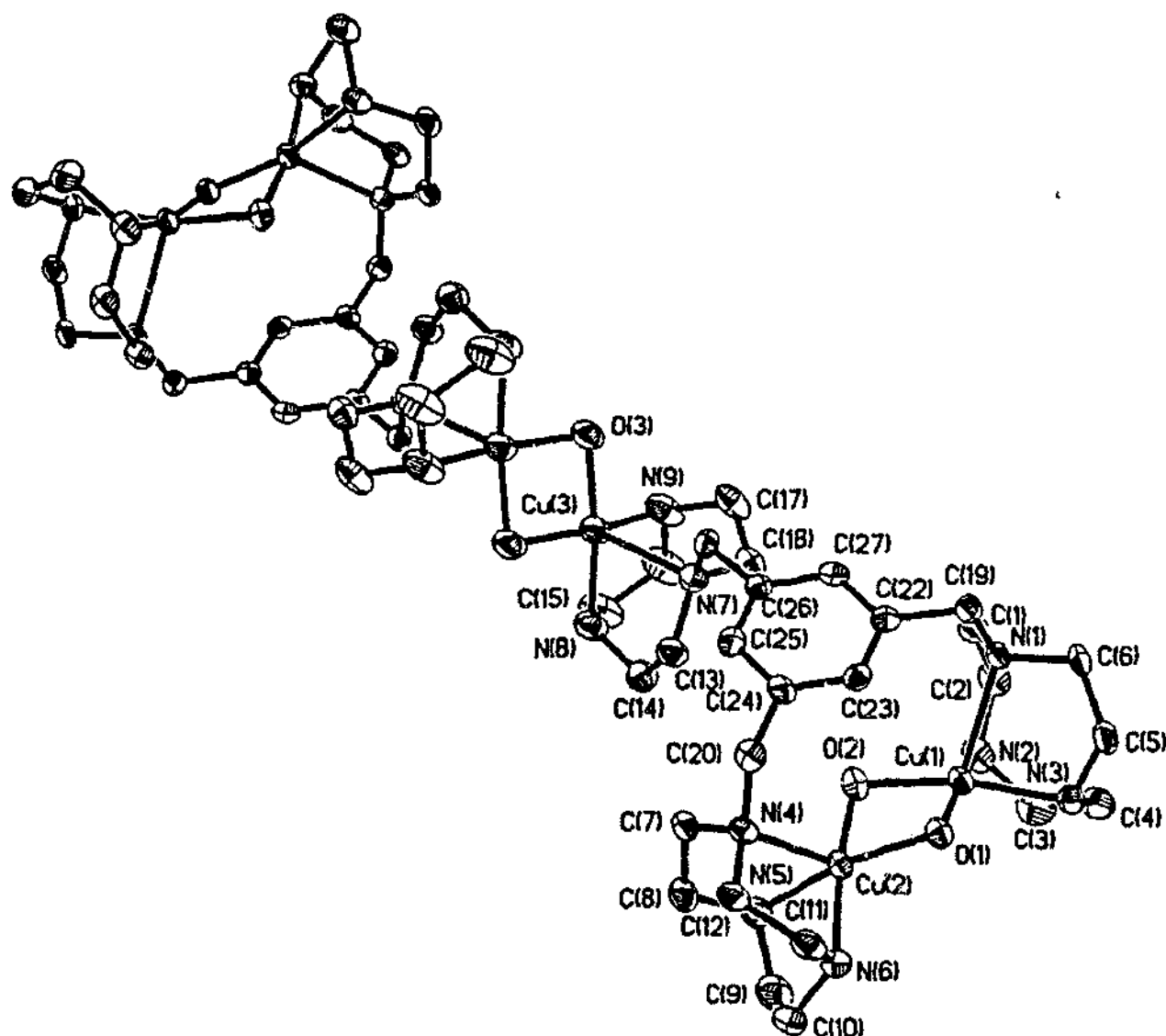


Figure 3.11 ORTEF plot of the molecular cation of $[\text{Cu}_6(\text{T}_3\text{mes})_2(\mu\text{-OH})_6](\text{ClO}_4)_6 \cdot (\text{H}_2\text{O})_6$, reported by Graham *et al.*³⁶

3.5 Copper Complexes Incorporating Phosphate Esters

Complexes incorporating phosphates or phosphate esters into their structure have been of interest in the modelling of phosphatase enzymes. Such enzymes generally have two or more metal centres at their active sites which act in concert in efficiently catalysing the cleavage of phosphate ester bonds (see Chapter 1). Investigations into the binding

of phosphate esters within bi- or tri-nuclear arrays, were aimed at deepening the understanding of relevant coordination chemistry, mechanism(s) and structures which may occur in enzymes.⁴⁴ Despite their relevance, the number of structurally characterised metal complexes incorporating phosphates or phosphate esters is not large.

3.5.1 Preparation of [Cu(tacn)₂](BNPP) (8)

Small blue crystals of 8 were deposited when a solution containing [Cu(tacn)Cl₂](ClO₄)₂ (5 mM), BNPP (5 mM) and HEPES at pH 7.4 buffer (50 mM) at a total volume of 4.02 mls, were left at 38°C overnight.

3.5.2 Crystal Structure of [Cu(tacn)₂](BNPP) (8)

The X-ray crystal structure of [Cu(tacn)₂](BNPP) was determined in order to confirm the presence of the phosphate moiety in the structure. Crystal parameters and details of the data collection, solution and refinement are presented in section 1.3 of the Appendix. The BNPP was found to be the counter ion for the [Cu(tacn)₂]²⁺ sandwich complex. The unit cell consists of a tacn unit, one BNPP counter ion and half a copper(II) centre. Figure 3.12 represents an ORTEP plot of the asymmetric unit, with an additional tacn ring and half a copper atom shown for clarity. Figure 3.13 shows the packing diagram of the complex. Table 3.6 lists selected bond distances and angles.

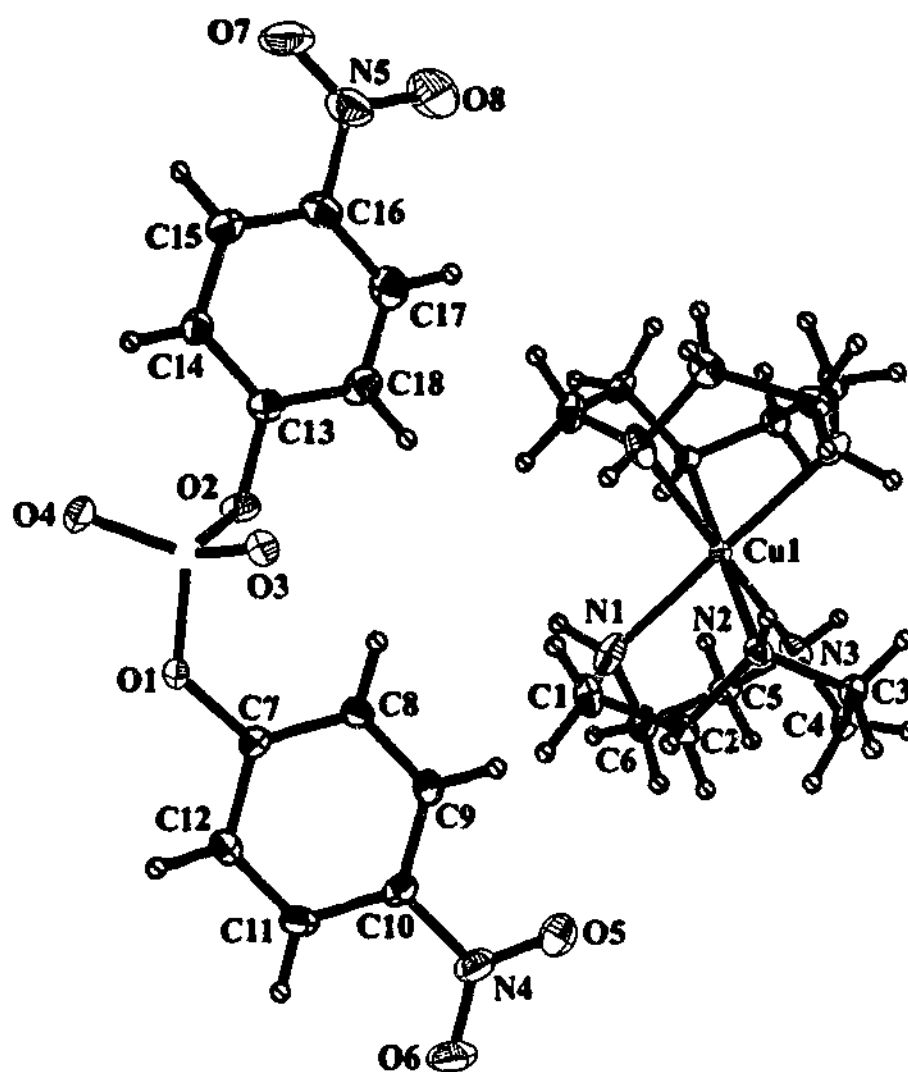


Figure 3.12 ORTEP plot of [Cu(tacn)₂](BNPP) (8) with atomic labelling scheme

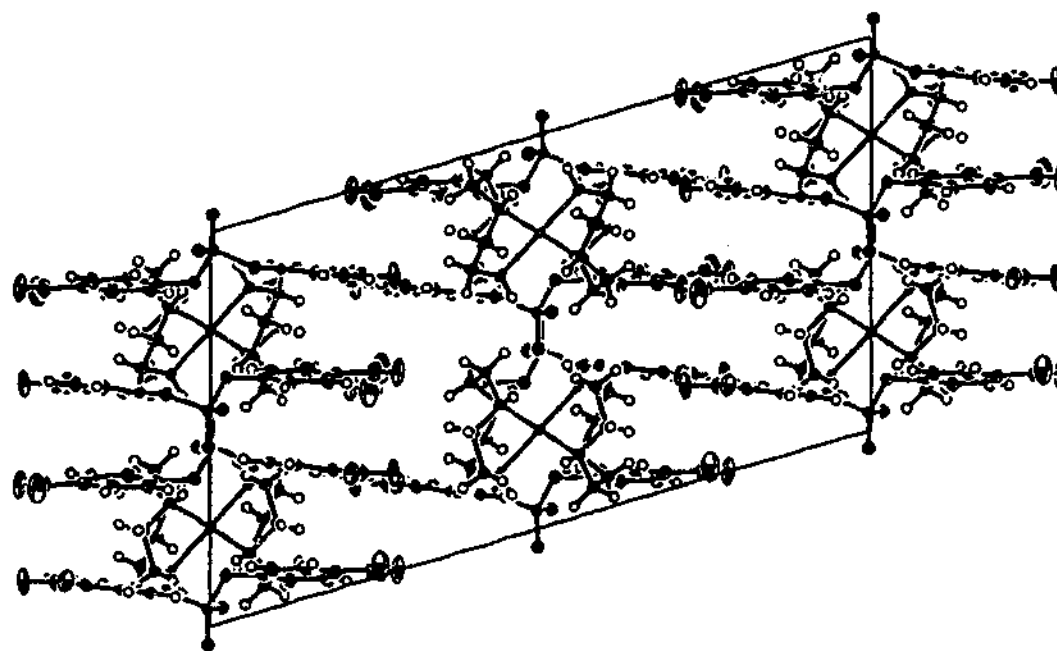


Figure 3.13 Packing diagram of [Cu(tacn)₂](BNPP) (8)

Chapter Three

Table 3.6 Selected bond distances (Å) and angles (°) for **8**

(#1 represents the second tacn ring)

P(1)-O(1)	1.505(2)	P(2)-O(2)	1.514(2)
P(1)-O(1)	1.6183(12)	P(1)-O(3)	1.4761(13)
P(1)-O(2)	1.6210(12)	P(1)-O(4)	1.4812(12)
Cu(1)-N(1)	2.1817(17)	Cu(1)-N(1)#1	2.1818(17)
Cu(1)-N(2)	2.0916(14)	Cu(1)-N(2)#1	2.0917(14)
Cu(1)-N(3)	2.1691(16)	Cu(1)-N(3)#1	2.1692(16)
O(1)-P(1)-O(2)	97.07(6)	O(2)-P(1)-O(3)	110.08(7)
O(1)-P(1)-O(3)	111.49(7)	O(2)-P(1)-O(4)	110.63(7)
O(1)-P(1)-O(4)	105.42(7)	O(3)-P(1)-O(4)	119.72(7)
N(1)-Cu(1)-N(2)	81.44(5)	N(2)-Cu(1)-N(3)#1	97.72(5)
N(1)-Cu(1)-N(3)	80.88(6)	N(3)-Cu(1)-N(1)#1	179.12(6)
N(1)-Cu(1)-N(1)#1	99.02(8)	N(3)-Cu(1)-N(2)#1	97.72(5)
N(1)-Cu(1)-N(2)#1	99.01(6)	N(3)-Cu(1)-N(3)#1	99.24(8)
N(1)-Cu(1)-N(3)#1	179.13(6)	N(1)#1-Cu(1)-N(2)#1	81.43(5)
N(2)-Cu(1)-N(3)	81.84(5)	N(1)#1-Cu(1)-N(3)#1	80.88(6)
N(2)-Cu(1)-N(1)#1	99.01(6)	N(2)#1-Cu(1)-N(3)#1	81.84(5)
N(2)-Cu(1)-N(2)#1	179.33(8)		

The copper centre lies in a distorted octahedral environment due to the constraints imposed by the tacn ring, with all N-Cu-N angles of the same tacn ring below 90°, being between 80.88(6) and 81.84(5)°. The angles between *trans* nitrogens in the tacn rings (*ca.* 179°) are all close to the ideal angle of 180°. The Cu-N distances are typical of such bond distances, being 2.1817(17), 2.0916(14) and 2.1691(16) Å for Cu-N(1), Cu-N(2) and Cu-N(3), respectively. From the packing diagram (Figure 3.13) the π -stacking of the phenyl rings can be seen. The shortest π - π interaction is between C(8) and C(18) of an adjacent unit (C(18A)) with a distance of 3.348 Å.

Chapter Three

This is not the first of this sandwich-type structure to be reported for the tacn ligand. The cation $[\text{Cu}(\text{tacn})_2]^{2+}$ was reported initially by Beveridge *et al.* in 1987.¹⁴ The bond angles and lengths for this complex are quite similar to those reported here. The formation of the sandwich complex under conditions used to conduct BNPP hydrolysis needs to be considered in the interpretation of the kinetics of BNPP hydrolysis conducted by other workers.⁴¹⁻⁴³

Many hydrolytic studies have been undertaken using $[\text{Cu}(\text{tacn})(\text{H}_2\text{O})_2]^{2+}$ to act as the catalyst to cleave P-OR bonds.^{41-43,45-48} The sandwich-type structure of **8** would be unreactive as a catalyst for the hydrolysis of the phosphate ester bond as there are no free coordination sites on the copper(II) centre for binding and activation of a substrate or to provide a nucleophile to attack the electropositive phosphorus centre. As complex **8** was synthesised from the starting material $[\text{Cu}(\text{tacn})(\text{H}_2\text{O})_2]^{2+}$, it is obvious that the sandwich complex will form in solution thereby making some of the copper(II) centres in solution inactive and leading to a reduction in the rate of hydrolysis. The hydrolytic system is further complicated, however, by the fact that the sandwich structure partially dissociates in solution, forming solvated bis-sandwich(tacn), $[\text{Cu}(\text{tacn})_2\text{S}_n]^{2+}$ (S = solvent molecule), where one of the tacn ligand is behaving as a mono- or bidentate ligand.¹⁴

3.5.3 Preparation of $[\text{Cu}_3(\text{Me}_3\text{tacn})_3(\text{PhP})_2](\text{ClO}_4)_2 \cdot \frac{1}{2}\text{H}_2\text{O}$ (**9**)

The product **9** was initially obtained by adding two molar equivalents of 1,4,7-trimethyl-1,4,7-triazacyclononane (Me_3tacn) in ethanol to an equimolar amount of $\text{Cu}(\text{ClO}_4)_2 \cdot 6\text{H}_2\text{O}$ in water followed by a one molar equivalent of disodium

Chapter Three

phenylphosphate (Na_2PhP). The resulting dark blue solution was allowed to slowly evaporate, producing dark blue crystals of crystallographic quality in a yield of 51%.

The second synthesis involved repeating the above method, but with the reactant mole ratios changed to match the product that was formed in the initial synthesis (yield 62%). The product isolated was found to be identical, with the unit cell of the crystal obtained from the second synthesis found to be the same as that from the first.

The infrared spectrum of the complex showed two sharp $\nu(\text{OH})$ stretches at 3616 and 3531 cm^{-1} due to the water in the lattice. Bands due to the perchlorate counter ion were observed at 1097 and 623 cm^{-1} . The strong band located at 1155 cm^{-1} is attributed to the phosphate. Two strong bands at 1595 and 767 cm^{-1} are assigned to the aromatic ring, with the first attributable to C=C vibrations and the latter due to out of plane bending of the ring. The microprobe and the microanalytical data confirmed that the bulk composition of the complex matched that of the single crystal used in X-ray crystallography (Table 3.7).

Table 3.7 Microanalytical data for compound 9

Calculated values are given in parenthesis

Complex	C (%)	H (%)	N (%)
9 $[\text{Cu}_3(\text{Me}_3\text{tacn})_3(\text{PhP})_2](\text{ClO}_4)_2 \cdot \frac{1}{2}\text{H}_2\text{O}$	37.2	5.9	10.1
	(37.3)	(5.9)	(10.0)

3.5.4 Crystal Structure of $[\text{Cu}_3(\text{Me}_3\text{tacn})_3(\text{PhP})_2](\text{ClO}_4)_2 \cdot \frac{1}{2}\text{H}_2\text{O}$ (9)

The structural analysis of compound (9) was undertaken in order to determine the coordination mode of the phenyl phosphate group and to determine the coordination environment around the copper(II) centres. Cell parameters and details of the data collection are presented in section 1.4 of the Appendix. The crystals consist of discrete $[\text{Cu}_3(\text{Me}_3\text{tacn})_3(\text{PhP})_2]^{2+}$ cations, perchlorate anions and water of crystallisation. Figure 3.14 represents the ORTEP plot of the cation, Figure 3.15 shows the extended packing array and Table 3.8 lists selected bond lengths and angles.

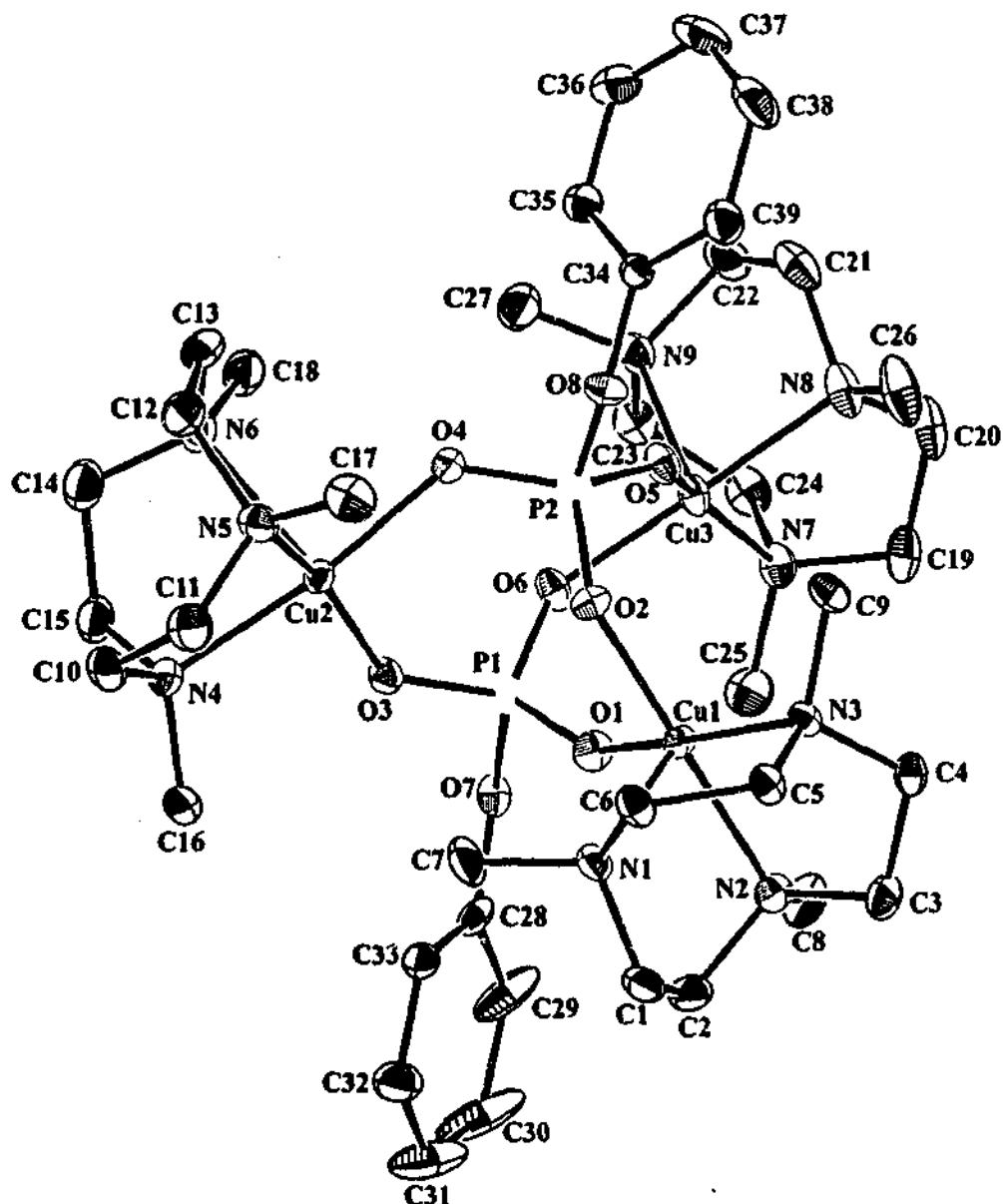


Figure 3.14 ORTEP plot of $[\text{Cu}_3(\text{Me}_3\text{tacn})_3(\text{PhP})_2]^{2+}$ cations (9) with atomic labelling scheme

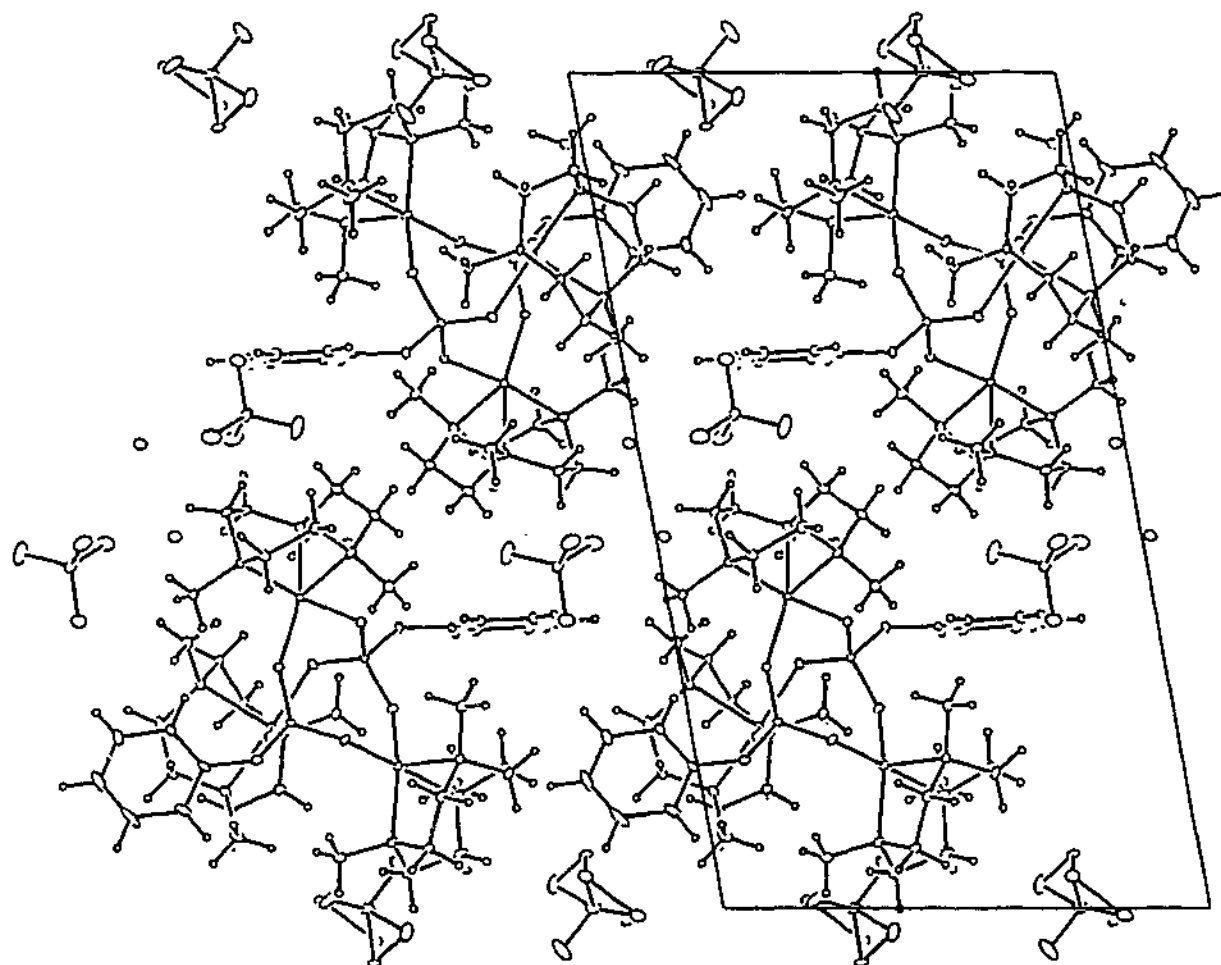


Figure 3.15 Extended packing array of 9

Chapter Three

Table 3.8 Selected bond distances (Å) and angles (°) for



P(1)-O(1)	1.505(2)	P(2)-O(2)	1.514(2)
P(1)-O(3)	1.514(2)	P(2)-O(4)	1.513(2)
P(1)-O(6)	1.511(2)	P(2)-O(5)	1.510(2)
P(1)-O(7)	1.635(2)	P(2)-O(8)	1.633(2)
Cu(1)-N(1)	2.224(2)	Cu(3)-N(7)	2.095(2)
Cu(1)-N(2)	2.073(2)	Cu(3)-N(8)	2.073(2)
Cu(1)-N(3)	2.057(2)	Cu(3)-N(9)	2.238(2)
Cu(1)-O(1)	1.917(2)	Cu(3)-O(5)	1.924(2)
Cu(1)-O(2)	1.932(2)	Cu(3)-O(6)	1.938(2)
Cu(2)-N(4)	2.092(2)		
Cu(2)-N(5)	2.089(2)		
Cu(2)-N(6)	2.248(2)		
Cu(2)-O(3)	1.959(2)		
Cu(2)-O(4)	1.944(2)		
O(1)-P(1)-O(3)	115.0(1)	O(2)-P(2)-O(4)	112.38(10)
O(1)-P(1)-O(6)	114.83(10)	O(2)-P(2)-O(5)	114.73(10)
O(1)-P(1)-O(7)	103.85(9)	O(2)-P(2)-O(8)	101.39(10)
O(3)-P(1)-O(6)	113.67(10)	O(4)-P(2)-O(5)	114.58(10)
O(3)-P(1)-O(7)	106.16(9)	O(4)-P(2)-O(8)	107.33(9)
O(6)-P(1)-O(7)	101.41(10)	O(5)-P(2)-O(8)	104.93(10)
N(1)-Cu(1)-N(2)	83.47(8)	N(7)-Cu(3)-N(8)	84.45(9)
N(1)-Cu(1)-N(3)	84.34(8)	N(7)-Cu(3)-N(9)	82.92(8)
N(1)-Cu(1)-O(1)	108.64(8)	N(7)-Cu(3)-O(5)	159.14(7)
N(1)-Cu(1)-O(2)	93.42(7)	N(7)-Cu(3)-O(6)	93.17(8)
N(2)-Cu(1)-N(3)	85.18(8)	N(8)-Cu(3)-N(9)	83.32(9)
N(2)-Cu(1)-O(1)	91.15(8)	N(8)-Cu(3)-O(5)	88.67(8)
N(2)-Cu(1)-O(2)	176.22(8)	N(8)-Cu(3)-O(6)	175.68(8)
N(3)-Cu(1)-O(1)	165.65(8)	N(9)-Cu(3)-O(5)	115.85(8)
N(3)-Cu(1)-O(2)	92.38(7)	N(9)-Cu(3)-O(6)	92.87(7)
O(1)-Cu(1)-O(2)	92.89(7)	O(5)-Cu(3)-O(6)	94.77(7)
N(4)-Cu(2)-N(5)	83.85(8)	Cu(1)-O(1)-P(1)	148.8(1)
N(4)-Cu(2)-N(6)	82.65(8)	Cu(1)-O(2)-P(2)	126.7(1)
N(4)-Cu(2)-O(3)	90.70(7)	Cu(2)-O(3)-P(1)	135.2(1)
N(4)-Cu(2)-O(4)	172.86(7)	Cu(2)-O(4)-P(2)	130.0(1)
N(5)-Cu(2)-N(6)	83.41(9)	Cu(3)-O(5)-P(2)	142.9(1)
N(5)-Cu(2)-O(3)	160.91(8)	Cu(3)-O(6)-P(1)	129.8(1)
N(5)-Cu(2)-O(4)	91.96(8)		
N(6)-Cu(2)-O(3)	114.10(8)		
N(6)-Cu(2)-O(4)	91.14(7)		
O(3)-Cu(2)-O(4)	95.07(7)		

Chapter Three

The complex cation consists of three $[\text{Cu}(\text{Me}_3\text{tacn})]^{2+}$ moieties linked together by two phosphate esters. The three terminal oxygens of the phosphate esters each link two of the $[\text{Cu}(\text{Me}_3\text{tacn})]^{2+}$ moieties, thus all three Cu(II) centres are linked to each other by two Cu-O-P-O-Cu bridging units. These phosphate groups lie above and below the plane defined by the Cu(Me₃tacn) units, with the phenoxy groups located perpendicular to the triangular array of copper atoms (Figure 3.16).

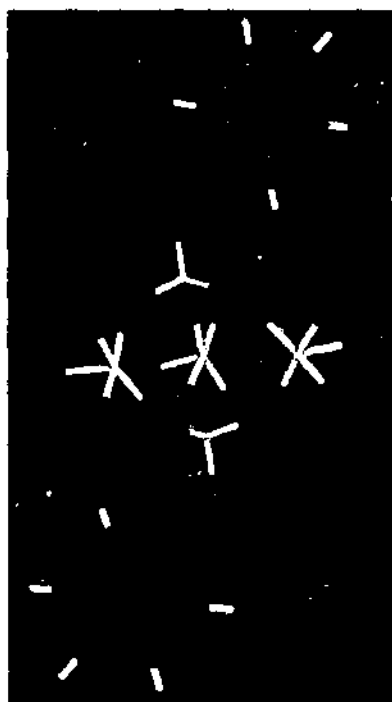


Figure 3.16 Schematic diagram of **9**. Only nitrogens of Me₃tacn units are shown for clarity

The geometry of each Cu(II) centre is best described as distorted SP with the Me₃tacn macrocycle occupying one face of the square pyramid and the phosphate oxygens in the other two positions. Using the method developed by Addison *et al.*,³⁸ τ values of 0.18, 0.20 and 0.28 are calculated for Cu(1), Cu(2) and Cu(3), respectively. The Cu...Cu

Chapter Three

distances of Cu(1)-Cu(2) 4.55 Å, Cu(2)-Cu(3) 5.04 Å and Cu(1)-Cu(3) 4.14 Å, clearly indicate that this trinuclear cluster is asymmetric.

For Cu(1), the Cu-N(1) distance to the apical nitrogen (2.224(2) Å) is, as expected, longer than those in the basal plane, reflecting the Jahn-Teller distortion imposed by the d^9 copper centre. The Cu-N(basal) bond distances are 2.073(2) and 2.057(2) Å for Cu(1)-N(2) and Cu(1)-N(3) respectively. The Cu-O distances are slightly shorter at 1.917(2) and 1.932(2) Å, but are typical of Cu-O-P bond lengths.⁴⁹ The Cu-N and Cu-O distances are typical for this type of structure.^{11,12,18,23,33} As seen in the previous complexes, the N-Cu-N distances are all below the ideal angle of 90°, being 83.47(8)°, 84.34(8)° and 85.18(8)° for N(1)-Cu(1)-N(2), N(1)-Cu(1)-N(3) and N(2)-Cu(1)-N(3), respectively, due to the constraints imposed by the tacn ring. Compensating for this, the bond angles between O(1)-Cu(1)-O(2), as well as those between N(tacn)-Cu(1)-O(phosphate) are all greater than 90°, ranging from 91.14(7)° to 108.68(8)°.

The geometry around the phosphate is distorted from a perfect tetrahedron. P-O bond lengths where coordinated to copper (*ca.* 1.51 Å), are shorter than the P-O bond in the phosphate ester (*ca.* 1.63 Å), but are typical of copper-coordinated P-O bonds.^{49,50} The O-P-O bond angle for the bridging oxygens are slightly smaller than for similar structures reported in the literature, at *ca.* 114°⁴⁹ *cf.* 118° and 119°.⁵⁰ This can also be compared to the BNPP anion in complex **8** as well as to a compound reported by Gieb *et al.*⁵¹ where the BNPP is also a counter ion. The O-P-O bond angle for the non-ester oxygens is 119.72(7)° for **8** (see Table 3.8) and 121.22° for that reported by Gieb. This illustrates that the coordination of the phosphate ester constricts the angle between the coordinated oxygens, subtended at the phosphorus centre.

Chapter Three

One interesting feature of the structure is the variation in the geometry of each Cu(II) centre. Some of the significant differences in the bond angles and distances around Cu(1), Cu(2) and Cu(3) can be gleaned from the data in Table 3.9.

Table 3.9 Comparison of selected bond lengths and angles for the copper(II) centres in **9**

Angles (°)	Cu(1)	Cu(2)	Cu(3)
N(apical)-Cu-N(basal)	83.47(8)	82.65(8)	82.92(8)
	84.34(8)	83.41(9)	83.32(9)
N(basal)-Cu-N(basal)	85.18(8)	83.65(8)	84.45(9)
N(apical)-Cu-O(phosphate)	108.64(8)	114.10(8)	115.85(8)
	93.72(7)	91.14(7)	92.87(7)
N(basal)-Cu-O(phosphate)	91.15(8)	90.70(7)	88.67(8)
	92.38(7)	91.96(8)	93.17(8)
Cu-O-P	165.65(8)	160.91(8)	159.14(7)
	176.22(8)	172.86(7)	175.68(8)
Cu-O-P	148.8(1)	135.2(1)	142.9(1)
	126.7(1)	130.0(1)	129.8(1)
Bond Distances (Å)			
Cu-N(apical)	2.224(2)	2.248(2)	2.238(2)
Cu-N(basal)	2.073(2)	2.092(2)	2.079(2)
	2.057(2)	2.089(2)	2.095(2)
Cu-O(phosphate)	1.917(2)	1.959(2)	1.924(2)
	1.932(2)	1.944(2)	1.938(2)

Chapter Three

This complex **9** is unique in the way it binds two organophosphates to three Cu(II) centres. Other Cu(II) complexes binding phosphates within the structure are usually binuclear, and often contain another bridging group between the two Cu(II) centres. An exception is the polymeric complex $\{[\text{Cu}_3(\text{T}_3\text{mes})(\mu\text{-OH})(\mu_3\text{-HPO}_4)(\text{H}_2\text{O})][\text{PF}_6]\cdot 3\text{H}_2\text{O}\}_n$.⁶ This complex contains a trinuclear Cu(II) array in which the three Cu(II) centres are linked by an HPO_4^{2-} bridge and two of the coppers are further linked by an hydroxo bridge. The ORTEP plot of this complex was presented in Figure 1.17 of the Introduction, and a schematic diagram is shown in Figure 3.17. This complex, as with other binuclear models, has an additional bridge (hydroxo) to the phosphate between the Cu(II) centres.

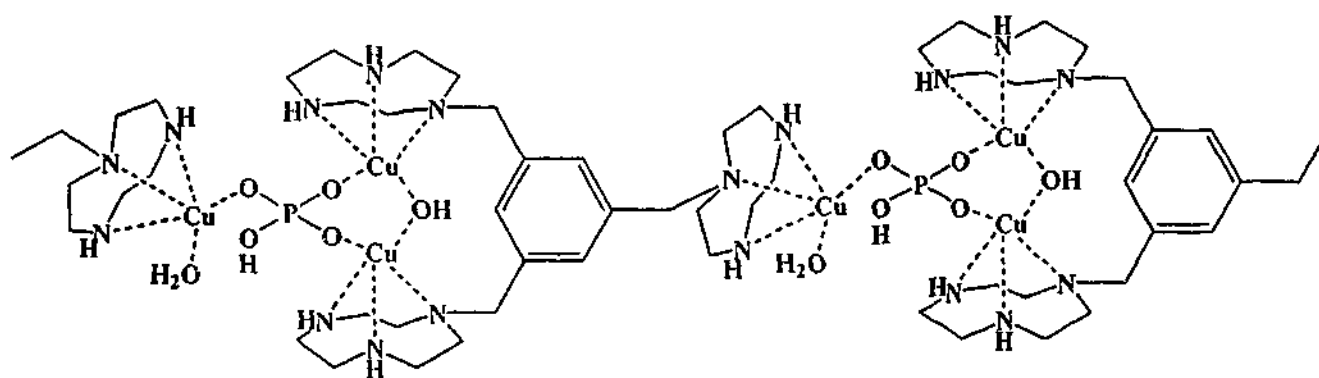


Figure 3.17 Schematic of $\{[\text{Cu}_3(\text{T}_3\text{mes})(\mu\text{-OH})(\mu_3\text{-HPO}_4)(\text{H}_2\text{O})][\text{PF}_6]\cdot 3\text{H}_2\text{O}\}_n$, with the repeating cation shown in blue⁶

A search of the Cambridge Crystallographic Database showed no similar type of structure to that of **9**. The only complexes with three metal centres bridged by two phosphates, through three phosphate from each, are non-copper cluster-type complexes.⁵²⁻⁵⁶ An example is shown in Figure 3.18.

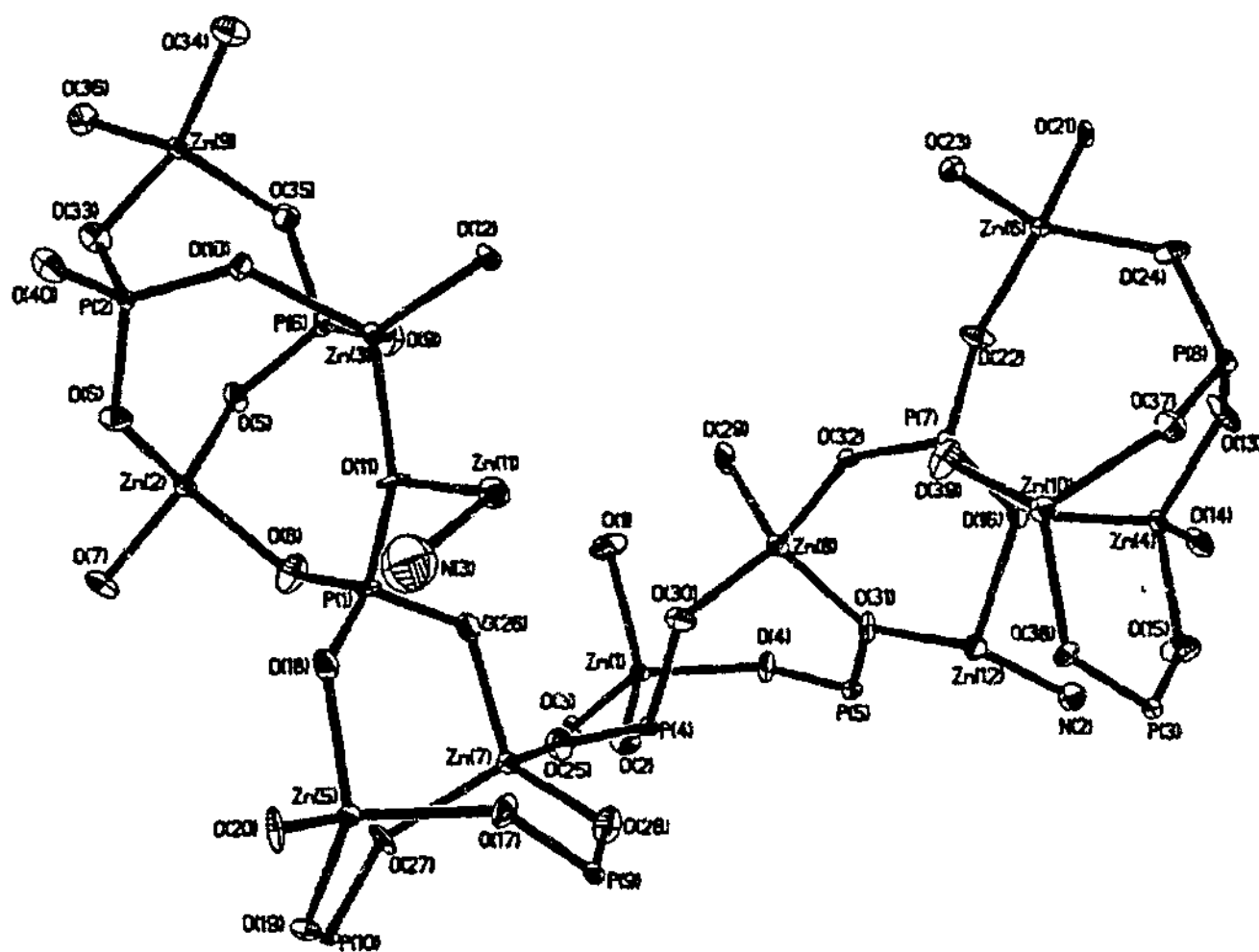


Figure 3.18 An example of a cluster complex where three metal centres are bridged by two phosphates. The ORTEP plot is of the framework of $[\text{NH}_3(\text{CH}_2)_3\text{NH}_3]_2[\text{NH}_3(\text{CH}_2)_3\text{NH}_2]_2[\text{Zn}_{12}(\text{OH}_2)_2(\text{PO}_4)_{10}]\cdot\text{H}_2\text{O}$ ⁵²

3.5.5 Synthesis of $[\text{Cu}_2(\text{T}_2\text{-}m\text{-X})(\text{NPP})(\mu\text{-OH})](\text{ClO}_4)\cdot\text{H}_2\text{O}$ (10)

Dark blue needles of **10** were obtained after mixing aqueous solutions of $[\text{Cu}_2\text{T}_2\text{-}m\text{-X}(\text{H}_2\text{O})_4](\text{ClO}_4)_4\cdot 3\text{H}_2\text{O}\cdot\text{NaClO}_4$ (**2**) (5mM, 1.0 ml) and disodium 4-nitrophenyl phosphate (Na_2NPP) (15 mM, 1.0 ml) to a HEPES solution (150 mM, 1.0 ml), at a pH was 7.4. The temperature was maintained at 38°C overnight, after which time needles of the product had formed in 79% yield.

Chapter Three

Bands in the infrared spectrum indicated the formation of the complex. Two sharp bands are observed at 3458 and 3577 cm^{-1} , due to the stretching vibrations of the bridging hydroxide and the water of crystallisation in the complex. NH stretches are observed at 3209 and 3329 cm^{-1} . The band at 1589 cm^{-1} is due to C=C stretches and indicates the presence of a benzene ring. The phosphate moiety cannot be conclusively confirmed through analysis of the infrared spectrum as the broad band for the perchlorate counter ion at 1098 cm^{-1} occurs in the same region. The other band confirming the presence of the perchlorate ion is at 625 cm^{-1} . The asymmetric and symmetric stretches of the nitro group on the phosphate moiety can, however, be seen at 1518 and 1345 cm^{-1} . There is excellent agreement between the calculated and observed microanalytical data (Table 3.10).

Table 3.10 Microanalytical Data for compound 10

Calculated values are given in parentheses

Complex	C (%)	H (%)	N (%)
10 $[\text{Cu}_2(\text{T}_2\text{-}m\text{-X})(\text{NPP})(\mu\text{-OH})]$	37.1	5.2	11.6
$(\text{ClO}_4)\cdot\text{H}_2\text{O}$	(37.2)	(5.2)	(11.7)

3.5.6. Crystal Structure of $[\text{Cu}_2(\text{T}_2\text{-}m\text{-X})(\text{NPP})(\mu\text{-OH})](\text{ClO}_4)\cdot\text{H}_2\text{O}$ (10)

Details of the X-ray structure determination of $[\text{Cu}_2(\text{T}_2\text{-}m\text{-X})(\text{NPP})(\mu\text{-OH})](\text{ClO}_4)\cdot\text{H}_2\text{O}$ are presented in section 1.5 of the Appendix. The ORTEP diagram (Figure 3.19) clearly shows that the NPP^{2-} anion bridges the two copper centres via two of its phosphate oxygens. An hydroxide bridge provides a further connection between the two copper

Chapter Three

centres. The unit cell consists of two copper-NPP-hydroxide cations, two perchlorate counter ions and half a water of crystallisation. The atom connectivity within each of the cations are the same, but there are some differences that are worthy of description. The bond distances and angles for each metal centre in one cation match those in the second cation within the asymmetric unit (see Table 3.11). The copper centres exhibit a distorted SP environment, with the bridge head nitrogen occupying the apical site. The values of τ for the copper centres are 0.002 for Cu(1), 0.18 for Cu(2) and Cu(3), and 0.003 for Cu(4). The copper(II) centres are 3.57 Å apart, which is comparable to compound 4, a complex which also has a hydroxide bridge between the copper(II) centres. An ORTEP diagram of the asymmetric unit is shown in Figure 3.20.

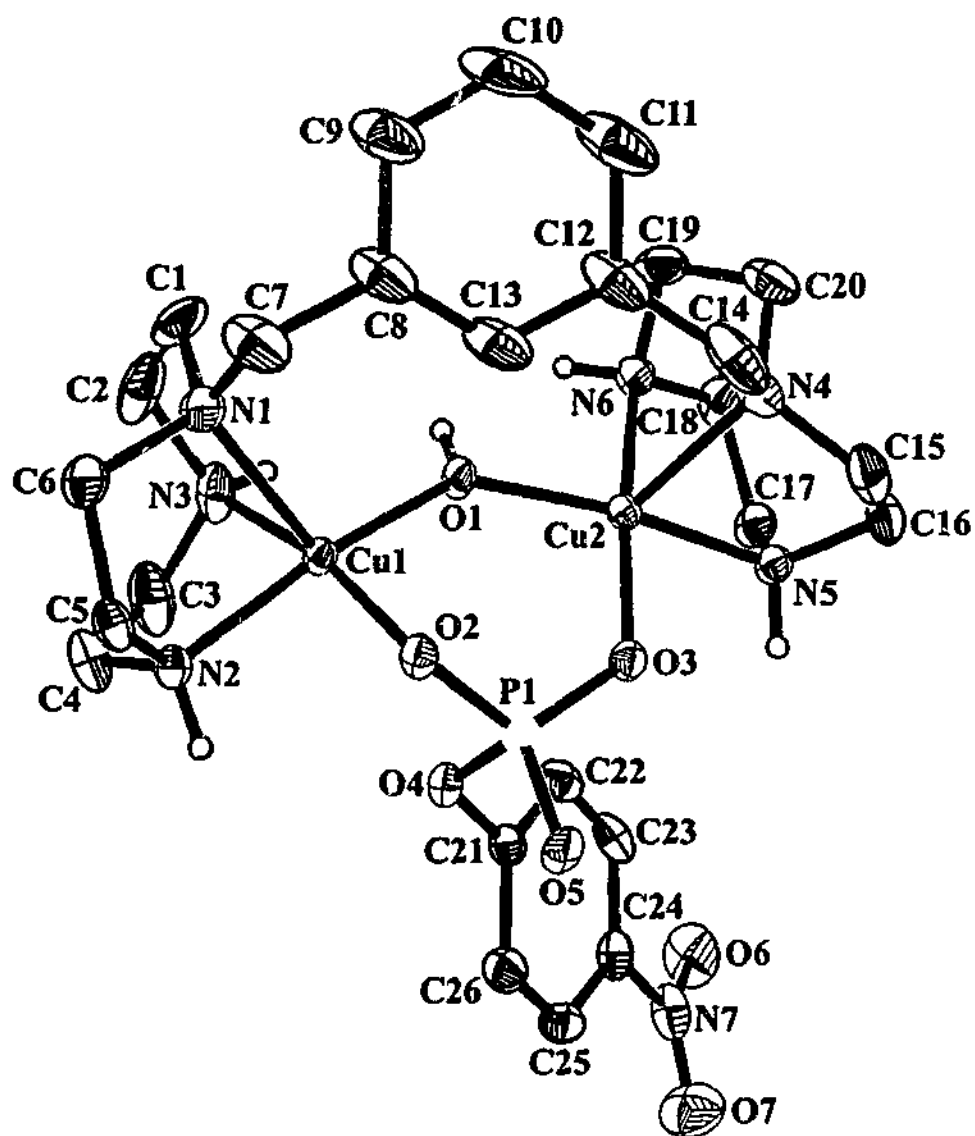


Figure 3.19 ORTEP plot of $[\text{Cu}_2(\text{T}_2\text{-}m\text{-X})(\text{NPP})(\mu\text{-OH})]^+$ (10) with atomic labelling

scheme

Chapter Three

Table 3.11 Selected bond distances (Å) and angles (°) for 10

Cu(1)-N(1)	2.320(4)	Cu(4)-N(11)	2.323(4)
Cu(1)-N(2)	2.029(4)	Cu(4)-N(12)	2.024(4)
Cu(1)-N(3)	2.034(4)	Cu(4)-N(13)	2.030(4)
Cu(1)-O(1)	1.901(3)	Cu(4)-O(8)	1.901(3)
Cu(1)-O(2)	1.967(3)	Cu(4)-O(10)	1.964(3)
Cu(2)-N(4)	2.305(4)	Cu(3)-N(8)	2.306(4)
Cu(2)-N(5)	2.048(4)	Cu(3)-N(10)	2.049(4)
Cu(2)-N(6)	2.028(4)	Cu(3)-N(9)	2.023(4)
Cu(2)-O(1)	1.915(3)	Cu(3)-O(8)	1.915(3)
Cu(2)-O(3)	1.950(3)	Cu(3)-O(9)	1.948(3)
Cu(1)-O(1)Cu(2)	138.23(17)	Cu(3)-O(8)-Cu(4)	138.26(16)
O(2)-P(1)-O(3)	115.53(18)	O(9)-P(2)-O(10)	115.56(18)
O(2)-P(1)-O(4)	101.67(17)	O(9)-P(2)-O(11)	107.18(17)
O(2)-P(1)-O(5)	113.32(18)	O(9)-P(2)-O(12)	111.97(18)
O(3)-P(1)-O(4)	107.09(17)	O(10)-P(2)-O(11)	101.63(17)
O(3)-P(1)-O(5)	111.75(18)	O(10)-P(1)-O(12)	113.16(18)
O(4)-P(1)-O(5)	106.32(19)	O(11)-P(2)-O(12)	106.15(18)
N(1)-Cu(1)-N(2)	81.93(15)	N(11)-Cu(4)-N(12)	82.08(15)
N(1)-Cu(1)-N(3)	81.88(16)	N(11)-Cu(4)-N(13)	81.88(17)
N(1)-Cu(1)-O(1)	108.96(14)	N(11)-Cu(4)-O(8)	108.58(14)
N(1)-Cu(1)-O(2)	106.43(14)	N(11)-Cu(4)-O(10)	106.44(14)
N(2)-Cu(1)-N(3)	83.66(16)	N(12)-Cu(4)-N(13)	83.85(16)
N(2)-Cu(1)-O(1)	168.16(15)	N(12)-Cu(4)-O(8)	168.41(15)
N(2)-Cu(1)-O(2)	88.93(14)	N(12)-Cu(4)-O(10)	88.99(14)
N(3)-Cu(1)-O(1)	93.12(15)	N(13)-Cu(4)-O(8)	93.00(15)
N(3)-Cu(1)-O(2)	168.03(16)	N(13)-Cu(4)-O(10)	168.21(17)
O(1)-Cu(1)-O(2)	92.25(13)	O(8)-Cu(4)-O(10)	92.18(12)
N(4)-Cu(2)-N(5)	82.75(15)	N(8)-Cu(3)-N(10)	82.59(15)
N(4)-Cu(2)-N(6)	82.68(16)	N(8)-Cu(3)-N(9)	82.53(16)
N(4)-Cu(2)-O(1)	113.28(15)	N(8)-Cu(3)-O(8)	113.24(15)
N(4)-Cu(2)-O(3)	93.40(14)	N(8)-Cu(3)-O(9)	98.29(14)
N(5)-Cu(2)-N(6)	83.20(15)	N(9)-Cu(3)-N(10)	83.27(15)
N(5)-Cu(2)-O(1)	162.53(15)	N(10)-Cu(3)-O(8)	162.65(15)
N(5)-Cu(2)-O(3)	90.16(14)	N(10)-Cu(3)-O(9)	91.17(14)
N(6)-Cu(2)-O(1)	91.73(14)	N(9)-Cu(3)-O(8)	91.55(14)
N(6)-Cu(2)-O(3)	173.09(14)	N(9)-Cu(3)-O(9)	173.25(14)
O(1)-Cu(2)-O(3)	94.08(13)	O(8)-Cu(3)-O(9)	94.26(12)

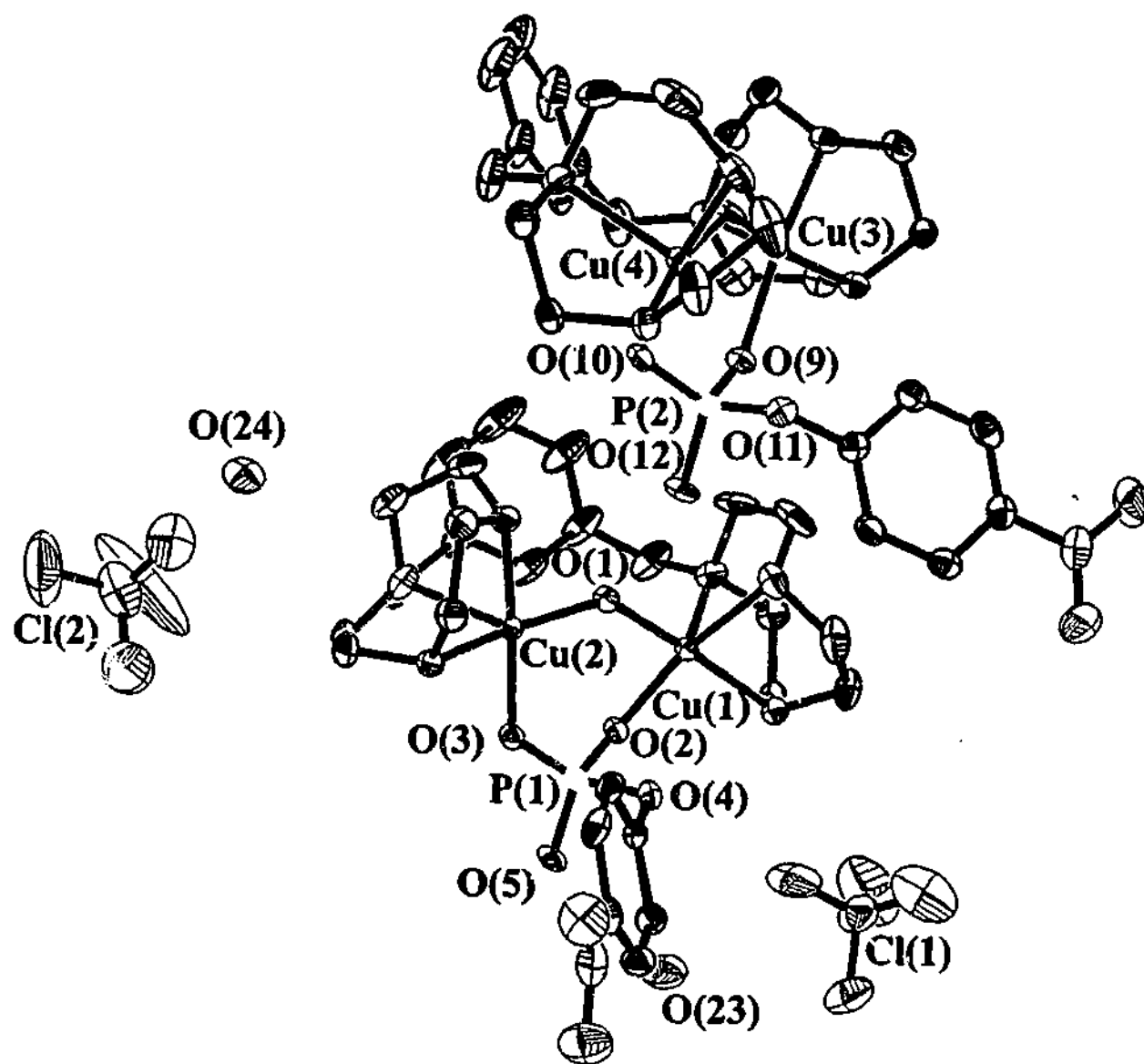


Figure 3.20 ORTEP plot of the asymmetric unit of
 $[\text{Cu}_2(\text{T}_2\text{-}m\text{-X})(\text{NPP})(\mu\text{-OH})]_2(\text{ClO}_4)_2 \cdot \text{H}_2\text{O}$ (10)

Chapter Three

As can be seen from Figure 3.21 and Table 3.12, the individual cations in the unit cell are connected via hydrogen bonding. For example, the non-coordinated phosphate oxygen in the second cationic unit (O(12)) forms contacts with hydrogens on the hydroxide oxygen (O(12)...O(1) = 2.7822 Å), closest amine hydrogens (O(12)...N(3) = 2.9012 Å and O(12)...N(6) = 2.9604 Å) and the water (O(12)...O(24B) = 2.7842 Å). This latter water in turn bonds to the adjacent perchlorate (O(20B)) (2.8102 Å) which further bonds to the hydrogen on N(12) (2.957(7) Å). These bonds are repeated in the following units, and form chains within the crystal (Figure 3.22).

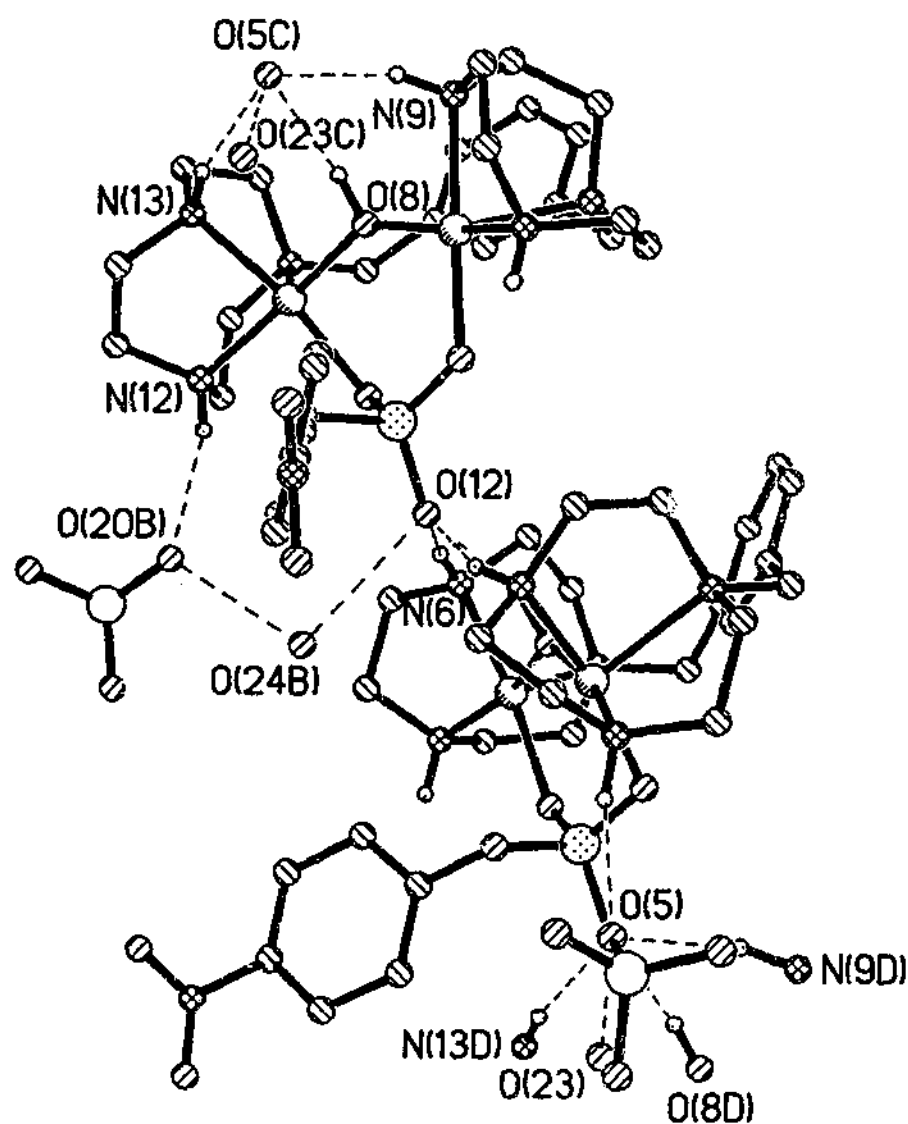
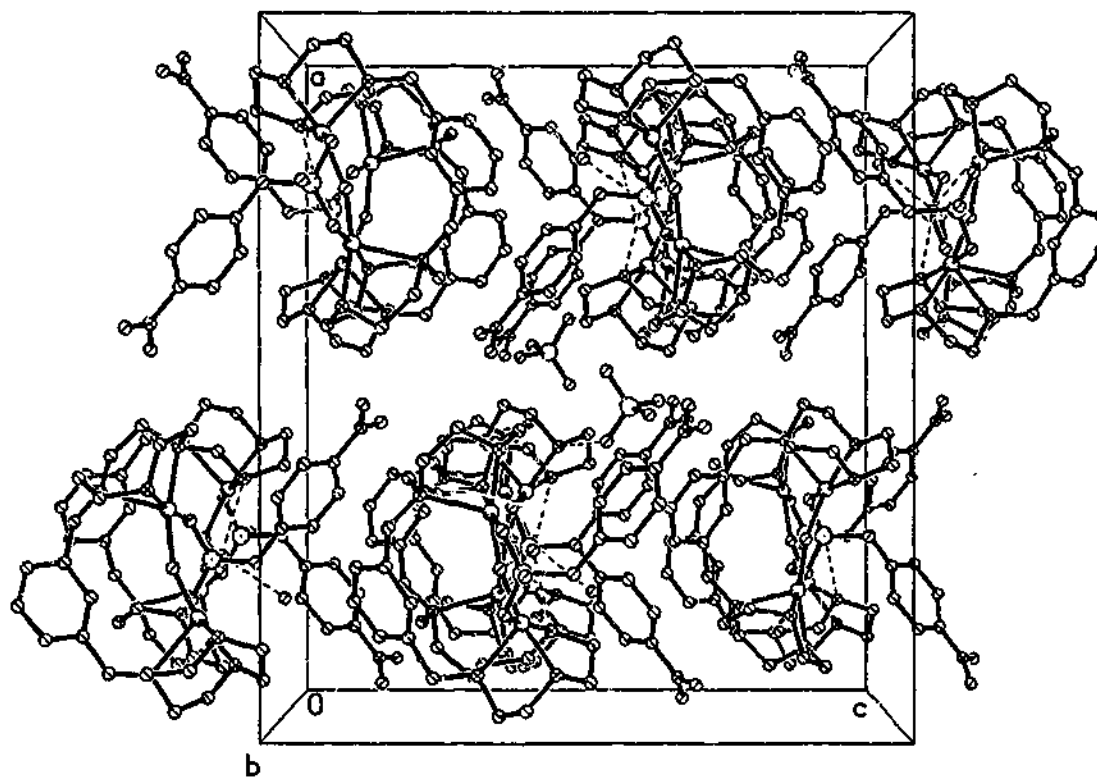


Figure 3.21 Diagram of 10 showing hydrogen bonding network

Table 3.12 Hydrogen bond distances (Å) and angles (°) for 10

O(1)-O(12)	2.782(5)
O(5)-O(23)	2.786(5)
O(20)-O(24)	2.810(7)
O(15)-O(23)	2.812(7)
O(12)-O(24) ^a	2.784(5)
O(5)-O(8) ^b	2.788(4)
O(12)-N(3)	2.901(5)
O(12)-N(6)	2.960(5)
O(15)-N(2)	2.949(6)
O(5)-N(9) ^b	2.954(5)
O(5)-N(13) ^b	2.895(5)
O(20) ^a -N(12)	2.957(7)
<hr/>	
O(12)-H(1)-O(1)	160(5)
O(5)-H(8) ^b -O(8) ^b	169(5)
O(12)-H(3)-N(3)	155(5)
O(12)-H(6)-N(6)	159(5)
O(5)-H(9N) ^b -N(9) ^b	160(5)
O(5)-H(3N) ^b -N(13) ^b	156(5)
O(20) ^a -H(12)-N(12)	150(5)
O(15)-H(2)-N(2)	149(5)
<hr/>	
a: x, -y, ½+z; b: x, 1+y, z	

**Figure 3.22** Extended packing array of 10, showing the chains formed within the crystal

Chapter Three

Table 3.13 Comparison of bond lengths (Å) between **10** and the structure reported by Spiccia⁶ (**A**, Figure 3.22)

Bond Length (Å)	10	A
Cu(1)-O-H	1.901(3)	1.89(1)
Cu(2)-O-H	1.915(3)	1.96(2)
Cu(1)-O-Phosphate	1.967(3)	1.94(1)
Cu(2)-O-Phosphate	1.950(3)	1.94(1)

A number of research groups have reported other structures in which two Cu(II) centres are bridged through an O-P-O bridge and an endogenous oxygen atom located on the ligand backbone, and not a hydroxo bridge.^{44,49,50} The structure reported by Wall *et al.*⁴⁹ is of a binuclear Cu(II) complex of the 2,6-bis[bis(2-benzimidazolylmethyl)aminomethyl]-4-methyl phenolate ligand (Figure 3.24). The dibenzyl phosphate bridges the two copper centres via an O-P-O linkage, and an endogenous phenolate bridge further links the two copper(II) centres. The Cu...Cu distance was found to be slightly longer at 3.670(4) Å, *cf.* 3.57 Å for **10**. The bond angles between the coppers and the bridging phenolate oxygen were smaller at 126.19°. In a similar structure reported by Karlin and coworkers⁴⁴ the Cu...Cu distance was found to be considerably larger at 3.773(4) Å. In a related dinuclear copper(II) complex reported by Yamaguchi *et al.*⁵⁰ of the ligand *N,N,N',N'*-tetrakis{(6-methyl-2-pyridyl)methyl}-1,3-diaminopropan-2-ol, where the endogenous oxygen in the propanol linking group bridges between the two copper(II) centres as does O-P-O bridge of a BNPP moiety, the Cu...Cu distance was 3.78 Å and the Cu-O-Cu bond angle was larger than that found in **10** at 140.18°.

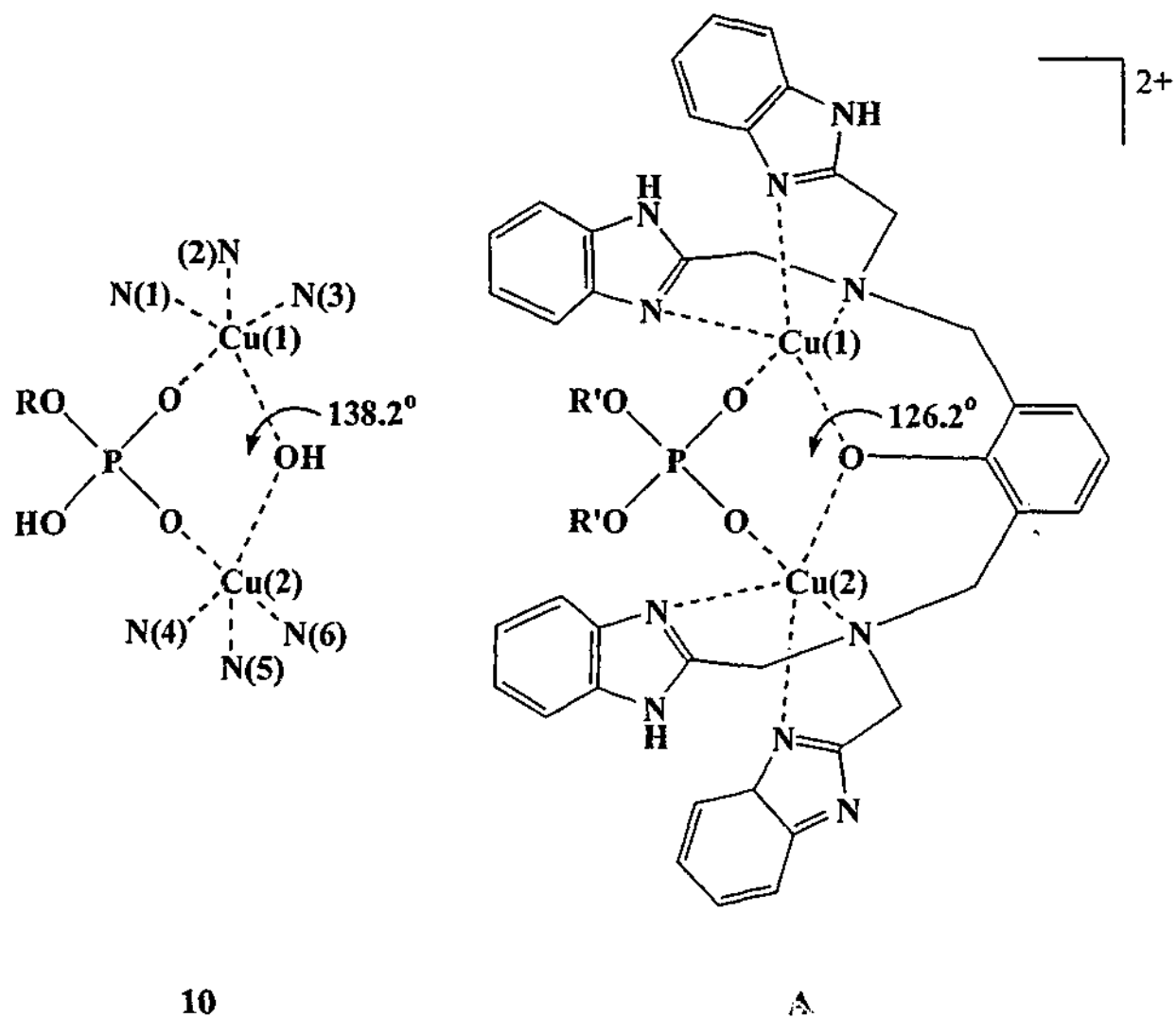


Figure 3.24 Comparison of **10** with structures reported by Wall *et al.*⁴⁹ (A)

3.6 Preparation of the Mononuclear Complex $[\text{Cu}^{\text{II}}\text{Me}_3\text{tacn}(\text{H}_2\text{O})_2](\text{ClO}_4)_2$ (**11**)

The copper complex of Me_3tacn was prepared for two reasons: (i) to be used in kinetic studies; and (ii) to compare the physicochemical properties of this mononuclear complex with those of **1-10**. The complex was made by the dropwise addition of an aqueous ethanol solution of the ligand to an ethanol solution of $\text{Cu}(\text{ClO}_4)_2 \cdot 6\text{H}_2\text{O}$. The pH was adjusted to *ca.* 6 with 2M NaOH and the dark blue solution was heated gently. The solvents were removed *in vacuo* and the residue taken up in EtOH. Diethyl ether was added until the solution turned cloudy and the solution was left at -20°C overnight.

Chapter Three

The blue crystalline solid was isolated in 79% yield. The analysis is consistent with the given formula.

3.7 Physicochemical Properties of Copper(II) Complexes

3.7.1 Electronic Spectra

Electronic spectra of complexes 1-7, 9-11 were recorded of both the solids and in solution. The solution spectra are shown in Figure 3.26 while the associated data is given in Table 3.14. The orbital energy diagrams for SP and TBP are shown in Figure 3.25.

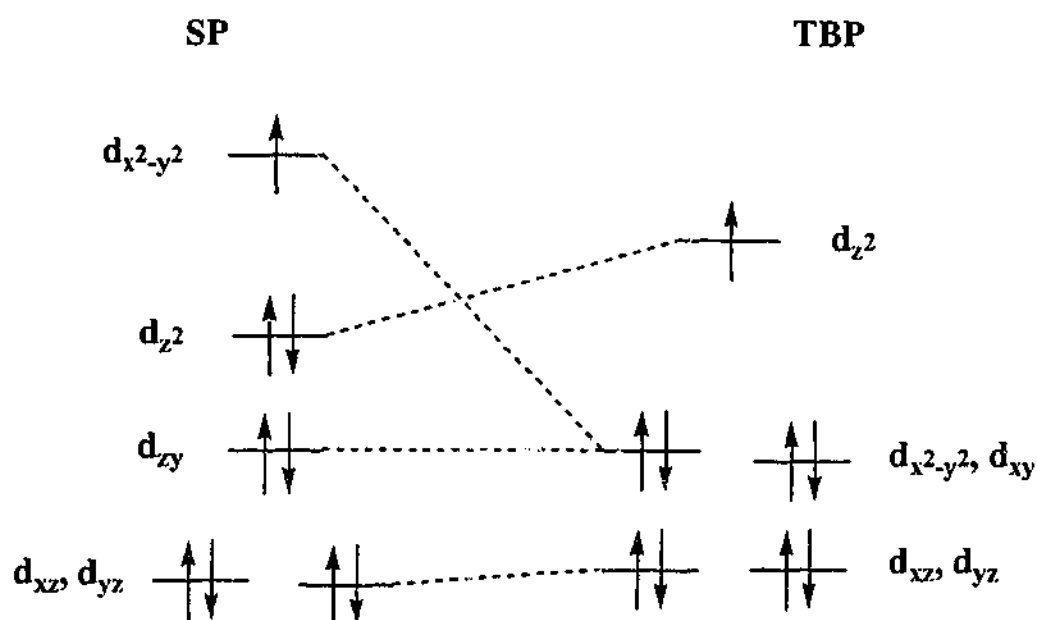


Figure 3.25 Orbital energy diagrams for five-coordinate, d^9 Cu(II) complexes

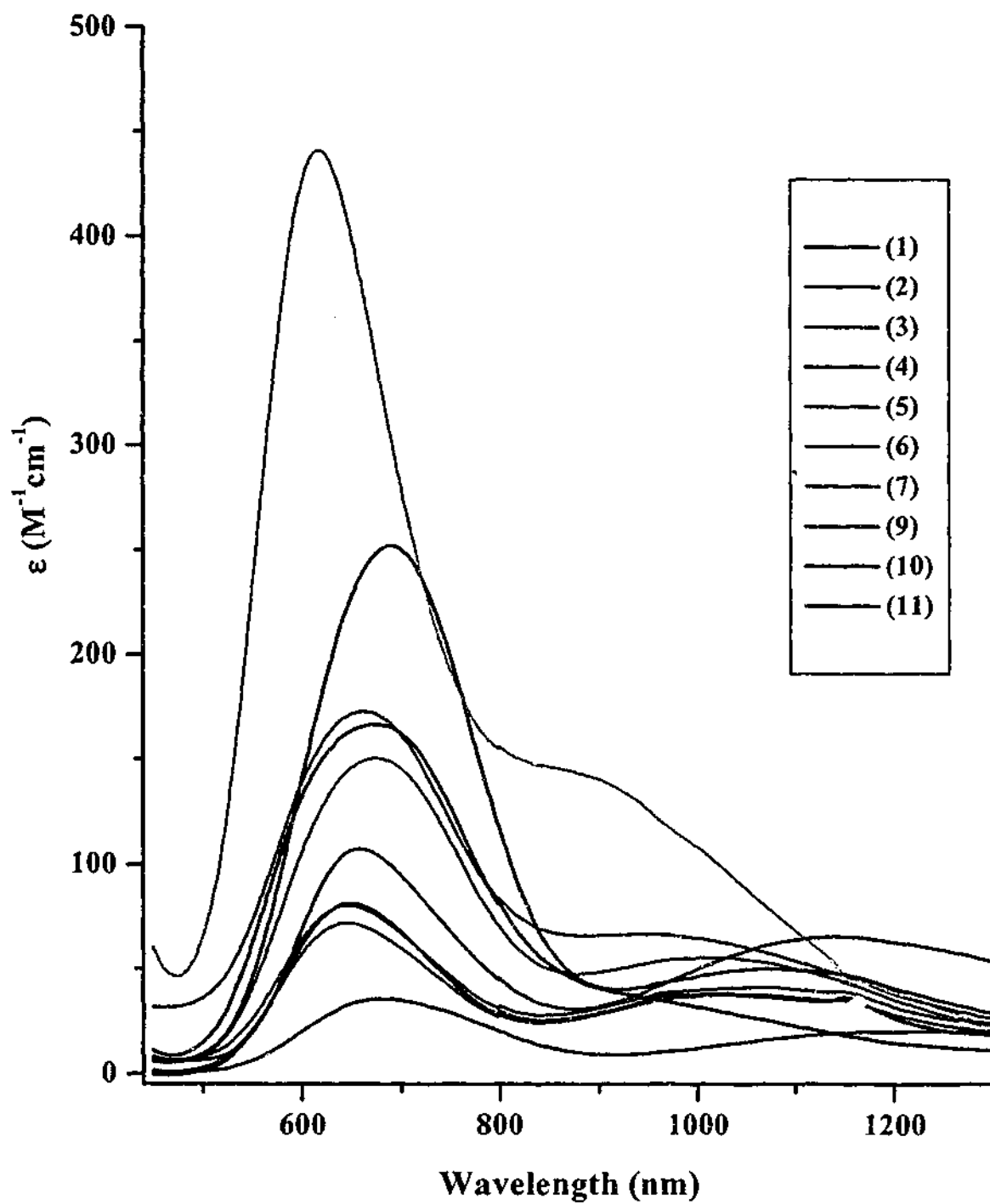


Figure 3.26 Electronic spectra of Cu(II) complexes recorded in water (1-7, 9 and 11), or DMF (10) (~1mM)

Chapter Three

Table 3.14 Electronic data for Cu(II) complexes

Complex	Solvent	λ_{\max} , nm, (ϵ_{\max} , $M^{-1}cm^{-1}$)		
1 [Cu ₂ (T _{2-o-X})Cl ₄]	H ₂ O	255 (5340)	649 (81)	1028 (39)
	Solid		636	1043
2 [Cu ₂ (T _{2-m-X})(H ₂ O) ₄] (ClO ₄) ₄ ·3H ₂ O·NaClO ₄	H ₂ O	250 (7779)	644 (72)	1043 (38)
	Solid		640	1072
3 [Cu ₂ (T _{2-p-X})Cl ₄]	H ₂ O	253 sh (5897)	644 (80)	1054 (41)
	Solid		636	981
4 [Cu ₂ (T _{2-PrO})Br ₂] Br·2H ₂ O	H ₂ O	270 (6291)	689 (252)	1072 (50)
	Solid		631	1081
5 [Cu ₂ (T _{2-o-X} Ac ₂)(H ₂ O) ₂] (ClO ₄) ₂ ·4H ₂ O	H ₂ O	257 (6916)	663 (173)	939 (67)
	Solid		658	1016
6 [Cu ₂ (T _{2-m-X} Ac ₂)(H ₂ O) ₂] (ClO ₄) ₂ ·4H ₂ O	H ₂ O	259 (6422)	675 (150)	1011 (55)
	Solid		670	1018
7 [Cu ₆ (T _{3mes}) ₂ (μ-OH) ₆] (ClO ₄) ₆ ·6H ₂ O	H ₂ O	252 (22620)	617 (440)	877 sh (143)
	Solid		610	~880 sh
9 [Cu ₃ (Me ₃ tacn) ₃ (PhP) ₂] (ClO ₄) ₂ ·½H ₂ O	H ₂ O	268 (12560)	658 (140)	1140 (85)
	DMF		663 (359)	1065 (142)
	Solid			650, 1049
10 Cu ₂ (T _{2-m-X})(NPP) (μ-OH)]ClO ₄ ·H ₂ O	DMF	263 (13314)	674 (166)	~1000 sh
		315 (12515)		
	Solid	336	620	~1000 sh
11 [Cu(Me ₃ tacn)(H ₂ O) ₂] (ClO ₄) ₂	H ₂ O	270 (3759)	682 (36)	1237 (20)
	Solid		685	

Chapter Three

The solution spectra of complexes 1-3 exhibit two weak $d \rightarrow d$ absorption maxima (λ_{\max}) at *ca.* 645 and 1040 nm. These values are typical for Cu(II) residing in a SP or distorted SP environment, and are due to the $d_{z^2} \rightarrow d_{x^2-y^2}$ and $d_{yz} \rightarrow d_{x^2-y^2}$ transition.^{15,23,27} This is also in the typical range for distorted SP copper(II) complexes with tacn based ligands.^{48,57} Complex 4 shows two $d \rightarrow d$ transitions, but these are shifted to higher wavelengths (689 and 1072 nm) relative to complexes 1-3. This shift is probably due to a distortion in the Cu(II) geometries towards TBP, as indicated from the crystallographic data. For a copper complex with the geometry about the Cu(II) centre intermediate between distorted SP and TBP, the λ_{\max} is shifted to higher wavelengths *cf.* SP, at around 720 nm,⁵⁷ while a Cu(II) complex with TBP geometry will exhibit an absorption maximum *ca.* 800-900 nm.⁵⁸ Complexes 5 and 6 also show a slight shift toward TBP geometry relative to 1-3, but not as great as that for 4, with values of 663 and 675 nm. Complex 9 showed a very similar spectrum to those of 1-3 with λ_{\max} values of 658 and 1140 nm. The spectrum of 9 showed no significant change with the change in solvent to DMF, and indeed, from the solid state. This indicates the trimer is stable in both aqueous and DMF solution, which has implications in the analysis of the ESR data (see section 3.7.2.2). The spectrum of 10 is also quite similar to those of the other Cu(II) complexes, with a small red shift *cf.* 1-3, but again, the shift is not as great as that seen for 4.

The spectra of the complexes in the solid state generally show only a slight shift to a lower wavelength compared with the solution spectra, indicating little change in stereochemistry on dissolution. The exceptions to this are 4 and 10, which in the solid state show about a 60 nm blue shift compared with the solution spectrum. This

Chapter Three

indicates that dissolution of these complexes causes a shift in Cu(II) geometry from distorted SP towards TBP geometry.

3.7.2 Magnetic and ESR Properties

3.7.2.1 Non-bridged Complexes

Room temperature magnetic moments for the copper complexes 1-3, 5-6 and 11 are in the range normally expected for mononuclear or polynuclear copper(II) complexes with un-coupled or weakly coupled d^9 copper(II) complexes ($1.8 - 2.0 \mu_B$ per Cu) (Table 3.15). These values are higher than the spin-only value of 1.73 BM, most likely due to mixing of the orbital angular momentum from the excited state due to spin-orbit coupling.⁵⁹ The magnetic moment for 1 is a little reduced from the normal range.

Table 3.15 Room temperature magnetic moments

Complex	Magnetic Moment (μ_B) per Cu
1 $[\text{Cu}_2(\text{T}_2\text{-}o\text{-X})\text{Cl}_4]$	1.63
2 $[\text{Cu}_2(\text{T}_2\text{-}m\text{-X})(\text{H}_2\text{O})_4](\text{ClO}_4)_4 \cdot 3\text{H}_2\text{O} \cdot \text{NaClO}_4$	1.85
3 $[\text{Cu}_2(\text{T}_2\text{-}p\text{-X})\text{Cl}_4]$	1.73
5 $[\text{Cu}_2(\text{T}_2\text{-}o\text{-X Ac}_2)(\text{H}_2\text{O})_2](\text{ClO}_4)_2 \cdot 4\text{H}_2\text{O}$	1.81
6 $[\text{Cu}_2(\text{T}_2\text{-}m\text{-X Ac}_2)(\text{H}_2\text{O})_2](\text{ClO}_4)_2 \cdot 4\text{H}_2\text{O}$	1.84

Variable temperature magnetic studies were carried out on powdered samples of complexes of 3, 5 and 6 over the temperature range 4.2-300 K. The results are shown in Figures 3.26 - 3.28. Complex 3 shows a decrease in μ_{eff} as the temperature decreases, which is indicative of weak antiferromagnetic coupling. The corresponding magnetic

Chapter Three

susceptibilities show a maximum at *ca.* 10 K. The data for 3 were fitted to a modified Bleaney-Bowers equation,⁶⁰ calculated for two $S = \frac{1}{2}$ centres under a $-2JS_1S_2$ spin Hamiltonian, using a non-linear least squares fitting routine. The susceptibility equation (Equation 3.1) allows for a monomeric impurity which is commonly seen in such systems,⁶¹ assuming the *g*-value is the same as the complex. All the symbols have their usual meaning and *P* is the amount of monomeric impurity. The data were fitted to Equation 3.1 and the parameters obtained are as follows: *g* value = 1.99, $J = -8 \text{ cm}^{-1}$ and $P = 0.18$. The coupling is unlikely to be intramolecular across the aromatic ring (Cu-Cu distance = 11.81 Å), but more likely to be intermolecular in nature and involving an H-bonded pathway through H-bonds between N(3) and Cl in an adjacent molecule (see Figure 3.7).

$$\chi_{Cu} = \frac{Ng^2\beta^2}{kT} \left[3 + \exp\left(\frac{-2J}{kT}\right) \right]^{-1} (1-P) + \frac{Ng^2\beta^2 P}{4kT} + N_{\alpha} \quad \text{Eq. 3.1}$$

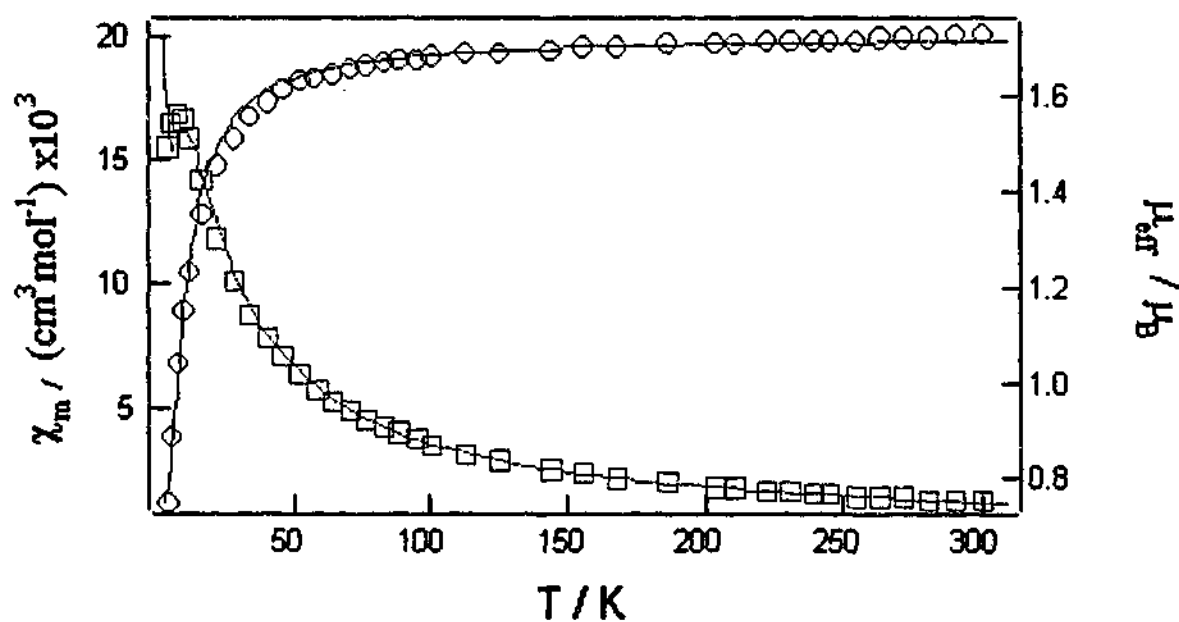


Figure 3.27 Plot of χ_m (\square) and μ_{eff} (\circ) (per Cu) versus temperature for complex 3 showing the fitted data

Complexes 5 and 6 show no change in the magnetic moment until very low temperatures, where a slight drop is observed. The χ_{Cu} values obey a Curie temperature dependence ($\chi_{\text{Cu}} = C/T$) This is indicative of no coupling or of very weak antiferromagnetic coupling between the copper centres.

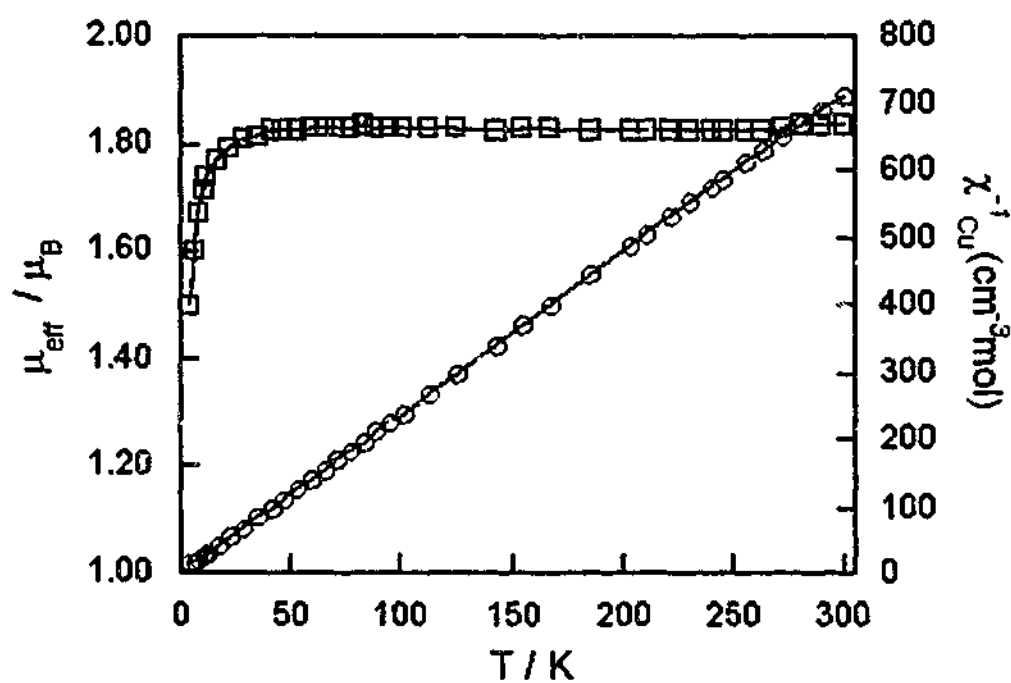


Figure 3.28 Plot of χ_{m}^{-1} (○) and μ_{eff} (□) (per Cu) versus temperature for complex 5.

Note: the lines joining the data points are not fitted lines.

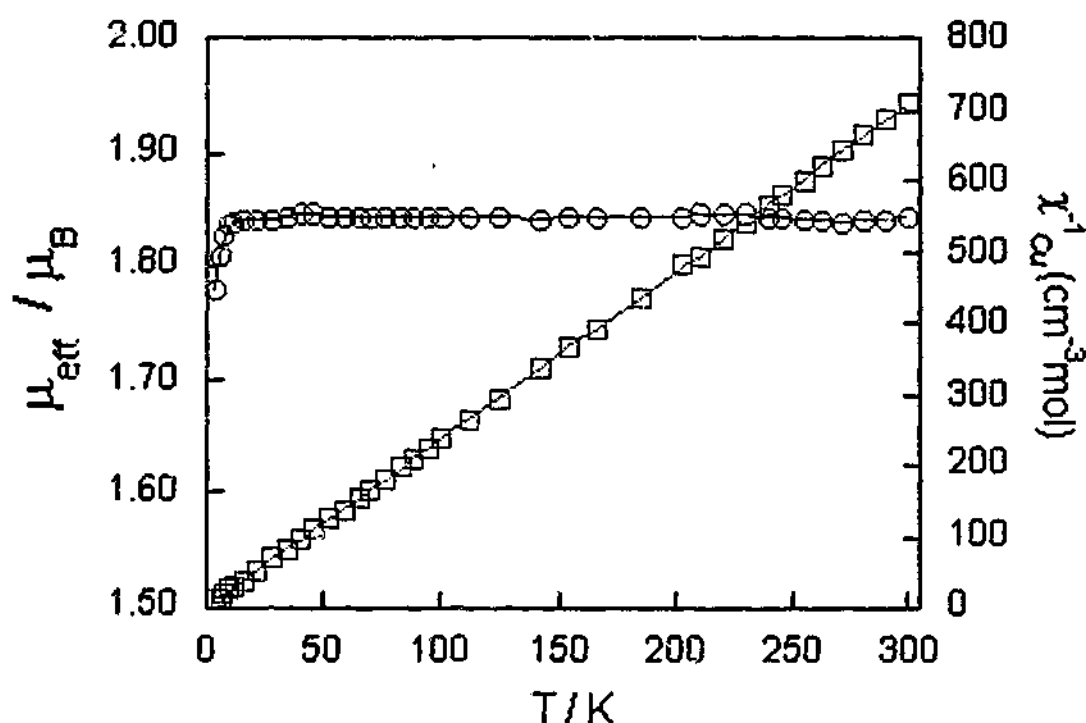


Figure 3.29 Plot of χ_m^{-1} (\square) and μ_{eff} (O) (per Cu) versus temperature for complex 6. Note: the lines joining the data points are not fitted lines.

X-band ESR spectra of the copper(II) complexes were recorded at 77 K for frozen solutions of ethylene glycol/water 1:1 for complexes 1-3 and DMF/toluene for complexes 5, 6 and 11 and are shown in Figure 3.30. The data are summarised in Table 3.16. The complexes show a strong signal centred around 3000 G. The spectrum for complex 11 shows a typical ESR spectrum for a mononuclear Cu(II) complex with nuclear spin of $3/2$, with all four hyperfine signals seen. The parameters obtained are typical of a SP environment around the Cu(II) centre with $g_{\parallel} > g_{\perp} > 2$.^{17,57} Three of the expected four hyperfine signals are seen for the binuclear complexes (1-3, 5 and 6), with the fourth hidden under the g_{\perp} line. Additional hyperfine lines are seen in the spectra for 1 and 2, which may be indicative of either different copper environments within the complexes, perhaps involving partial solvation, or of the existence of weak dipole-

Chapter Three

dipole coupling between the copper centres. Brudenell *et al.* have described the latter phenomena in binuclear copper-tacn complexes, with the former explanation ruled out through crystallographic analysis of the complexes.¹⁷ They reported that the increasing Cu...Cu separations, brought about by the increasing length of the bridge between two tacn units, decreased the dipole-dipole coupling between the copper centres. This coupling was seen for complexes of the ethane and propane bridged ligands, but not for those of butane or *m*-xylyl bridged ligands. In contrast, the complexes of the *ortho* and *meta* xylyl bridged ligands described here show additional hyperfine lines due to the dipole-dipole coupling. This phenomenon has also been documented in other studies of copper(II) complexes.^{62,63} Weak half-field ($\Delta m_s = \pm 2$) lines would be predicted at *ca.* 1500 G if dipole-dipole coupling was operative.

Table 3.16 ESR data for complexes 1-3, 5, 6 and 11

Complex	g_{\parallel}	A_{\parallel} $\times 10^{-4} \text{ cm}^{-1}$	g_{\perp}
1 [Cu ₂ T ₂ - <i>o</i> -X Cl ₄]	2.29	165	2.06
2 [Cu ₂ T ₂ - <i>m</i> -X (H ₂ O) ₄](ClO ₄) ₄ .3H ₂ O.NaClO ₄	2.29	170	2.05
3 [Cu ₂ T ₂ - <i>p</i> -X Cl ₄]	2.30	176	2.06
5 [Cu ₂ T ₂ - <i>o</i> -X Ac ₂ (H ₂ O) ₂](ClO ₄) ₂ .6H ₂ O	2.27	166	2.05
6 [Cu ₂ T ₂ - <i>m</i> -X Ac ₂ (H ₂ O) ₂](ClO ₄) ₂ .4H ₂ O	2.27	175	2.05
11 [Cu Me ₃ Tacn (H ₂ O) ₂](ClO ₄) ₂	2.34	161	2.06

Chapter Three

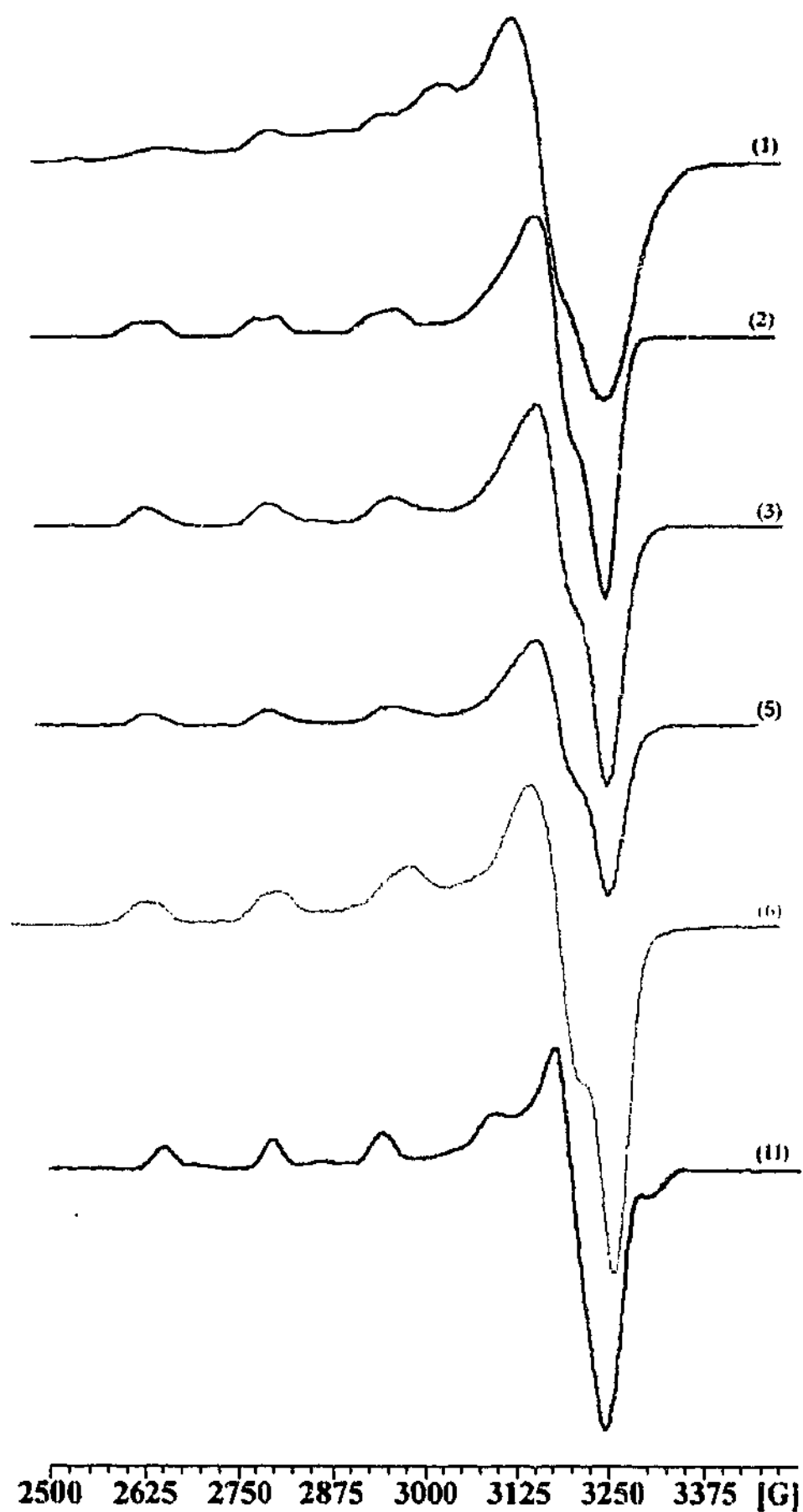


Figure 3.30 ESR spectra of complexes 1-3, 5, 6 and 11 recorded at 77K for frozen solutions of ethylene glycol/water (1:1) for 1-3 and DMF/toluene for 5, 6 and 11

3.7.2.2 Bridged Complexes

Room temperature magnetic moments for the bridged copper(II) complexes 4, 9 and 10 were performed on powdered samples (Table 3.17). The value for complex 4 is a little reduced while that for 9 is in the range normally expected for mononuclear or polynuclear copper(II) complexes. Complex 10 shows a moment which is well below the expected value due to antiferromagnetic coupling between the metal centres.

Table 3.17 Room temperature magnetic moments per Cu(II) for complexes 4, 9 and 10

Complex	Magnetic Moment (μ_B) per Cu
4 $[\text{Cu}_2(\text{T}_2\text{PrO})\text{Br}_2]\text{Br}\cdot 2\text{H}_2\text{O}$	1.56
9 $[\text{Cu}_3(\text{Me}_3\text{tacn})(\text{PhP})_2](\text{ClO}_4)_2\cdot \frac{1}{2}\text{H}_2\text{O}$	1.85
10 $[\text{Cu}_2(\text{T}_2\text{-}m\text{-X})(\text{NPP})(\mu\text{-OH})](\text{ClO}_4)\cdot \text{H}_2\text{O}$	0.82

3.7.2.2.1 Magnetism and ESR Data for $[\text{Cu}_2(\text{T}_2\text{PrO})\text{Br}_2]\text{Br}\cdot 2\text{H}_2\text{O}$ (4)

Magnetic susceptibilities of complex 4 were determined in a field of 1T over the temperature range of 300 – 4.2 K. The plots are shown in Figures 3.31 and 3.32. The plot of 4 was fitted to Equation 3.1 (see previous section). The small increase in the magnetic susceptibility observed at low temperatures for complex 4 is due to a trace of monomeric impurity, which is a feature commonly observed within complexes possessing antiferromagnetic interactions between the metal centres.⁶¹

Chapter Three

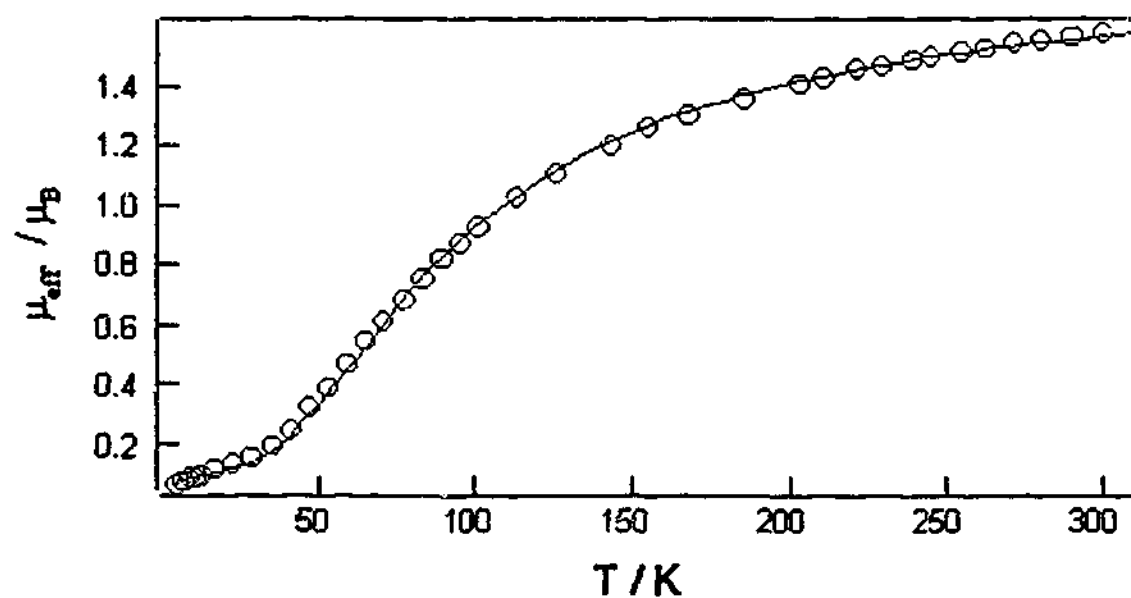


Figure 3.31 Plot of μ_{eff} (per Cu) versus temperature for complex 4

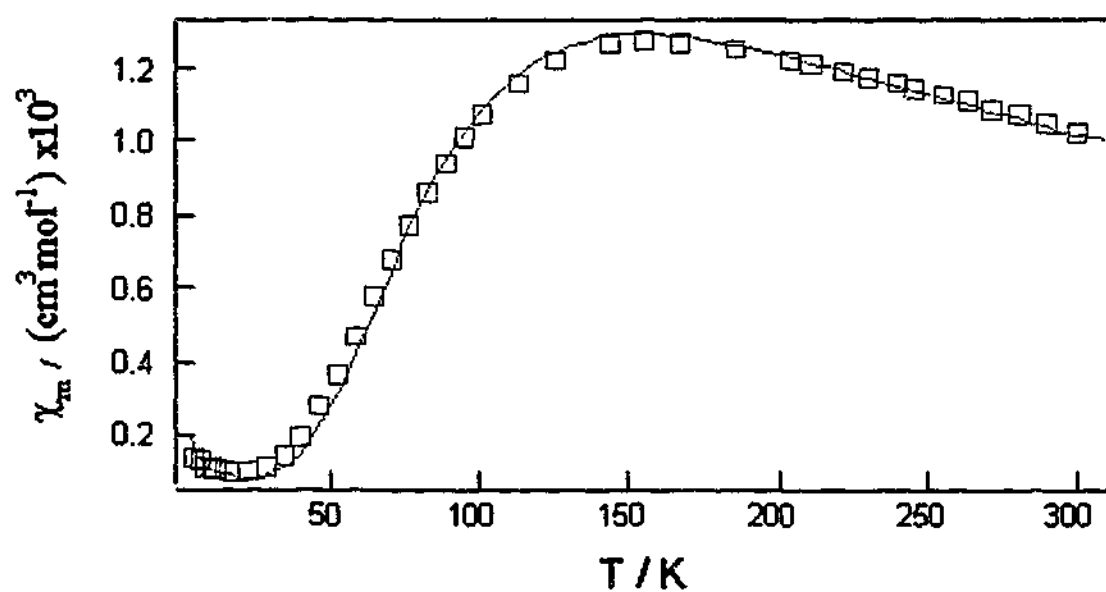


Figure 3.32 Plot of χ_m (per Cu) versus temperature for complex 4

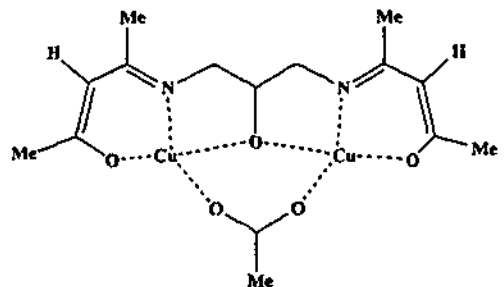
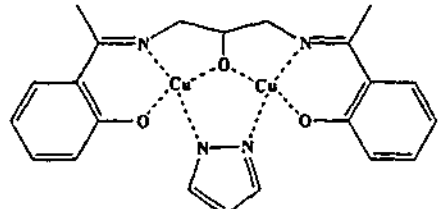
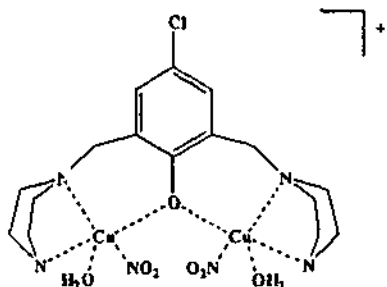
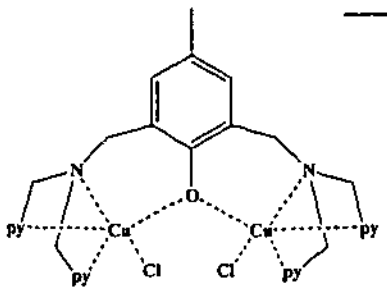
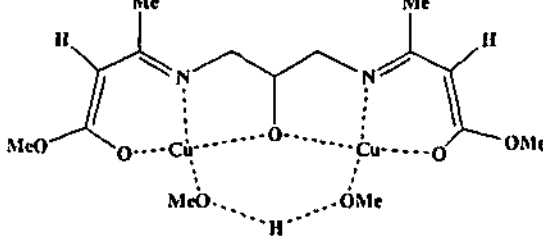
The variable temperature magnetic moment plot of 4 shows a steady decrease in magnetic moment from $1.57 \mu_B$ (per Cu) at 300 K to $0.05 \mu_B$ at 4.2 K, which is indicative of moderate strength antiferromagnetic coupling between the copper(II) centres. The data were fitted to Equation 3.1 and the parameters obtained are as follows, g value = 2.01, $J = -86 \text{ cm}^{-1}$ and $P = 0.0012$. This value of J can be compared

Chapter Three

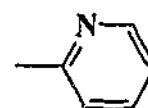
to other 2-propanolato or phenolato bridged complexes, most of which have a second (or third) exogenous bridge such as OAc^- or pyrazolate (see Table 3.18).⁶⁴⁻⁶⁸ One complex which contains a single alkoxo bridge as part of a Schiff-base ligand, together with an H-bonded link (MeO-H-OMe) was reported to display very strong coupling with $J = -318 \text{ cm}^{-1}$. The Cu-O-Cu bridge angle of $137.7(5)^\circ$ compared well to the present $136.2(2)^\circ$. Such large angles and corresponding large Cu...Cu separations normally lead to very strong antiferromagnetic coupling⁶⁴ and thus the smaller J value for 4 needs explanation. Normally the "end groups" (acac, sal, tacn, $\text{N}(\text{CH}_2\text{py})_2$, halide) play a minor part in the net J value when they lead to unusual geometries around each Cu with consequent effects on the Cu "magnetic orbitals" used in the bridging pathways (e.g. $J = 0$ for the Cl-complex shown in Table 3.18⁶⁹ because the PhO^- bridge is in the apical (z) position relative to Cu ($d_{x^2-y^2}$) magnetic orbitals). More important is the nature of the Cu(II) orbitals (i.e. $d_{x^2-y^2}$) for planar or SP geometry and their coplanarity and bridging geometry (Cu-O-Cu) relative to the RO^- (or PhO^-) bridging atom. The more coplanar, the more negative is the J value. Dihedral angles between the Cu SP basal planes, which incorporate the RO^- (or PhO^-) bridging oxygen lead to smaller J values (see the NO_2 derivative in Table 3.18⁷⁰). Other features such as non-trigonal O(bridging) geometry⁷⁰ and the presence of exogenous bridges (counter-complementarity effects^{64,69}) will also reduce the antiferromagnetic coupling. In complex 4 the dihedral angle of $76.35(8)^\circ$ shows that the SP basal planes of each Cu(II) are not coplanar and thus this leads to a diminution in the size of J relative to other μ -alkoxo (only) systems.⁶⁴ In the NO_2 (phenolate only) complex, shown in Table 3.18, the dihedral angle is 83.7° and a lower than expected J value (-122 cm^{-1}) is observed.

Chapter Three

Table 3.18 Cu-O-Cu bond angles, Cu...Cu distances and J values for binuclear copper(II) complexes

Complex	Cu-O-Cu Angle (°)	Cu...Cu distance (Å)	J value (cm ⁻¹)	Ref.
4 [Cu ₂ (T ₂ -PrO)Br ₂].2H ₂ O	136.2	3.57	-86	TW
	133.3(3)	3.502(2)	-83	64
	125.1	3.359(4)	-120	68
	130.1(6)	3.603(4)	-122	70
	140.2(5)	4.128(3)	0	69
	137.7(5)	3.644(2)	-318	64

Note: TW = This Work; py =



An X-band ESR spectrum of **4** was recorded at 77 K for a frozen solution in DMF/toluene. The signal was very weak and could not be distinguished from the cavity signal of the instrument. This is not unexpected due to the medium strength coupling between the Cu(II) centres as seen in the magnetic susceptibility plots (Figures 3.30 and 3.31), although, in principal, a triplet state line should be visible at 77 K for such a J value.

3.7.2.2.2 ESR Data for $[\text{Cu}_6(\text{T}_3\text{mes})_2(\mu\text{-OH})_6](\text{ClO}_4)_6 \cdot 6\text{H}_2\text{O}$ (**7**)

An X-band ESR spectrum of the copper(II) complex **7** was recorded of a frozen solution in DMF/toluene. Complex **7** shows a strong signal centred around 3000 G. The parameters obtained are typical of a SP environment around the Cu(II) centre with $g_{\parallel} > g_{\perp} > 2$, and are similar to those seen in the previous section. The spectrum of **7** is shown in Figure 3.33 and the parameter values are $g_{\parallel} = 2.27$, $A_{\parallel} = 154 \times 10^{-4} \text{ cm}^{-1}$ and $g_{\perp} = 2.06$. This spectrum arises either from monomeric impurities or from the uncoupled trimer.



Figure 3.33 X-band ESR spectrum of complex **7** recorded at 77 K for a frozen DMF/Toluene solution

3.7.2.2.3 Magnetism and ESR Data for $[\text{Cu}_3(\text{Me}_3\text{tacn})(\text{PhP})_2](\text{ClO}_4)_2 \cdot \frac{1}{2}\text{H}_2\text{O}$ (9)

Variable temperature magnetic susceptibilities of 9 were obtained on powdered samples in the temperature range of 300-4.2 K, in a field of 1T. The χ values, per trimer are Curie-like in this temperature range (Figure 3.34). The corresponding magnetic moments, per Cu_3 , shown in Figure 3.35 A, show a small decrease from $3.2 \mu_B$ (1.85 per Cu) at 300 K, to $3.1 \mu_B$ at 14 K, then more rapidly to $3.01 \mu_B$ (1.73 per Cu) at 4.2 K, indicative of very weak antiferromagnetic coupling. Such weak coupling is not unexpected in phosphate bridged Cu(II) and other metals systems.^{6,71,72} In complex 9, weak coupling probably also relates to the mode of bridging (Figure 3.17) in which two adjacent basal positions of each Cu(II) SP are linked via O-P-O from the organophosphate, above and below the plane defined by the three Cu(II) centres. Unlike the classical strongly coupled $[\text{Cu}_2(\text{acetate})_4]$ case (O-C-O arms), the basal planes, in which the $d_{x^2-y^2}$ "magnetic" orbital are situated, are not parallel or close to each other. Attempts were made to quantitatively fit the susceptibility data. In the first instance, an isosceles triangle model was used as an approximation and this involved two J-values. The data were fitted according to Equation 3.2, and the general approach is outlined in the books of Kahn⁷³ and of Mabbs and Machin.⁷⁴

$$\chi_m = \frac{N\beta^2 g^2 \left[\exp\left(\frac{-2J}{kT}\right) + \exp\left(\frac{-2J_{12}}{kT}\right) + 10 \exp\left(\frac{J}{kT}\right) \right]}{\exp\left(\frac{-2J}{kT}\right) + \exp\left(\frac{-2J_{12}}{kT}\right) + 2 \exp\left(\frac{J}{kT}\right)} + N_a \quad \text{Eq. 3.2}$$

Chapter Three

A good fit to the μ/T data was obtained (Figure 3.35 A) using a very small J -value of J_1 (-0.5 cm^{-1}) and of J_2 ($+0.5 \text{ cm}^{-1}$), with $g = 2.09$ and temperature independent paramagnetism (TIP) (N_A) of $180 \times 10^{-6} \text{ cm}^3 \text{ mol}^{-1}$. As can be seen, a negative J_1 and a positive J_2 gave the best fit to the data. Use of a negative J_1 and a negative J_2 gave a poorer fit. It is not clear from the structure, even allowing for different Cu...Cu distances and differences in bridge angles, why there should be a difference in sign. It is probably best to conclude that the coupling is very weak and overall antiferromagnetic (J negative). There is, unfortunately, no large change in μ (per Cu_3) with temperature of the type noted in $[\text{Cu}_3(\text{T}_3\text{mes})(\mu_2\text{-OH})(\mu_3\text{-HPO}_4)(\text{H}_2\text{O})]^{3+}$ yielding a $S = \frac{1}{2}$ ground state at low temperature,⁶ or of the type noted in $[\text{Cu}_3(\text{pyridine-2-aldoximate})_3(\mu_3\text{-OH})]^{2+}$ in which μ (per Cu_3) remains constant at $1.77 \mu_B$ due to an isolated $S = \frac{1}{2}$ ground state at low temperature.⁷⁵ It is clear, however, from the size of μ at 300 K and at 4.2 K, that both J -values are not positive (i.e. $S = \frac{3}{2}$ ground state which would require μ (per Cu_3) at 4.2 K to be $> 3.87 \mu_B$). A second attempt at fitting the data employed a scalene triangle model. The data were fitted according to Equation 3.3, and the general approach is outlined in the books of Kahn⁷³ and of Mabbs and Machin.⁷⁴ The model is parameterised using the energy gaps Δ_1 and Δ_2 which relate to the energies of the three levels $E(^3/2)$ and $E(^3/2, \pm)$. A reasonable fit was obtained in the range 300-14 K, using $\Delta_1 = 5.0 \text{ cm}^{-1}$, $\Delta_2 = 2.0 \text{ cm}^{-1}$ and $g = 2.08$, but the rapid and small decrease which occurs in μ below 10 K was poorly reproduced (Figure 3.35 B). The individual J_{12} , J_{23} and J_{13} values can not be extracted unambiguously from these Δ values. Suffice to say that the energy gaps are small, in line with a very weakly coupled trimer.

$$\chi_m = \frac{\frac{N\beta^2 g^2}{kT} \left[0.5 + 0.5 \exp\left(\frac{-\Delta_1}{kT}\right) + 5 \exp\left(\frac{-\Delta_2}{kT}\right) \right]}{2 + 2 \exp\left(\frac{-\Delta_1}{kT}\right) + 4 \exp\left(\frac{-\Delta_2}{kT}\right)} + N_\alpha \quad \text{Eq. 3.3}$$

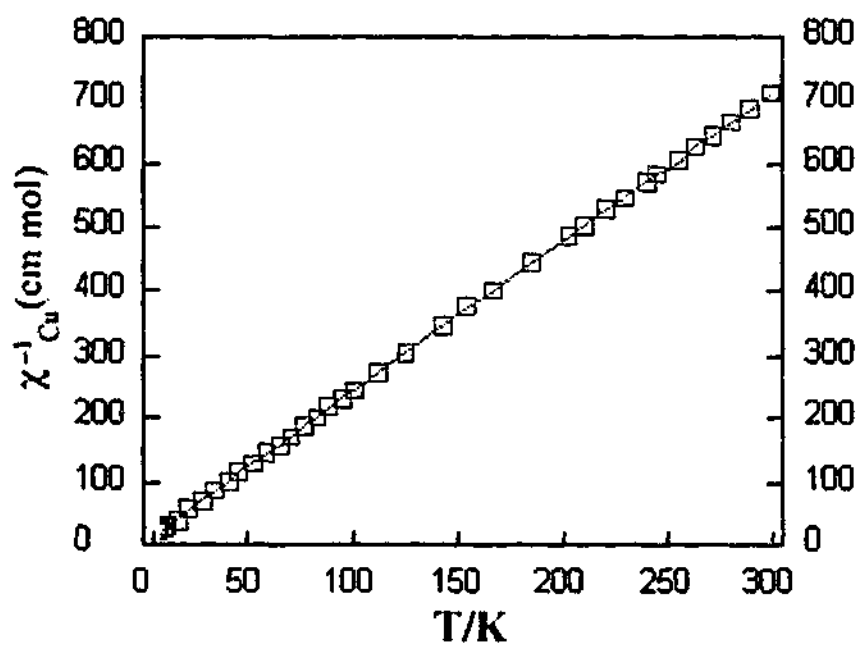
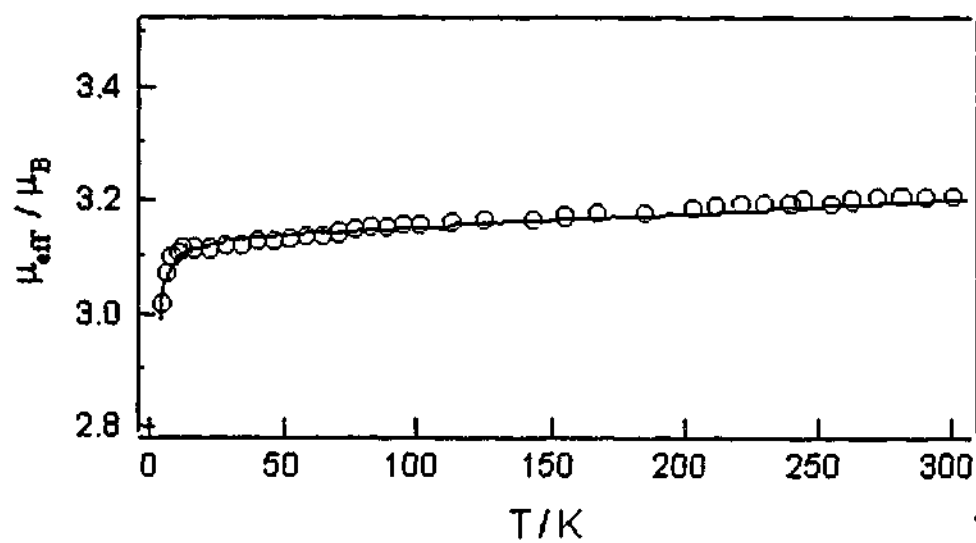
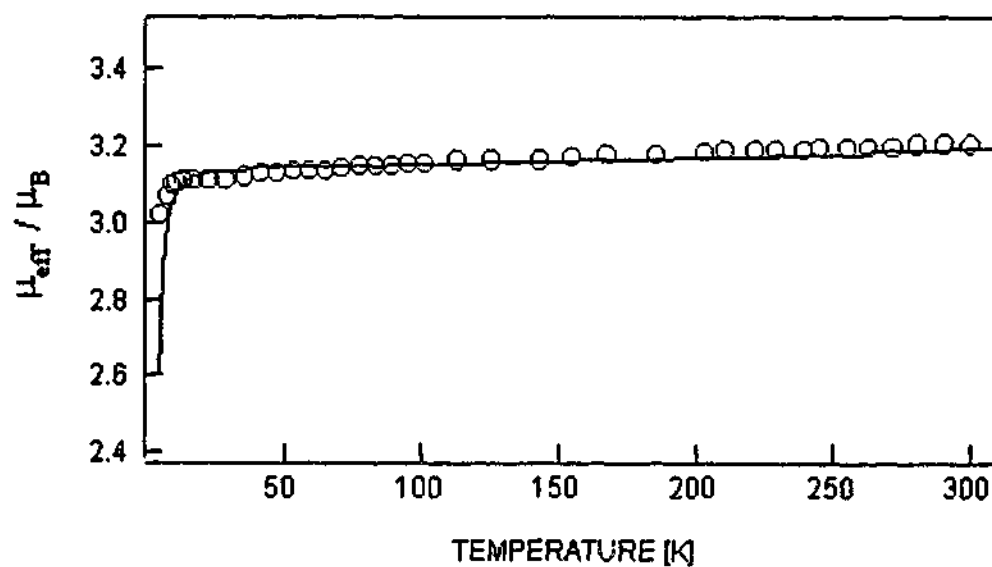


Figure 3.34 Plot of χ_m^{-1} (□) (per Cu) versus temperature for complex 9

Chapter Three



(A)



(B)

Figure 3.35 Plots of μ_{eff} (per Cu_3) versus temperature for complex **9**. The solid lines were calculated using Equation 3.2 and 3.3, respectively, with the parameter values given in the text

The ESR spectrum of **9** was recorded at 77K of a frozen DMF/toluene solution at very high gain (Figure 3.36). The spectrum shows two sets of signals, with one set having

Chapter Three

larger $A_{||}$ than the other. The set with $A_{||} = 154 \times 10^{-4} \text{ cm}^{-1}$ has $g_{||} = 2.31$, and that with $A_{||} = 178 \times 10^{-4} \text{ cm}^{-1}$ has $g_{||} = 2.24$. This suggests that one of the Cu(II) centres is in a different environment to the other two or that the DMF (partially) causes the complex to dissociate. As seen in Section 3.7.1, the electronic spectra of **9** in the solid state, in aqueous solution and in DMF solution show very little differences. Crystallographically, Cu(2) and Cu(3) are in similar environments, while Cu(1) is in a more distorted geometry (Table 3.9). The parameters obtained, however, are still indicative of a mononuclear SP environment around all Cu(II) centres. The magnetic susceptibility plot of the neat powder shows very weak antiferromagnetic coupling within the trinuclear moiety. Since ESR spectroscopy, particularly at the gain setting used (4×10^4), is a sensitive technique and capable of detecting monomeric signals, perhaps brought about by trimer dissociation in DMF, it is hard to know with certainty whether the two signals seen in frozen solution are from the weakly coupled trimer, or from some monomer species. Electronic spectra of **9** in the solid state, in aqueous solution and DMF between 1200 and 400 nm showed no significant shift in the absorption maxima centred at *ca.* 650 nm, showing no evidence of dissociation of the complex in solution. A more detailed study of "half-field" ($\Delta M_s = 2$) ESR signals would be required to identify any spin-coupled signals.⁶²

Chapter Three

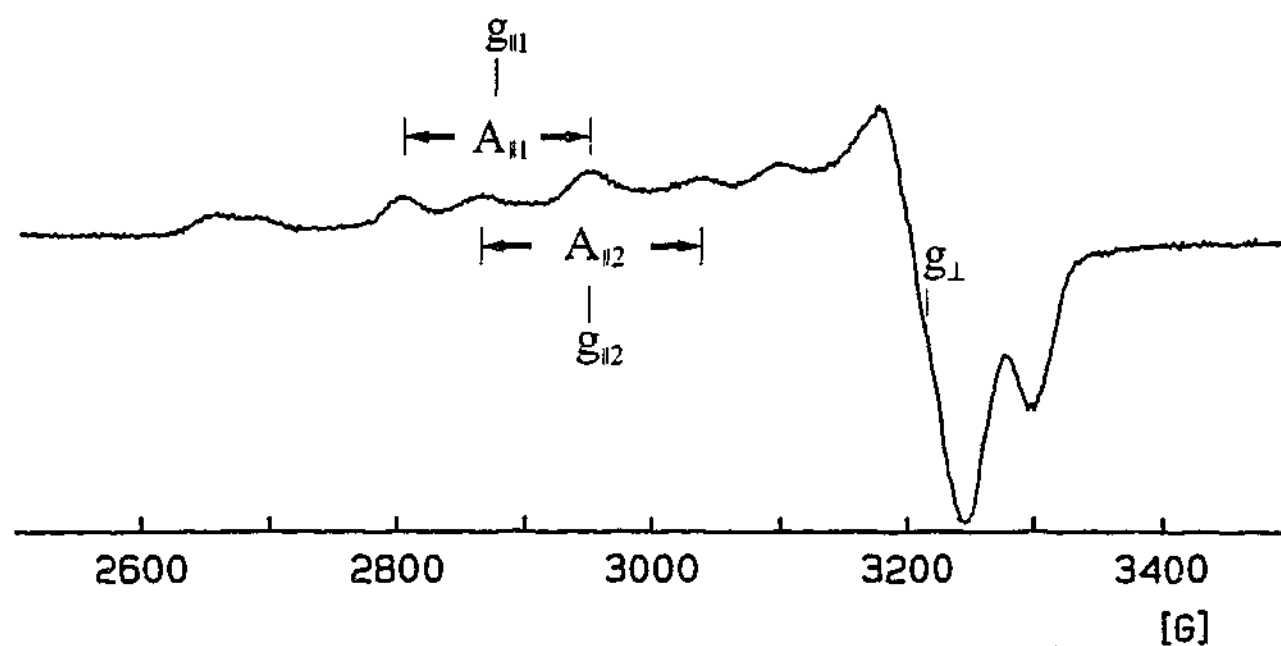


Figure 3.36 ESR spectrum of a frozen DMF/Toluene solution of **9** at 77 K

Table 3.19 ESR data of a frozen DMF/Toluene solution of **9** at 77 K

Complex	$g_{ }$	$A_{ }$ $\times 10^{-4} \text{ cm}^{-1}$	g_{\perp}
9 $[\text{Cu}_3(\text{Me}_3\text{tacn})(\text{PhP})_2](\text{ClO}_4) \cdot \frac{1}{2}\text{H}_2\text{O}$	2.31	154	2.06
	2.24	178	~ 2.06

3.7.2.2.4 Magnetism and ESR Data for $[\text{Cu}_2(\text{T}_2\text{-}m\text{-X})(\text{NPP})(\mu\text{-OH})](\text{ClO}_4) \cdot \text{H}_2\text{O}$

(10)

Magnetic susceptibilities of complex **10** were measured in a field of 1T over the temperature range of 300 – 4.2 K. The plots are shown in Figure 3.37. The variable temperature magnetic moment plot of **10** shows a decrease in magnetic moment with temperature which is indicative of strong antiferromagnetic coupling between the

Chapter Three

copper(II) centres. The plot reaches a minimum value of 0.10 BM at *ca.* 90 K, after which the magnetic moment is fairly constant. The increase in the corresponding magnetic susceptibility observed at low temperatures is due to a monomeric impurity, which is a feature commonly observed within Cu(II) complexes possessing antiferromagnetic interactions between the metal centres.⁶¹ The data were fitted to Equation 3.1 (see previous section) and the parameters obtained are as follows, *g* value = 2.00, *J* = -275 cm⁻¹ and *P* = 0.004. This large, negative value of *J* arises primarily due to strong antiferromagnetic coupling across the Cu-O(H)-Cu bridge, since the NPP bridge and the *m*-xylyl moiety are poor superexchange pathways.¹⁵ The OH link joins the Cu *d*_{x²-y² orbitals. The Cu...Cu distance of 3.57 Å and the Cu-O-Cu angle of 138.2° are predicted to lead to a *J* value of -515 cm⁻¹ by use of Thompson's data⁷⁶ for single μ -OH bridged complexes. This angular correlation, however, applies to a series of dinuclear compounds which contain an aromatic diazine (N-N) as the second bridge and this does not allow for large Cu-O-Cu angles of the magnitude observed for **10**. It also has a different superexchange ability than does the organophosphate and so the angular correlation gives poor agreement with the present system, although strong antiferromagnetic coupling is anticipated, largely via the Cu-O(H)-Cu angle.}

A more appropriate comparison is made with compounds such as [(bpy)₂Cu(μ -OH)(μ -ClO₄)Cu(bpy)₂](ClO₄)₂⁷⁷ for which *J* is -161 cm⁻¹, Cu-O-Cu = 141.6(3)° and Cu-Cu distance = 3.642(2) Å. Few [Cu(μ -OH)(μ -phosphate)Cu] bridged complexes are available for comparison. In Graham's trimer,⁶ the [Cu(1)(OH)(O₂PO₂)Cu(2)] moiety yielded *J*₁₂ = -161 cm⁻¹, less than observed for **10**, even though the bridging geometry is rather similar (Figure 3.22). Clearly more examples of μ -OH, μ -phosphate are required.

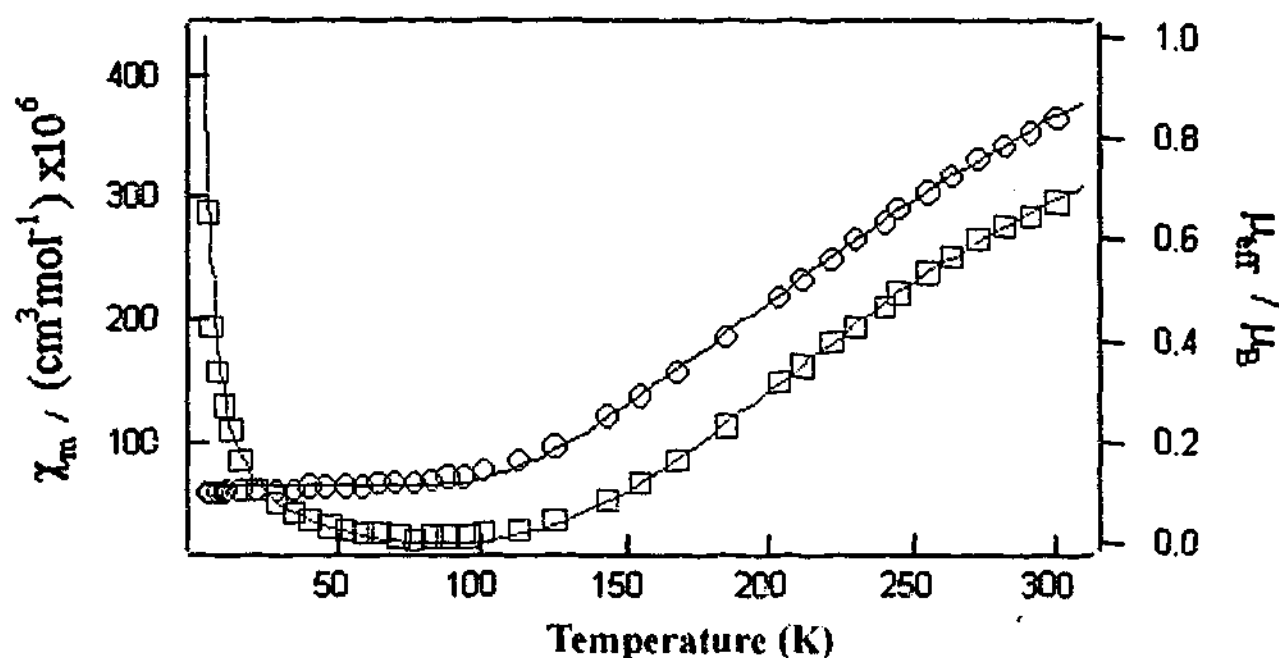


Figure 3.37 Plot of χ_m (□) and μ_{eff} (○) (per Cu) versus temperature for complex 10

The X-band ESR spectrum of 10 was recorded in a frozen solution of DMF/toluene at 77 K. The spectrum of 10 also shows a very weak signal centred at *ca.* 3000 G, ($g = 2.04$) however, the signal is thought to be due to a monomeric impurity as seen in the magnetic susceptibility plot. As with 4 this is not unexpected due to the strong coupling seen at low temperature in the magnetic susceptibility plot (Figure 3.37).

3.8 Concluding Remarks

A series of copper(II) complexes of mono- and poly-nucleating derivatives of 1,4,7-triazacyclononane have been prepared and characterised, using the ligands presented in Chapter 2. In each case, the tacn macrocycle bound to one of the four triangular faces of the square pyramid. This is a general feature of these complexes. Complex 11 was prepared in order to compare its reactivity with phosphate esters. It was chosen over the simpler $[\text{Cu}(\text{tacn})(\text{H}_2\text{O})_2]^{2+}$ due to the smaller likelihood of formation of sandwich type structures that the latter is known to form in solution.¹⁴

Chapter Three

From structural and analytical data, complexes 1-7 were concluded to have at least one free coordination site available for the coordination of substrates or for generation of nucleophiles, making them suitable for phosphate ester hydrolytic studies. Reaction of several of these complexes with various phosphates formed compounds with the phosphate moiety incorporated. Reaction of $[\text{Cu}(\text{tacn})(\text{H}_2\text{O})_2]^{2+}$ with BNPP results in the formation of the sandwich complex, $[\text{Cu}(\text{tacn})_2]^{2+}$ (8), which will ultimately inhibit the hydrolysis of phosphate esters. Compound 9, in which three $\text{Cu}(\text{Me}_3\text{tacn})$ units are linked together by three oxygen atoms from each of two phenyl phosphate moieties, illustrates possible cooperative effects of up to three $[\text{Cu}(\text{Me}_3\text{tacn})]^{2+}$ able to work in concert to hydrolyse phosphate esters. Likewise, compound 10 shows two copper tacn rings able to work together in binding phosphate esters, and thereby increasing the rate of hydrolysis. This complex also illustrates the benefits of using bis(tacn) ligands over the mononucleating tacn ligand, as the bridge inhibits the formation of the sandwich type structure, thereby making more reactive sites available for the hydrolysis.

Magnetic susceptibility studies show that the copper(II) complexes which are bridged through a hydroxide or alkoxide bridges have medium to strong antiferromagnetic coupling between the copper centres (compounds 4 and 10). In contrast, compound 9 shows very little interaction between the copper centres, indicating that the phosphate bridge in 10 is not the primary source of coupling between the two or more copper centres. Comparisons have been made to related systems.

3.9 Experimental

Laboratory chemicals and solvents

All reagents were of reagent grade quality, obtained from commercial suppliers and used without further purification. Solvents were used as received or dried over 4Å molecular sieves. Distilled water was used throughout.

Physical Measurements

Infrared spectra

Infrared spectra were recorded using KBr disks or nujol mulls on a Perkin-Elmer 1600 series FTIR spectrophotometer at a resolution of 4.0 or 8.0 cm^{-1} . Abbreviations used to describe intensities are: s (strong), m (medium), w (weak) and br (broad).

Electronic spectra

UV-Visible-NIR spectra of complexes were measured on a Cary 5G spectrophotometer. The maximum absorbance wavelengths (λ_{max} , nm) are reported with the corresponding extinction coefficients (ϵ , $\text{M}^{-1}\text{cm}^{-1}$) in parentheses. Solution spectra were recorded using 1 cm quartz cells and solid state spectra were recorded on powdered samples.

Magnetic susceptibility measurements

Room temperature magnetic moments were measured on a Faraday balance which incorporated a four inch Newport electromagnet fitted with Faraday-profile pole faces. Samples were held in a small quartz bucket suspended from a Cahn RG microbalance by a nylon thread. Diamagnetic corrections were made using Pascal's constants.

Chapter Three

Variable temperature magnetic susceptibility measurements were performed by Dr B. Mobaraki, Monash University, on a Quantum Design MPMS Squid magnetometer over a temperature range of 4.2 to 300 K, at a field strength of 10 000 G (1 T). Samples were contained in calibrated gelatine capsules and held in the centre of a drinking straw fused to the end of the sample rod. The temperature and field were checked against a standard Pd sample and $\text{CuSO}_4 \cdot 5\text{H}_2\text{O}$. Fitting of the data employed a non-linear least squares program called POLYMER which was written at Monash University.

Microprobe analyses

Electron microprobe analyses were recorded by Mr A. Van den Bergen, Monash University, with a Jeol JSM-1 scanning electron microscope through an NEC X-ray detector and pulse-processing system connected to a Packard multi-channel analyser. Solid samples were mounted on an aluminium planchet using double sided conducting carbon impregnated sticky tape.

Microanalyses

Analyses of C, H and N were performed by Chemical and Microanalytical Services Pty. Ltd. (CMAS), Melbourne, Australia, or the Campbell Microanalytic Services, University of Otago, Dunedin, New Zealand.

Electron spin resonance spectra

ESR spectra were carried out by Simon Drew, Monash University, on a Varian E12 spectrometer operating at X-band frequency (9.1 GHz). The spectra were recorded at 77 K in a 2:1 mixture of ethylene glycol/water or 1:1 DMF/toluene. The solution was placed in an iron-free quartz tube.

Chapter Three

Conductivity measurements

Solution conductivity measurements were made using a Crison 522 Conductimeter with Pt black electrodes. A 0.020 M KCl solution was used to calibrate the meter.

Synthesis of Complexes**[Cu₂(T₂-o-X)Cl₄] (1)**

T₂-o-X·6HCl (0.50 g, 0.90 mmol) was dissolved in water (10 ml) and a solution of CuCl₂·2H₂O (0.61 g, 3.6 mmol) in water (10 ml) was added. The pH of the dark blue solution was adjusted to 7 with 2M NaOH. The precipitated Cu(OH)₂ was removed and the solution heated to reduce the volume by approximately half. The solution was allowed to cool then left to slowly evaporate. After 2 weeks a small number of blue crystals had formed and were collected by vacuum filtration.

Yield: 0.15 g (27%). Analytical data: Found (%): C 37.9; H 5.9; N 13.2. Calculated for Cu₂C₂₀H₃₆N₆Cl₄ (%): C 38.2; H 5.8; N 13.4. UV-Vis spectrum: Solid (λ_{\max} , nm) 330, 636, 1043. Solution: (H₂O; λ_{\max} , nm (ϵ , M⁻¹cm⁻¹)): 255 (5340), 649 (81), 1028 (39). IR spectrum (KBr; ν , cm⁻¹): 3417 s, 3225 s, 2905 m, 2849 m, 1638 w, 1619 w, 1561 w, 1488 m, 1446 m, 1385 w, 1356 w, 1285 w, 1233 w, 1198 w, 1150 w, 1095 m, 1012 m, 993 w, 944 w, 893 w, 862 w, 833 w, 775 w, 731 w, 656 m, 633 w, 580 w, 457 w, 420 w. Electron microprobe: Cu, Cl present. Magnetic moment: $\mu_{\text{eff}}(\text{per Cu}) = 1.63 \mu_{\text{B}}$ at 295 K. Electron spin resonance (H₂O/Ethylene glycol); $g_{\parallel} 2.29$ $A_{\parallel} 165 \times 10^{-4} \text{ cm}^{-1}$; $g_{\perp} 2.06$. Molar conductivity (H₂O): 48 Scm²mol⁻¹.

Chapter Three

$$([\text{Cu}_2(\text{T}_2\text{-}m\text{-X})(\text{H}_2\text{O})_4](\text{ClO}_4)_4 \cdot 3\text{H}_2\text{O} \cdot \text{NaClO}_4) \text{ (2)}$$

$\text{T}_2\text{-}m\text{-X} \cdot 6\text{HCl}$ (0.50 g, 0.90 mmol) was dissolved in water (10 ml) and a solution of $\text{Cu}(\text{ClO}_4)_2 \cdot 6\text{H}_2\text{O}$ (1.33 g, 3.60 mmol (excess)) in water (10 ml) was added. The pH of the dark blue solution was adjusted to 7 with 1M NaOH. The precipitated $\text{Cu}(\text{OH})_2$ was removed by filtration and the filtrate loaded onto an ion-exchange column. The complex was eluted with 0.1 M NaClO_4 . Two bands separated on the column, the first due to excess Cu(II). The second band was collected and reduced in volume to about 20 ml and the solvent was left to slowly evaporate. After several days a blue powder formed and was collected by vacuum filtration and washed with a small amount of acetone.

Yield: 0.64 g (77%). Analytical data: Found (%): C 21.2; H 4.3; N 7.4. Calculated for $\text{Cu}_2\text{C}_{22}\text{H}_6\text{N}_6\text{O}_{27}\text{Cl}_5\text{Na}$ (%): C 21.2; H 4.4, N 7.4. UV-Visible-NIR spectrum: Solid (λ_{max} , nm): 305, 640, 1072. Solution: (H_2O ; λ_{max} , nm (ϵ , $\text{M}^{-1}\text{cm}^{-1}$): 250 (7779), 644 (72), 1043 (38). IR spectrum (KBr; ν , cm^{-1}): 3424 m br, 3306 m, 2940 m, 2880 m, 2021 w, 1738 w, 1638 w, 1544 w, 1491 w, 1459 m, 1362 w, 1285 w, 1239 w, 1286 s br, 948 m, 860 w, 826 w, 737 w, 675 w, 625 m, 582 w, 500 w, 423 w. Electron microprobe: Cu, Cl and Na present. Magnetic moment: μ_{eff} (per Cu) = 1.85 μ_{B} at 295 K. Electron spin resonance (H_2O /Ethylene glycol); g_{\parallel} 2.29; A_{\parallel} $170 \times 10^{-4} \text{ cm}^{-1}$; g_{\perp} 2.05. Molar conductivity (H_2O): $572 \text{ Scm}^2\text{mol}^{-1}$.

$$([\text{Cu}_2(\text{T}_2\text{-}p\text{-X})\text{Cl}_4] \text{ (3)}$$

Dark blue crystals of 3 were obtained from $\text{T}_2\text{-}p\text{-X} \cdot 6\text{HCl}$ (0.50g, 0.90 mmol) and CuCl_2 (0.61g, 3.6 mmol) using the same procedure as described for compound 1.

Yield: 0.19g (33%). Analytical data: Found (%): C 37.6; H 5.9; N 13.4. Calculated for $\text{Cu}_2\text{C}_{20}\text{H}_{36}\text{N}_6\text{C}_4$ (%): C 38.2; H 5.8; N 13.4. UV-Visible-NIR spectrum: Solid (λ_{max} ,

Chapter Three

nm): 326, 636, 981. Solution: (H₂O; λ_{\max} , nm (ϵ , M⁻¹cm⁻¹)): 253 (sh) (5897), 644 (80), 1054 (41). IR spectrum (KBr; ν , cm⁻¹): 3449 br w, 3270 s, 2943 m, 2846 m, 1638 w, 1544 w, 1511 w, 1492 w, 1459 w, 1380 w, 1347 w, 1282 w, 1234 w, 1149 w, 1099 m, 1040 m, 1004 s, 946 m, 894 w, 864 m, 829 m, 766 w, 732 w, 629 w, 581 w, 495 w, 430 w. Electron microprobe: Cu, Cl present. Magnetic moment: μ_{eff} (per Cu) = 1.73 μ_{B} at 297 K. Electron spin resonance (H₂O/Ethylene glycol); g_{\parallel} =2.30 ; A_{\parallel} =176 $\times 10^{-4}$ cm⁻¹; g_{\perp} =2.06. Molar conductivity (H₂O): 456 Scm²mol⁻¹.

[Cu₂(T₂-PrO)Br₂]Br·2H₂O (4)

T₂-PrOH·6HBr (0.30 g, 0.38 mmol) was dissolved in water (10 ml) and the pH was adjusted to 6 with 1 M NaOH. An aqueous solution (5 ml) of Cu(ClO₄)₂·6H₂O (0.56 g, 1.5 mmol) was added. During the addition the pH dropped back to *ca.* 3. The pH was adjusted up to 10 with 1M NaOH and the Cu(OH)₂ that formed was removed and the pH adjusted back to 7 with HCl. The solution was allowed to stand and after 2 weeks blue crystals of the product had formed. These were collected by vacuum filtration, washed with MeOH and air dried.

Yield = 0.17 g (63%). Analytical data: Found (%): C 25.0, H 5.1, N 11.4. Calculated for Cu₂C₁₅H₃₇N₆O₃Br₃ (%): C 25.2, H 5.2, N 11.7. UV-Visible-NIR spectrum: Solid, (λ_{\max} , nm): 631, 1081. Solution: (H₂O; λ_{\max} , nm (ϵ , M⁻¹cm⁻¹)): 270 (6291), 689 (252), 1072 (50). IR spectrum (KBr; ν , cm⁻¹): 3463 s, 3335 m, 3290 s, 3216 m, 2942 s, 2896 s, 2848 s, 2050 w, 1738 w, 1648 w, 1613 m, 1490 w, 1455 m, 1380 m, 1357 m, 1333 w, 1283 w, 1242 w, 1178 w, 1155 w, 1110 s, 1087 s, 1010 s, 987 m, 927 m, 900 m, 870 m, 844 m, 820 m, 776 m, 748 w, 687 w, 569 w, 543 w, 504 w, 412 w. Electron microprobe: Cu, Cl present. Magnetic moment: μ_{eff} (per Cu) = 1.56 μ_{B} at 300 K.

Chapter Three

Electron spin resonance: g_{\parallel} 2.27, A_{\parallel} 161×10^4 cm; g_{\perp} 2.05. Molar conductivity (H_2O): $397 \text{ Scm}^2\text{mol}^{-1}$.

$[\text{Cu}_2(\text{T}_2\text{-}o\text{-X Ac}_2)(\text{H}_2\text{O})_2](\text{ClO}_4)_2 \cdot 4\text{H}_2\text{O}$ (5)

The crude oil of $\text{T}_2\text{-}o\text{-X Ac}_2 \cdot 6\text{HCl}$ was used directly in the synthesis of the copper complex. $\text{T}_2\text{-}o\text{-X Ac}_2$ (0.72 g, 1.0 mmol) was dissolved in water (20 ml) and an aqueous solution of $\text{CuCl}_2 \cdot 2\text{H}_2\text{O}$ (2.24 g, 13.1 mmol, in excess) was added resulting in a dark blue solution. The pH was adjusted to 5 with 2M NaOH and the $\text{Cu}(\text{OH})_2$ which formed was removed. The resulting solution was diluted to 2L with water and loaded onto a Sephadex SP-C25 cation exchange column (2.5×25 cm). Addition of 0.1 M NaClO_4 eluted several pale blue bands followed by the main band containing the desired complex. The eluent containing the complex was reduced in volume *in vacuo* to ~30 mls and left to slowly evaporate. A blue powder formed the following day, was collected by vacuum filtration and washed with MeOH. The blue product was left to air dry.

Yield = 0.31g (32%). Analytical data: Found (%): C 30.6, H 5.0, N 8.9. Calculated for $\text{Cu}_2\text{C}_{24}\text{H}_{54}\text{N}_6\text{O}_{20}\text{Cl}_2$ (%): C 30.5; H 5.8; N 8.9. UV-Visible-NIR spectrum: Solid (λ_{max} , nm): 276, 658, 1016. Solution: (H_2O ; λ_{max} , nm (ϵ , $\text{M}^{-1}\text{cm}^{-1}$)): 257 (6916), 663 (173), 939 (67). IR spectrum (KBr; ν , cm^{-1}): 3420 m, 3297 m, 2928 m, 2110 w, 1598 s, 1494 m, 1448 m, 1400 m, 1370 m, 1318 w, 1237 w, 1099 s, 929 w, 870 w, 833 w, 784 w, 732 w, 624 s, 460 w, 421 w. Electron microprobe: Cu, Cl present only. Magnetic moment: μ_{eff} (per Cu) = $1.81 \mu_{\text{B}}$ at 25°C . Electron spin resonance (DMF/Toluene); g_{\parallel} =2.27, A_{\parallel} $166 \times 10^4 \text{ cm}^{-1}$, g_{\perp} =2.05. Molar conductivity (H_2O): $284 \text{ Scm}^2\text{mol}^{-1}$. Electrospray mass spectroscopy ($\text{H}_2\text{O}:\text{CH}_3\text{CN}$) m/z : 701 (6%) $[\text{Cu}_2(\text{T}_2\text{-}o\text{-X Ac}_2)]\text{ClO}_4^+$.

Chapter Three

[Cu₂(T₂-*m*-X Ac₂)(H₂O)₂](ClO₄)₂·4H₂O (6)

Compound 6 was prepared in an identical manner to 5 using T₂-*m*-X Ac₂·6HCl (1.3 g, 1.8 mmol) and CuCl₂·2H₂O (1g, 6 mmol excess). The blue powder was collected, washed with MeOH and air dried.

Yield = 0.66 g (39%). Analytical data: Found (%): C 31.7; H 4.9; N 9.4. Calculated for Cu₂C₂₄H₅₀N₆O₁₈Cl₂ (%): C 31.7; H 5.6; N 9.3. UV-Visible-NIR spectrum Solid, (λ_{max}, nm): 310, 670, 1018. Solution: (H₂O; λ_{max}, nm (ε, M⁻¹cm⁻¹)): 670 (166), 1010 (58). IR spectrum (KBr; ν, cm⁻¹): 3423 br m, 3316 m, 2938 m, 2883 w, 2030 w, 1596 s, 1493 w, 1444 w, 1405 m, 1368 m, 1320 w, 1288 w, 1239 w, 1090 s, 981 m, 932 w, 867 w, 823 w, 792 w, 735 w, 700 w, 625 s, 571 w, 541 w, 505 w, 458 w. Electron microprobe: Cu, Cl present. Magnetic moment: μ_{eff} (per Cu) = 1.84 μ_B at 20°C. Electron spin resonance (DMF/Toluene); g₁=2.27, A₁ 175 × 10⁻⁴ cm⁻¹, g₂=2.06. Molar conductivity (H₂O): 340 Scm²mol⁻¹. Molar conductivity (H₂O): 411 Scm²mol⁻¹. Electrospray mass spectroscopy (H₂O:CH₃CN) *m/z*: 701 (13%) [Cu₂(T₂-*m*-X Ac₂)]ClO₄⁺.

[Cu₆(T₃mes)₂(μ-OH)₆](ClO₄)₆·6H₂O (7)

Complex 7 was synthesised according the procedure as outlined by Graham *et al.*³⁶ using the free base of the ligand T₃mes (1.06 g, 2.11 mmol) and Cu(ClO₄)₂·6H₂O (4.68 g, in excess). Blue crystals formed which were suitable for X-ray crystallography and the unit cell confirmed the presence of the product.

Yield = 0.94 g (58%). Unit Cell: a=14.3579 Å, b=13.9231 Å, c=21.4261 Å, β=109.6°. (Lit.³⁶ a=14.4299(4) Å, b=13.9410(6) Å, c=21.463(1) Å, β=109.377(1)°.

UV-Visible-NIR spectrum: Solid (λ_{max}, nm): 610, ~880 sh. Solution: (H₂O; λ_{max}, nm (ε, M⁻¹cm⁻¹)): 252 (22620), 617 (440), 877 sh (143).

[Cu(tacn)₂]BNPP (8)

Crystals of 8 were deposited from a solution of total volume 4 mls with concentrations of 5 mM BNPP, 5 mM [Cu(tacn)Cl₂] and 50 mM HEPES at pH 7.4, with the temperature maintained for 6 days at 38°C. After cooling the solution and standing overnight, a small amount of blue crystals deposited which were suitable for single crystal X-ray analysis. No further analysis of the sample was undertaken due to the small amount of product obtained.

[Cu₃(Me₃tacn)₃(PhP)₂](ClO₄)₂·½H₂O (9)

1,4,7-trimethyl-1,4,7-triazacyclononane (Me₃tacn) (0.145g, 0.849 mmol) was dissolved in EtOH (5 cm³) and added to an aqueous solution of disodium phenyl phosphate (Na₂PhP) (0.104 g, 0.424 mmol), followed by the addition CuClO₄·6H₂O (0.314g, 0.849 mmol). A precipitate formed immediately which dissolved within *ca.* one minute. The resulting dark blue solution was heated gently to reduce the volume before being allowed to slowly evaporate at ambient temperature. Dark blue crystals had formed after several days which were suitable for X-ray crystallographic studies.

Yield = 0.18 (51%). Analytical data: Found (%): C 37.2, H 5.9, N 10.1. Calculated for Cu₃C₃₉H₇₄N₉O_{16.5}Cl₂P₂ (%): C 37.3, H 5.9, N 10.0. UV-Visible-NIR spectrum: Solid: (λ_{max}, nm): 650, 1049. Solution: (H₂O; λ_{max}, nm (ε, M⁻¹cm⁻¹)): 268 (12557), 658 (140), 1140 (85). IR spectrum (KBr, ν, cm⁻¹): 3616 m, 3531 m, 3063 w, 2915 m, 2675 m, 2826 m, 2475 w, 2023 w, 1801 w, 1736 w, 1595 s, 1494 s, 1464 s, 1364 m, 1303 m, 1240 s, 1155 s, 1097 s, 1009 s, 882 s, 767 s, 743 m, 696 m, 623 s, 575 m, 556 m, 530 s, 443 w, 412 w. Electron microprobe: Cu, P, Cl present only. Magnetic moment: μ_{eff} (per Cu) =

1.85 μ_B at 293 K. Electron spin resonance (DMF/Toluene); $g_{11}=2.31$, A_{11} 154×10^{-4} cm^{-1} , $g_{12}=2.24$, A_{12} 178×10^{-4} cm^{-1} , $g_{\perp}=2.06$. Molar conductivity (H_2O): $340 \text{ Scm}^2 \text{ mol}^{-1}$.

[Cu₂(T₂-*m*-X)(NPP)(μ -OH)](ClO₄) \cdot H₂O (10)

Blue crystals of 10 were grown from a solution used to conduct a preliminary kinetic run. The solution consisted of [Cu₂(T₂-*m*-X)(H₂O)₄](ClO₄)₄ \cdot 3H₂O \cdot NaClO₄ (2) (5 mM), Na₂NPP (5 mM), HEPES buffer (50 mM) at pH 7.4 and NaClO₄ (0.04 mM). The solution was kept at 38°C overnight, after which time dark blue needles were collected and washed with water. These crystals were suitable for crystallographic analysis.

Yield: 0.71 mg (79%). Analytical data: Found (%): C 37.1; H 5.2; N 11.6. Calculated for Cu₂C₂₆H₄₃N₇O₁₂ClP (%): C 37.2; H 5.2; N 11.7. UV-Visible-NIR spectrum Solid; (λ_{max} , nm): 336, 620, ~950 (sh). Solution: (DMF; λ_{max} , nm (ϵ , $\text{M}^{-1}\text{cm}^{-1}$)): 315 (12515), 674 (166), 1000 (sh). IR spectrum (KBr; ν , cm^{-1}): 3577 m, 3458 m, 3329 m, 3209 m, 3072 w, 2938 m, 2831 m, 1639 w, 1605 m, 1589 m, 1518 s, 1491 m, 1458 m, 1345 s, 1243 s, 1098 s, 1039 m, 1023 m, 997 s, 952 m, 882 s, 829 m, 752 m, 726 m, 700 w, 625 m, 582 m, 535 m, 445 w. Electron microprobe: Cu, Cl, P present only. Magnetic moment: 0.82 μ_B at 298 K.

[Cu(Me₃tacn)(H₂O)₂](ClO₄)₂ (11)

To an aqueous solution of copper perchlorate hexahydrate (11.51 g, 31.06 mmol) was added 1,4,7-trimethyl-1,4,7-triazacyclononane (Me₃tacn) (5.31 g, 0.0311 mol) in 50 ml of a 50% ethanol in water mix. The resulting dark blue solution was adjusted to pH 6 with 2M NaOH and then the solution was taken to dryness. The residue was then taken

Chapter Three

up in EtOH and Et₂O was added until the solution became cloudy. The flask was left at -20°C overnight, after which time blue crystals had formed. The dark blue crystals were collected by filtration, washed with Et₂O and air dried.

Yield = 11.48g (79%). Analytical data: Found (%): C 23.1, H 5.4, N 8.9. Calculated for CuC₉H₂₅N₃O₁₀Cl₂ (%): C 23.0, H 5.3, N 8.9. UV-Visible-NIR spectrum: Solid: (λ_{max} , nm): 685. Solution: (H₂O; λ_{max} , nm (ϵ , M⁻¹cm⁻¹)): 270 (3759), 682 (36), 1237 (20). IR spectrum (KBr; ν , cm⁻¹): 3424 br m, 2982 w, 2908 m, 2856 m, 2812 w, 1638 w, 1498 w, 1451 m, 1298 m, 1145 s, 1090 s, 1011 m, 940 w, 894 w, 781 w, 745 w, 628 m, 576 w, 441 w, 411 w. Electron microprobe: Cu, Cl present. Electron spin resonance (DMF/Toluene); g_{\parallel} =2.34, A_{\parallel} 161×10^{-4} cm⁻¹, g_{\perp} =2.06.

Chapter Three

3.10 References

- (1) Cotton, F. A., Wilkinson, G. *Advanced Inorganic Chemistry*; Fifth ed.; John Wiley & Sons: New York, 1988.
- (2) Frausto da Silva, J. J. R., Williams, R. J. P. *The Biological Chemistry of the Elements*; Clarendon Press: Oxford, 1991.
- (3) Halfen, J. A., Jazdzewski, B. A., Mahapatra, S., Berreau, L. M., Wilkinson, E. C., Que, L., Jr., Tolman, W. B. *J. Am. Chem. Soc.* **1997**, *119*, 8217.
- (4) McCue, K. P., Voss, D. A., Jr, Marks, C., Morrow, J. R. *J. Chem. Soc., Dalton Trans.* **1998**, 2961.
- (5) McCue, K. P., Morrow, J. R. *Inorg. Chem.* **1999**, *38*, 6136.
- (6) Spiccia, L., Graham, B., Hearn, M. T. W., Lazarev, G., Moubaraki, B., Murray, K. S., Tiekink, E. R. T. *J. Chem. Soc., Dalton Trans.* **1997**, 4089.
- (7) Adams, H., Bailey, N. A., Dwyer, M. J. S., Fenton, D. E., Hellier, P. C., Hempstead, P. D., Latour, J. M. *J. Chem. Soc., Dalton Trans.* **1993**, 1207.
- (8) McKee, V., Zvagulis, M., Dagobian, J. V., Patch, M. G., Reed, C. A. *J. Am. Chem. Soc.* **1984**, *106*, 4765.
- (9) Kövári, E., Krämer, R. *J. Am. Chem. Soc.* **1996**, *118*, 12704.
- (10) Yang, R., Zompa, L. J. *Inorg. Chem.* **1976**, *15*, 1499.
- (11) Bereman, R. D., Churchill, M. R., Schaber, P. M., Winkler, M. E. *Inorg. Chem.* **1979**, *18*, 3123.
- (12) Schwindinger, W. F., Fawcett, T. G., Lalancette, R. A., Potenza, J. A., Schugar, H. J. *Inorg. Chem.* **1980**, *19*, 1379.
- (13) Chaudhuri, P., Oder, K., Weighardt, K., Weiss, J., Reedjik, J., Hinrichs, W., Wood, J., Ozarowski, A. M., Stratemaier, H., Reinen, D. *Inorg. Chem.* **1986**, *25*, 2951.

Chapter Three

- (14) Beveridge, A. D., Lavery, A. J., Walkinshaw, M. D., Schröder, M. *J. Chem. Soc., Dalton Trans.* **1987**, 373.
- (15) Graham, B., Fallon, G. D., Hearn, M. T. W., Hockless, D. C. R., Lazarev, G., Spiccia, L. *Inorg. Chem.* **1997**, *36*, 6366.
- (16) Brudenell, S. J., Spiccia, L., Tiekink, E. R. T. *Inorg. Chem.* **1996**, *35*, 1974.
- (17) Brudenell, S. J., Spiccia, L., Bond, A. M., Comba, P., Hockless, D. C. R. *Inorg. Chem.* **1998**, *37*, 3705.
- (18) Schultz, D., Weyhermüller, T., Weighardt, K., Butzlaff, C., Trautwein, A. X. *Inorg. Chim. Acta* **1996**, *246*, 387.
- (19) Kavana, M., Powell, D. R., Burstyn, J. N. *Inorg. Chim. Acta* **2000**, *297*, 351.
- (20) DasGupta, B., Katz, C., Israel, T., Watson, M., Zompa, L. J. *Inorg. Chim. Acta* **1999**, *292*, 172.
- (21) Behle, L., Neuburger, M., Aehnder, M., Kaden, T. A. *Helv. Chim. Acta* **1995**, *78*, 693.
- (22) Auerbach, U., Eckert, U., Weighardt, K., Nuber, B., Weiss, J. *Inorg. Chem.* **1990**, *29*, 938.
- (23) Chaudhuri, P., Oder, K., Weighardt, K., Nuber, B., Weiss, J. *Inorg. Chem.* **1986**, *25*, 2818.
- (24) Chaudhuri, P., Ventur, D., Weighardt, K., Peters, E-M., Peters, K., Simon, A. *Angew. Chem., Int. Ed. Engl.* **1985**, *24*, 57.
- (25) Blake, A. J., Fallis, I. A., Gould, R. O., Parsons, S., Ross, S. A., Schröder, M. *J. Chem. Soc., Chem. Commun.* **1994**, 2467.
- (26) Weighardt, K., Tolksdorf, I., Herrmann, W. *Inorg. Chem.* **1985**, *24*, 1230.
- (27) Haidar, R., Ipek, M., DasGupta, B., Yousaf, M., Zompa, L. J. *Inorg. Chem.* **1997**, *36*, 3125.

Chapter Three

-
- (28) Zhang, X., Hseih, W-Y., Margulis, T. N., Zompa, L. J. *Inorg. Chem.* 1995, 34, 2883.
- (29) Young, M. J., Chin, J. *J. Am. Chem. Soc.* 1995, 117, 10577.
- (30) Farrugia, L. J., Lovatt, P. A., Peacock, R. D. *J. Chem. Soc., Dalton Trans.* 1997, 911.
- (31) Tolman, W. B. *Acc. Chem. Res.* 1997, 30, 227.
- (32) Blake, A. J., Donlevy, T. M., England, P. A., Fallis, I. A., Parsons, S., Ross, S. A., Schröder, M. *J. Chem. Soc., Chem. Commun.* 1994, 1981.
- (33) Fry, F. H., Graham, B., Spiccia, L., Hockless, D.C.R., Tiekink, E.R.T. *J. Chem. Soc., Dalton Trans.* 1997, 827.
- (34) Blake, A. J., Danks, J. P., Li, W-S., Lippolis, V., Schröder, M. *J. Chem. Soc., Dalton Trans.* 2000, 3034.
- (35) Graham, B., Grannas, M. J., Hearn, M. T. W., Kepert, C. M., Spiccia, L., Skelton, B. W., White, A. H. *Inorg. Chem.* 2000, 39, 1092.
- (36) Graham, B., Spiccia, L., Fallon, G.D., Hearn, M. T. W., Mabbs, F. E., Moubaraki, B., Murray, K. S. *J. Chem. Soc., Dalton Trans.*, In press.
- (37) Graham, B., Hearn, M. T. W., Junk, P. C., Kepert, C. M., Mabbs, F. E., Moubaraki, B., Murray, K. S., Spiccia, L. *Inorg. Chem.* 2001, 40, 1536.
- (38) Addison, A. W., Rao, T. N. *J. Chem. Soc., Dalton Trans.* 1984, 1349.
- (39) Sessler, J. L., Sibert, J. W., Burrell, A. K., Lynch, V. *Inorg. Chem.* 1993, 32, 4277.
- (40) Deacon, G. B., Huber, F. *Inorg. Chim. Acta* 1985, 104, 41.
- (41) Burstyn, J., Deal K. *Inorg. Chem.* 1993, 32, 3585.
- (42) Deal, K., Burstyn, J. *Inorg. Chem.* 1996, 35, 2792.
- (43) Deal, K., Hengge, A. C., Burstyn, J. N. *J. Am. Chem. Soc.* 1996, 118, 1713.

Chapter Three

-
- (44) Mahroof-Tahir, M., Karlin, K. D., Chen, Q., Zubieta, J. *Inorg. Chim. Acta* **1993**, *207*, 135.
- (45) Hegg, E. L., Burstyn, J. N. *J. Am. Chem. Soc.* **1995**, *117*, 7015.
- (46) Hegg, E. L., Burstyn, J. N. *Inorg. Chem.* **1996**, *35*, 7474.
- (47) Hegg, E. L., Deal, K. A., Kiessling, L. L., Burstyn, J. N. *Inorg. Chem.* **1997**, *36*, 1715.
- (48) Hay, R. W., Govan, N. *Polyhedron* **1998**, *17*, 463.
- (49) Wall, M., Humes, R. M., Chin, J. *Angew. Chem. Int. Ed. Engl.* **1993**, *32*, 1633.
- (50) Yamaguchi, K., Akagi, F., Fujinami, S., Shionota, M., Suzuki, S. *Chem. Commun.* **2001**, 375.
- (51) Gieb, S. J., Hirst, S. C., Vincent, C., Hamilton, A. D. *Chem. Commun.* **1991**, 1283.
- (52) Vaidhyanathan, R., Natarajan, S., Rao, C. N. R. *J. Mater. Chem.* **1999**, 2789.
- (53) Lu, J., Xu, Y., Goh, N. K., Chia, L. S. *Chem. Commun.* **1998**, 2733.
- (54) Choudhury, A., Natarajan, S., Rao, C. N. R. *Chem. Commun.* **1999**, 1305.
- (55) Inoue, M., Yamase, T. *Bull. Chem. Soc., Jpn* **1996**, *69*, 2863.
- (56) Soghomonian, V., Chen, Q., Zhang, Y., Haushalter, R. C., Tao, C., Zubieta, J. *Chemistry of Materials* **1995**, *7*, 1221.
- (57) McLachlan, G. A., Fallon, G. D., Martin, R. L., Spiccia, L. *Inorg. Chem.* **1995**, *34*, 254.
- (58) Hathaway, B. J., in ; Wilkinson, G., Gillard, R. D., McCleverty, J. A., Ed.; Pergamon: Oxford, 1987; Vol. 5, pp 533-774 and referenced therein.
- (59) Bencini, A., Bertini, I., Gatteschi, D., Scozzafava, A. *Inorg. Chem.* **1978**, *17*, 3194.
- (60) Bleaney, B., Bowers, K. D. *Proc. R. Soc. London, Ser. A.* **1952**, *214*, 451.

Chapter Three

-
- (61) Kruger, P. E., Moubaraki, B., Fallon, G. D., Murray, K. S. *J. Chem. Soc., Dalton Trans.* 2000, 713.
- (62) Smith, T. D., Pilbrow, J. R. *Coord. Chem. Rev.* 1974, 13, 173.
- (63) Murase, I., Hamada, S., Ueno, S., Kida, S. *Synth. React. Inorg. Met.-Org. Chem.* 1983, 13, 191.
- (64) Nishida, Y., Kida, S. *J. Chem. Soc., Dalton Trans.* 1986, 2633.
- (65) Bertocello, K., Fallon, G.D., Hodgkin, J.H., Murray, K. *Inorg. Chem.* 1988, 27, 4750.
- (66) Maloney, J. J., Glogowski, M., Rohrbach, D. F., Urbach, F. L. *Inorg. Chim. Acta* 1987, 127, L33.
- (67) Nishida, Y., Kida, S. *Inorg. Chem.* 1988, 27, 447.
- (68) Mazurek, W., Kennedy, B. J., Murray, K. S., O'Conner, M. J., Rodgers, J. R., Snow, M. R., Wedd, A. G., Zwack, P. R. *Inorg. Chem.* 1985, 24, 3258.
- (69) Nishida, Y., Shimo, H., Maehara, H., Kida, S. *J. Chem. Soc., Dalton Trans.* 1985, 1945.
- (70) Bertocello, K., Fallon, G. D., Hodgkin, J. H., Murray, K. S. *Inorg. Chem.* 1988, 27, 4750.
- (71) Ainscough, E. W., Brodie, A. M., Ranford, J. D., Waters, J. M. *J. Chem. Soc., Dalton Trans.* 1997, 1251.
- (72) Mourabaki, B., Murray, K. S., Ranford, J. D., Vittal, J. J., Wang, X., Xu, Y. *J. Chem. Soc. Dalton Trans.* 1999, 3573.
- (73) Kahn, O. *Molecular Magnetism*; VCH: New York, 1993.
- (74) Mabbs, F. E., Machin, D. J. *Magnetism and Transition Metal Complexes*; Chapman and Hall: London, 1973.

Chapter Three

- (75) Beckett, R., Colton, R., Hoskins, B. F., Martin, R. L., Vince, P. G. *Aust. J. Chem.* **1969**, *22*, 2527.
- (76) Thompson, L. K., Lee, F. L., Gabe, E. J. *Inorg. Chem.* **1988**, *27*, 39.
- (77) Haddad, M. S., Wilson, S. C., Hodgson, D. J., Hendrickson, D. N. *J. Am. Chem. Soc.* **1981**, *103*, 384.

Chapter Four

Synthesis and Characterisation of Zinc(II) Complexes of 1,4,7-triazacyclononane derivatives

4.1 Introduction

Once referred to as the "boring" element because of the lack of spectroscopic properties, the chemistry of zinc has been a rapidly expanding area of research. Zinc exists in the metallic and divalent state. Zinc(II) commonly adopts 4, 5 or 6 coordination states, most commonly forming colourless or yellow to brown complexes.

Zinc(II) is found in many enzymes in which it fulfils both functional and structural roles.¹ It is represented in all six classes of enzymes (see section 1.2), where it generally acts as a strong Lewis acid in a catalytic role.² Other features which make zinc(II) an ideal metal in active sites of hydrolase enzymes are its flexible coordination geometry, fast ligand exchange, its inactivity to redox reactions and the Brønsted acidity of coordinated aquo ligands, enabling the generation of nucleophiles at physiological pH. Such enzymes include carbonic anhydrase, DNA polymerase I, carboxypeptidase A, alkaline phosphatase and phospholipase C (see also section 1.3). In modelling of the active sites of such enzymes, polyamine macrocyclic zinc(II) complexes have proved extremely beneficial. Their high thermodynamic stability allowed zinc(II)-polyamine complexes to be formed at physiological pH in aqueous solution.³

The first zinc(II)-tacn complex was reported by Zompa and coworkers in 1977.⁴ In a solution study, these workers found that tacn and zinc(II) formed very stable 1:1

Chapter Four

complexes. In the same year, the first Zn(II) complex of a bis(tacn) ligand, dtne, was reported, but again, the complex was only studied in solution.⁵ The zinc(II) complex of this ligand was isolated in 1985 by Weighardt and coworkers,⁶ reporting the mononuclear zinc(II) complex of the dtne ligand (Figure 4.1 A). In 1989, the first Zn(II) complex incorporating a tacn-derivative with a single pendant arm was reported.⁷ The ligand consists of a tacn unit functionalised with a single bipyridylmethyl pendant arm, and is capable of acting as a pentadentate ligand. The zinc(II) complex was particularly interesting as it was found to be seven a coordinate complex, established by X-ray crystallography, with two weakly bound perchlorate anions completing the coordination sphere (Figure 4.1 B).

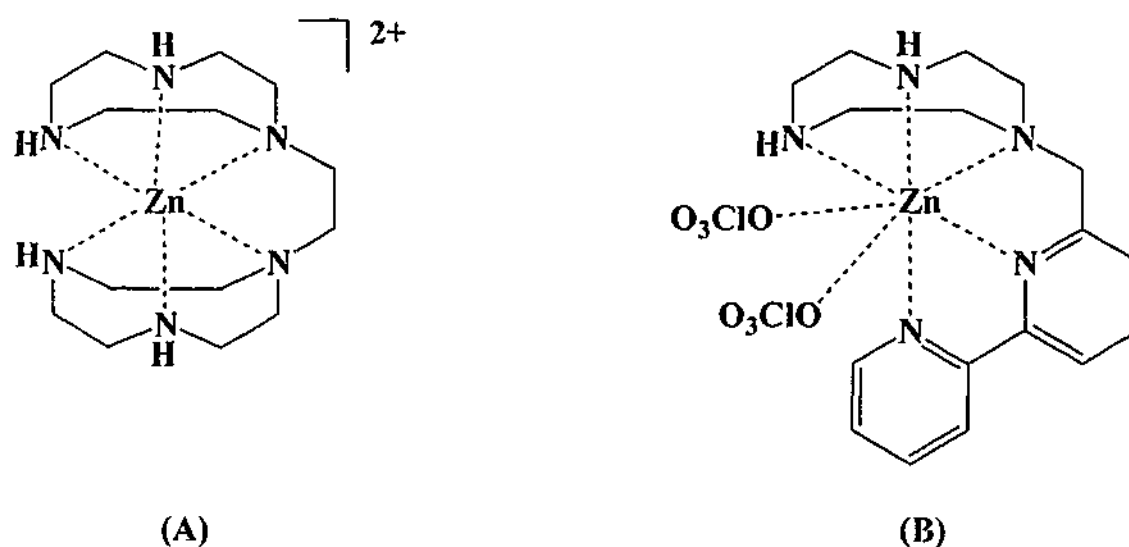


Figure 4.1 Two zinc(II) complexes of tacn

Since these complexes appeared in the literature, relatively few further examples of zinc(II) complexes of tacn-derivatives have been reported. Most of these have been mononuclear in nature.⁸⁻¹⁷ Figure 4.2 shows a selection of mononuclear zinc(II)

Chapter Four

complexes of tacn-derivatives whose structures have been determined crystallographically.

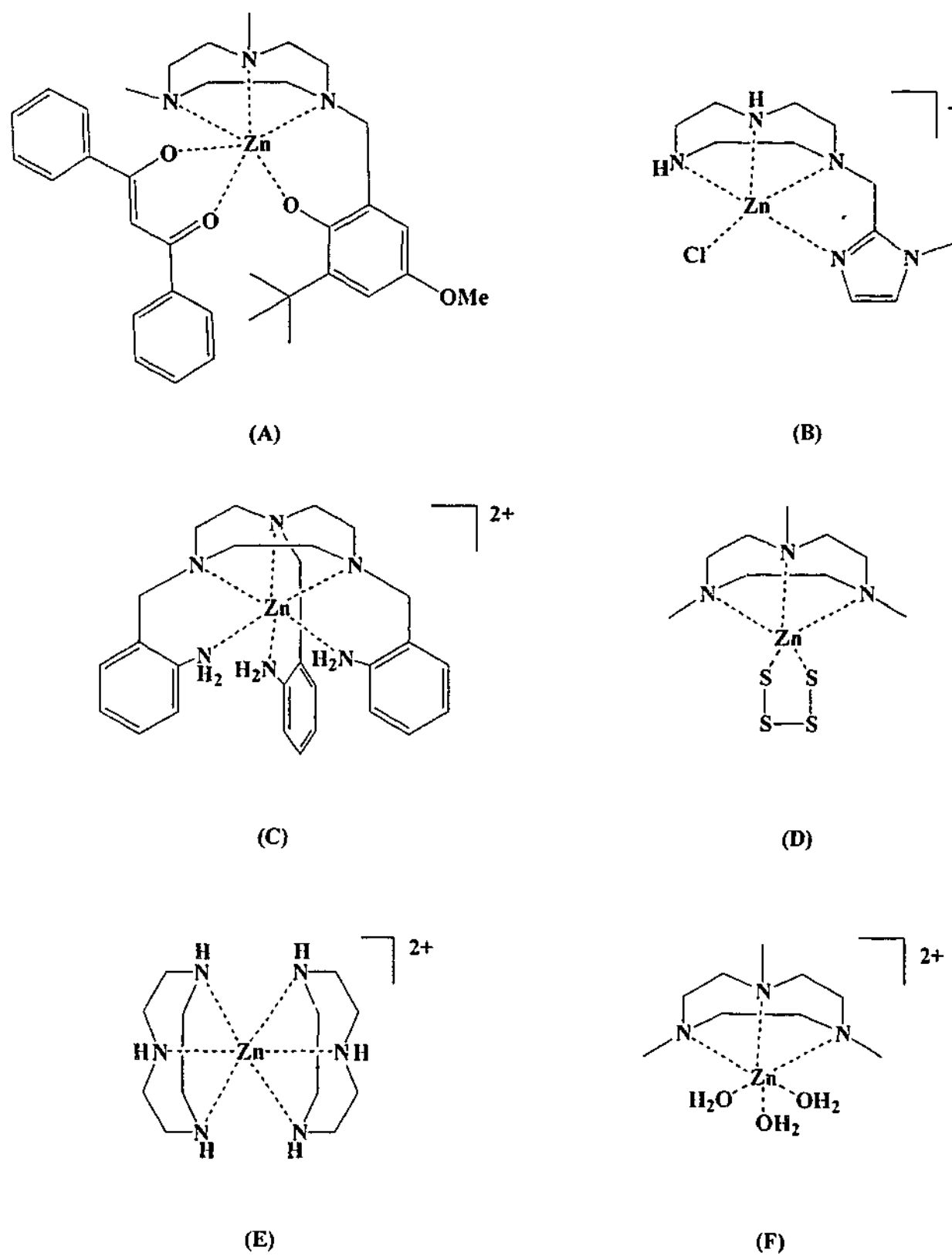


Figure 4.2 Selection of mononuclear zinc(II) complexes incorporating tacn

A,⁹ B,¹⁰ C,¹¹ D,¹² E,¹⁶ and F¹⁵

Chapter Four

Binuclear complexes are far less common, with only a few such complexes reported to date. Three of these complexes are comprised of two mononuclear Zn(II) moieties linked together via bridging anions. There are only three papers reporting binuclear zinc(II) complexes of bis(tacn) ligands.

Chaudhuri *et al.* in 1992¹⁶ reported two complexes consisting of two Zn(II)-1,4,7-trimethyl-1,4,7-triazacyclononane units linked together by either two μ -OH bridges, or by one μ -OH and two μ -O₂CCH₃ bridges (Figure 4.3 A & B). These complexes served as structural models for two of the zinc(II) centres in phospholipase C from *Bacillus Cereus* and leucine aminopeptidases from bovine lens, respectively. The same research group later reported two complexes with similar structures, but in which three halogen bridges connect the two zinc(II) cations (Figure 4.3 C & D).¹⁸ In 1996, Ellis *et al.*¹⁹ reported the structure of a Zn(II) binuclear complex of a ligand functionalised with a phenylphosphine pendant arm. In this complex, the two zinc-tacn units are bridged weakly by a Cl⁻ anion (one Zn-Cl bond is quite long (2.909(6) Å) and the Zn centre is better considered as being 5-coordinate (see Figure 4.3 E)).

Chapter Four

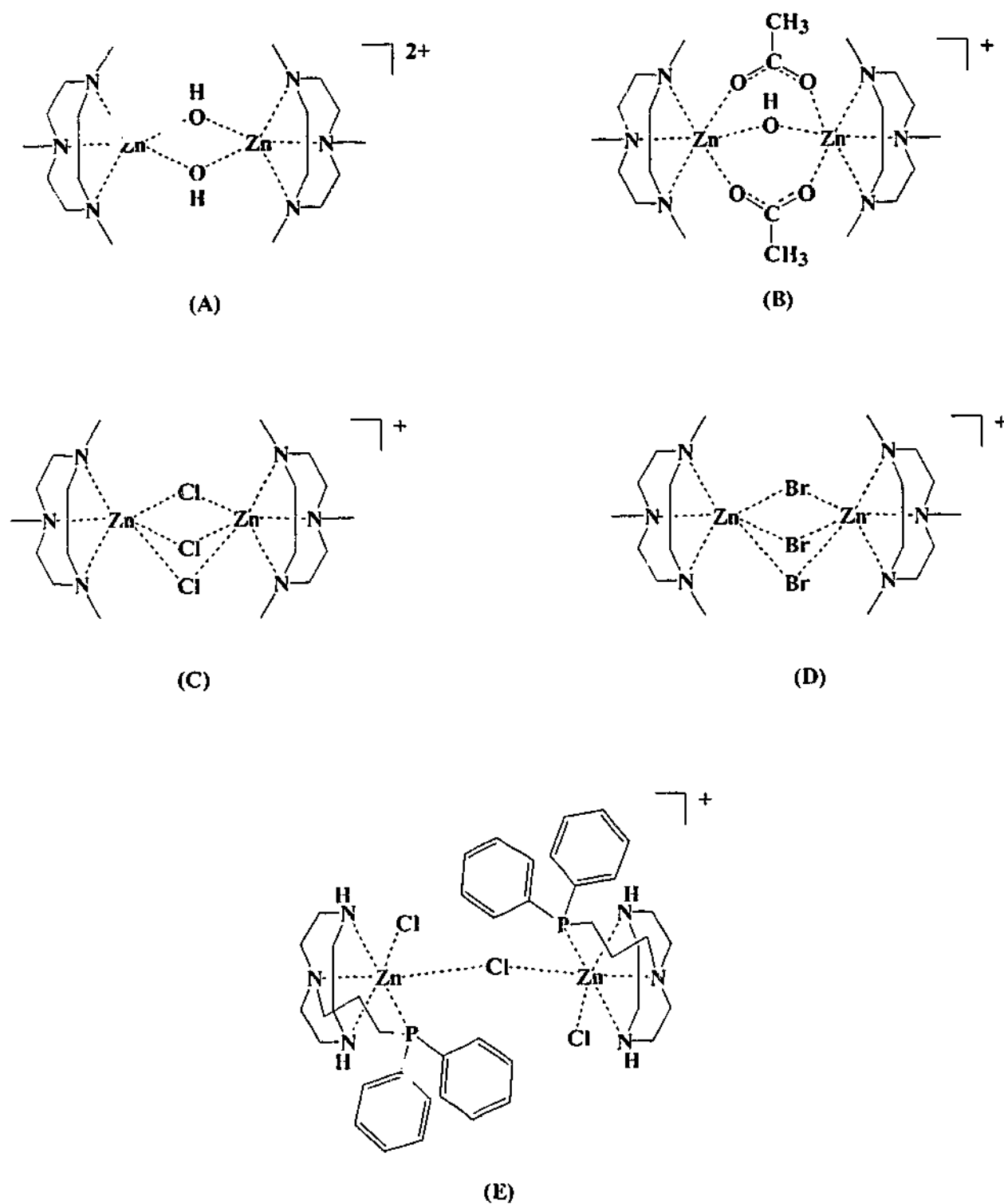


Figure 4.3 Structures of binuclear zinc(II)-tacn complexes

Three papers have reported zinc(II) complexes of the bis(tacn) ligands. Two of these relate to bis(pentadentate) ligands which bind one zinc(II) centre in each pentadentate macrocyclic compartment. Schröder and coworkers²⁰ in 1994 reported the complex of a

Chapter Four

ligand consisting of two tacn units linked with an ethane bridge, which was further functionalised with alcohol pendant arms (Figure 4.4 A). Subsequent to this publication, Spiccia and coworkers²¹ reported the binuclear complexes of a series of binucleating ligands obtained by *N*-functionalisation of various bis(tacn) ligands with 2-pyridylmethyl pendant arms (Figure 4.4 B & C). The third paper focuses on the coordination chemistry of ligand comprised of two tacn moieties linked via alkyl bridges.¹⁷ For the pentane bridged ligand, zinc(II) centres were found to bind to each macrocyclic compartment. Each Zn(II) centre is connected to a second centre from another Zn(II)₂-ligand moiety via three chloride bridges. The result is a tetranuclear complex (Figure 4.4 D). This paper also reports the solution chemistry of Zn(II)₂-ligand complexes connected by polymethylene chains with 2-8 carbons.

Chapter Four

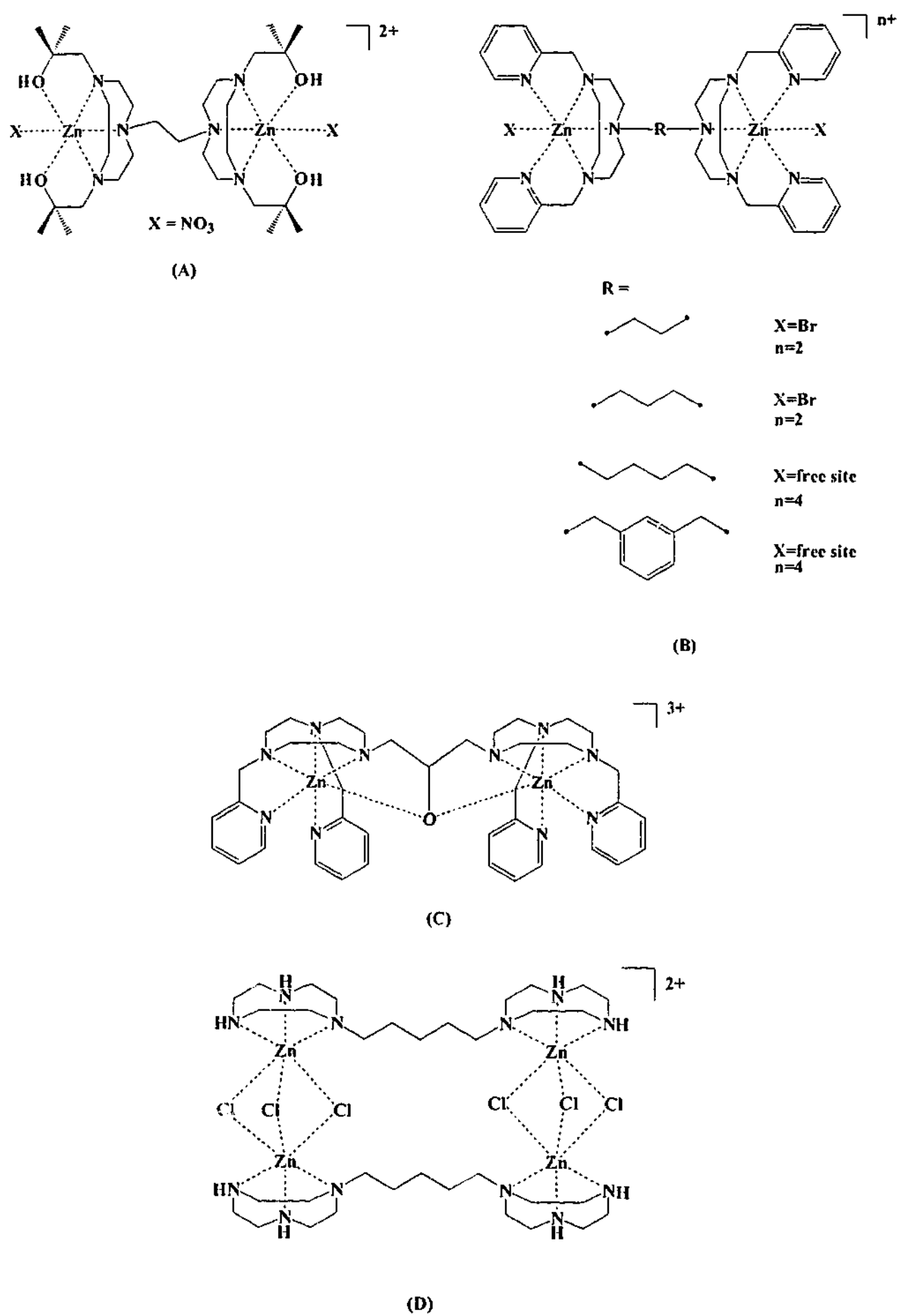


Figure 4.4 Zinc(II) complexes of bis(tacn) ligands

Chapter Four

The knowledge of zinc(II) coordination chemistry, although an area of increasing interest, is a topic which has a great capacity for expansion. This chapter deals with the coordination chemistry of zinc(II) with the ligands presented in Chapter 2. The complexes described in this chapter show the ability of bis(tacn) ligands to form complexes with different structural features, depending on the nature of the bridge linking the tacn units. Polynuclear zinc(II) complexes were of particular interest in this study as it was anticipated that such complexes would give enhanced rates of hydrolysis with phosphate esters.

4.2 Zinc(II) complexes of bis(tacn) ligands

4.2.1 Preparation of Complexes

The zinc(II) complexes of $T_2\text{-}o\text{-}X$ and $T_2\text{-}p\text{-}X$ were synthesised by addition of aqueous solutions of the hexahydrochloride salt of the ligands to aqueous solutions containing two equivalents of $Zn(ClO_4)_2 \cdot 6H_2O$ (complex 12) or $ZnCl_2 \cdot xH_2O$ (complex 14) in water. The pH of each solution was adjusted to *ca.* 5 with 1M NaOH and any precipitate of the metal hydroxide was removed by filtration. Colourless to pale yellow solutions resulted. Crystals of $[Zn(T_2\text{-}o\text{-}X)](ClO_4)_2$ (12) were grown by slow evaporation of the solution and isolated in a low yield (37%). Crystals of $[Zn_2(T_2\text{-}p\text{-}X)(H_2O)_4(DMF)_2][ZnCl_4]_2$ (14) (yield 15%) were isolated after an initial crop of $[Zn_2(T_2\text{-}p\text{-}X)(H_2O)_6Cl_4] \cdot xZnCl_2$ (~50%) was collected by filtration and DMF was added to the filtrate and the solution left to slowly evaporate. The synthesis of the zinc complex with $T_2\text{-}m\text{-}X$ (complex 13) differed in that the solvent used was acetone and the free ligand was reacted with two molar equivalents of $ZnBr_2$. A white precipitate formed immediately and was collected in high yield (95%). The zinc(II) complex of

Chapter Four

T₂PrOH was formed by dissolution of the hexahydrobromide salt of the ligand in water and adjustment of the pH to *ca.* 6. The solution was added to an aqueous solution of Zn(ClO₄)₂·6H₂O and the pH was adjusted to *ca.* 10. After removal of any precipitate of zinc hydroxide that formed, the pH was adjusted back to *ca.* 7 and the solution allowed to slowly evaporate. Complex 15 precipitated as a colourless crystalline solid in a yield of 41%. The structures of these complexes, either determined by X-ray crystallography or proposed on the basis of analytical data described herein, are shown in Figure 4.5.

Chapter Four

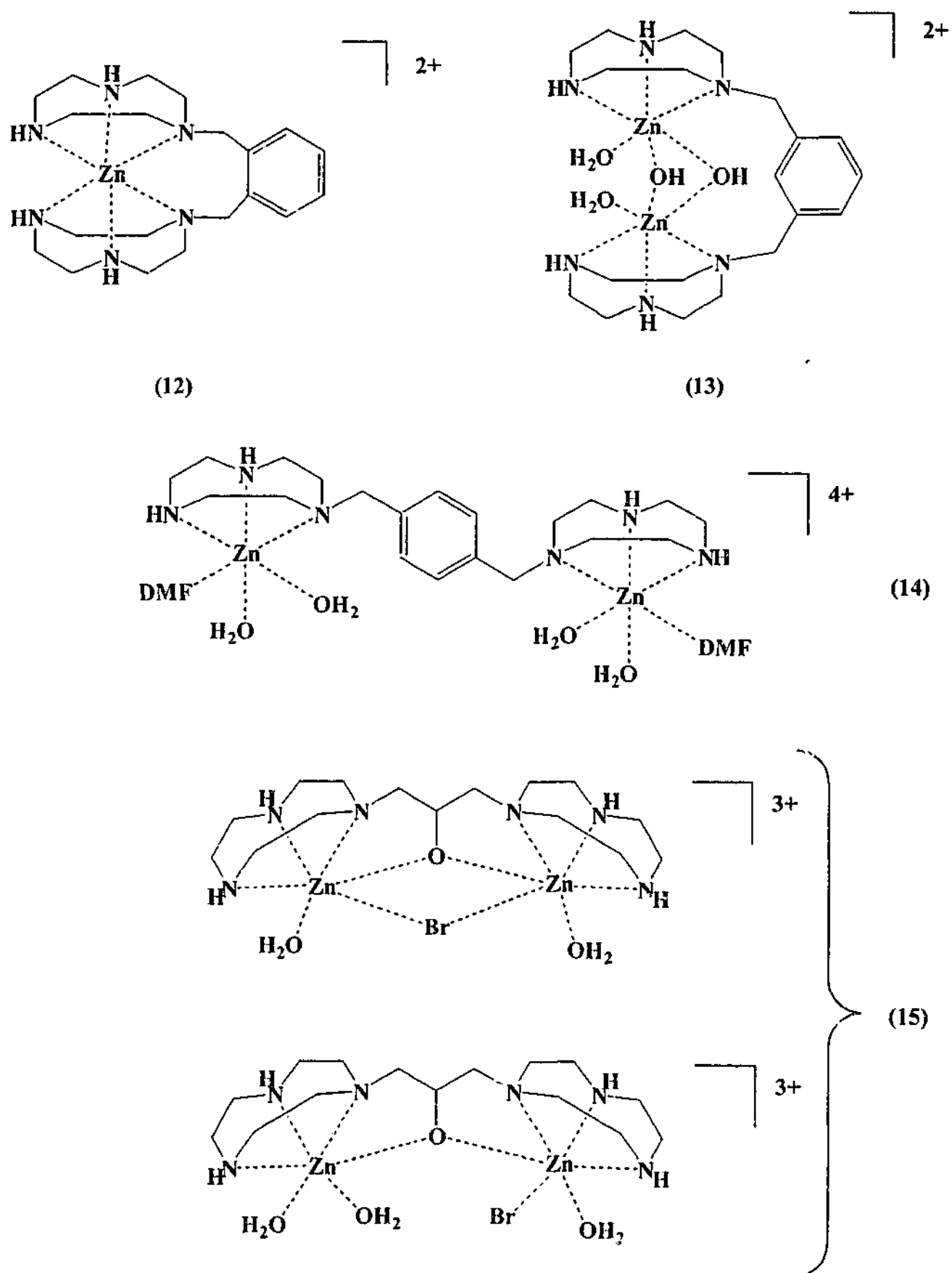


Figure 4.5 Zinc(II) complexes of T_2 -(*o*, *m*, *p*)-X and T_2 -PrOH ligands

Chapter Four

The IR spectra of the complexes show sharp bands due to the NH stretch of the tacn ring in the region of 3225 - 3306 cm^{-1} and compound 12 showed bands at *ca.* 1100 and 630 cm^{-1} due to the perchlorate counter ions. Compound 14 showed a sharp band at 1617 cm^{-1} attributed to the $\nu(\text{CO})$ of the coordinated DMF. The complexes with the xylyl bridge show a number of peaks in the fingerprint region between at *ca.* 1450 and 1490 cm^{-1} , due to the benzene ring. The C-H out-of-plane bending vibrations can also be seen for 12 and 13, with bands at 751 and 815 cm^{-1} for the *ortho* and *meta* substitution, respectively. The equivalent band for the *para* substituted benzene ring, expected at *ca.* 800-860 cm^{-1} , is not clearly distinguishable in the spectrum. The $\nu(\text{NH})$ region for 15 shows two bands, at 3291 and 3259 cm^{-1} indicating the presence of more than one type of NH in the structure. Also seen in the IR spectrum of 15 is a band at 3434 cm^{-1} due to water present in the lattice. Analytical data for the compounds agree well with the given formula of the complexes and are shown in Table 4.1.

Table 4.1 Elemental data for compounds 12 - 15

Calculated data is given in parentheses

Complex	C (%)	H (%)	N (%)
12 $[\text{Zn}(\text{T}_2\text{-}o\text{-X})](\text{ClO}_4)_2 \cdot \text{H}_2\text{O}$	37.6 (37.4)	6.0 (6.0)	13.1 (13.1)
13 $[\text{Zn}_2(\text{T}_2\text{-}m\text{-X})(\mu\text{-OH})_2]\text{Br}_2 \cdot 3\text{H}_2\text{O}$	32.7 (32.7)	5.5 (5.5)	11.0 (11.4)
14 $[\text{Zn}_2(\text{T}_2\text{-}p\text{-X})(\text{H}_2\text{O})_4(\text{DMF})_2][\text{ZnCl}_4]_2$	27.9 (27.8)	5.2 (5.2)	10.2 (10.0)
15 $[\text{Zn}_2(\text{T}_2\text{-PrO})(\text{H}_2\text{O})_2\text{Br}]\text{Br}_2 \cdot \text{H}_2\text{O}$	24.4 (24.4)	5.1 (5.3)	11.4 (11.4)

Chapter Four

Electrospray mass spectroscopy of the complexes (Table 4.2) is also consistent with the analytical data given in Table 4.1.

Table 4.2 Electrospray mass spectroscopy of compounds 12 – 15

Complex	Peak (<i>m/z</i>)	Assignment
12 [Zn(T ₂ - <i>o</i> -X)](ClO ₄) ₂ .H ₂ O	541.2	{Zn(T ₂ - <i>o</i> -X)(ClO ₄)(H ₂ O)} ⁺
	523.3	{Zn(T ₂ - <i>o</i> -X)ClO ₄ } ⁺
13 [Zn ₂ (T ₂ - <i>m</i> -X)(μ-OH) ₂]Br ₂ .3H ₂ O	583.0	{Zn ₂ (T ₂ - <i>m</i> -X)(μ-O)Br} ⁺
14 [Zn ₂ (T ₂ - <i>p</i> -X)(H ₂ O) ₄ (DMF) ₂][ZnCl ₄] ₂	751.0	{Zn ₂ (T ₂ - <i>p</i> -X)(ZnCl ₄)(H ₂ O)Cl} ⁺
	597.1	{Zn ₂ (T ₂ - <i>p</i> -X)Cl ₃ } ⁺
	497.2	{Zn ₂ (T ₂ - <i>p</i> -X)(H ₂ O) ₂ Cl} ⁺
15 [Zn ₂ (T ₂ -PrO)Br ₃ (H ₂ O)].2H ₂ O	602.9	{Zn ₂ (T ₂ -PrO)Br ₂ } ⁺

To aid in the determination of the composition of the complexes, the conductivities were measured in water, and in the case of **15**, in water and methanol. The conductivities of complexes **12-14** were consistent with the proposed structures (Figure 4.5). The molar conductivity of **15** in methanol of 199 Scm²mol⁻¹ is indicative of a 2:1 electrolyte,²² which corresponds to two uncoordinated and one coordinated bromide. Two structures are possible for **15** that are consistent with the analytical data. Both are shown in Figure 4.5. The conformation shown in **A** is not symmetrical, with a bromide

Chapter Four

and a water ligand on one of the zinc(II) centres, and two water ligands on the second zinc(II). A second proposed structure is depicted in B, and includes a bridging bromide, connecting between the two zinc(II) ions. This structure is symmetrical, with the bromide connecting to both metal centres. This type of structure has been seen in a previous complex isolated by Brooker *et al.*²³ This complex comprised of an endogenous alkoxo bridge and a chloride, both bridging between two Mn(II) centres (Figure 4.6). This complex also has a further chloride bridge to a second unit, forming a tetranuclear complex.

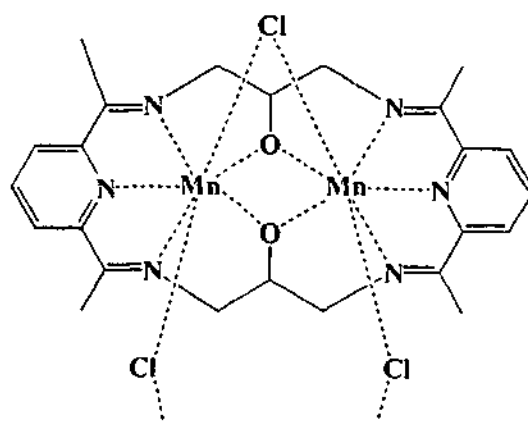


Figure 4.6 Complex isolated by Brooker *et al.*²³ with an alkoxo and a chloride bridging between two Mn(II) centres. The chlorides at the bottom of the diagram bridge to an identical unit to that shown, forming the tetranuclear complex.

4.2.2 Crystal Structure of $[\text{Zn}(\text{T}_2\text{-}o\text{-X})](\text{ClO}_4)_2 \cdot \text{H}_2\text{O}$ (12)

The single-crystal X-ray structure of compound (12) was determined in order to confirm the mononuclear nature of this complex, in which the $\text{T}_2\text{-}o\text{-X}$ ligand sandwiches a single zinc(II) centre. Cell parameters and details of the data collection are presented in

Chapter Four

section 1.7 of the Appendix. The molecular structure consists of discrete $[\text{Zn T}_2\text{-o-X}]^{2+}$ units and two perchlorate anions. Figure 4.7 represents and ORTEP plot of the complex and Table 4.3 lists selected bond lengths and angles.

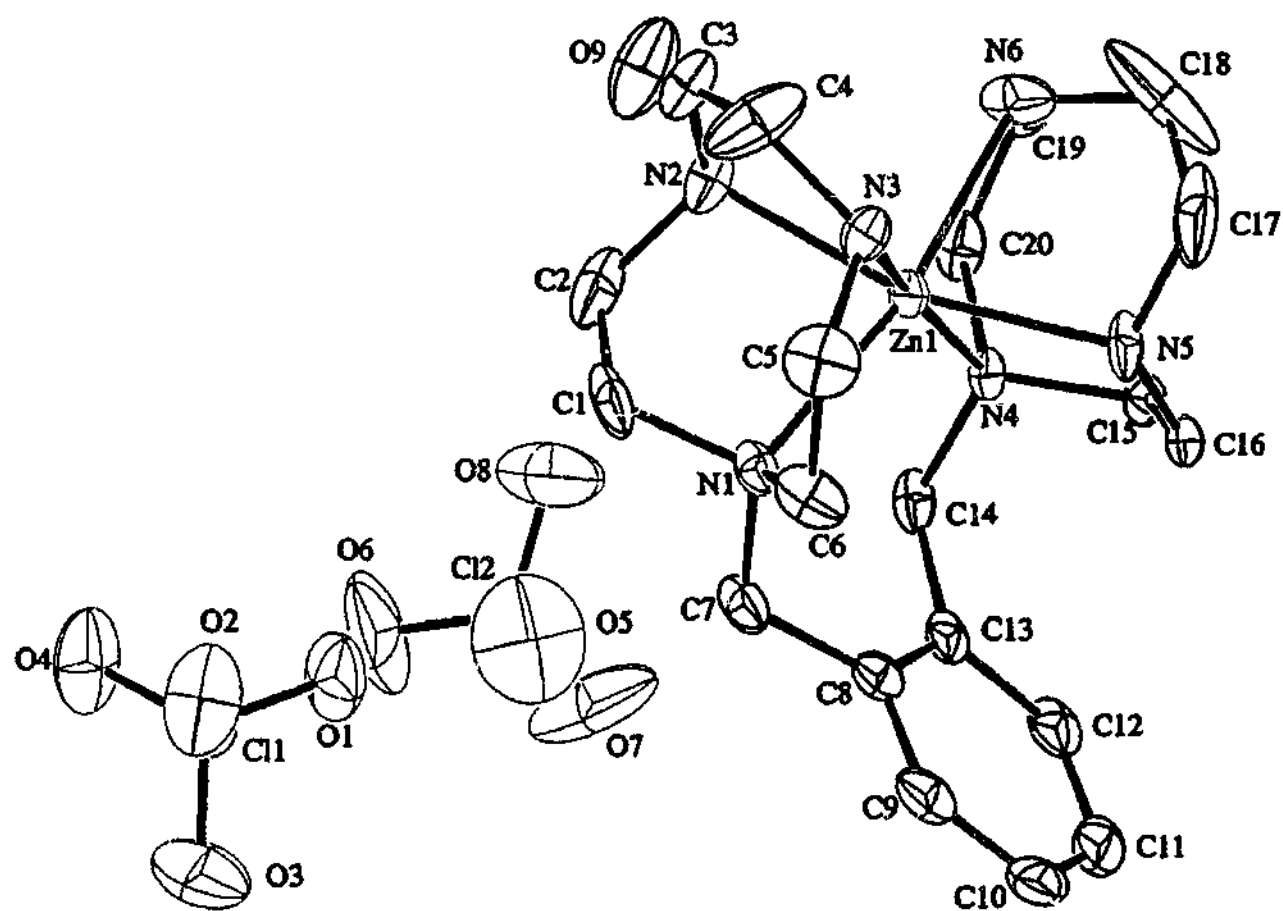
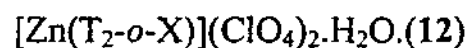


Figure 4.7 ORTEP plot of $[\text{Zn}(\text{T}_2\text{-o-X})](\text{ClO}_4)_2$ (12) with atomic labelling scheme

Chapter Four

Table 4.3 Selected bond distances (Å) and angles (°) for



Zn-N(1)	2.249(4)	Zn-N(4)	2.191(4)
Zn-N(2)	2.181(4)	Zn-N(5)	2.189(4)
Zn-N(3)	2.185(4)	Zn-N(6)	2.203(5)
N(1)-Zn-N(2)	80.5(2)	N(2)-Zn-N(6)	87.8(2)
N(1)-Zn-N(3)	78.8(2)	N(3)-Zn-N(4)	168.9(1)
N(1)-Zn-N(4)	102.4(2)	N(3)-Zn-N(5)	88.4(2)
N(1)-Zn-N(5)	111.3(2)	N(3)-Zn-N(6)	100.3(2)
N(1)-Zn-N(6)	168.3(2)	N(4)-Zn-N(5)	80.9(1)
N(2)-Zn-N(3)	81.8(2)	N(4)-Zn-N(6)	80.7(2)
N(2)-Zn-N(4)	109.3(2)	N(5)-Zn-N(6)	80.3(2)
N(2)-Zn-N(5)	163.0(2)		

The structural analysis of compound **12** shows that the geometry around the zinc(II) centre is distorted octahedral, with each tacn ring coordinated to one face of the octahedron of the zinc(II) centre. The Zn-N bond lengths fall into the same range as for other six coordinate complexes with tacn derivatives.¹⁶ The intra-ring N_{cis}-Zn-N_{cis} "bite" angles (*ca.* 80°) are all well below the ideal octahedral value of 90° due to constraints imposed by the rigidity of the tacn ring. The distortion is also evident in the *trans* angles about the Zn(II) centre (N(1)-Zn-N(6) = 168.3(2)°; N(2)-Zn-N(5) = 163.0(2)°; N(3)-Zn-N(4) = 168.9(1)°), with all angles being well below the 180° expected for the idealised octahedron. Additional distortion of the octahedron is imposed by the *o*-xylyl bridge, with a dihedral angle 10.6° between the plane passing through the N(1), N(2) and N(3) and the plane dissecting N(4), N(5) and N(6). The value of the dihedral angle is very similar to that found in the analogous Cu(II) and Ni(II) analogues, being 9.5° and 9.0° for Cu(II) and Ni(II), respectively.²⁴

Chapter Four

It is interesting to note that in **12** one of the Zn-N bonds lengths (Zn-N(1) = 2.249(4) Å) is longer than the remaining Zn-N distances (2.181(4) - 2.203(5) Å). This is due to the shifting of the benzene ring towards the tacn ring containing N(4), N(5) and N(6), thus pulling N(1) away from the Zn centre. This effect has also been observed in the analogous Ni complex, with the elongated Ni-N bond at 2.182(4) Å and the remaining bonds in the octahedron lying between 2.110(4) Å and 2.142(4) Å.²⁴ By contrast, in the copper analogue, elongation of two *trans* Cu-N bonds is observed due to the Jahn-Teller distortion of the Cu(II) centre. In **12**, the benzene ring is tilted towards one of the tacn rings as seen in the nickel analogue.

The sandwich-type structure exhibited in complex **12** has been demonstrated in other zinc(II) complexes with tacn and tacn derivatives. The 2:1 complex of tacn and zinc has been prepared by Weighardt and coworkers,¹⁶ while more intricate mononuclear sandwich-structures have been reported by DasGupta *et al.*¹⁷ This latter paper reports that the ethane and propane bridged bis(tacn) ligands form zinc(II) complexes with sandwich structures in solution.

4.2.3 Crystal Structure of $[\text{Zn}_2(\text{T}_2\text{-}p\text{-X})(\text{H}_2\text{O})_4(\text{DMF})_2][\text{ZnCl}_4]$ (**14**)

The structural analysis of compound **14** was undertaken in order to determine the coordination environment around the zinc(II) centres and to confirm the binucleating nature of the ligand. Cell parameters and details of the data collection are presented in section 1.8 of the Appendix. The crystals consist of discrete $[\text{Zn}_2(\text{T}_2\text{-}p\text{-X})(\text{H}_2\text{O})_4(\text{DMF})_2]^{4+}$ cations and $[\text{ZnCl}_4]^{2-}$ counter anions. Figure 4.8 represents the ORTEP plot of the cation and Table 4.4 lists selected bond lengths and angles.

Chapter Four

The structural analysis of **14** shows the ligand, T₂-p-X coordinates a zinc(II) centre to each of the macrocyclic compartments of the ligand. The remaining three coordination sites of the zinc are occupied by two water molecules and a DMF moiety. The presence of the coordinated DMF solvent molecules in **14** demonstrates the ability of zinc(II) centres to coordinate amide molecules through the oxygen of the carbonyl group. This has been proposed as an important feature of zinc(II) hydrolytic enzymes that catalyse the cleavage of amide bonds (peptidases). The binding of DMF in complex **14** indicates that simple amides do have an affinity for zinc(II) centres which may also be exhibited by more complex polypeptide structures.

Chapter Four

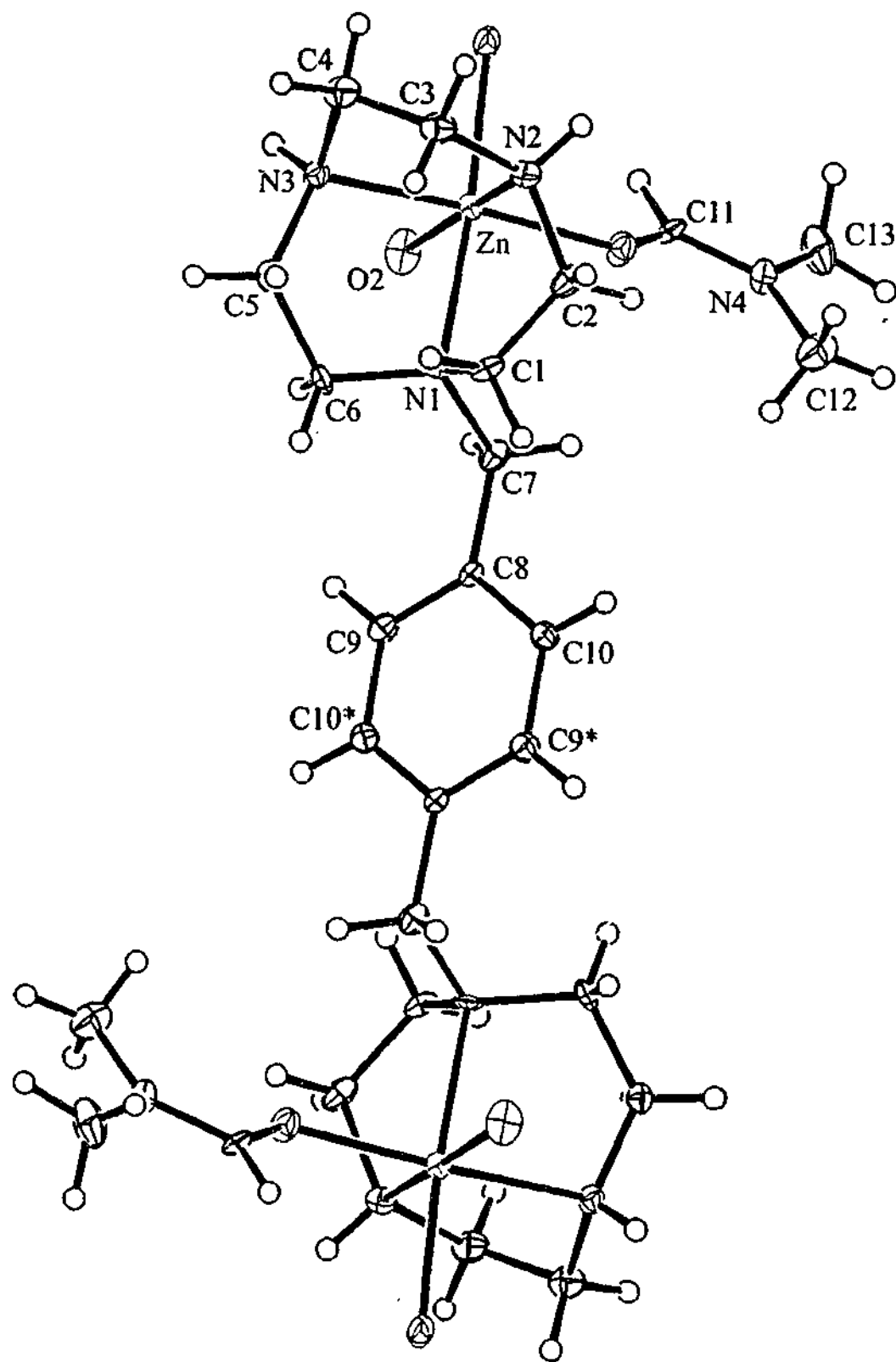


Figure 4.8 ORTEP plot of $[\text{Zn}_2(\text{T}_2\text{-p-X})(\text{H}_2\text{O})_4(\text{DMF})_2]^{4+}$ (14) with atomic labelling scheme

Chapter Four

Table 4.4 Selected bond distances (Å) and angles (°) for
 $[\text{Zn}_2(\text{T}_2\text{-}p\text{-X})(\text{H}_2\text{O})_4(\text{DMF})_2][\text{ZnCl}_4]$ (**14**)

Zn(1)-N(1)	2.204(6)	Zn(1)-O(1)	2.118(5)
Zn(1)-N(2)	2.118(6)	Zn(1)-O(2)	2.175(5)
Zn(1)-N(3)	2.131(6)	Zn(1)-O(3)	2.043(5)
N(1)-Zn(1)-N(2)	82.8(2)	N(2)-Zn(1)-O(3)	92.1(2)
N(1)-Zn(1)-N(3)	81.8(2)	N(3)-Zn(1)-O(1)	92.0(2)
N(1)-Zn(1)-O(1)	172.9(2)	N(3)-Zn(1)-O(2)	94.3(2)
N(1)-Zn(1)-O(2)	93.5(2)	N(3)-Zn(1)-O(3)	173.4(2)
N(1)-Zn(1)-O(3)	93.5(2)	O(1)-Zn(1)-O(2)	90.4(2)
N(2)-Zn(1)-N(3)	82.7(2)	O(1)-Zn(1)-O(3)	92.4(2)
N(2)-Zn(1)-O(1)	93.1(2)	O(2)-Zn(1)-O(3)	90.5(2)
N(2)-Zn(1)-O(2)	175.6(2)		

The Zn(1)...Zn(1) distance was found to be quite long at 11.75 Å due to the *anti*-conformation adopted by the two macrocyclic compartments of the ligand. The Zn centre is found to adopt a distorted octahedral geometry, with the tacn chelate ring constraining the N-Zn(1)-N angles below the ideal octahedral geometry angle of 90°. The other three coordination sites are taken by two water molecules and one DMF molecule. The bond angles between these molecules are much closer the ideal as no constraints are imposed. The *trans* angles in the octahedron (172.9(2) - 175.6(2) Å) are also less than the ideal angle of 180°, but the distortion is not as great as that in **12**, due to the greater flexibility of the coordination sphere in **14** compared with **12**. The Zn-N(secondary amine) bond distances (2.118(6) and 2.131(6) Å) are shorter than the Zn-N(tertiary amine) distance (2.204(6) Å) which reflects the stronger binding properties of secondary amines compared to tertiary amine groups.

Chapter Four

The structures of the T_2 - pX ligands with Cu(II) (complex 1) and Ni(II)²⁴ both show *anti*-conformation, with the metals orientated on opposite sides of the ligand, as seen in 14. The metal-metal distance of the zinc complex lies between those of Cu(II) and Ni(II), at 11.81 Å and 11.68 Å, respectively. In each of the complexes (Cu(II), Zn(II) and Ni(II)) the tacn ring is coordinated to one face of the polyhedron, with the bridgehead nitrogen occupying the apical site of a square pyramid (Cu(II)) or the octahedron (Ni(II) and Zn(II)).

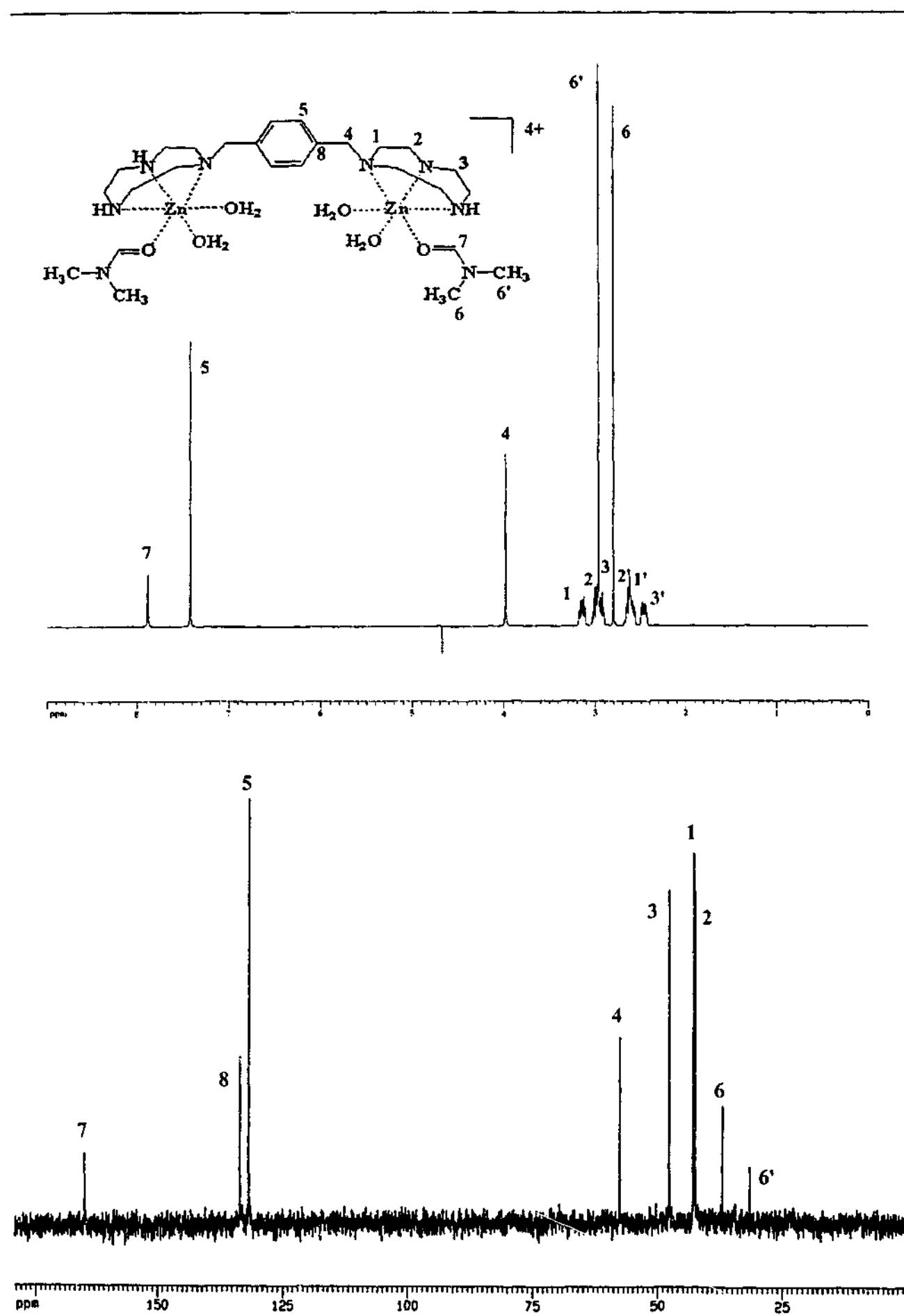
4.2.4 Solution NMR Spectroscopic Analysis of [Zn(T_2 - o -X)](ClO₄)₂ (12), [Zn₂(T_2 - m -X)(μ -OH)₂]Br₂·3H₂O (13), [Zn₂(T_2 - p -X)(H₂O)₄(DMF)₂][ZnCl₄] (14) and [Zn₂(T_2 -PrO)(H₂O)₂Br]Br₂·H₂O (15)

The room temperature (300K) ¹H NMR and ¹³C NMR spectra of 12-15 were measured in D₂O. The spectra for 12 are shown in Figure 4.9, while those for 15 are shown in Figure 4.11. The ¹H NMR spectrum for the *p*-xylyl bridged complex shows a series of multiplets at 2.46, 2.61, 2.98 and 3.12 ppm, integrating to 4, 8, 8 and 4, respectively. The multiplets at 2.61 and 2.98 ppm are a combination of two overlapping multiplets, each of 4 protons. The peaks are assigned to the three methylene environments within the tacn ring. Each proton on these carbon atoms appears at a different chemical shift, implying the two protons are different. The assignments are shown in Figure 4.9, and were confirmed by a proton-carbon correlation experiment. Overlapping this region are two singlets at 2.80 and 2.96 ppm which arise from the methyl groups of the DMF ligand. Two signals are seen due to the two resonance forms of DMF. The amide proton in the DMF unit is observed as a singlet at 7.87 ppm. The bridge methylene protons within the bis(tacn) unit give a singlet at 3.97 ppm and the remaining singlet at

Chapter Four

7.41 ppm arises from the aromatic protons in the *para*-xylyl unit. In the ^{13}C NMR spectrum, two signals are again observed for the methyl carbons in the DMF substituent, at 31.32 and 36.86 ppm. The C=O in the DMF moiety gives a peak at 165.0. Three signals at 42.36, 42.68 and 47.52 ppm are attributed to the methylene carbons in the tacn ring. The signal at 57.56 ppm is due to the methylene carbons in the xylyl bridge, while two peaks are observed in the aromatic region, at 131.51 ppm for the aromatic CH, and at 133.22 ppm for the quaternary carbons in the xylyl bridging unit.

Chapter Four

Figure 4.9 ^1H (top) and ^{13}C (bottom) spectra of 14

Chapter Four

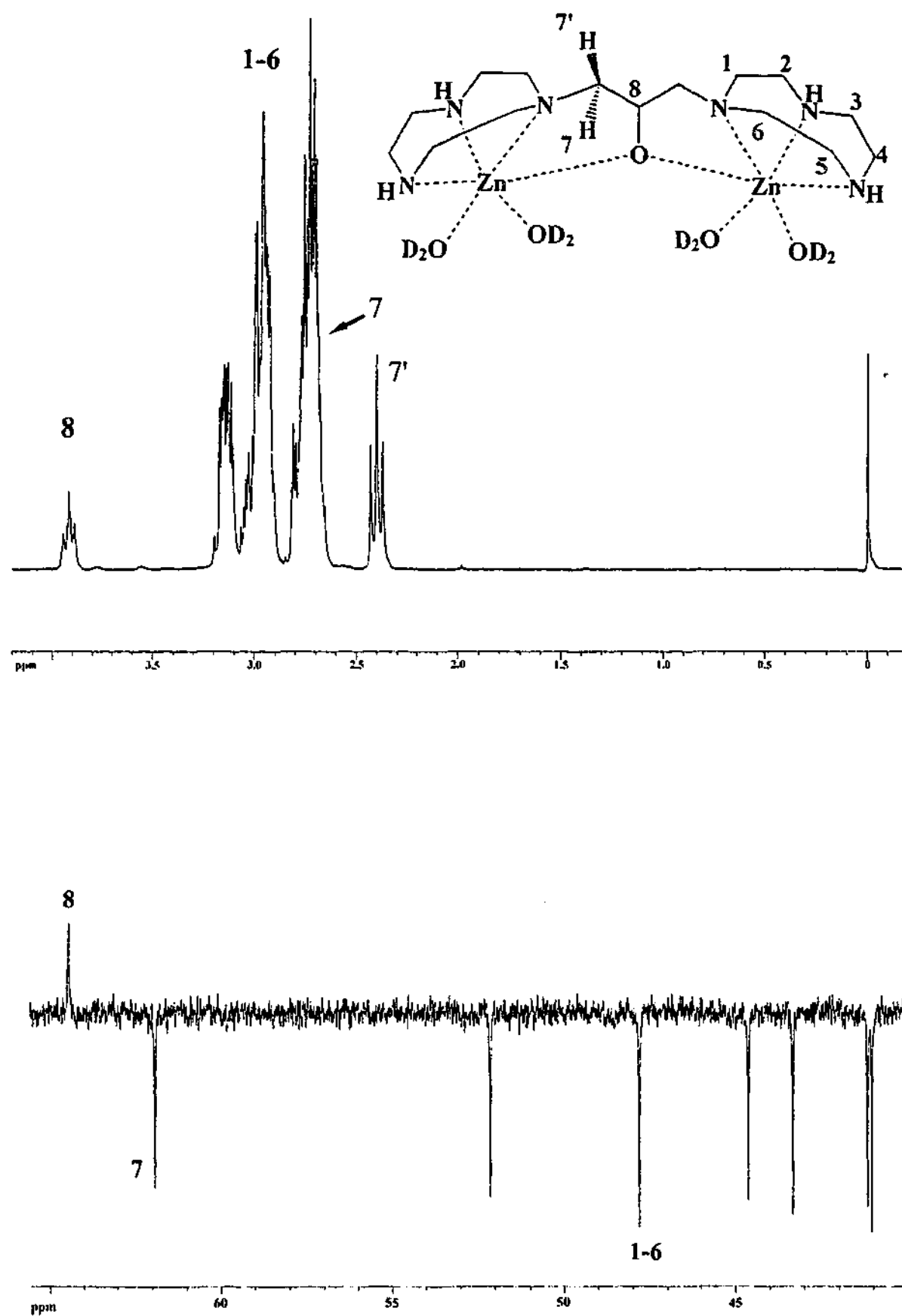
The NMR spectra of compounds **12** and **13** are similar to those of **14**, with more signals in the aromatic regions as expected. Both the *ortho*- and *meta*-bridged complexes show multiplets in the proton NMR spectra, at 7.45 and 7.50 ppm, respectively. The carbon NMR spectra show typical patterns for the 1,2- and 1,3-disubstituted benzene rings, the *ortho* complex showing two aromatic CH signals at 132.37 and 134.30 ppm, while the *meta* complex shows three at 131.07, 131.89 and 135.93 ppm. The spectrum for **12** shows an additional signal in the proton NMR *cf.* **13** and **14**, with a broad peak at 3.45 ppm equating to two protons and is presumed to be an impurity. This impurity remains unidentified. The ^{13}C NMR spectrum has 4 methylene signals in the tacn region, instead of the expected 3. Three of these peaks are very close together at 44.19, 44.30 and 44.43 ppm, one of which is thought to be due to the impurity.

The NMR spectra of **15** were recorded in D_2O at room temperature. Although the composition in the solid state is unclear, in solution any coordinated bromide ions will exchange with D_2O in solution, as shown by the conductivity in water, giving the structure as shown in Figure 4.10. The ^1H NMR shows three multiplets at 2.77 and 2.94 and 3.14 ppm due to the methylene protons in the tacn ring. These signals compare favourably to those of a related zinc complex, of the $\text{T}_2\text{-PrOH}$ ligand functionalised by 2-methylpyridyl pendant arms,²¹ which also shows three multiplets centred at 2.70, 3.00 and 3.20 ppm. The protons in the bridge of the ligand give rise to three signals. The signal furthest downfield in the spectrum at 3.91 ppm corresponds to the central CH group in the propanol bridge. This signal appears as a triplet of multiplets. The two inequivalent methylene protons in the bridge give rise to two signals each integrating to two protons. The first is clearly seen as a triplet at 2.41 ppm, and the second signal

Chapter Four

hidden under the multiplet due to the tacn protons (see Figure 4.10, signals 7 and 7'). Two sets of signals for these protons are also seen in the analogous compound by Brudenell *et al.*²¹. The ¹³C NMR spectrum of 15 shows six peaks for the six carbon environments in the tacn ring, at 41.04, 41.18, 43.33, 44.62, 47.81 and 52.14 ppm. Six carbon signals were also observed for the related complex by Brudenell *et al.*²¹. The carbons in the bridge give two signals, one at 61.93 ppm due to the methylene carbon and the second at 64.46 ppm due to the central bridging CH carbon. In solution, each half of the complex is equivalent indicated by one observed resonance for each of the carbon environments in the tacn ring and the bridge.

Chapter Four

Figure 4.10 ^1H (top) and ^{13}C (bottom) spectra of 15

Chapter Four

4.3 Complexes of bis(tacn) ligands with acetate pendant arms

4.3.1 Preparation of Complexes

Addition of two molar equivalents of $\text{Zn}(\text{ClO}_4)_2 \cdot 6\text{H}_2\text{O}$ to an aqueous solution of the crude oil of $\text{T}_2\text{-}o\text{-X Ac}_2$ and $\text{T}_2\text{-}m\text{-X Ac}_2$ and adjustment of the pH to *ca.* 5, produced pale yellow solutions. The solutions were loaded onto a cation exchange column and the complexes eluted with 0.1 M NaClO_4 solution. After concentration of the eluent *in vacuo*, the solutions were left to slowly evaporate, producing white powders in yields of 19% and 62% for *ortho* and *meta*, respectively. Experienced here and previously,²⁵ complexes of this type incorporating acetate pendant arms have proven to be extremely soluble in water and are therefore difficult to crystallise. Proposed structures based on the analytical data that follows are shown in Figure 4.11.

Chapter Four

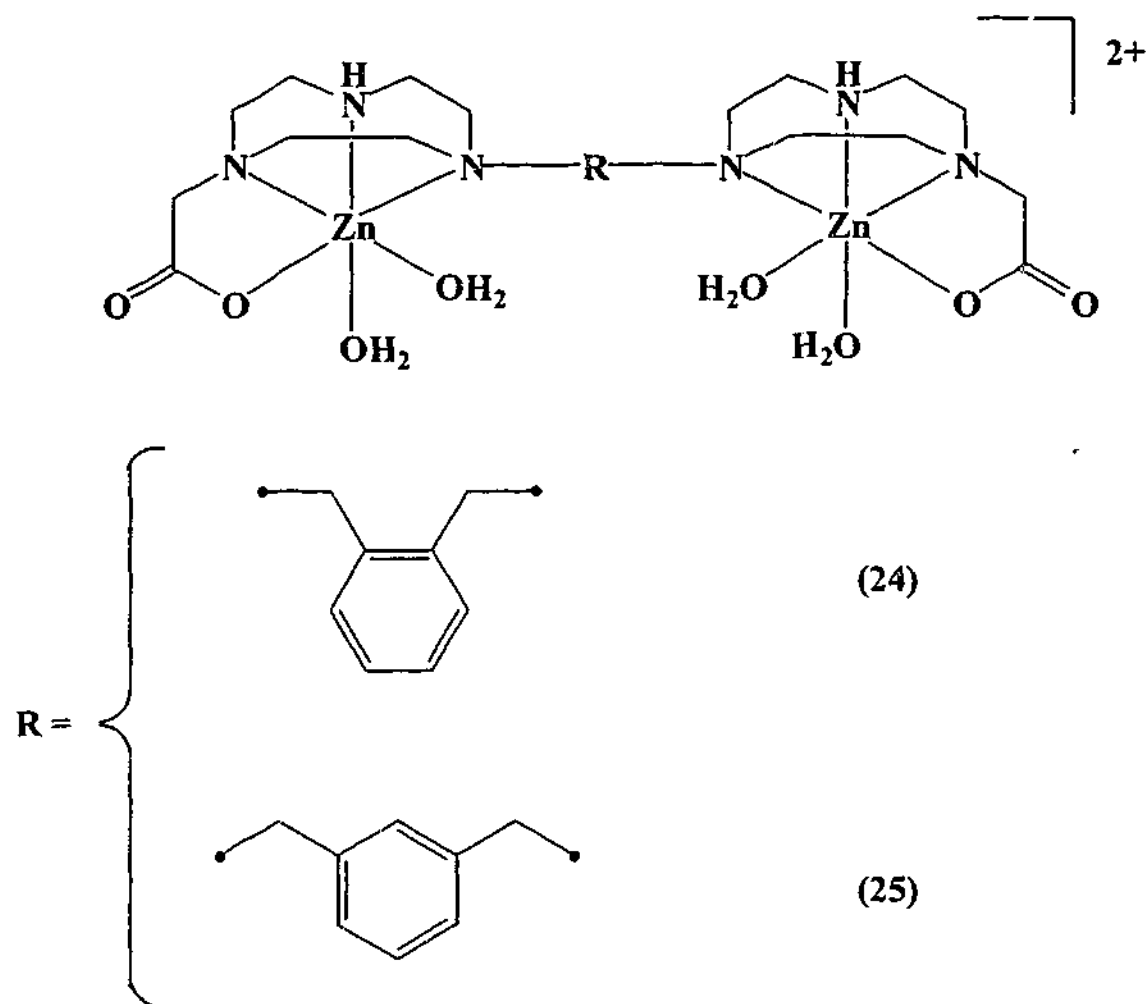


Figure 4.11 Proposed structures of compounds 16 and 17. Counter ions are perchlorate ions.

The IR spectra of complexes 16 and 17 are virtually identical. Sharp bands 3329 and 3325 cm^{-1} for 16 and 17, respectively, are attributed to the NH stretch of the ligands, while bands around 1100 and 625 cm^{-1} are due to the perchlorate counter ions. Strong bands at 1589 and 1591 cm^{-1} (16 and 17 respectively) and a weaker band at *ca.* 1404 cm^{-1} is assigned to the asymmetric and the symmetric stretching modes of the carboxylate group, respectively. The shifts in ν_{as} and ν_{s} are indicative of unidentate coordination of the acetate pendant arm.²⁶ The spectra also confirm the presence of

Chapter Four

water, with strong, broad OH stretches around 3450 cm^{-1} . Analytical data agree well with the given formula of the complexes shown in Table 4.5.

Table 4.5 Elemental Analysis for complexes 16–17

Calculated values are given in parenthesis

Complex	C (%)	H (%)	N (%)
16 $[\text{Zn}_2(\text{T}_2\text{-}o\text{-X Ac}_2)(\text{H}_2\text{O})_4](\text{ClO}_4)_2 \cdot 2\text{H}_2\text{O}$	31.6 (31.6)	5.2 (5.5)	9.1 (9.2)
17 $[\text{Zn}_2(\text{T}_2\text{-}m\text{-X Ac}_2)(\text{H}_2\text{O})_4](\text{ClO}_4)_2 \cdot 2\text{H}_2\text{O}$	31.8 (31.6)	5.2 (5.5)	9.2 (9.2)

The electrospray mass spectra are also consistent with the given compositions. Both complexes show three peaks at m/z 701.0, 639.1 and 539.1 which correspond to the following monopositively charged species, $\{\text{Zn}_2(\text{T}_2\text{-}(o,m)\text{-X Ac}_2)\text{ClO}_4\}^+$, $\{\text{Zn}(\text{T}_2\text{-}(o,m)\text{-X Ac}_2\text{H}_2)\text{ClO}_4\}^+$ and $\{\text{Zn}(\text{T}_2\text{-}(o, m)\text{-X Ac}_2\text{H})\}^+$. The molar conductivity of each complex was measured in water and gave similar values ($271\text{ Scm}^2\text{mol}^{-1}$ and $244\text{ Scm}^2\text{mol}^{-1}$) which are in the typical range for a 1:2 electrolyte.²²

4.3.2 Solution NMR Spectroscopy of $[\text{Zn}_2(\text{T}_2\text{-}o\text{-X Ac}_2)(\text{H}_2\text{O})_4](\text{ClO}_4)_2 \cdot 2\text{H}_2\text{O}$ (16) and $[\text{Zn}_2(\text{T}_2\text{-}m\text{-X Ac}_2)(\text{H}_2\text{O})_4](\text{ClO}_4)_2 \cdot 2\text{H}_2\text{O}$ (17)

The solution ^1H and ^{13}C NMR spectra of compounds 16 and 17 were recorded in D_2O at 300K and are shown in Figures 4.12 and 4.13. The spectra of these complexes were expected to be complicated, as on coordination of the metal, each carbon within each half of the molecule is inequivalent. In these complexes there are eight different methylene environments giving signals in the region of 2.2 – 4.3 ppm in the ^1H NMR

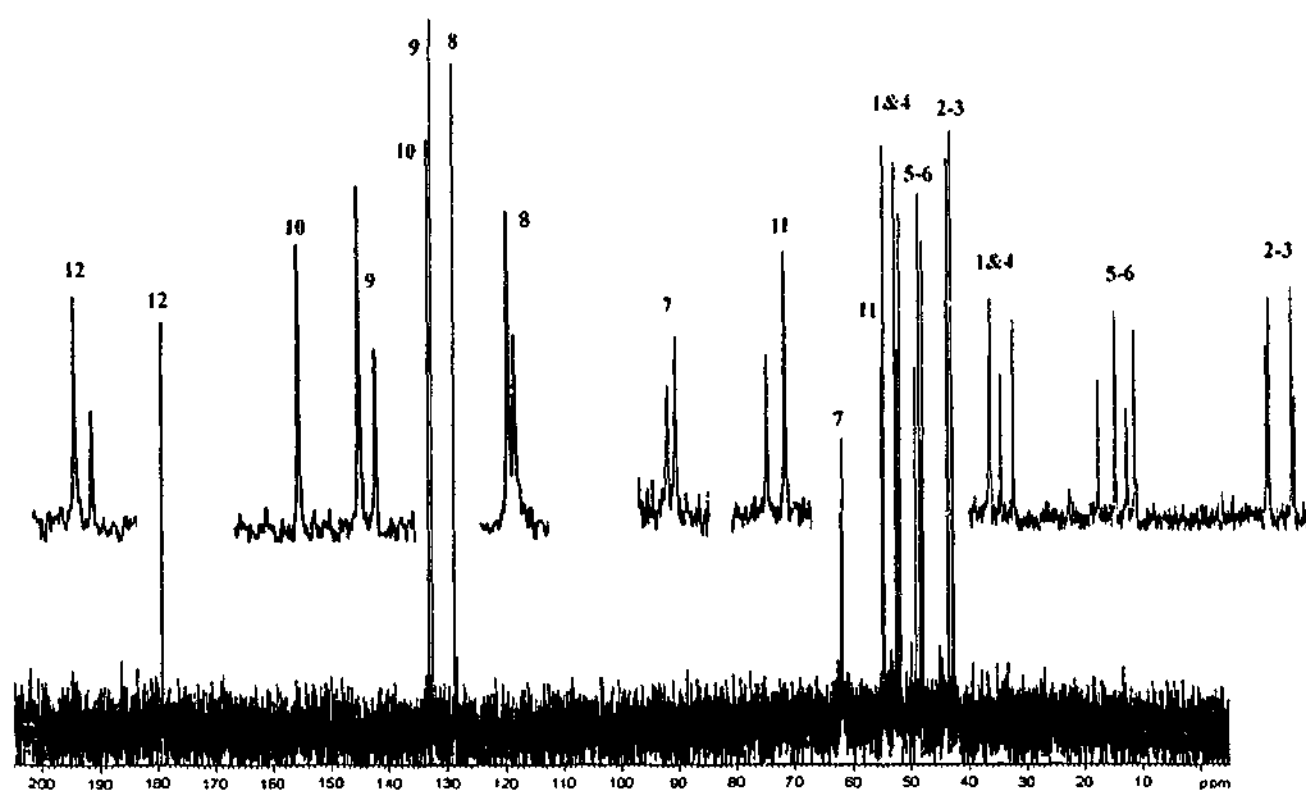
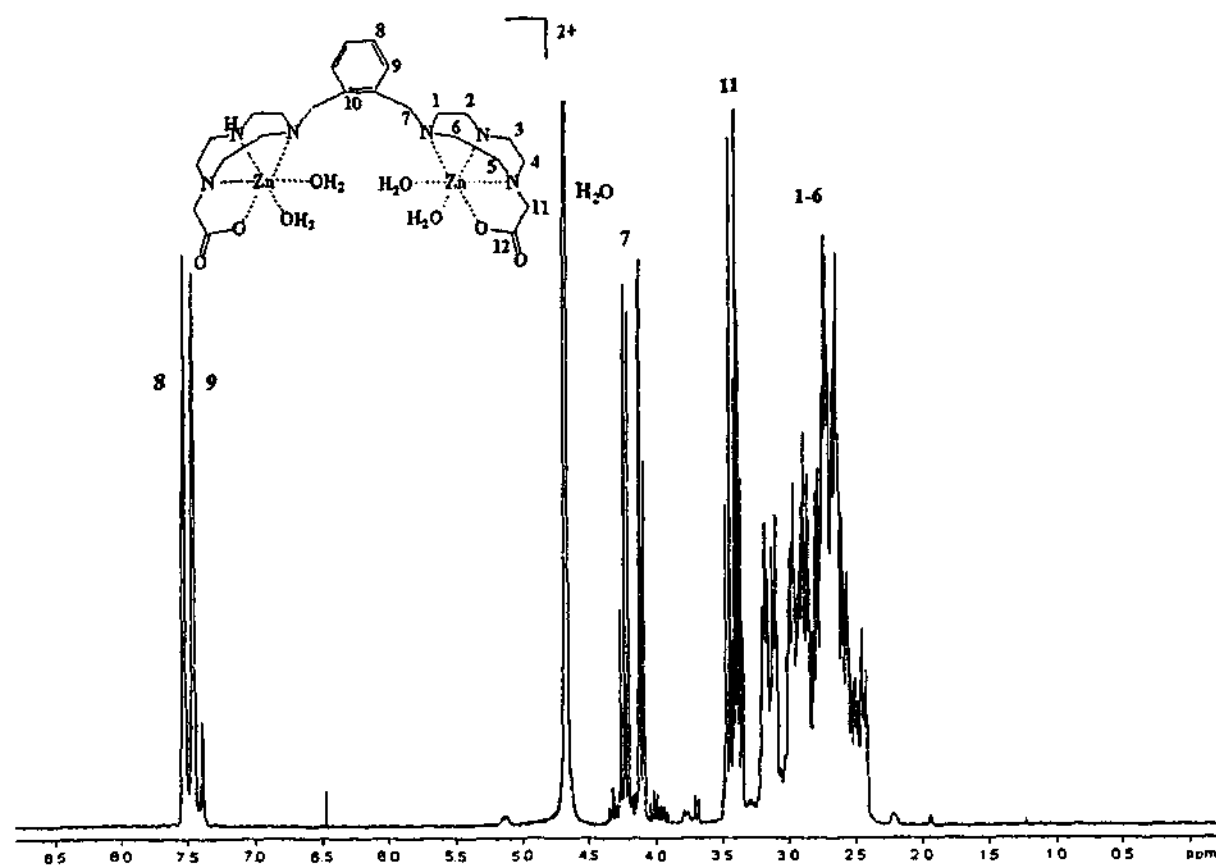
Chapter Four

spectrum. The signals due to the methylene protons in the tacn ring give rise to a very complicated spectrum, with peaks overlapping and no signals able to be individually assigned. These regions (2.39 – 3.22 ppm for the *ortho* species and 2.30 – 3.27 ppm for the *meta* species) however, each integrate to 24 protons, relative to the aromatic region. The methylene protons in the pendant arm give signals at 3.41 and 3.35 ppm for **16** and **17** respectively, each integrating to 4 protons. Each of these signals is not the expected singlet, but rather multiplets. This may be caused by the rigidity of the complexed species, making each of the methylene protons slightly different. The methylene protons in the xylyl bridge also give multiplets, at 4.20 ppm (**16**) and 4.00 ppm (**17**). In the spectrum of **16** the aromatic protons give rise to two multiplets at 7.48 and 7.54 ppm, while compound **17** shows a singlet at 7.46 ppm. The latter simplicity is unexpected, however, the anticipated three signals may have coalesced. The presence of the *meta* xylyl-bridged ligand is confirmed in the ^{13}C NMR spectrum with 3 sets of peaks arising due to the aromatic CH groups in the ring at 128.83 and 128.87, 131.76 and 131.78 and 134.15 and 134.37 ppm, with a fourth set at 133.74 and 133.84 ppm due to the quaternary carbon. The expected four signals for the *meta*-xylyl bridge actually appears as four sets of two signals. The feature is also observed with the remaining resonances in each of the complexes. The aromatic region for the *ortho* species (**16**) shows two sets of peaks due to the aromatic CH peaks at 128.82 and 128.87, and 132.52 and 132.67 ppm, with the quaternary carbon appearing as only one signal at 133.24 ppm. The spectra show the carbonyl peak at 179.05 and 179.18 ppm, and 178.81 and 178.93 ppm for **16** and **17**, respectively. Further upfield are the signals due to the methylene carbons in the tacn ring, the pendant carboxylate arm and the xylyl bridge. The bridge protons resonate at 61.75 and 61.94 ppm, and 61.51 and 61.67 ppm for **16**

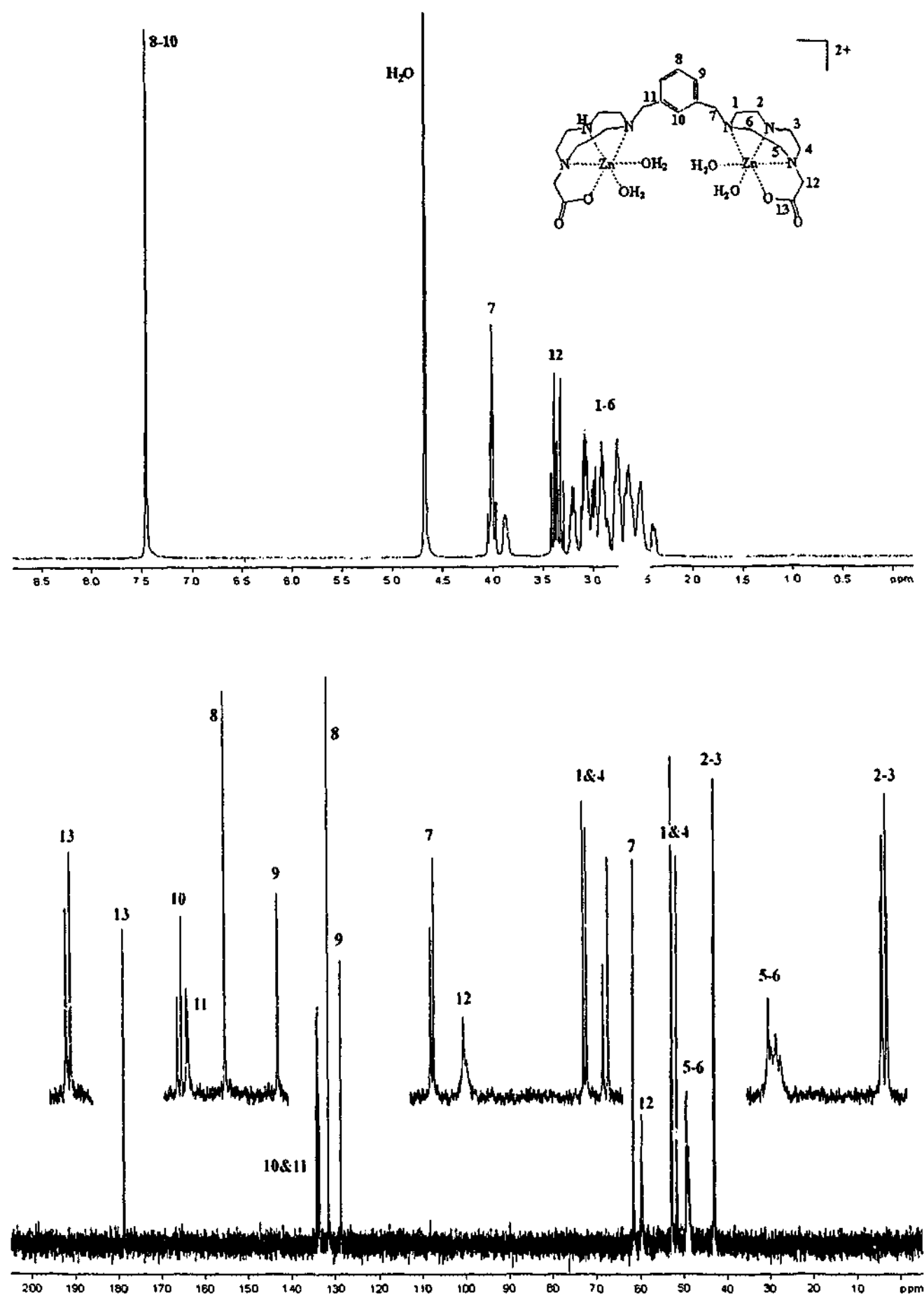
Chapter Four

and 17, respectively. For compound 16, the pendant arm methylene carbon give signals at 54.83 and 53.51 ppm, while for 17 the signal appears at 59.62 ppm. The methylene carbons in the tacn ring give rise to signals between 42.67-52.62 ppm (16) and 42.83-52.68 ppm (17), with two signals per carbon. The additional resonances will appear if the conformation or the structure of the complex changes slightly in solution. If, for instance, the zinc exists in both a 5- and a 6-coordinate environment in solution, there will be two signals for each carbon in the ligand. In the two cases where only one signal is observed (quaternary C in 16 and the bridge CH₂ in 17) the separation of these peaks may be such that it is too small to see two different signals. This doubling up of the signals due possibly to the presence of both 5- and 6-coordinate species in solution may also account for the complicated ¹H NMR spectra.

Chapter Four

Figure 4.12 ^1H and ^{13}C NMR spectra of 16

Chapter Four

Figure 4.13 ^1H and ^{13}C NMR spectra of 17

Chapter Four

4.4 Complex of a tris(tacn) ligand (18)

4.4.1 Preparation of the Complex

Complex 18 was synthesised by addition of an aqueous solution of the hydrochloride salt of the ligand, T₃mes, to an aqueous solution of Zn(ClO₄)₂·6H₂O. Addition of NaClO₄·H₂O to the solution and adjustment of the pH to *ca.* 7 with 1 M NaOH followed by gentle heating, precipitated a white powder on cooling. This was washed with methanol and allowed to air dry. The powder was isolated 37% yield.

The IR spectrum for 18 shows a broad water peak at 3261 cm⁻¹, which is overlapping with the NH stretching region and as a result, no ν(NH) can be seen. The perchlorate counter ions give a strong band at 1099 cm⁻¹ and a weaker band at 626 cm⁻¹. Peaks in the fingerprint region are indicative of the presence of the mesitylene linker group. Elemental analysis is consistent with the proposed structure and is given in Table 4.6.

Table 4.6 Elemental analysis for 18

Calculated values are in parenthesis

Complex	C (%)	H (%)	N (%)
18 Zn ₆ (T ₃ mes) ₂ (μ-OH) ₆ (H ₂ O) ₆](ClO ₄) ₆ ·H ₂ O	29.6	5.3	10.9
	(29.2)	(5.5)	(11.4)

Chapter Four

4.4.2 Solution NMR Spectroscopic Analysis of $[\text{Zn}_6(\text{T}_3\text{mes})_2(\mu\text{-OH})_6(\text{H}_2\text{O})_6](\text{ClO}_4)_6 \cdot \text{H}_2\text{O}$ (18)

The room temperature (300K) ^1H NMR and ^{13}C NMR spectra of 18 were run in D_2O are shown in Figure 4.14. The ^1H NMR spectrum shows a singlet in the aromatic region at 7.51 ppm due to the three equivalent protons on the aromatic bridge group. The methylene protons in the bridge are seen as a singlet at 4.09 ppm. The methylene protons on the tacn ring give rise to a more complicated set of signals centred at 2.88 ppm. The pattern is the same as seen for the other Zn(II)-poly(tacn) complexes (see Figure 4.9) and was again confirmed by a proton-carbon correlation spectrum. The ^{13}C NMR spectrum shows the expected 6 peaks. Three signals from the methylene protons on the tacn ring resonate at 41.51, 41.87 and 46.85 ppm. The protons in the linker group give a methylene signal at 56.93, the aromatic CH at 133.61 ppm and the quaternary at 132.79 ppm.

Chapter Four

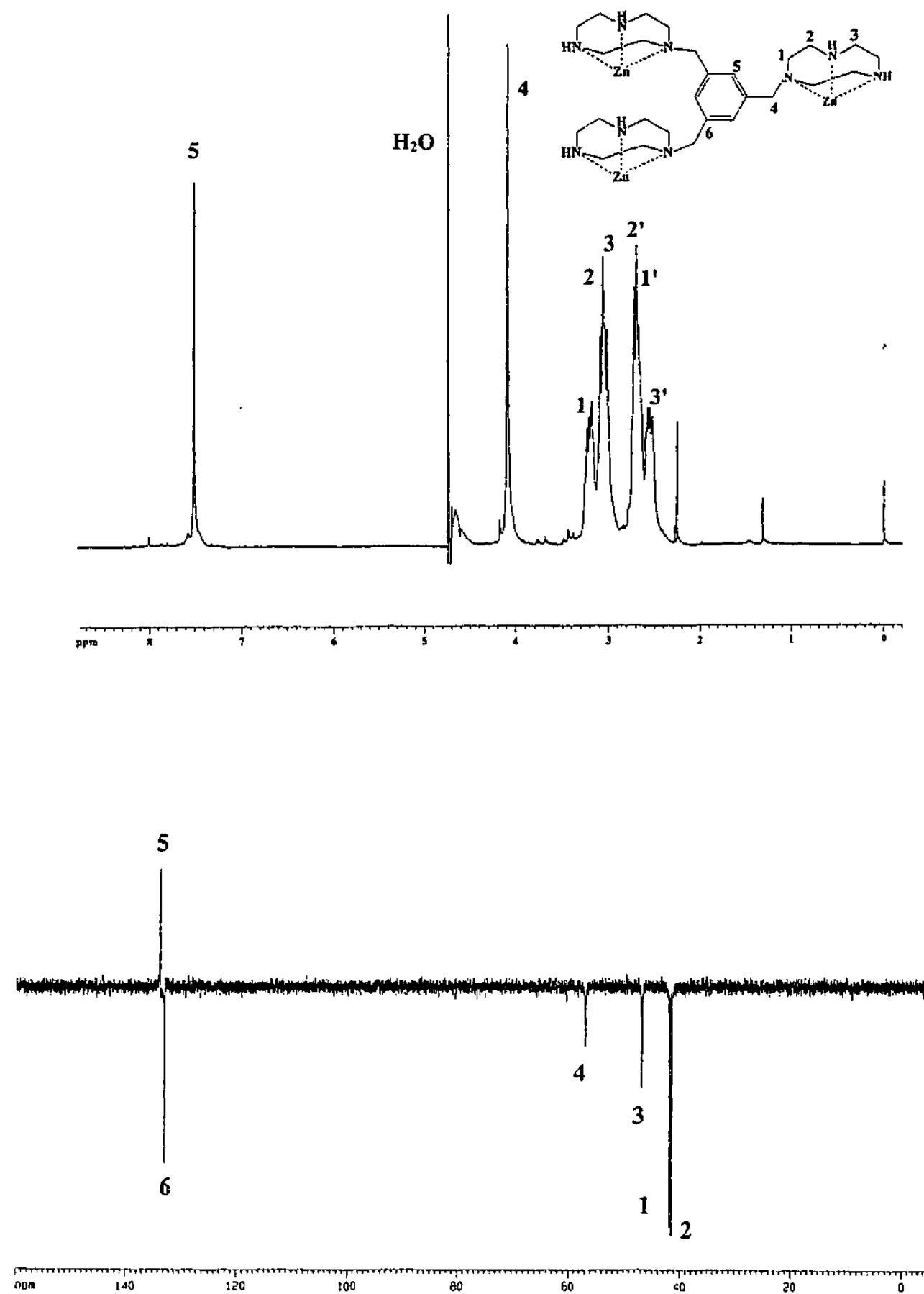


Figure 4.14 ^1H (top) and ^{13}C NMR (bottom) spectra of 18

Note the structure shown is only a partial representation

Chapter Four

It was initially theorised that the structure of the complex was analogous to the copper complex (complex 7, Section 3.4), based on the microanalytical data (Figure 4.15). Due to the simplicity of the NMR spectra, however, a more detailed study was undertaken. If the structure shown in Figure 4.15 was indeed indicative of the complex isolated, one may expect a more complicated ^{13}C NMR spectrum as the aromatic carbons are not all equivalent. A variable pD NMR study was undertaken to determine the structure of the complex isolated.

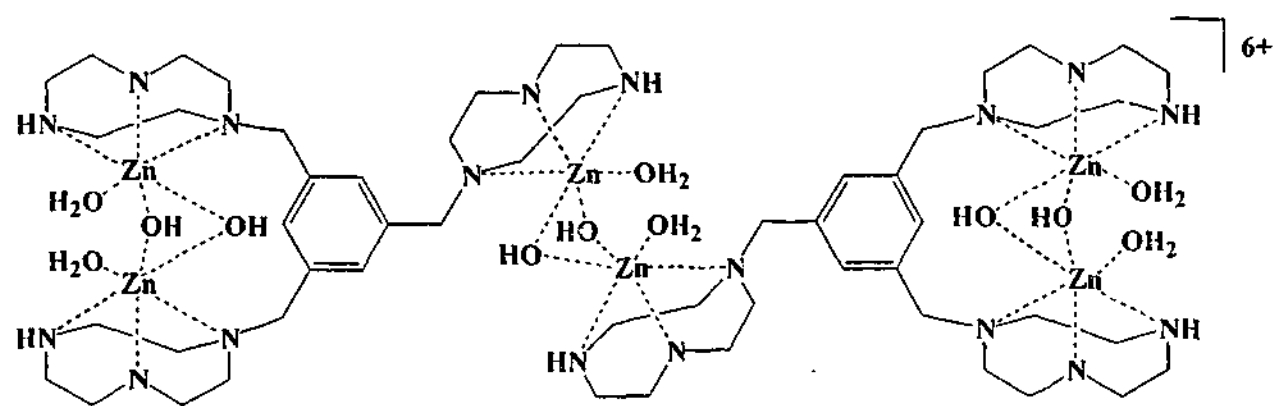


Figure 4.15 Analogous structure of 18 to that of
 $[\text{Cu}_6(\text{T}_3\text{mes})_2(\mu\text{-OH})_6(\text{H}_2\text{O})_6](\text{ClO}_4)_6 \cdot \text{H}_2\text{O}$ (7)

The pD of the complex dissolved in D_2O is 7. The pD of the solution was taken down to *ca.* 5 and the ^1H NMR showed a mixture of the above spectrum, and that of the free ligand. The integration showed that approximately a third of the complex had dissociated to the free ligand. The ^{13}C NMR spectrum was also in agreement with this observation. There was no evidence at the lower pD that a zinc(II) complex analogous to the hydroxo bridged trinuclear complex (Figure 4.16) isolated by Graham *et al.*²⁷

Chapter Four

$[\text{Cu}_3(\text{T}_3\text{mes})(\mu\text{-OH})_2(\text{H}_2\text{O})_2](\text{ClO}_4)_4 \cdot 7\text{H}_2\text{O}$ was formed. One might expect formation of this type of structure with decrease in pD, if a complex with the structure shown in Figure 4.15 was present.

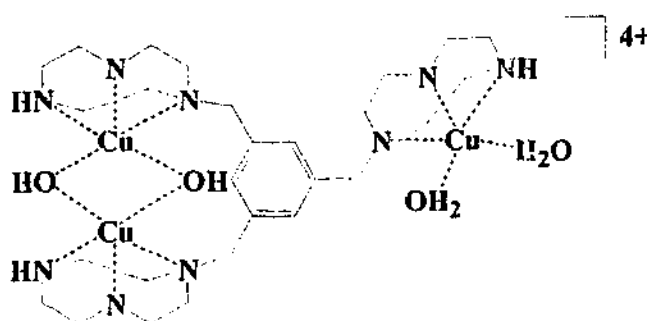
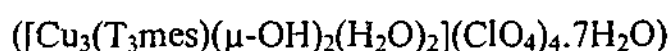


Figure 4.16 Hydroxo bridged trinuclear complex isolated by Graham *et al.*²⁷



Increasing the pD to *ca.* 9 also gave different spectra, relative to the those of the complex dissolved in D_2O (*i.e.* pD 7). The spectra became more simple with increasing pD. Two singlets still arise in the ^1H NMR spectrum due to the aromatic CH groups (7.62 ppm) and the methylene CH_2 groups (4.10 ppm) in the bridge. The tacn methylene protons, however, no longer give the pattern seen in Figure 4.14, and indeed in the other xylyl bridged binuclear complexes (13 and 14), but give rise to a doublet of multiplets centred at 2.88 ppm. The ^{13}C NMR spectrum is also extremely simple. Two signals at 134.19 and 134.85 ppm arise from the CH and the quaternary C in the methylene linker, while signals due to the methylene carbons appear at 42.52, 43.13 and 50.33 ppm. The bridge methylene carbons resonate at 60.83 ppm. A comparison of the spectra of the free ligand at this pD discounted dissociation of the complex at high

Chapter Four

pD, since the spectra of the ligand were found to be quite similar to those at the lower pD.

A more symmetrical structure was sought to explain the simplicity of the NMR spectra. Figure 4.17 shows the proposed structure for the complex $[\text{Zn}_6(\text{T}_3\text{mes})_2(\mu\text{-OH})_6(\text{H}_2\text{O})_6](\text{ClO}_4)_6 \cdot \text{H}_2\text{O}$. Modelling studies using Insight II,²⁸ however, indicated that the structure presented below is too sterically hindered to form, and therefore the proposed structure is that presented in Figure 4.15.

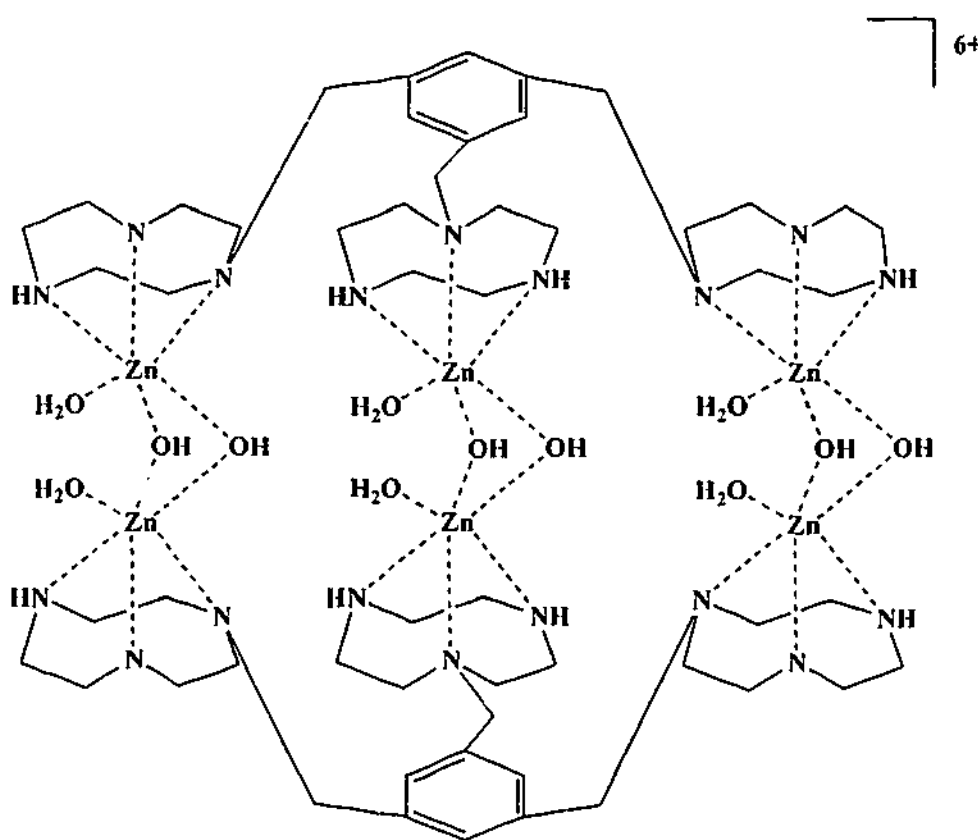
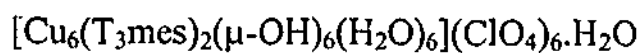


Figure 4.17 A theoretical symmetrical structure of



Chapter Four

It may well be that the Cu(II) structure is preferred and that there is some coincidence of the signals, or there is rapid exchange which simplifies the observed spectra. For example, the water ligands may exchange rapidly with the bridging hydroxide (see Figure 4.15), which will give an overall more symmetrical structure.

4.5 Zinc(II) Complex Incorporating Phosphate

4.5.1 Preparation of $[(\text{Zn}_2(\text{Me}_3\text{tacn})_2(\text{H}_2\text{O})_4\text{PhP})(\text{ClO}_4)_2 \cdot \text{H}_2\text{O}]$ (19)

Synthesis of the complex was achieved by the addition of equimolar amounts of an ethanol solution of Me_3tacn (0.55 g, 2.9 mmol) and an aqueous solution of $\text{Zn}(\text{ClO}_4)_2 \cdot 6\text{H}_2\text{O}$ (1.10 g, 2.90 mmol), followed by addition of a half molar amount of disodium phenyl phosphate (Na_2PPh) (0.25 g, 0.97 mmol). After slow evaporation, colourless crystals were deposited which were suitable for X-ray diffraction studies (Yield = 34%). The infrared spectrum showed an absorption at 3496 cm^{-1} due to coordinated water. A broad band centered at 1090 cm^{-1} was observed. Both perchlorate and phosphate have stretching frequencies in this area, so the presence of phosphate could not be determined conclusively by infrared spectroscopy. The presence of perchlorate was confirmed by the absorption at 626 cm^{-1} . Several bands occurring in the range of $700 - 800 \text{ cm}^{-1}$ are indicative of a phenyl group in the structure. Elemental analysis is consistent with the composition as determined by X-ray crystallography, however the bulk sample was found to precipitate with additional water molecules within the powder, compared with the crystal structure (Table 4.7). The electrospray mass spectrum also confirm the composition with peaks at m/z 817 and 741 due to $\{[\text{Zn}(\text{Me}_3\text{tacn})_2(\text{H}_2\text{O})_4\text{PhP}](\text{ClO}_4)\}^+$ and $\{[\text{Zn}(\text{Me}_3\text{tacn})_2\text{PhP}](\text{ClO}_4)\}^+$, respectively.

Chapter Four

Table 4.7 Elemental analysis for 19

Calculated values are in parenthesis

Complex	C (%)	H (%)	N (%)
19 $Zn_2(Me_3tacn)_2(H_2O)_4PhP](ClO_4)_2 \cdot 3H_2O$	29.9	6.0	8.7
	(29.7)	(6.3)	(8.7)

4.5.2 Crystal Structure of $[(Zn_2(Me_3tacn)_2(H_2O)_4PhP)(ClO_4)_2 \cdot H_2O]$ (19)

The single-crystal X-ray structure of 19 was determined in order to establish the binuclear nature of the complex and to confirm the coordination mode of the phenyl phosphate ligand. Cell parameters and details of the data collection are presented in section 1.9 of the Appendix. The molecular structure consists of discrete $[Zn_2(Me_3tacn)(H_2O)_4(PhP)]^{2+}$ units, perchlorate anions and water of crystallisation. Figure 4.18 represents and ORTEP plot of the complex, with the extended packing array shown in Figure 4.19. Table 4.8 lists selected bond lengths and angles.

Chapter Four

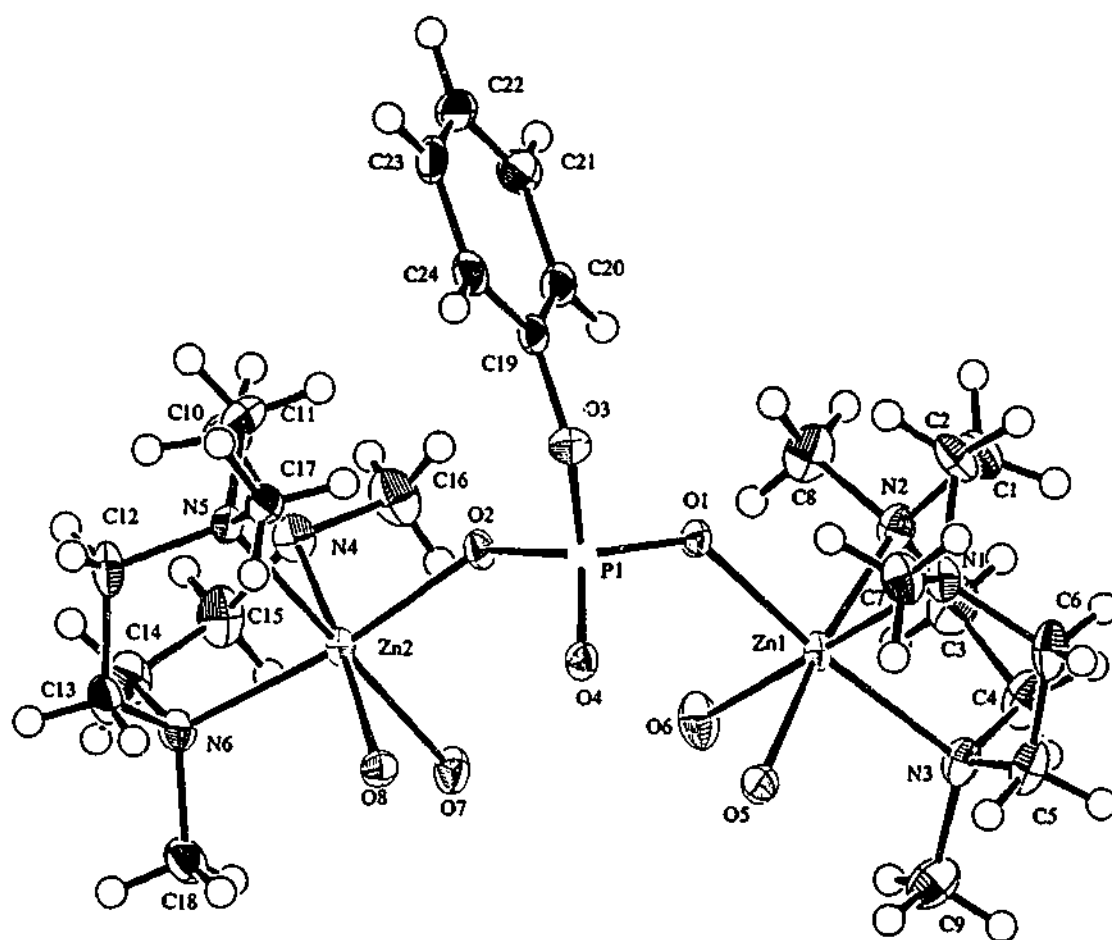


Figure 4.18 ORTEP plot of $[(Zn_2(Me_3tacn)_2(H_2O)_4PhP)]^{2+}$ cation 19 with atomic labelling scheme

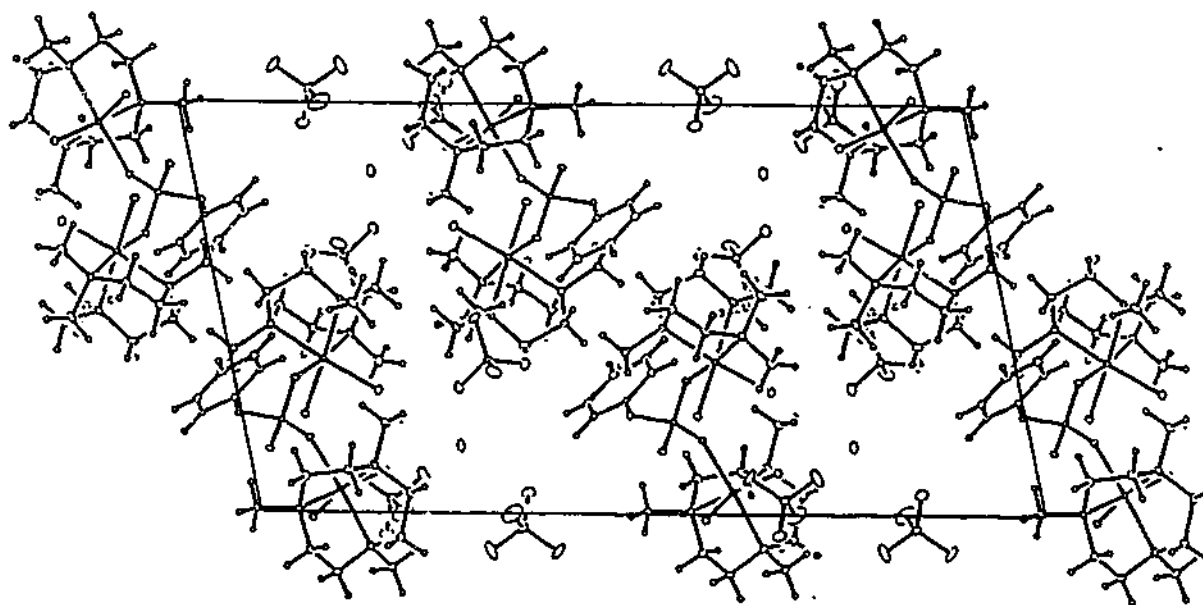
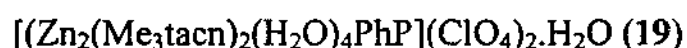


Figure 4.19 Packing diagram of 19

Chapter Four

Table 4.8 Selected bond distances (Å) and angles (°) for



Zn(1)-N(1)	2.173(3)	Zn(2)-N(4)	2.170(3)
Zn(1)-N(2)	2.167(2)	Zn(2)-N(5)	2.188(2)
Zn(1)-N(3)	2.172(2)	Zn(2)-N(6)	2.176(3)
Zn(1)-O(1)	1.997(2)	Zn(2)-O(2)	2.006(2)
Zn(1)-O(5)	2.155(2)	Zn(2)-O(7)	2.232(2)
Zn(1)-O(6)	2.185(2)	Zn(2)-O(8)	2.126(2)
N(1)-Zn(1)-N(2)	82.34(10)	N(4)-Zn(2)-N(5)	82.85(9)
N(1)-Zn(1)-N(3)	82.83(10)	N(4)-Zn(2)-N(6)	82.29(10)
N(1)-Zn(1)-O(1)	91.37(9)	N(4)-Zn(2)-O(2)	93.79(9)
N(1)-Zn(1)-O(5)	93.51(9)	N(4)-Zn(2)-O(7)	95.35(9)
N(1)-Zn(1)-O(6)	175.69(8)	N(4)-Zn(2)-O(8)	173.85(9)
N(2)-Zn(1)-N(3)	82.48(9)	N(5)-Zn(2)-N(6)	82.14(9)
N(2)-Zn(1)-O(1)	94.59(8)	N(5)-Zn(2)-O(2)	91.52(9)
N(2)-Zn(1)-O(5)	172.71(8)	N(5)-Zn(2)-O(7)	177.76(8)
N(2)-Zn(1)-O(6)	93.82(9)	N(5)-Zn(2)-O(8)	100.35(8)
N(3)-Zn(1)-O(1)	173.79(9)	N(6)-Zn(2)-O(2)	172.89(9)
N(3)-Zn(1)-O(5)	91.08(8)	N(6)-Zn(2)-O(7)	96.33(9)
N(3)-Zn(1)-O(6)	94.76(9)	N(6)-Zn(2)-O(8)	92.89(8)
O(1)-Zn(1)-O(5)	91.49(7)	O(2)-Zn(2)-O(7)	89.92(8)
O(1)-Zn(1)-O(6)	90.89(8)	O(2)-Zn(2)-O(8)	91.40(8)
O(5)-Zn(1)-O(6)	90.10(8)	O(7)-Zn(2)-O(8)	81.33(7)

The important feature of this complex is the presence of a bridging phosphate ester. In the complex, two Zn-Me₃tacn moieties are bridged by a single phosphate monoester. This has implications in phosphate ester hydrolysis studies as this complex may show cooperative effects of two zinc atoms as seen in the enzyme alkaline phosphatase. In contrast to [Cu₃(Me₃tacn)₃(PhP)₂](ClO₄)₂·½H₂O (9) and [Cu₂(T₂-*m*-X)(NPP)(μ-OH)]ClO₄·H₂O (10), complex 19 features four-coordinated water molecules, which on deprotonation could act as internal nucleophiles capable of enhancing the phosphate ester cleavage.

Chapter Four

The structural analysis of **19** indicates that each zinc(II) centre adopts a distorted octahedral geometry, however, each side of the molecule is slightly different. The N-Zn-N bond angles are all quite similar ($\sim 82^\circ$) and below the ideal octahedral angle of 90° , due to the constraining effects of the tacn ring. The bond angles between N-Zn-O(H₂O), and the angles between O(H₂O)-Zn-O(H₂O), vary on each side of the molecule. For example, the angle O(5)-Zn(1)-O(6) is close to the ideal octahedral angle ($89.33(7)^\circ$) with no constraints imposed, however the equivalent bond angle between O(5)-Zn(1)-O(7) is considerably less at $81.33(7)^\circ$. All six bond lengths from Zn-centres are similar with an average value of 2.174 \AA . The Zn-O(phosphate) distances ($1.997(2) - 2.006(2) \text{ \AA}$) are shorter than the Zn-O(OH₂) distances ($2.126(2) \text{ \AA} - 2.232(2) \text{ \AA}$). The zinc atoms themselves lie at a distance of 5.05 \AA apart. The non-bonded interatomic distances show a hydrogen bonding network between the bound and free waters and the perchlorate counter ions.

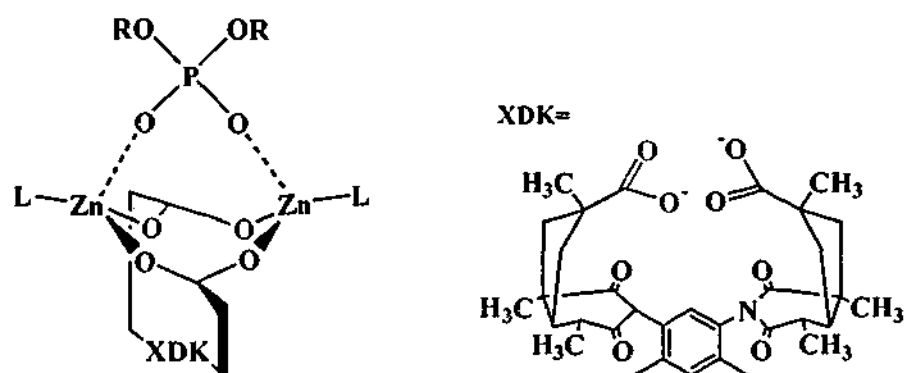
Other groups have also isolated zinc complexes in which two zinc centres are linked by an O⁻-P-O⁻ bridge.²⁹⁻³² Lippard and coworkers reported a binuclear complex in a 1:1 diphenyl phosphate to binuclear zinc complex (proposed structure see Figure 4.20 A),²⁹ while Adams *et al.* report the structure of two mononuclear zinc units linked by an NPP unit (Figure 4.20 B).³⁰ The structure of the latter is similar to **19**, but in this case the ligand is the tetradentate ligand tris[(2-pyridyl)methyl]amine (tpa). The Zn-Zn distance for this complex, 5.97 \AA , is slightly longer than that of the complex isolated in this work (5.05 \AA). In structure **B**, the zinc(II) centres lie in a disordered pentagonal-bipyramidal geometry, with the coordination sphere containing no coordinated water molecules which could be vital to generate nucleophiles to enhance phosphate ester cleavage.

Chapter Four

Another structure where two mononuclear zinc(II) complexes have been linked by a phosphate moiety was reported by Kitajima and coworkers,³² where the ligand used was hydro-tris(3,5-diisopropyl-1-pyrazolyl)borate. The complex was synthesised by addition of 2 mole equivalents of mononuclear complex to 1 mole equivalent of NPP. A schematic representation of the resulting complex is shown in Figure 4.20 C. The Zn-Zn distance was considerable shorter than that of Adams *et al.* at 5.14 Å, and is slightly longer than that found in **19**. It should be noted, however, that interzinc distances in these model complexes are well in excess of the distance found in Alkaline Phosphatase (AP) (3.94 Å). The zinc(II) centres in Kitajima's complex adopt a distorted tetrahedral geometry.

Comparison of the Zn(II)...Zn(II) distance of **19** with the Cu(II)...Cu(II) separation of complex **9** ($[\text{Cu}_3(\text{Me}_3\text{tacn})_3(\text{PhP})_2]\text{ClO}_4 \cdot \frac{1}{2}\text{H}_2\text{O}$) shows the metal-metal separation to be similar to the largest separation found in **9** (4.14, 4.55 and 5.04 Å). The distance of the hydroxo-phosphate-bridged complex **10** ($[\text{Cu}_2(\text{T}_2\text{-}m\text{-X})(\text{NPP})(\mu\text{-OH})]\text{ClO}_4 \cdot \text{H}_2\text{O}$), however, shows the metal-metal separation to be much shorter (3.57 Å), and in fact less than the distance found in AP. This shorter distance results from the connection of the two copper(II) centres via a single atom hydroxo bridge.

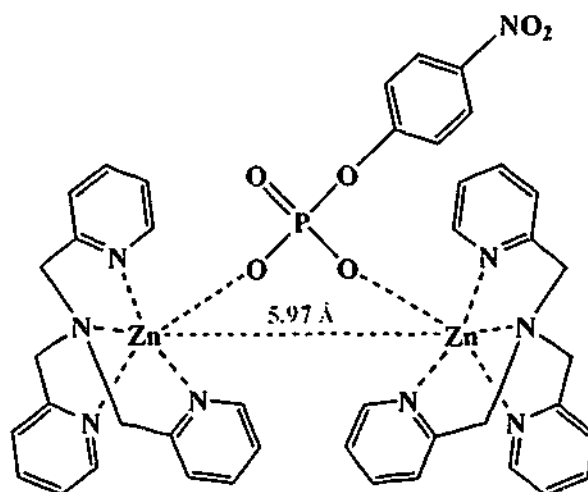
Chapter Four



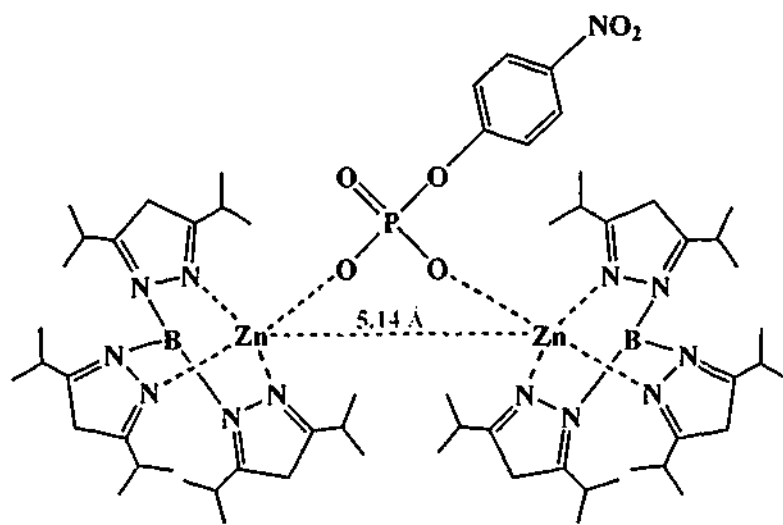
R = Ph or *p*-NO₂Ph

(A)

L = MeOH or py



(B)



(C)

Figure 4.20 Binuclear zinc(II) structures with bridging phosphate esters

Chapter Four

A comparison of **19** with the active sites of phosphatase enzymes shows the distances between metal centres within the catalytic centre are considerably shorter (see section 1.3). The distance between the two Zn centres in the AP enzymes, isolated with coordinated phosphate is 3.94 Å (see Figure 4.21). In the enzyme, the zinc(II) centres are coordinated to the less bulky inorganic phosphate molecule, which may contribute to the smaller Zn-Zn distance found in the enzyme. In addition, the synthetic models are not subjected to the constraints imposed by the presetting of the metal-binding cleft in the protein.³¹ In the enzyme phospholipase C (PLC) with coordinated inorganic phosphate, where the phosphate coordinates to all three zinc centres, the distances are: Zn(1)...Zn(2) = 5.7 Å; Zn(1)...Zn(3) = 3.5 Å; Zn(2)...Zn(3) = 4.5 Å.³³ As the coordination mode of the phosphate is different to that of these complexes, *i.e.* a single phosphate oxygen bridging between two zinc(II) centres (see Figure 4.21 C), a comparison is not valid in this case.

Chapter Four

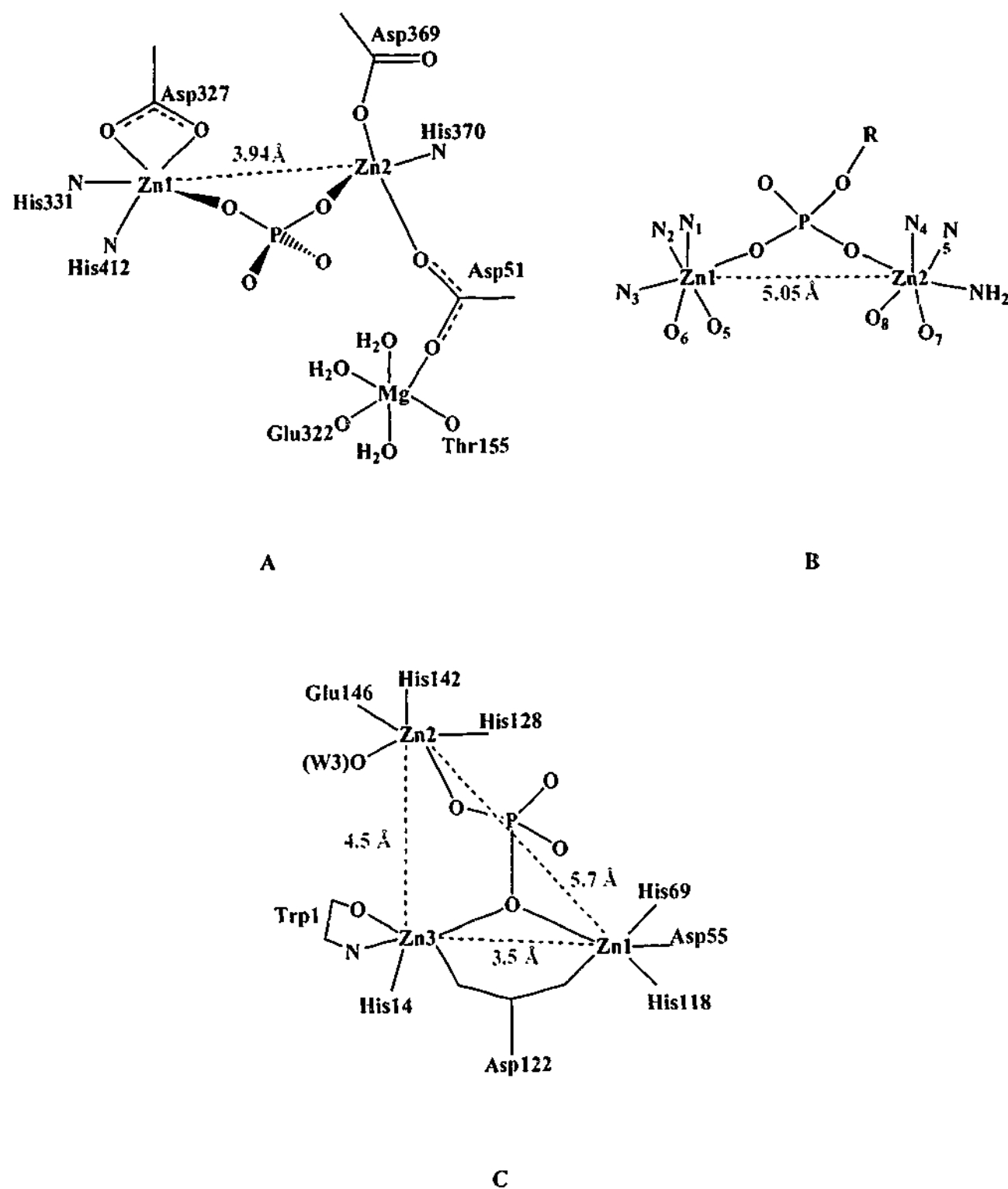


Figure 4.21 Comparison of the active site of AP with coordinated inorganic phosphate (A) and 19 (B) and the active site of phospholipase C with coordinated inorganic phosphate (C)

Chapter Four

4.5.3 Solution NMR Spectroscopic Analysis of
 $[(Zn_2(Me_3tacn)_2(H_2O)_4)PhP](ClO_4)_2 \cdot H_2O$ (19)

The room temperature (300K) 1H and ^{13}C NMR spectra of 19 were recorded in D_2O are shown in Figure 4.22. The proton NMR spectrum of 19 shows a singlet at 2.54 ppm arising from the methyl groups on the tacn ring nitrogens. The methylene protons in the tacn ring give rise to a multiplet centred at 2.74 ppm, which arise from the different orientations of the tacn nitrogens relative to the phosphate ester bridge (i.e. *cis* or *trans*). This result is unexpected in light of the single CH_3 signal, however, it is possible that the complex is undergoing exchange or reorganisation in solution and that the rates of exchange for the methyl and the methylene groups are different. The remaining signals in the spectrum appear in the aromatic region, with three signals for each of the three different environments in the phenyl phosphate moiety. These signals appear as a triplet of multiplets centred at δ 7.11 for the single proton in the *para* position relative to the phosphate group, a doublet of multiplets centred at 7.21 ppm for the proton in the *ortho* position and a triplet of multiplets at δ 7.36 for the remaining protons in the *meta* position. The ^{13}C NMR spectrum is also a simple spectrum. A signal at 45.76 ppm is attributable to the methyl groups while a single peak at 52.45 ppm arises from the methylene carbons within the tacn ring. The three signals from the aromatic CH appear at 120.16, 122.60 and 129.36 ppm and the quaternary carbon gives the signal at 152.73 ppm. The ^{31}P NMR gives a single peak at 1.03 ppm, due to the phosphate bridging group of the complex.

Chapter Four

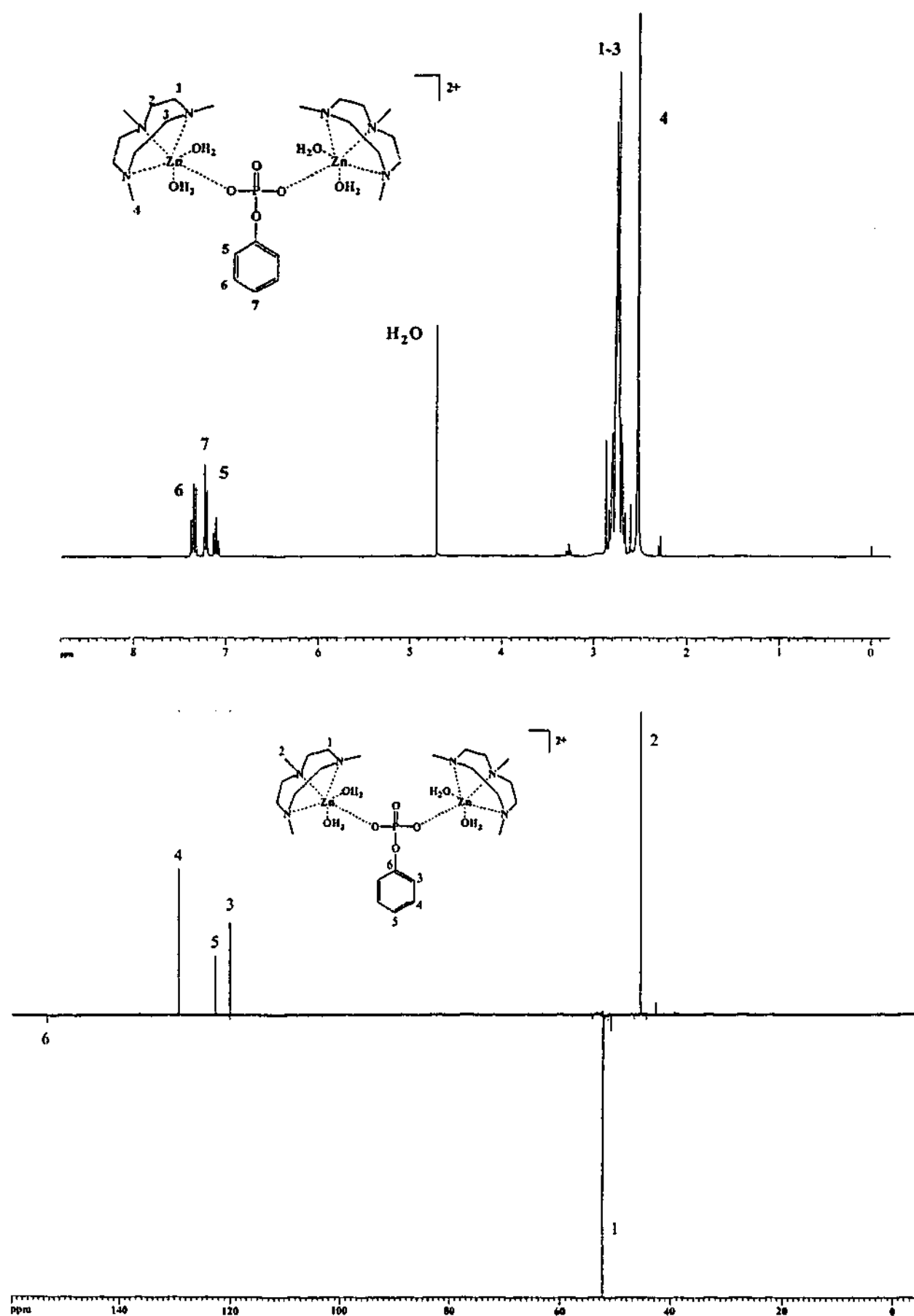


Figure 4.22 ¹H (top) and ¹³C (bottom) NMR spectra of 19 recorded in D₂O

Chapter Four

4.6 Concluding Remarks

The results presented in this chapter clearly demonstrate the different binding capacities of the bis(tacn) ligands. The three different structures formed by the *ortho*, *meta* and *para* ligands show how the change in the length of the organic group linking the macrocyclic compartments can alter the preferred structure of the metal complex that is formed. A mononuclear complex is formed on complexation with the *o*-xylyl bridged ligand, a hydroxo bridged complex with the *m*-xylyl bridged ligand, while in the case of the *p*-xylyl bridged ligand one zinc(II) ion binds to each of the tacn moiety without further bridging between the metal centres. The complex with the alkoxo bridge between each of the zinc(II) centres may also have an additional bridge between them, namely a bromide. The zinc(II) complex with the T₃mes ligand forms a dimeric species, with one [Zn₃(T₃mes)] moiety linked to a second through two hydroxo bridged between each of the zinc(II) centres.

The preparation of the complexes with the bis(tacn) ligands incorporating the acetate pendant arms, with an additional binding site on the ligand, enables the binuclear species to form with no bridging units between the metals. This clearly leaves two free sites on each metal centre for possible substrate binding and the potential for the complexes to act as catalysts for phosphate ester hydrolysis.

The isolation of $[(\text{Zn}(\text{Me}_3\text{tacn})(\text{H}_2\text{O})_2)_2(\text{PhP})]^{2+}$ shows possible cooperative effects of the $[\text{Zn}(\text{Me}_3\text{tacn})]^{2+}$ moiety, making it a potential reagent in the catalytic cleavage of phosphate esters. For this complex, an internal nucleophile may be created by adjustment of the pH, and thus could be used for the cleavage of phosphate ester bonds.

Chapter Four

4.7 Experimental

Reagents and Instruments

Laboratory chemicals, solvents, and nitrogen gas

All reagents were of reagent grade quality, obtained from commercial suppliers and used without further purification. Solvents were used as received or dried over 4Å molecular sieves. Nitrogen gas (CIG, high purity) was used directly from the cylinder. Water was distilled prior to use.

^1H , ^{13}C and ^{31}P Nuclear Magnetic Resonance (NMR) spectra

^1H and broad band decoupled ^{13}C NMR spectra were recorded on either a Bruker AC200, BrukerDPX300 or Bruker DRX400 spectrometer. Internal standards of tetramethylsilane (TMS) for non-aqueous solvents and sodium(2,2,3,3-d₄-3-(trimethylsilyl))propionate (TMSP-D) for D₂O were used as references, while phosphoric acid was used as the reference in ^{31}P NMR. The chemical shifts (δ) are reported in ppm using the high frequency positive convention. Abbreviations used to describe the resonances are: s (singlet), d (doublet), t (triplet), m (multiplet) and br (broad).

Infrared spectra

Infrared spectra were recorded using KBr disks or nujol mulls on a Perkin-Elmer 1600 series FTIR spectrophotometer at a resolution of 4.0 or 8.0 cm^{-1} . Abbreviations used to describe intensities are: s (strong), m (medium), w (weak) and br (broad).

Chapter Four

Microprobe analyses

Electron microprobe analyses were recorded by Mr A. Van den Bergen, Monash University, with a Jeol JSM-1 scanning electron microscope through an NEC X-ray detector and pulse-processing system connected to a Packard multi-channel analyser. Solid samples were mounted on an aluminium planchet using double sided conducting carbon impregnated sticky tape.

Microanalyses

Analyses of C, H and N were performed by Chemical and Microanalytical Services Pty. Ltd. (CMAS), Melbourne, Australia, or University of Otago, Dunedin, New Zealand.

Conductivity measurements

Solution conductivity measurements were made using a Crison 522 Conductimeter with Pt black electrodes. A 0.020 M KCl solution was used to calibrate the meter.

Synthesis of Complexes

$[\text{Zn}(\text{T}_{2-o}\text{-X})](\text{ClO}_4)_2$ (12)

$\text{T}_{2-o}\text{-X}\cdot 6\text{HCl}$ (0.50 g, 0.90 mmol) was dissolved in water (10 ml) and a solution of $\text{ZnCl}_2\cdot 2\text{H}_2\text{O}$ (0.61 g, 3.6 mmol) in water (10 ml) was added. The pH of the solution was adjusted to 6 with 2M NaOH. The precipitate of $\text{Zn}(\text{OH})_2$ was removed and the solution heated to reduce the volume. The solution was allowed to cool and then left to slowly evaporate. After 2 weeks crystals suitable for X-ray diffraction had formed and were collected by vacuum filtration.

Chapter Four

Yield = 0.29 g (37%). Analytical data: Found (%): C 37.6; H 6.0; N 13.1. Calculated for $\text{ZnC}_{20}\text{H}_{38}\text{N}_6\text{O}_9\text{Cl}_2$ (%): C 37.4; H 6.0; N 13.1. IR spectrum (KBr; ν , cm^{-1}): 3600 m, 3531 m, 3332 m, 2939 m, 2862 m, 1628 m, 1493 m, 1462 m, 1396 w, 1365 w, 1342 w, 1313 w, 1283 w, 1251 w, 1099 br s, 986 m, 938 m, 904 w, 858 m, 817 m, 798 w, 751 m, 624 s, 563 w, 507 w, 460 w, 422 w. ^1H NMR (D_2O): δ 2.78 (24H, m, $12 \times \text{CH}_2$ tacn), 3.45 (2H, br s, impurity), 4.03 (4H, s, $2 \times \text{CH}_2$ *o*-xylyl bridge), 7.45 (4H, m, ArCH). ^{13}C NMR (D_2O): δ 44.19 (CH_2 tacn), 44.30 (CH_2 tacn), 44.43 (CH_2 tacn), 51.04 (CH_2 tacn), 59.96 (CH_2 *o*-xylyl bridge), 128.34 (ArCH), 132.37 (ArCH), 134.30 (quaternary C). Electron microprobe : Zn, Cl present. Molar conductivity (H_2O) : 273 $\text{Scm}^2\text{mol}^{-1}$. Electrospray mass spectrum ($\text{H}_2\text{O}/\text{MeOH}$) (m/z): 541.2 (8%) $\{\text{Zn}(\text{T}_2\text{-o-X})(\text{ClO}_4)(\text{H}_2\text{O})\}^+$, 523.3 (6%) $\{\text{Zn}(\text{T}_2\text{-o-X})(\text{ClO}_4)\}^+$.

$[\text{Zn}_2(\text{T}_2\text{-}m\text{-X})(\mu\text{-OH})_2(\text{H}_2\text{O})_2]\text{Br}_2 \cdot \text{H}_2\text{O}$ (13)

Compound 13 was prepared by dissolving the free base of $\text{T}_2\text{-}m\text{-X}$ (0.20 g, 0.52 mmol) in acetone (5 ml) and adding it to a warm solution of ZnBr_2 (0.23 g, 1.0 mmol) in acetone (5 ml). A white precipitate formed immediately. The mixture was allowed to cool to room temperature before it was collected by vacuum filtration. The white powder was washed with acetone and air dried.

Yield = 0.41 g (95%). Analytical data : Found (%): C 32.7; H 5.5; N 11.4. Calculated for $\text{Zn}_2\text{C}_{20}\text{H}_{40}\text{N}_6\text{O}_5\text{Br}_2$ (%): C 32.7; H 5.5; N 11.4. IR spectrum (KBr; ν , cm^{-1}): 3409 br s, 3222 br s, 2984 m, 2874 m, 1638 m, 1489 m, 1458 m, 1363 m, 1313 w, 1282 w, 1241 w, 1151 w, 1105 m, 1036 m, 946 m, 883 m, 855 w, 815 m, 758 w, 734 w, 703 w, 671 w, 633 w, 572 w, 413 w. ^1H NMR (D_2O): 2.90 (24H, m, CH_2 tacn), 4.09 (4H, s,

Chapter Four

CH₂ *m*-xylyl bridge), 7.50 (4H, m, ArCH). ¹³C NMR (D₂O): δ 47.84 (CH₂ tacn), 49.96 (CH₂ tacn), 54.61 (CH₂ tacn), 63.51 (CH₂ *m*-xylyl bridge), 131.07 (ArCH), 131.89 (ArCH), 135.93 (ArCH), 137.85 (quaternary C). Electron microprobe : Zn and Br present only. Molar conductivity (H₂O): 570 Scm²mol⁻¹. Electrospray mass spectrum (H₂O/MeOH) (*m/z*): 583.0 (6%) {Zn₂(T₂-*m*-X(μ-O))} Br⁺.

[Zn₂(T₂-*p*-X)(H₂O)₄(DMF)₂][ZnCl₄]₂ (14)

Compound (14) was made following the same procedure as compound (12) using T₂-*p*-X.6HCl (0.50 g, 0.90 mmol) and ZnCl₂.xH₂O (0.49 g, excess). After an impure initial crop of [Zn₂(T₂-*p*-X)(H₂O)₆Cl₄].xZnCl₂ (Yield = ~50%) was collected, DMF was added to the filtrate and left to slowly evaporate. Colourless needles were deposited, collected by vacuum filtration, washed with methanol and air dried.

Yield = 0.15g (15%). Analytical data: Found (%): C 27.9; H 5.2; N 10.2. Calculated for Zn₄C₂₆H₅₄N₈O₆Cl₈ (%): C 27.8; H 5.2; N 10.0. IR spectrum (KBr; ν, cm⁻¹): 3445 s, 3288 s, 2975 m, 2937 m, 2872 m, 1663 s, 1620 m, 1545 w, 1487 w, 1455 m, 1375 m, 1285 w, 1254 w, 1148 w, 1100 m, 1055 w, 995 m, 936 w, 889 w, 863 m, 819 w, 781 w, 732 w, 693 w, 631 w, 574 w, 490 w, 420 w. ¹H NMR (D₂O): δ 2.46 (4H, m, 2 × CH₂ tacn), 2.61 (8H, m, 4 × CH₂ tacn), 2.80 (6H, s, 2 × CH₃ DMF), 2.96 (6H, s, 2 × CH₃ DMF), 2.98 (8H, m, 4 × CH₂ tacn), 3.12 (4H, m, 2 × CH₂ tacn), 3.97 (4H, s, 2 × CH₂ *p*-xylyl bridge), 7.40 (4H, s, ArCH), 7.87 (2H, 2 × CH (DMF)). ¹³C NMR (D₂O): δ 31.31 (CH₃ DMF), 36.86 (CH₃ DMF), 42.36 (CH₂ tacn), 47.68 (CH₂ tacn), 47.52 (CH₂ tacn), 57.56 (CH₂ bridge), 91.73 (CH DMF), 131.51 (ArCH), 133.22 (quaternary C). Electron microprobe : Zn and Cl present. Molar conductivity : 973 Scm²mol⁻¹. Electrospray

Chapter Four

mass spectrum (H₂O/MeOH) (*m/z*): 751 (6%) {Zn₂(T₂-*p*-X)[ZnCl₄](H₂O)Cl}⁺, 597.1 (11%) {Zn₂(T₂-*p*-X)Cl₃}⁺, 497.2 (27%) {Zn(T₂-*p*-X)(H₂O)₂Cl}⁺.

[Zn₂(T₂-PrO)(H₂O)₂Br]Br₂·H₂O (15)

Compound 15 was synthesised by dissolving T₂-PrOH·6HBr (0.30 g, 0.38 mmol) in water, adjustment of the pH to *ca.* 6 with 1M NaOH and addition of this solution to an aqueous solution of Zn(ClO₄)₂·6H₂O (0.56 g, 1.5 mmol, excess). The pH of the solution was taken to 10 and any precipitate which formed was removed. The pH was adjusted back to 7 with 1M HBr. The solution was warmed gently for 10 minutes and then allowed to stand at room temperature. After several days a colourless crystalline product deposited, was collected, washed with acetone and air dried.

Yield = 0.11 g (41%). Analytical Data: Found (%): C 24.4, H 5.1, N 11.4. Calculated for Zn₂C₁₅H₃₉N₆O₄Br₃ (%): C 24.4, H 5.3, N 11.4. IR spectrum (KBr, ν, cm⁻¹): 3464 m, 3291 s, 3259 s, 2939 m, 2881 m, 2855 m, 1687 w, 1487 m, 1455 m, 1430 w, 1362 w, 1289 w, 1269 w, 1248 w, 1186 w, 1159 w, 1125 m, 1104 w, 1055 w, 1013 m, 989 m, 940 m, 888 m, 859 m, 814 w, 674 m, 576 w, 538 w, 516 w, 454 m. ¹H NMR (D₂O): δ 2.41 (t, 2H, CH₂ bridge), 2.77 (10H, m, CH₂ tacn and 2H, CH₂ bridge), 2.94 (10H, m, CH₂ tacn), 3.14 (4H, m, CH₂ tacn) 3.91 (1H, t, CH bridge). ¹³C NMR (D₂O): δ 41.04 (CH₂ tacn), 41.18 (CH₂ tacn), 43.33 (CH₂ tacn), 44.62 (CH₂ tacn), 47.81 (CH₂ tacn), 52.14 (CH₂ tacn), 61.93 (CH₂ bridge), 64.46 (CH bridge). Electron Microprobe: Zn and Br present. Molar conductivity (H₂O): 507 Scm²mol⁻¹; (MeOH) 380 Scm²mol⁻¹. Electrospray mass spectrum (H₂O/MeOH) (*m/z*): 602.9 (53%) {Zn₂(T₂-PrO)Br₂}⁺.

Chapter Four

 $[\text{Zn}_2(\text{T}_2\text{-}o\text{-X Ac}_2)(\text{H}_2\text{O})_4](\text{ClO}_4)_2 \cdot 2\text{H}_2\text{O}$ (16)

The yellow solid of $\text{T}_2\text{-}o\text{-X Ac}_2 \cdot 6\text{HCl}$ (0.70 g, *ca.* 1.0 mmol) was dissolved in water (40 ml) and a solution consisting of $\text{Zn}(\text{ClO}_4)_2 \cdot 6\text{H}_2\text{O}$ (2.22 g, 5.96 mmol, 2 fold excess) dissolved in water (40 ml) was added. The pH of the solution was adjusted to 5-6 with 1M NaOH and the solution heated on the steam bath for 10 minutes. The fluffy white precipitate of $\text{Zn}(\text{OH})_2$ was removed. The solution was loaded on to a Sephadex SP-C20 cation exchange column and eluted with 0.1 M NaClO_4 . The eluent was concentrated *in vacuo*, the solution was left to stand and slowly evaporate and after several weeks, a cream precipitate deposited. This was collected by vacuum filtration, washed with MeOH (20 ml) and allowed to air dry. The filtrate was allowed to continue to evaporate and another crop was collected.

Total yield = 0.17 g (19%). Analytical Data: Found (%): C 31.6, H 5.2, N 9.1. Calculated for $\text{Zn}_2\text{C}_{24}\text{H}_{50}\text{N}_6\text{O}_{18}\text{Cl}_2$ (%): C 31.6, H 5.5, N 9.2. IR spectrum (KBr, ν , cm^{-1}): 3424 br s, 3329 s, 2941 m, 1589 s, 1493 w, 1456 m, 1440 m, 1403 m, 1315 m, 1238 w, 1099 br s, 999 m, 982 m, 930 w, 899 w, 853 w, 817 w, 783 w, 719 w, 665 w, 625 s, 571 w, 523 w. ^1H NMR (D_2O): 2.39-3.22 (24H, m, CH_2 tacn), 3.41 (4H, m, CH_2 pendant arm), 4.20 (4H, m, CH_2 bridge), 7.48 (2H, m, ArCH), 7.54 (2H, m, ArCH). ^{13}C NMR (D_2O): 42.67 (CH_2 tacn), 43.59 (CH_2 tacn), 48.09 (CH_2 tacn), 48.49 (CH_2 tacn), 49.07 (CH_2 tacn), 51.83 (CH_2 tacn), 52.25 (CH_2 tacn), 52.62 (CH_2 tacn), 54.78 (CH_2 pendant arm), 61.71 (CH_2 bridge), 128.82 (ArCH), 132.62 (ArCH), 133.17 (quaternary C), 179.18 (C=O). Electron Microprobe: Zn and Cl present. Molar conductivity (H_2O): $271 \text{ Scm}^2\text{mol}^{-1}$. Electrospray mass spectrum ($\text{H}_2\text{O}/\text{MeOH}$) (m/z): 701.0 (27%) $[\text{Zn}_2(\text{T}_2\text{-}o\text{-X Ac}_2)]\text{ClO}_4^+$, 639.1 (19%) $\{\text{Zn}(\text{T}_2\text{-}o\text{-X Ac}_2\text{H}_2\text{ClO}_4)^+\}$, 539.2 (16%) $\{\text{Zn T}_2\text{-}o\text{-X Ac}_2\text{H}\}^+$.

Chapter Four

 $[\text{Zn}_2(\text{T}_2\text{-}m\text{-X Ac}_2)(\text{H}_2\text{O})_4](\text{ClO}_4)_2 \cdot 2\text{H}_2\text{O}$ (17)

The yellow solid of $\text{T}_2\text{-}m\text{-X Ac}_2 \cdot 6\text{HCl}$ (0.70 g, *ca.* 1.0 mmol) was dissolved in water (40 ml) and a solution containing $\text{Zn}(\text{ClO}_4)_2 \cdot 6\text{H}_2\text{O}$ (2.19 g, 5.88 mmol, 2 fold excess) dissolved in water (40 ml) was added. The pH of the solution was adjusted to 5-6 with 1M NaOH and the solution heated on the steam bath for 10 minutes. The fluffy white precipitate of $\text{Zn}(\text{OH})_2$ was removed. The solution was loaded on to a Sephadex SP-C20 cation exchange column and eluted with 0.1 M NaClO_4 . The eluent was concentrated *in vacuo* and the solution was left to stand and slowly evaporate and after several weeks, a cream precipitate deposited. This was collected by vacuum filtration, washed with MeOH (10 mls) and allowed to air dry. The filtrate was allowed to continue to evaporate and two more crops were collected.

Yield = 0.57 g (62%). Analytical Data: Found (%): C 31.8, H 5.2, N 9.2. Calculated for $\text{Zn}_2\text{C}_{24}\text{H}_{50}\text{N}_6\text{O}_{18}\text{Cl}_2$ (%): C 31.6, H 5.5, N 9.2. IR spectrum (KBr, ν , cm^{-1}): 3447 s br, 3325 s, 2939 m, 2879 m, 2026 w, 1591 s, 1492, w, 1459 m, 1406 m, 1326 w, 1262 w, 1101 s, 1004 m, 930 w, 854 w, 818 w, 787 w, 724 w, 670 w, 625 s, 534 w, 476 w, 414 w. ^1H NMR (D_2O): δ 2.30-3.27 (24H, m, CH_2 tacn), 3.35 (4H, m, CH_2 pendant arm), 4.00 (4H, m, CH_2 bridge), 7.46 (4H, s, ArCH). ^{13}C NMR (D_2O): 42.83 (CH_2 tacn), 42.92 (CH_2 tacn), 43.12 (CH_2 tacn), 43.25 (CH_2 tacn), 48.83 (CH_2 tacn), 49.18 (CH_2 tacn), 51.52 (CH_2 tacn), 51.85 (CH_2 tacn), 52.68 (CH_2 tacn), 59.62 (CH_2 pendant arm), 61.50 (CH_2 bridge), 128.81, 131.74, 133.62 (quaternary C), 134.13 (ArCH), 178.81 (C=O). Electron Microprobe: Zn and Cl present. Molar Conductivity (H_2O): 244 $\text{Scm}^2\text{mol}^{-1}$. Electrospray mass spectrum ($\text{H}_2\text{O}/\text{MeOH}$) (m/z): 701.0 (26%) $\{\text{Zn}_2(\text{T}_2\text{-}m\text{-X Ac}_2)\text{ClO}_4\}^+$, 639.1 (18%) $\{\text{Zn}(\text{T}_2\text{-}m\text{-X Ac}_2\text{H}_2\text{ClO}_4)\}^+$, 539.2 (14%) $\{\text{Zn T}_2\text{-}m\text{-X Ac}_2\text{H}\}^+$.

Chapter Four

 $[\text{Zn}_6(\text{T}_3\text{mes})_2(\mu\text{-OH})_6(\text{H}_2\text{O})_6](\text{ClO}_4)_6 \cdot \text{H}_2\text{O}$ (18)

Compound 18 was synthesised by adding an aqueous solution of $\text{T}_3\text{mes} \cdot 9\text{HCl}$ (2.00 g, 2.41 mmol) (10 ml) to an aqueous solution containing $\text{Zn}(\text{ClO}_4)_2 \cdot 6\text{H}_2\text{O}$ (2.69 g, 7.23 mmol) dissolved in water (10 ml). The pH of the solution was adjusted to *ca.* 6 and $\text{NaClO}_4 \cdot \text{H}_2\text{O}$ (1 g) was added. The solution was warmed gently to reduce the volume by half. A white powder precipitated upon cooling. This was collected by vacuum filtration, washed with methanol and air dried. A second crop was collected after leaving the filtrate to slowly evaporate.

Total yield = 0.98 g (37%). Analytical data : Found (%): C 29.6; H 5.3; N 10.9. Calculated for $\text{Zn}_6\text{C}_{54}\text{H}_{122}\text{N}_{18}\text{O}_{37}\text{Cl}_6$ (%): C 29.2; H 5.5; N 11.4. IR spectrum (KBr; ν , cm^{-1}): 3261 br m, 2937 m, 1623 w, 1491 w, 1457 m, 1364 w, 1284 w, 1090 s, 1004 m, 942 w, 882 w, 857 w, 822 w, 739 w, 626 m, 420 w. ^1H NMR (D_2O , pD 7): δ 2.55 (m, 6H, CH_2 tacn), 2.68 (m, 12H, CH_2 tacn), 3.04 (m, 12H, CH_2 tacn), 3.21 (m, 6H, CH_2 tacn), 4.09 (s, 6H, CH_2 bridge), 7.51 (s, 3H, ArCH). ^{13}C NMR (D_2O , pD 7): δ 41.51 (CH_2 tacn), 41.87 (CH_2 tacn), 46.85 (CH_2 tacn), 56.93, (CH_2 bridge), 132.79 (quaternary C bridge), 133.61 (ArCH bridge). ^1H NMR (D_2O , pD 5): δ 2.60 (m, 6H, CH_2 tacn complex), 2.69 (m, 12H, CH_2 tacn complex), 3.03 (m, 12H, CH_2 tacn complex and 5H CH_2 tacn ligand), 3.24 (m, 6H, CH_2 tacn complex and 5H CH_2 tacn ligand), 3.62 (s, 5H, CH_2 tacn ligand), 3.98 (s, 2.5H, CH_2 bridge ligand), 4.06 (s, 6H, CH_2 bridge complex), 7.45 (s, 1.9H, ArCH, ligand), 7.46 (s, 3H, ArCH complex). ^{13}C NMR (D_2O , pD 5): δ 42.19 (CH_2 tacn complex), 42.54 (CH_2 tacn complex), 42.86 (CH_2 tacn ligand), 43.66 (CH_2 tacn ligand), 47.34 (CH_2 tacn ligand), 47.69 (CH_2 tacn complex), 57.76, (CH_2 bridge complex), 58.13 (CH_2 bridge ligand), 133.01 (ArCH bridge ligand), 134.37

Chapter Four

(quaternary C bridge complex), 134.62 (ArCH bridge complex), 136.11 (quaternary C bridge ligand). ^1H NMR (D_2O , pD 9): δ 2.88 (dm, 6H, CH_2 tacn), 4.10 (s, 6H, CH_2 bridge), 7.62 (s, 3H, ArCH). ^{13}C NMR (D_2O , pD 9): δ 42.52 (CH_2 tacn), 43.13 (CH_2 tacn), 50.33 (CH_2 tacn), 60.83, (CH_2 bridge), 134.19 (ArCH bridge), 134.85 (quaternary C bridge). Electron microprobe: Zn and Cl present.

$[(\text{Zn}_2(\text{Me}_3\text{tacn})_2(\text{H}_2\text{O})_4\text{PhP})(\text{ClO}_4)_2 \cdot \text{H}_2\text{O}]$ (19)

To an ethanol solution of Me_3tacn (0.50 g, 2.9 mmol) (20 ml) was added an aqueous solution of $\text{Zn}(\text{ClO}_4)_2 \cdot 6\text{H}_2\text{O}$ (1.10 g, 2.90 mmol) (10 ml), followed by addition of a third molar amount of disodium phenyl phosphate (Na_2PPh) (0.25 g, 0.97 mmol) (10 ml). After slow evaporation, colourless crystals suitable for X-ray crystallography were deposited. These were collected by vacuum filtration and allowed to air dry.

Yield = 0.32 g (34%). Analytical data: Found (%): C 29.9; H 6.0; N 8.7. Calculated for $\text{Zn}_2\text{C}_{24}\text{H}_{61}\text{N}_6\text{O}_{19}\text{PCl}_2$ (%): C 29.7; H 6.3; N 8.7. IR spectrum (KBr; ν , cm^{-1}): 3496 s br, 2870 m, 2825 m, 1654 m, 1639 m, 1594 m, 1570 w, 1560 w, 1541 w, 1522 w, 1490 s, 1467 m, 1426 w, 1366 m, 1303 m, 1235 m, 1090 s br, 1015 s, 994 s, 891 m, 770 m, 746 m, 696 m, 668 w, 626 s, 575 w. 554 m, 516 w, 441 w, 421 w, 408 w. ^1H NMR (D_2O): δ 2.54 (s, 9H, CH_3), 2.74 (m, 12H, CH_2 tacn ring), 7.11 (tm, 1H ArCH), 7.21 (dm, 2H, CH_2 tacn ring), 7.36 (t m, 2H, ArCH). ^{13}C NMR (D_2O): δ 45.76 (CH_3) 52.45 (CH_2), 120.16 (ArCH), 122.60 (ArCH), 129.36 (ArCH), 157.73 (quaternary C). ^{31}P NMR (D_2O): δ 1.03 (s, $\text{C}_6\text{H}_5\text{PO}_4$). Electron microprobe : Zn and Cl and P present. Molar conductivity : $767 \text{ Scm}^2 \text{ mol}^{-1}$. Electrospray mass spectrum ($\text{H}_2\text{O}/\text{MeOH}$) (m/z): 817 (45%) $\{[\text{Zn}_2(\text{Me}_3\text{tacn})_2(\text{PhP})(\text{H}_2\text{O})_4]\text{ClO}_4\}^+$, 741 (16%) $\{[\text{Zn}_2(\text{Me}_3\text{tacn})_2(\text{PhP})]\text{ClO}_4\}^+$.

Chapter Four

4.8 References

- (1) Powell, A. K., Deveson, A. C., Collison, D., Harper, D. R., Mabbs, F. E. In *The Chemistry of the Copper and Zinc Triads*; Welch, A. J., Chapman, S.K., Ed.; The Royal Society of Chemistry: Cambridge, 1993.
- (2) Fenton, D. E. *Biocoordination Chemistry*; Oxford University Press: New York, 1995.
- (3) Kimura, E., Kituta, E. *J. Bioinorg. Chem.* **2000**, *5*, 139.
- (4) Yang, R., Zompa, L. J. *Inorg. Chem.* **1976**, *15*, 1499.
- (5) Tanaka, N., Kobayashi, Y., Takamoto, S. *Chem. Lett.* **1977**, 107.
- (6) Weighardt, K., Tolksdorf, I., Herrmann, W. *Inorg. Chem* **1985**, *24*, 1230.
- (7) Alcock, N. W., McLaren, F., Moore, P., Pike, G. A., Roe, S. M. *J. Chem. Soc., Chem. Commun.* **1989**, 629.
- (8) Halfen, J. A., Jazdzewski, B. A., Mahapatra, S., Berreau, L. M., Wilkinson, E. C., Que, L., Jr., Tolman, W. B. *J. Am. Chem. Soc.* **1997**, *119*, 8217.
- (9) Sokolowski, A., Müller, J., Weyhermüller, T., Schnepf, R., Hilderbrandt, P., Hildenbrand, K., Bothe, E., Weighardt, K. *J. Am. Chem. Soc.* **1997**, *119*, 8889.
- (10) Di Vaira, M., Mani, F., Stoppioni, P. *Inorg. Chim. Acta* **2000**, *303*, 61.
- (11) Schlager, O., Weighardt, K., Grondy, H., Rufinska, A., Nuber, B. *Inorg. Chem.* **1995**, *34*, 6440.
- (12) Pafford, R. J., Chou, J-H., Rauchfuss, T.B. *Inorg. Chem.* **1999**, *38*, 3779.
- (13) Watson, A. A., Willis, A. C., Fairlie, D. P. *Inorg. Chem.* **1997**, *36*, 752.
- (14) Chen, H., Olmstead, M. M., Albright, R. L., Deveson, J., Fish, R. H. *Angew. Chem. Int. Ed. Engl.* **1997**, *36*, 642.
- (15) Silver, G. C., Gantzel, P., Trogler, W. C. *Inorg. Chem.* **1995**, *34*, 2487.

Chapter Four

-
- (16) Chaudhuri, P., Stockheim, C., Weighardt, K., Deck, W., Gregorzik, R., Vahrenkamp, H., Nuber, B., Weiss, J. *Inorg. Chem.* **1992**, *31*, 1451.
- (17) DasGupta, B., Haidar, R., Hsieh, W-Y., Zompa, L. *J. Inorg. Chim. Acta* **2000**, *306*, 78.
- (18) Bossek, U., Nühlen, D., Bill E., Glaser, T., Krebs, C., Weyhermüller, T., Weighardt, K., Lengen, M., Trautwein, A. X. *Inorg. Chem.* **1997**, *36*, 2834.
- (19) Ellis, D., Farrugia, L. J., Hickman, D. T., Lovatt, P. A., Peacock, R. D. *Chem. Commun.* **1996**, 1817.
- (20) Blake, A. J., Donlevy, T. M., England, P. A., Fallis, I. A., Parsons, S., Ross, S. A., Schröder, M. *J. Chem. Soc., Chem. Commun.* **1994**, 1981.
- (21) Brudenell, S. J., Spiccia, L., Hockless, D. C. R., Tiekink, E. R. T. *J. Chem. Soc., Dalton, Trans.* **1999**, 1475.
- (22) Geary, W. J. *Coord. Chem. Rev.* **1971**, *7*, 81.
- (23) Brooker, S., McKee, V. *Chem. Commun.* **1989**, 619.
- (24) Graham, B., Fallon, G. D., Hearn, M. T. W., Hockless, D. C. R., Lazarev, G., Spiccia, L. *Inorg. Chem.* **1997**, *36*, 6366.
- (25) Fry, F. H., Graham, B., Spiccia, L., Hockless, D.C.R., Tiekink, E.R.T. *J. Chem. Soc., Dalton Trans.* **1997**, 827.
- (26) Deacon, G. B., Huber, F. *Inorg. Chim. Acta* **1985**, *104*, 41.
- (27) Graham, B., Spiccia, L., Fallon, G.D., Hearn, M. T. W., Mabbs, F. E., Moubaraki, B., Murray, K. S. *J. Chem. Soc., Dalton Trans.*, In press.
- (28) Insight II 4.0.0Pt Molecular Modelling Program. Discover3 minimisation (esff).
- (29) Tanase, T., Yun, J. W., Lippard, S. J. *Inorg. Chem* **1995**, *34*, 4220.

Chapter Four

-
- (30) Adams, H., Bailey, N. A., Fenton, D. E., He, Q. Y. *J. Chem. Soc. Dalton Tran.* **1995**, 697.
- (31) Adams, H., Bailey, N. A., Fenton, D. E., He, Q-Y. *J. Chem. Soc., Dalton Trans.* **1997**, 1533.
- (32) Hikichi, S., Tanaka, M., Moro-oka, Y., Kitajima, N. *Chem. Commun.* **1992**, 814.
- (33) Hansen, S., Harzen, L. K., Hough, E. *J. Mol. Biol.* **1992**, 225, 543.

Chapter Five

Kinetics of the Hydrolysis of Phosphate Esters

5.1 Introduction

Metal promoted hydrolytic studies are an active area of research, with many publications appearing in the literature in recent years.¹⁻¹⁶ It is an important area of research as the backbones of the macromolecules DNA and RNA are both comprised of phosphodiester bonds (Figure 5.1). Development of active catalysts that cleave such linkages may find application in medicinal and biochemical research² and also has relevance to detoxification issues surrounding chemical weapons and insecticides, as these chemical toxins also contain phosphate esters.¹⁷ The aim in designing synthetic hydrolases is to discover and take advantage of the mechanisms which nature utilises to achieve such great rate enhancements.⁸ Determining the role of metal ions within model systems will give both a better understanding of the mechanisms by which the enzyme functions, as well as aiding the development of improved synthetic hydrolases.⁷

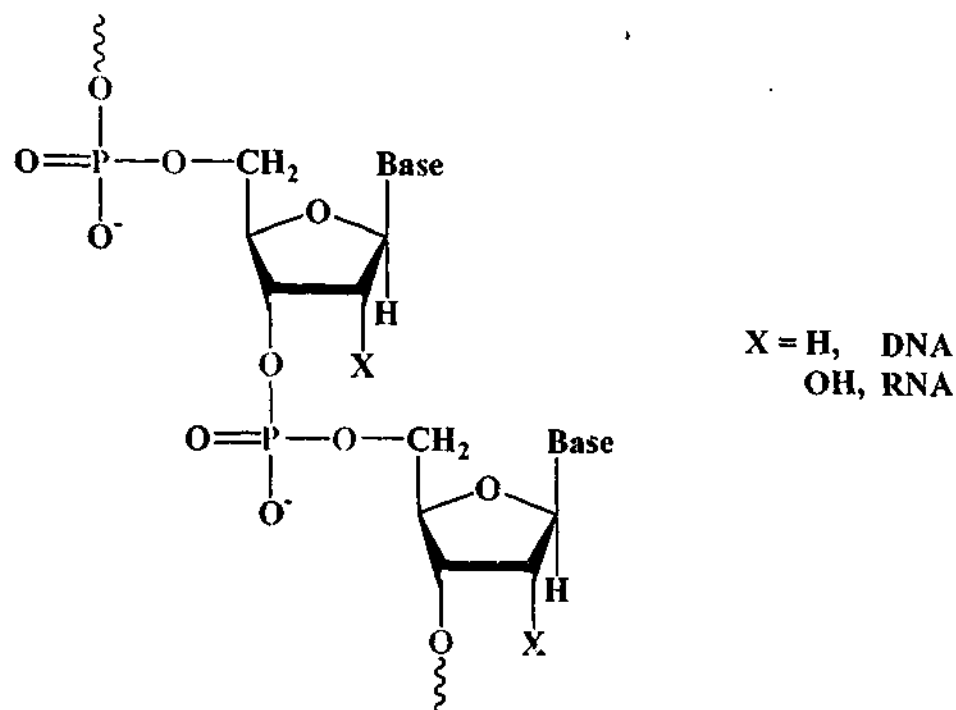
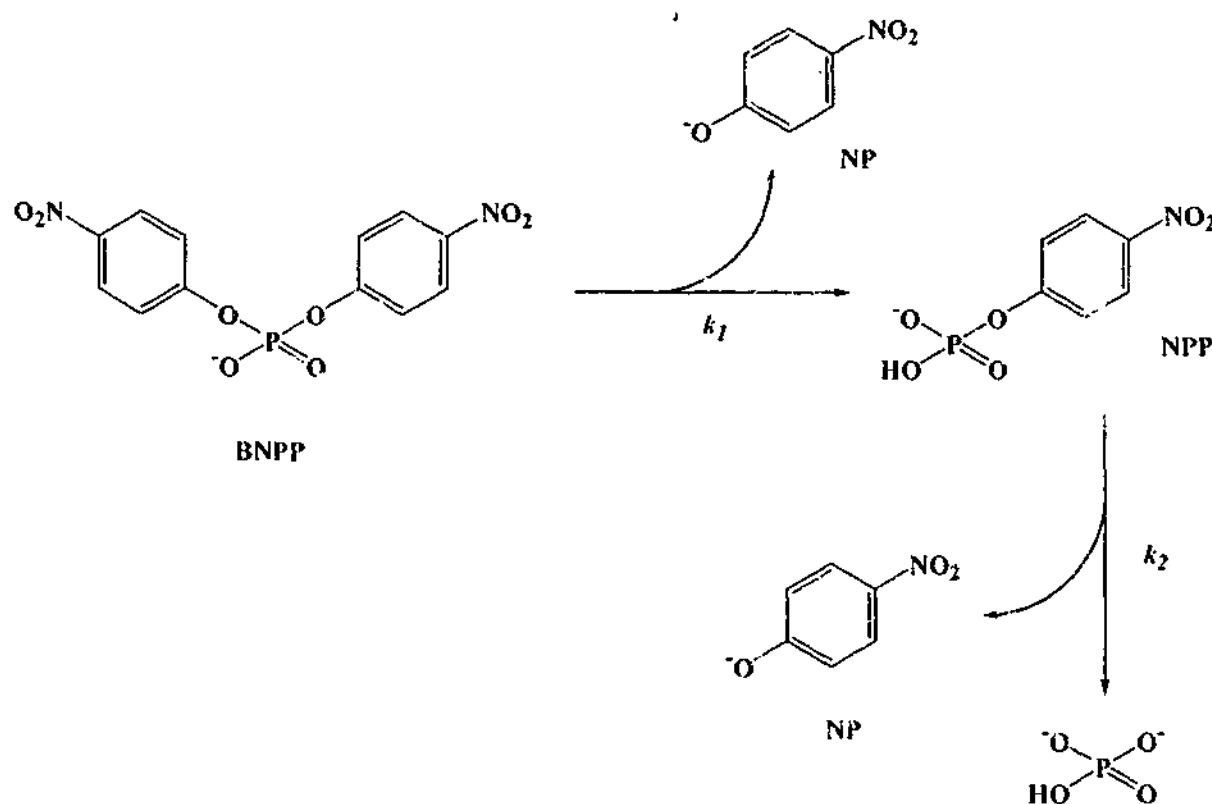


Figure 5.1 Schematic diagram of DNA/RNA, showing phosphodiester bonds

The phosphate ester bond is extremely resistant to hydrolysis. For example, the half-life for the cleavage P-O-R bonds in DNA is estimated to be approximately 130 000 years at neutral pH and 25°C,^{7,18} while that for RNA is around 4 years under identical conditions. The faster rate of RNA cleavage can be attributed to the presence of the 2'-hydroxyl group on the ribose ring.⁷

The small molecule bis(4-nitrophenyl) phosphate (BNPP) is a phosphodiester that has been commonly used in hydrolytic studies, and is the focus of the current work. Other examples of phosphodiester applied in hydrolytic studies include ethyl (4-nitrophenyl) phosphate (ENPP), and 2-hydroxypropyl 4-nitrophenyl phosphate (HPNP). For each of these esters hydrolysis can be conveniently monitored by the release of 4-nitrophenolate (NP), a chromophore which absorbs at 400 nm (Scheme 5.1). These are useful models for phosphate esters found in nature as their hydrolysis leads to the easily detected NP.



Scheme 5.1 The Hydrolysis of BNPP

A variety of complexes and their ability to hydrolyse phosphate esters have been previously discussed in Chapter 1 (section 1.5). Burstyn and Deal¹⁹ have compared the rate constants of the hydrolysis of phosphate esters of several complexes with their own well studied [Cu(tacn)Cl₂] system. The comparisons used pH vs. rate profiles data from the original source to calculate approximate rate constants at pH 7.2. The data are listed in Table 5.1.

Table 5.1 Calculated rate constants for the hydrolysis of phosphate esters by various complexes and comparison with [Cu(tacn)Cl₂], as presented by Burstyn and coworkers.⁷

Nucleophile ^{†‡}	Substrate [†]	<i>k</i> (pH 7.2)	T (°C)	Original Ref.
OH ⁻	BNPP	$4 \times 10^{-7} \text{ s}^{-1}$	100	20
[(tacn)Cu-OH] ⁺	BNPP	$9 \times 10^{-4} \text{ s}^{-1}$	100	19
[(bpy)Cu-OH] ⁺	ENPP	$1 \times 10^{-2} \text{ M}^{-1} \text{ s}^{-1}$	75	21
[(tacn)Cu-OH] ⁺	BNPP	$5 \times 10^{-2} \text{ M}^{-1} \text{ s}^{-1}$	75	19
[(en) ₂ Co-OH] ²⁺	BNPP	$3 \times 10^{-5} \text{ s}^{-1}$	50	22
[(tacn)Cu-OH] ⁺	BNPP	$9 \times 10^{-6} \text{ s}^{-1}$	50	19
[[12]Zn-OH] ⁺	BNPP	$6 \times 10^{-5} \text{ M}^{-1} \text{ s}^{-1}$	35	14
[(tacn)Cu-OH] ⁺	BNPP	$8 \times 10^{-4} \text{ M}^{-1} \text{ s}^{-1}$	35	19
[(en) ₂ Ir-OH] ²⁺	ENPP	$3 \times 10^{-5} \text{ s}^{-1}$	25	23
[(tacn)Cu-OH] ⁺	BNPP	$5 \times 10^{-7} \text{ s}^{-1}$	25	19

[†]Abbreviations: tacn = 1,4,7-triazacyclononane; [12] = 1,5,9-triazacyclodecane; bpy = 2,2'-bipyridine; en = ethylenediamine; BNPP = bis(4-nitrophenylphosphate); ENPP = ethyl 4-nitrophenylphosphate.

[‡]Additional water ligands on the metals have not been included.

Of the many studies of such complexes, some report simply the observed rate constant for a given set of conditions, while others report a more detailed study. A brief look at a select group of complexes is presented below. In the tables below (Tables 5.2 and 5.3), a similar comparison to that presented by Burstyn⁷ has been made of rate constants of other complexes appearing in the literature. Table 5.2 includes rate constants where a pH vs. rate profile has been included in the paper, while Table 5.3 lists rate constants under a given set of conditions.

Table 5.2 Comparison of second order rate constants of various complexes

Nucleophile [†]	Substrate	k (M ⁻¹ s ⁻¹)	pH	T (°C)	Ref.
[ZnL ¹ -O] ⁺	BNPP	3×10^{-4}	7.2	35	10
[Zn ₂ L ² (OH) ₂] ²⁺	BNPP	1.15×10^{-4}	10.5	35.1	24
[Zn ₂ L ³ (OH) ₂] ²⁺	BNPP	9.08×10^{-5}	10.9	35.1	25

[†]Abbreviations: L¹ = (S)-1-(2-hydroxy-2-phenylethyl)-1,4,7,10-tetraazacyclododecane; L² = [12]aneN₃; L³ = [12]andN₄;

Table 5.3 Comparison of observed rate constant of various complexes

Complex [†]	Substrate [†]	[Complex]	[Substrate]	pH	T (°C)	Rate (s ⁻¹)	Ref.
[Zn(tren)OH ₂] ²⁺	BNPP	1.0 mM	20 μM	8.5	50	5.5 × 10 ⁻⁷	26
[ZnL ¹ OH ₂] ²⁺	BNPP	1.0 mM	20 μM	8.5	50	1.8 × 10 ⁻⁶	26
[ZnL ² OH ₂] ²⁺	BNPP	1.0 mM	20 μM	8.5	50	1.0 × 10 ⁻⁵	26
[ZnFeL ³] ⁴⁺	HPNP	0.5 mM	0.82 mM	8.5	25	2.4 × 10 ⁻⁵	27
[EuL ⁴] ^{3+ a}	BNPP	5.0 mM	37.6 μM	7.0	50	3.1 × 10 ⁻⁴	28
[EuL ⁵] ^{3+ a}	BNPP	5.0 mM	37.6 μM	7.0	50	1.1 × 10 ⁻³	28
La(III)/Fe(III) ^b	BNPP	10 mM	Not given	7.0	50	2.8 × 10 ⁻⁴	29
[EuL ⁶] ³⁺	BNPP	0.4 mM	40 μM	8.5	50	1.5 × 10 ⁻³	30

[†]Abbreviations: tren = tris(2-aminoethyl)amine; L¹ = *N,N',N''*-tris(2-benzylaminoethyl)amine; L² = *N,N',N''*-tris(im-benzyl-L-histylethylaminoethyl)amine; L³ = 2,6-bis[*bis*(2-pyridylmethyl)amino]methyl-4-methoxyphenolate; L⁴ = *N*-(propylcarboxylic acid)benzoaza-15-crown-5 ether; L⁵ = *N*-(butylcarboxylic acid)benzoaza-15-crown-5 ether; L⁶ = 4,7,13,16,21-penta-oxo-1,10-diazabicyclo[8.8.5]tricosane

[†]HPNP = 2-hydroxypropyl 4-nitrophenyl phosphate.

^aComplex made *in situ* and additional ligands not specified.

^bNo multidentate ligand present, metals added as chlorides, each metal in a concentration of 10 mM; *cf.* La(III) alone, rate = 8.3 × 10⁻⁶ s⁻¹; Fe(III) alone, rate = 5.5 × 10⁻⁶ s⁻¹.

Many types of metal complexes have been studied for their ability to cleave phosphate esters. These include complexes which hydrolyse BNPP,^{31,32} RNA,³³⁻⁴⁰ DNA^{5,6,17,28,31,41-46} and diribonucleotides.⁴⁷⁻⁵¹ Studies of complexes which hydrolyse these biological molecules have included a variety of metal ions as well as the ligands which bind them. Metals from the transition series as well as from the lanthanide series, and some actinides⁵² have been used to study the hydrolysis of RNA and DNA. Zinc(II)^{31,39,53,54} and copper(II)^{5,6,31,35,36,41,54-57} are the most common transition metals to

be used in hydrolytic studies, however iron(III)⁴³ and others^{31,54,58,59} are also included.⁴³ Lanthanides and actinides used in these studies include La(III),^{33,36,38,54} Ce(III),⁵⁸ Eu(III),^{28,33,36,44} Lu(III)³⁶ and Th(IV).⁵²

These studies have led to the identification of the features of model compounds that contribute to faster phosphate ester cleavage rates. Two important features are that the metal centre must have a free coordination site for the coordination of the phosphate ester, and also a water ligand *cis* to the coordinated phosphate ester. On deprotonation, this water ligand forms a coordinated hydroxide, which then acts as a nucleophile in attacking the phosphate ester.²³

The focus of the present work was to test a variety of complexes, including those reported in Chapters 3 and 4, for their ability to enhance the rate of phosphate ester hydrolysis. Polynuclear complexes were chosen as it was anticipated that by increasing the number of metal centres, each with a free coordination site, would increase the rate of hydrolysis by having more sites available for the coordination of the substrate, BNPP. This chapter describes the screening of such complexes for their ability to hydrolyse BNPP, and since the $[\text{Cu}(\text{Me}_3\text{tacn})(\text{H}_2\text{O})_2]^{2+}$ complex was found to exhibit the fastest rate of BNPP cleavage, the remainder of the chapter therefore concentrates on a more detailed study and analysis of the kinetic behaviour of this complex.

5.2 Hydrolytic Studies: Preliminary Screening of Complexes

Complexes synthesised in the preceding two chapters (Chapter 3 and 4) were tested for their ability to hydrolyse the activated phosphate diester, bis(4-nitrophenyl)phosphate, (BNPP).

The initial reaction conditions consisted of a solution containing 1.7 mM of the complex, 0.15 mM of BNPP in 50 mM HEPES buffer at pH 7.4. The reactions were maintained at 50°C and were monitored for 8000 minutes, taking a single reading at 400 nm every 10 minutes. The data obtained from the initial screening experiments are shown in Figure 5.2.

The rates for the hydrolysis of BNPP were estimated from the plots by the initial rates method for all complexes with the exception of $[\text{Cu}(\text{Me}_3\text{tacn})(\text{H}_2\text{O})_2](\text{ClO}_4)_2$ and $[\text{Cu}_6(\text{T}_3\text{mes})_2(\mu\text{-OH})_6]^{6+}$. Such a fitting procedure has been used by other research groups to determine the initial rate.^{10,19,25,32,60} Fitting of the data for the remaining two complexes involved a double exponential fit, explained in detail later in Section 5.3.2. The plots show an increase in absorbance with time, the slope being indicative of the rate of hydrolysis of BNPP. The top plot in Figure 5.2 shows the absorbance traces for complexes tested in the study, without the traces for $[\text{Cu}(\text{Me}_3\text{tacn})(\text{H}_2\text{O})_2](\text{ClO}_4)_2$ and $[\text{Cu}_6(\text{T}_3\text{mes})_2(\mu\text{-OH})_6]^{6+}$ to show the relative rates more clearly. In the lower plot, inclusion the traces for $[\text{Cu}(\text{Me}_3\text{tacn})(\text{H}_2\text{O})_2](\text{ClO}_4)_2$ and $[\text{Cu}_6(\text{T}_3\text{mes})_2(\mu\text{-OH})_6]^{6+}$, clearly shows rate enhancements by these latter complexes are much greater than any other complex tested. This is borne out by the data presented in Table 5.4. As the complex $[\text{Cu}_6(\text{T}_3\text{mes})_2(\mu\text{-OH})_6]^{6+}$ has been shown to undergo dissociation to the trinuclear complex, $[\text{Cu}_3(\text{T}_3\text{mes})(\mu\text{-OH})_2(\text{H}_2\text{O})_2]^{4+}$ at pH 6-7, the complex will be predominantly in the latter form at the screening pH. Consequently, the concentration will be double that of the other complexes tested (see Scheme 5.2). Therefore, the complex $[\text{Cu}(\text{Me}_3\text{tacn})(\text{H}_2\text{O})_2](\text{ClO}_4)_2$ exhibits the fastest rate of cleavage of BNPP of all the complexes tested.

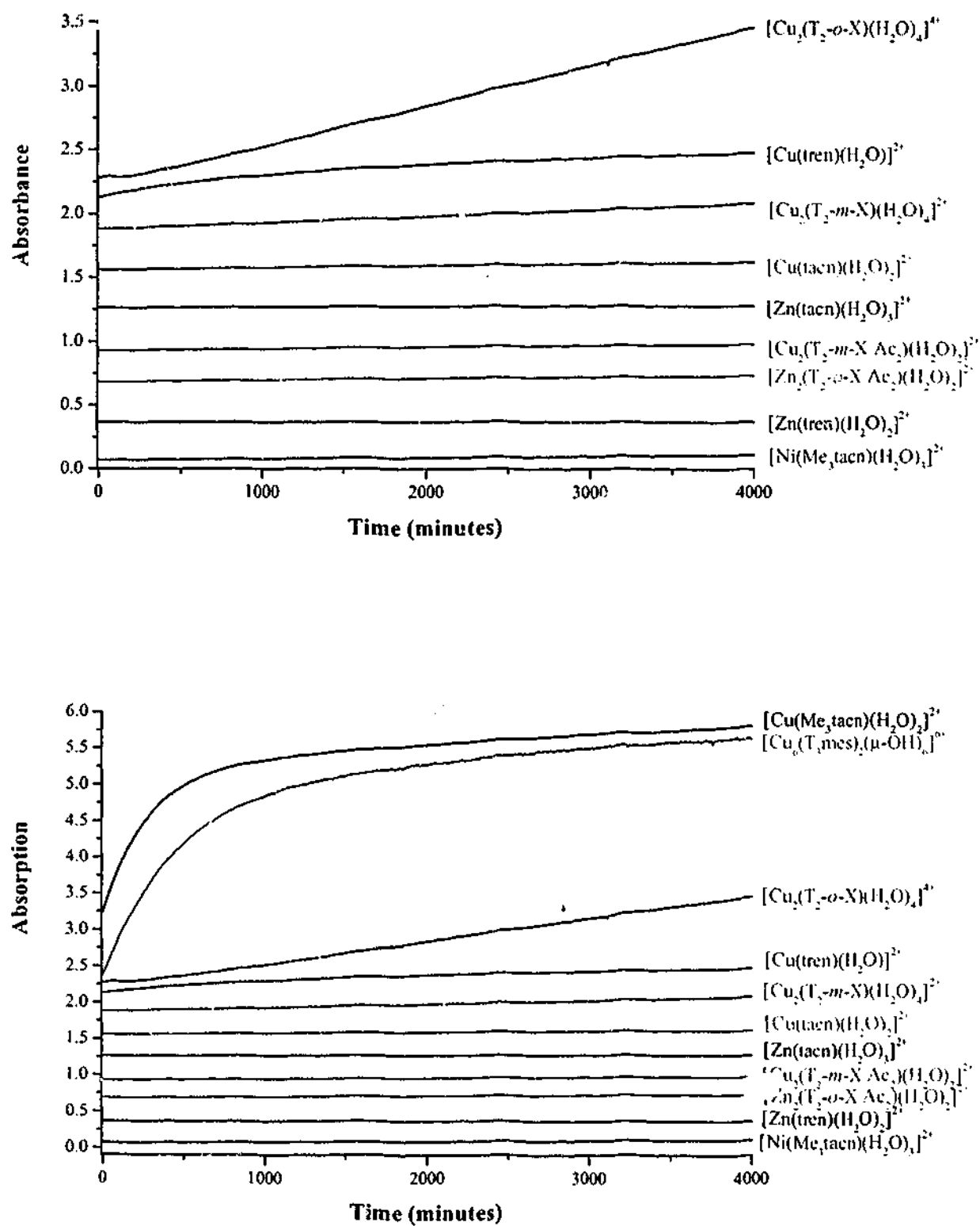


Figure 5.2 Absorbance vs. time plots for the catalysis of NNPP by various complexes.

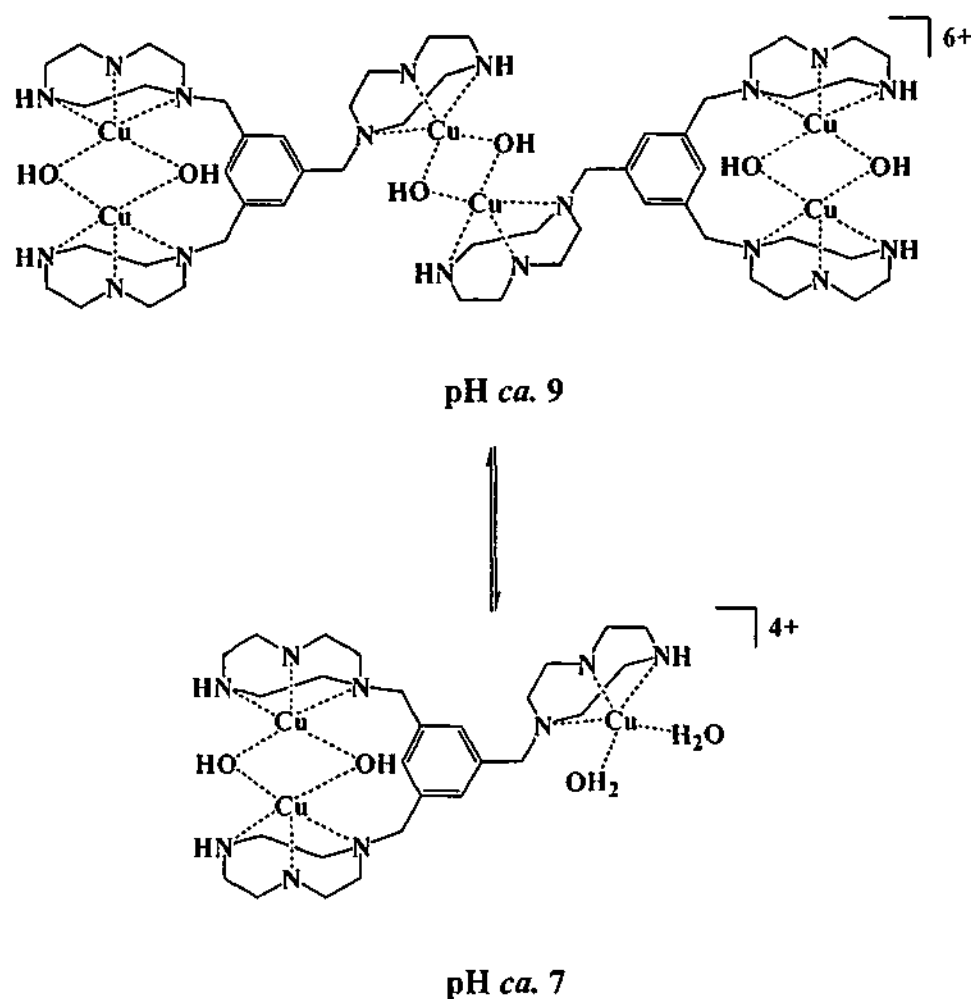
The top graph shows the rates without $[\text{Cu}(\text{Me}_3\text{tacn})(\text{H}_2\text{O})_2]^{2+}$ and $[\text{Cu}_6(\text{T}_3\text{mes})_2(\mu\text{-OH})_6]^{6+}$, while the bottom graph includes data for these complexes.

Table 5.4 Observed rate constants of various complexes tested.

pH 7.4; [BNPP]=0.15 mM; [Complex] = 1.7 mM; Temperature 50°C.

Note: the values left blank were too small to be measured

[Complex]	$10^7 \times k_{obs} (s^{-1})$
$[Cu(Me_3tacn)(H_2O)_2]^{2+}$	630
$[Cu_6(T_3mes)_2(\mu-OH)_6]^{6+}$	450
$[Cu_2(T_2-o-X)Cl_4] (1)$	52
$[Cu(tren)(H_2O)]^{2+}$	82
$[Cu_2(T_2-m-X)(H_2O)_4]^{4+} (2)$	8.6
$[Cu(tacn)(H_2O)_2]^{2+}$	2.5
$[Zn(tacn)(H_2O)_3]^{2+}$	-
$[Cu_2(T_2-m-X Ac_2)(H_2O)_2]^{2+} (6)$	2.1
$[Zn_2(T_2-o-X Ac_2)(H_2O)_2]^{2+} (16)$	2.7
$[Zn(tren)(H_2O)_2]^{2+}$	-
$[Ni(Me_3tacn)(H_2O)_3]^{2+}$	1.8



Scheme 5.2 pH dependent dissociation of $\text{Cu}_6(\text{T}_3\text{mes})_2(\mu\text{-OH})_6]^{6+}$ to
 $[\text{Cu}_3(\text{T}_3\text{mes})(\mu\text{-OH})_2(\text{H}_2\text{O})_2]^{4+}$ at pH 7.2

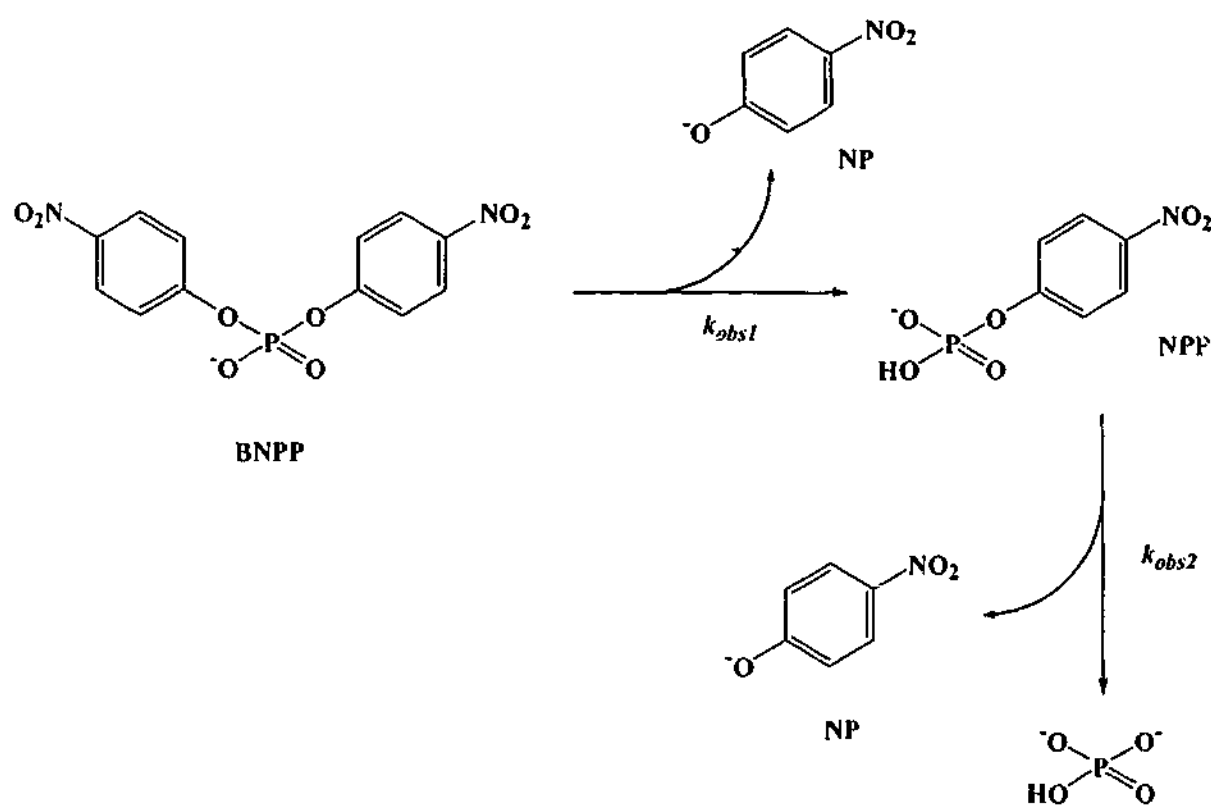
5.3 Kinetic Study of $[\text{Cu}(\text{Me}_3\text{tacn})(\text{H}_2\text{O})_2](\text{ClO}_4)_2$ (11)

As determined from the initial screening experiments, the rate of cleavage of BNPP by $[\text{Cu}(\text{Me}_3\text{tacn})(\text{H}_2\text{O})_2](\text{ClO}_4)_2$ is significantly faster than for any other complex tested in this study. Consequently, a detailed study of the reaction of BNPP with $[\text{Cu}(\text{Me}_3\text{tacn})(\text{H}_2\text{O})_2](\text{ClO}_4)_2$ was undertaken.

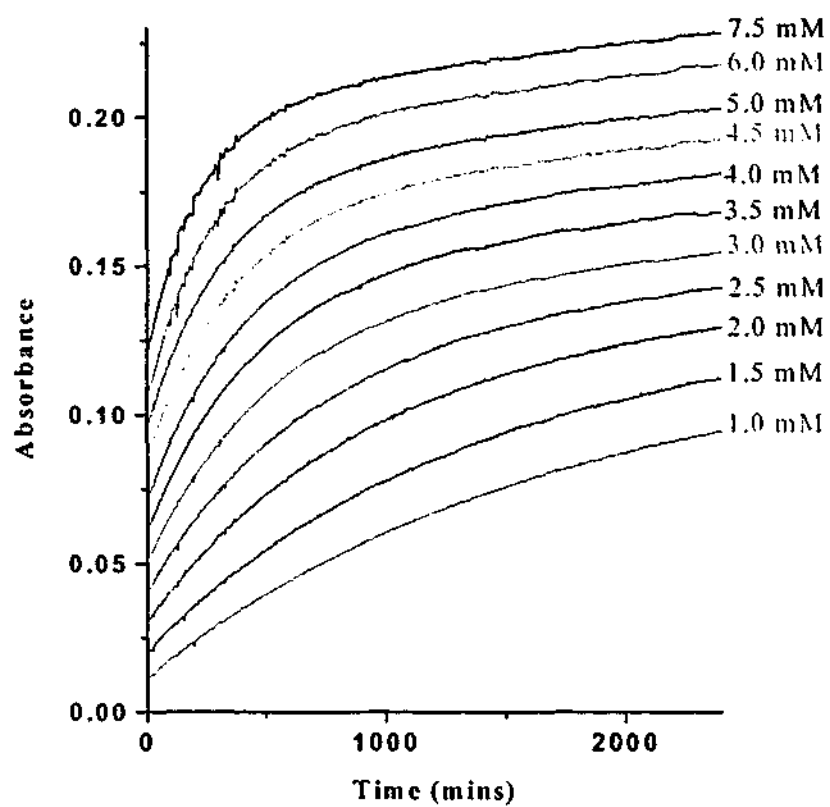
5.3.1 Reaction Conditions

Experiments were carried out with variation in temperature (42.5, 50.0, 57.5 and 65.0°C), complex concentration (1.0-7.5 mM), and pH (5.9-9.1). The pH of the

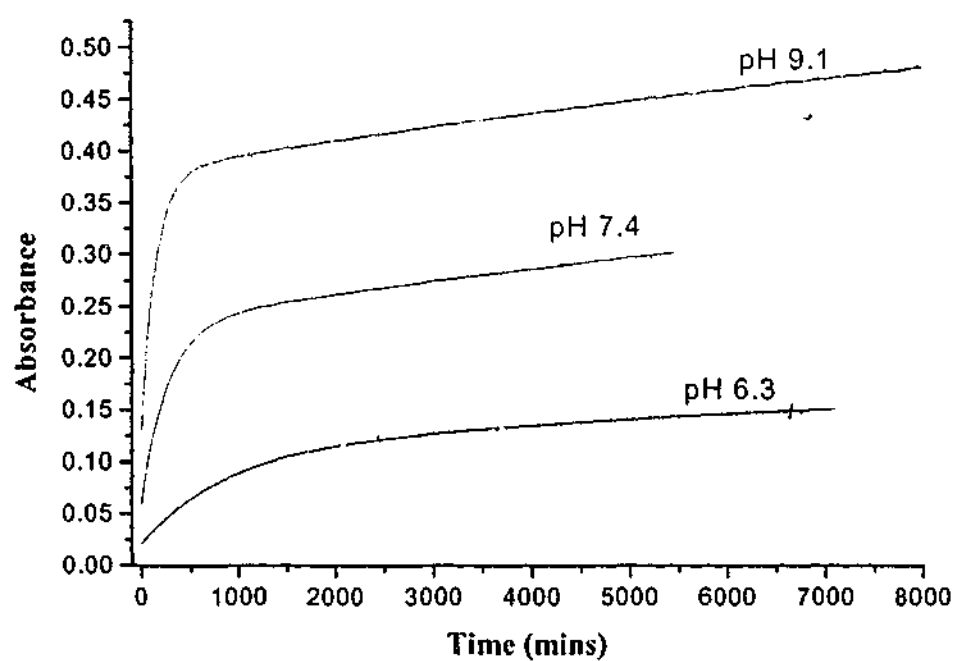
experiment was maintained through the use of buffers (MES 5.9, 6.3; MOPS 6.7, 7.0; HEPES 7.4, 7.8; TAPS 8.2, 8.4, 8.7; CHES 9.1). The concentration of BNPP was kept constant at 15 μM , hence the complex was in large excess relative to the substrate. The release of the 4-nitrophenylate anion was monitored at a single wavelength (400 nm) for period of up to 8000 minutes, depending on the rate of reaction. The resulting plots of absorbance versus time shows an increase in absorption with time, the slope of which shows a marked decrease after a time (Figure 5.3). The reactions of $[\text{Cu}(\text{Me}_3\text{tacn})(\text{H}_2\text{O})_2]^{2+}$ with BNPP were found to be biphasic in nature, due to the consecutive release of two 4-nitrophenylate (NP) ions from BNPP (Scheme 5.3 k_{obs1} and k_{obs2}).



Scheme 5.3 Release of 2 moles of 4-nitrophenyl phosphate (NP) and the corresponding observed rate constants, k_{obs1} and k_{obs2}



Conditions: pH 6.3, Temperature = 50°C; [BNPP] = 15 μ M



Conditions: Temperature 50°C; [Complex] = 2.0 mM; [BNPP] = 15 μ M

Figure 5.3 Typical plots of the absorbance increase over time due to the release of 4-nitrophenylate. Concentration dependence (top) and pH dependence (bottom).

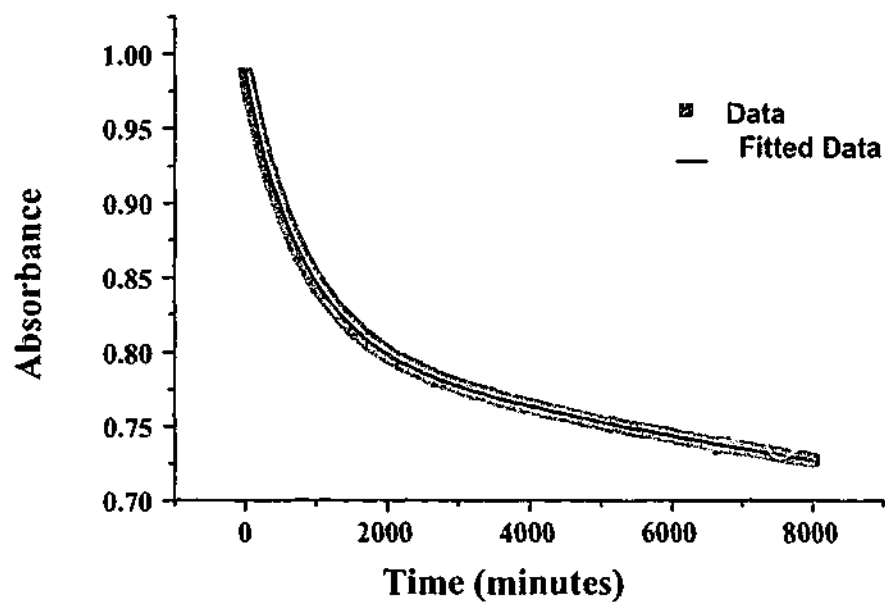
The release of the first NP ion is *ca.* 100 times faster than the rate of the second cleavage. Such differences in the rates for the release of the first and second NP has been observed in previous studies.^{2,61} As expected the rate of release also increased with increasing complex concentration and temperature.

5.3.2 Determination of the Observed Rate Constants

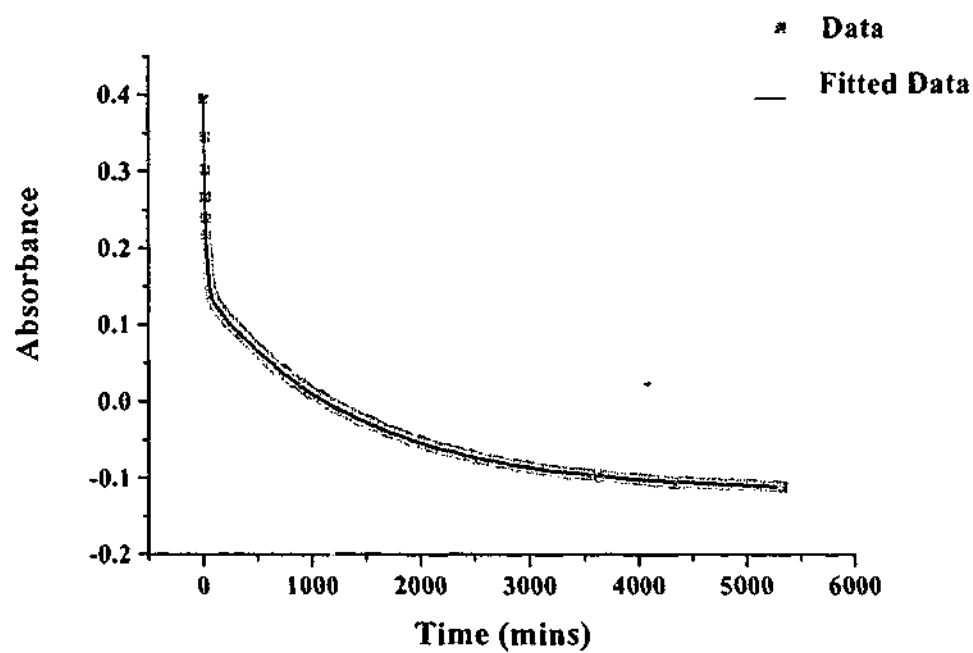
The treatment of the data required the fit of an equation to determine the observed rate constants for both reactions, *i.e.* the production of two mole equivalents of 4-nitrophenylate. As the complex was in a large excess relative to BNPP, the reaction is first order in terms of the substrate and therefore pseudo first-order kinetics can be applied. Each release of NP was treated as a first order process and the data was fitted to an exponential function.

The raw data was transposed and fitted to a double exponential equation (Equation 5.1) to determine k_{obs1} and k_{obs2} , where k_{obs1} = the rate of production of the first mole of 4-nitrophenylate and k_{obs2} = the rate of production of the second. Examples of the fit are shown in Figure 5.4 and the calculated rates are shown in Tables 5.5 and 5.6.

$$Abs = A + Be^{-k_{obs1}t} + Ce^{-k_{obs2}t} \quad \text{Eq. 5.1}$$



[Cu(II) complex] = 2 mM; Temperature = 50°C; [BNPP] = 15 μ M; pH 6.3



[Cu(II) complex] = 6.0 mM; Temperature = 65°C; [BNPP] = 15 μ M; pH 9.1

Figure 5.4 Examples of the fits of Equation 5.1 to experimental data, showing the fit of the equation to a fast hydrolysis (bottom) and a slower hydrolysis (top).

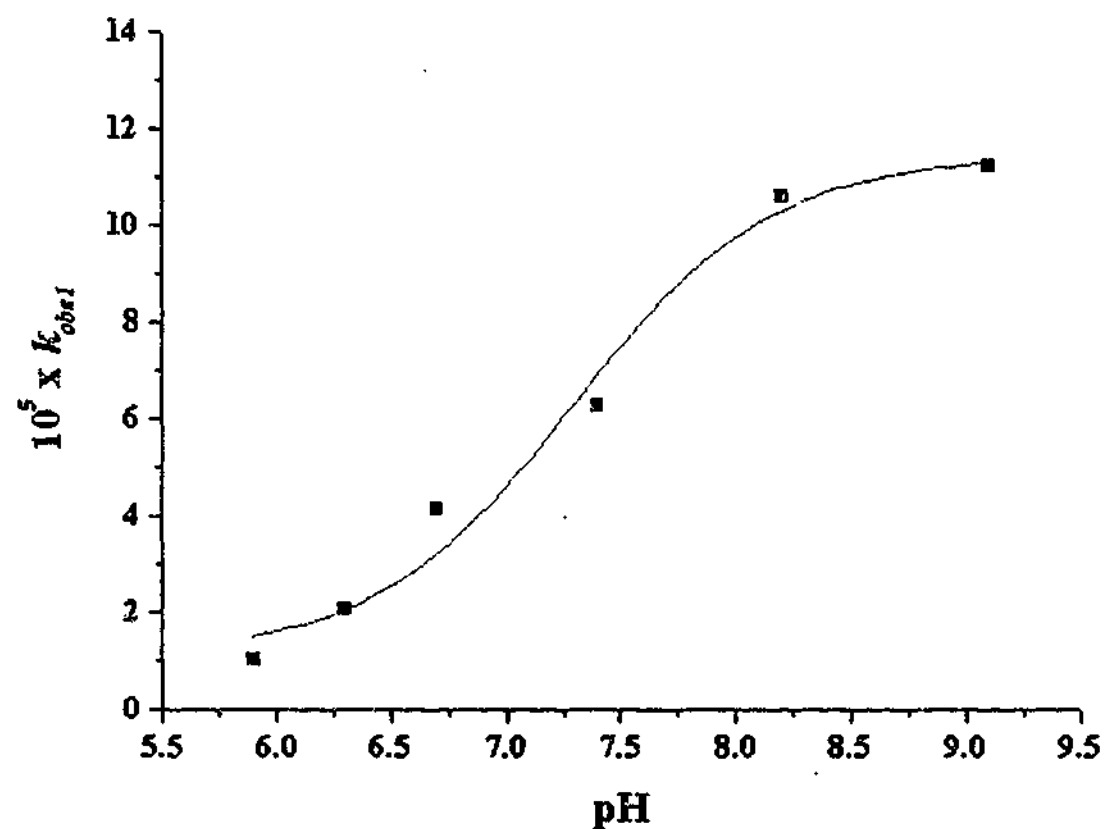
5.3.2 Release of the first 4-nitrophenylate anion, k_{obs1}

Presented below in Table 5.5 are the rate constants, k_{obs1} , as determined from Equation 5.1.

Table 5.5 Calculated values of $10^5 \times k_{obs1}$ (s^{-1}) at 50°C

	pH 5.9	pH 6.3	pH 6.7	pH 7.0	pH 7.4	pH 7.8	pH 8.2	pH 9.1
1.0mM	0.36±0.01	1.115±0.007	2.02±0.02		3.67±0.01		5.50±0.03	-
1.5mM	0.90±0.09	1.50±0.01	3.02±0.02		5.06±0.07		9.22±0.04	8.61±0.01
2.0mM	1.02±0.04	2.04±0.01	4.12±0.03		6.26±0.01		10.60±0.05	11.20±0.01
2.5mM	1.23±0.03	2.541±0.007	5.27±0.03		7.88±0.02		12.56±0.06	14.0±0.2
3.0mM	1.80±0.05	3.22±0.001	7.17±0.05		8.92±0.02	3.1±0.4		16.0±0.5
3.5mM	1.98±0.05	3.74±0.04	8.02±0.07		10.25±0.02	7.44±0.07		17.1±0.3
4.0mM	2.10±0.05	4.17±0.04	9.0±0.8		11.16±0.02	5.03±0.06		
4.5mM	2.45±0.05	4.70±0.04	8.85±0.07		12.55±0.05	10.1±0.1		
5.0mM	2.92±0.07	5.18±0.05	9.73±0.08	8.18±0.05	12.77±0.04	12.3±0.1		
6.0mM	3.32±0.05	6.61±0.08	10.77±0.03	10.41±0.07	15.17±0.07	15.9±0.2		
7.5mM	4.08±0.07	7.50±0.08	12.7±0.1	13.0±0.1	17.28±0.09	19.9±0.2		

From the calculated value of k_{obs1} , it is seen that the rate generally increases with pH, temperature and increasing [complex]. A rate-pH profile is shown in Figure 5.5 and shows the characteristic S-shaped curve, typical for a process involving a deprotonation.



Conditions: [Complex] = 2.0 mM; [BNPP] = 15 μ M; Temperature = 50°C

Figure 5.5 Rate-pH profile for k_{obs1}

5.3.3 Release of the second 4-nitrophenylate anion, k_{obs2}

Presented in the table below (Table 5.6) are the calculated rate constants for k_{obs2} as determined by fitting the absorbance data to Equation 5.1.

Table 5.6 Calculated values of $10^6 \times k_{obs2}$ (s^{-1}) at 50°C

	pH 5.9	pH 6.3	pH 6.7	pH 7.0	pH 7.4	pH 7.8	pH 9.1
1.0mM		0.2±0.1			0.21±0.09		0.42±0.03
1.5mM	2.2±0.5	1.82±0.07	0.09±0.06		1.18±0.02		0.83±0.01
2.0mM	0.77±0.4	1.92±0.08	0.67±0.05		1.57±0.02		1.10±0.06
2.5mM	0.76±0.4	2.01±0.03	1.33±0.04		1.89±0.03		1.30±0.01
3.0mM	2.3±0.2	2.19±0.05	1.67±0.04		1.93±0.03	1.1±0.8	1.71±0.01
3.5mM	0.9±.2	2.3±0.1	2.00±0.03		2.24±0.02	1.2±0.1	1.67±.01
4.0mM	2.2±0.2	2.70±0.08	2.17±0.04		2.50±0.01	1.1±0.5	
4.5mM	1.7±0.2	2.76±0.08	2.50±0.04		2.44±0.02	1.4±0.3	
5.0mM	2.1±0.2	2.83±0.07	2.50±0.03	1.46±0.07	2.84±0.02	1.3±0.2	
6.0mM	1.7±0.1	5.71±0.09	2.67±0.03	1.81±0.07	2.51±0.02	2.0±0.2	
7.5mM	2.0±0.1	3.24±0.07	3.00±0.03	2.59±0.07	3.71±0.02	2.5±0.1	

Interestingly, the values for k_{obs2} do not show a clear dependence on pH. To fully confirm this observation, the reactions would need to be monitored for a longer period of time, or a more detailed study of the hydrolysis of the monoester, 4-nitrophenyl phosphate, NPP, by $[Cu(Me_3tacn)(H_2O)_2]^{2+}$ would need to be undertaken. As the current work is focussed on the hydrolysis of phosphate diesters, the analysis of the hydrolysis of NPP was not pursued further. Consequently, the current analysis is limited to the release of the first NP from BNPP.

5.3.4 Determination of the Equilibrium Constants, K_a and K_{dim}

In order to analyse the kinetic data successfully, the determination of the acid dissociation constant for the Cu(II) complex and the constant for dimerisation of the monodeprotonated form, $[\text{Cu}(\text{Me}_3\text{tacn})(\text{H}_2\text{O})(\text{OH})]^+$ to $[(\text{Me}_3\text{tacn})\text{Cu}(\mu\text{-OH})_2\text{Cu}(\text{Me}_3\text{tacn})]^{2+}$ was undertaken. The dihydroxo bridged binuclear complex, previously structurally characterised by Chaudhuri *et al.* in 1985,⁶² was found to crystallise in some of the solutions used in kinetic analysis, particularly at high concentrations of $[\text{Cu}(\text{Me}_3\text{tacn})(\text{H}_2\text{O})_2]^{2+}$ and at high pH. Consequently, a thermodynamic study of this system was conducted by UV-Visible spectrophotometry pH titrations. The spectra of $[\text{Cu}(\text{Me}_3\text{tacn})(\text{H}_2\text{O})_2](\text{ClO}_4)_2$ were recorded at varying concentrations (1.0 – 7.5 mM), temperatures (42.5 – 65°C) and pH values (pH 5.9, 7.0 and 9.1). As the pH was increased from 5.9 to 9.1, a blue shift in the absorbance maxima of the copper(II) *d-d* transition, as well as an increase in the molar extinction coefficient was observed (Figure 5.6). As [complex] increased, so did the absorption of the solution (Figure 5.7).

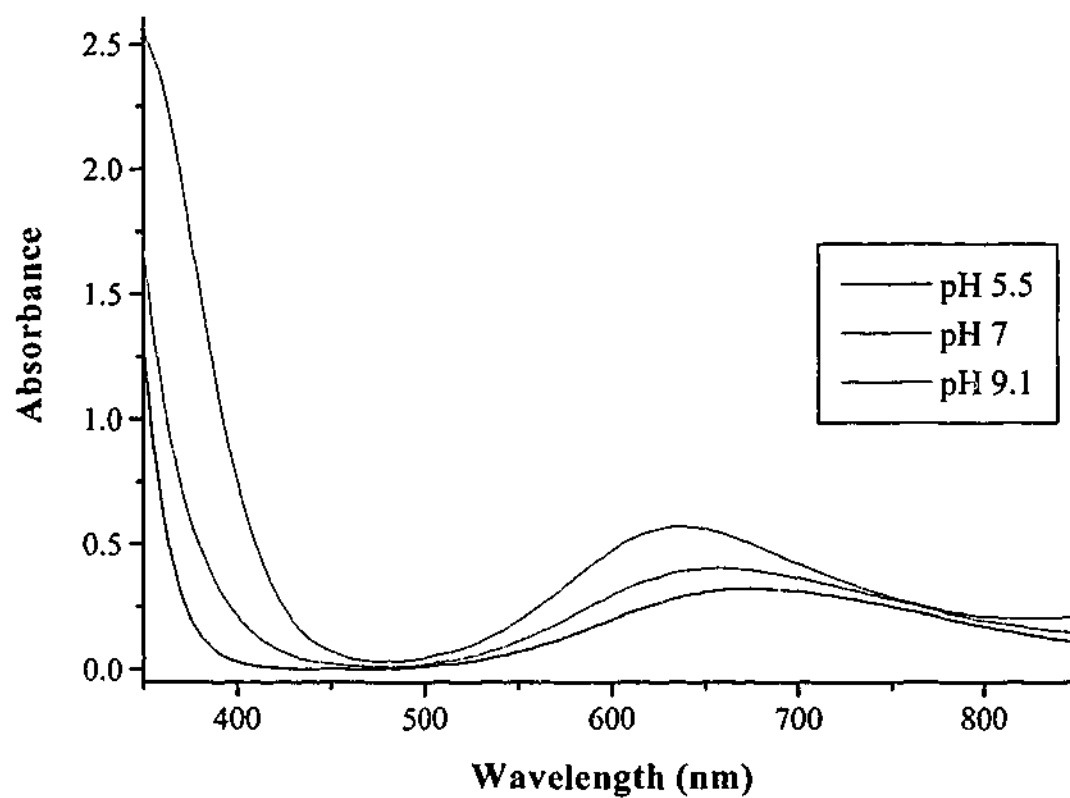


Figure 5.6 Spectra of $[\text{Cu}(\text{Me}_3\text{tacn})(\text{H}_2\text{O})_2](\text{ClO}_4)_2$ at Temperature 50°C and $[\text{Complex}] = 7.5 \text{ mM}$

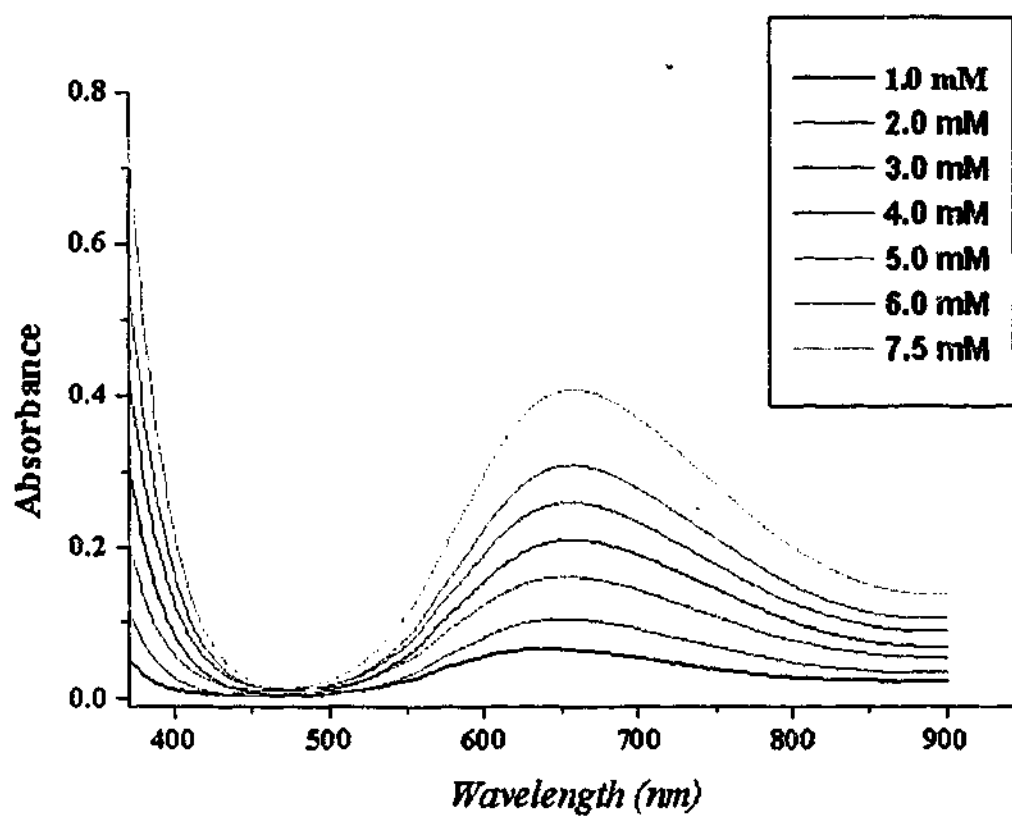
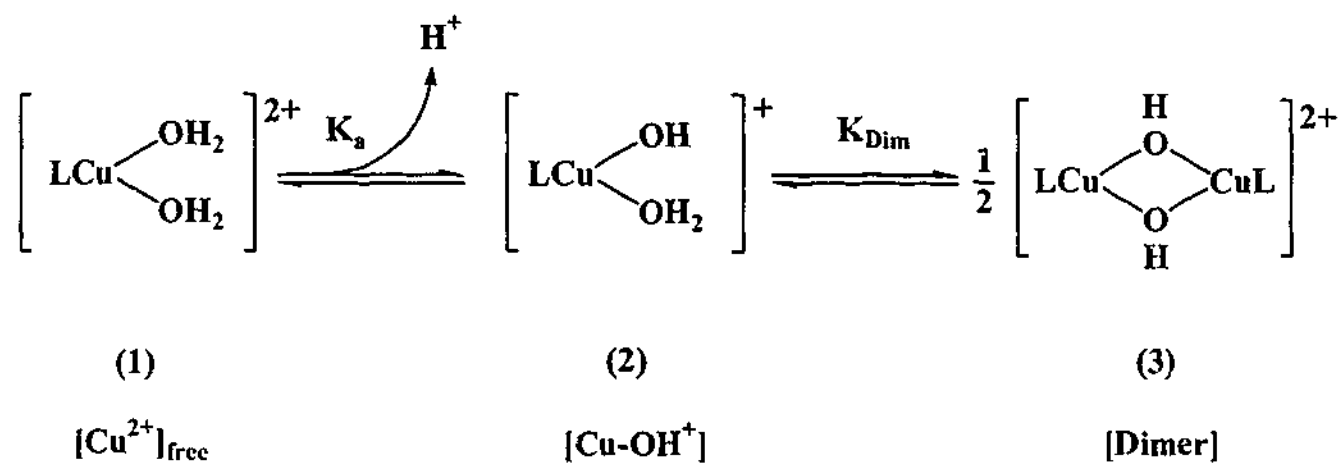


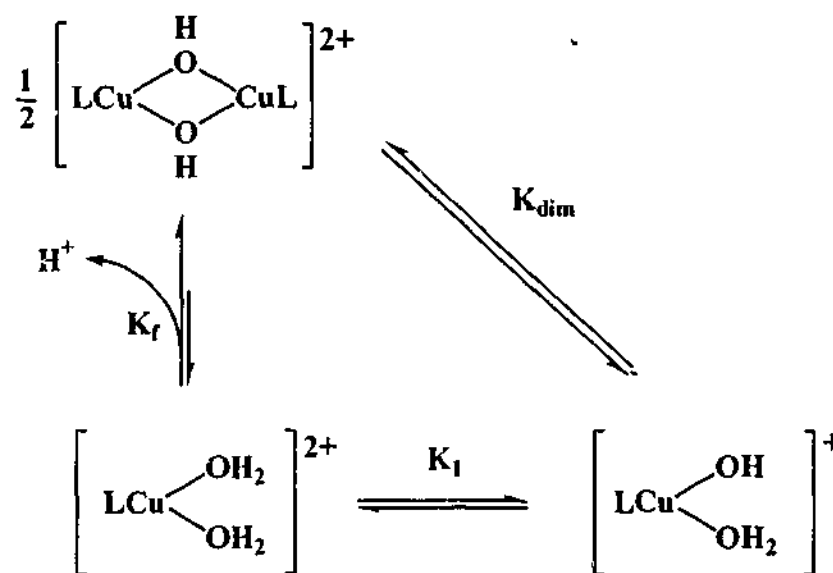
Figure 5.7 Spectra of $[\text{Cu}(\text{Me}_3\text{tacn})(\text{H}_2\text{O})_2]^{2+}$ at Temperature 50°C and $\text{pH } 7.0$

The pH and [complex] dependence of the spectra and the postulation that the hydroxo bridged binuclear complex forms at high pH and [complex] are consistent with the reaction sequence shown in Scheme 5.4.



Scheme 5.4 pH dependent solution equilibrium of $[\text{Cu}(\text{Me}_3\text{tacn})(\text{H}_2\text{O})_2]^{2+}$ (11)

An equivalent scheme has been proposed by Burstyn and coworkers^{8,19} for the dimerisation of $[\text{Cu}(\text{tacn})(\text{H}_2\text{O})_2]^{2+}$ (Scheme 5.5).



Scheme 5.5 Reaction pathway for dimer formation from the diaqua Cu-tacn complex^{8,19}

The variable temperature, [complex] and pH spectrophotometric data were used in the determination of the equilibrium constants for the formation of the species $[(\text{Me}_3\text{tacn})\text{Cu}(\text{H}_2\text{O})(\text{OH})]^+$ (Scheme 5.4 (Complex 2)) and $[(\text{Me}_3\text{tacn})\text{Cu}(\mu\text{-OH})_2\text{Cu}(\text{Me}_3\text{tacn})]^{2+}$ (Scheme 5.4 (Complex 3)). It was anticipated that this analysis would facilitate the interpretation of the kinetic data. The analysis was carried out with the assistance of Dr Joël Brugger from The South Australian Museum and Department of Geology and Geophysics, University of Adelaide.

Principal Component Analysis

The initial step in the analysis was to determine the number of species that contribute to the absorption spectra. Principal component analysis (PCA) was used to determine the number of mathematical factors required to describe the experimental spectra.⁶³ The residuals (R) are calculated according to Equation 5.2, so that the number of species is above the minimum percentage experimental error.

$$R=100\sqrt{\frac{\sum(x_i-x)^2}{\sum x_i^2}} \quad \text{Eq. 5.2}$$

where x_i and x are the measured and the calculated absorbance values, respectively.

The PCA of this system indicates that three species are required to describe the measured spectra to within experimental uncertainty, confirming the model depicted in Scheme 5.4.

The spectra were modelled using a method of non-linear least squares regression.⁶³ A detailed explanation of the principles involved is given in a paper by Brugger *et al.*,⁶⁴ and hence only a brief explanation of the background principles involved for the interpretation of the spectra is presented here. The Beer-Lambert law states that the absorbance of a solution, S , at a wavelength, λ , is a function of the pathlength, l_{path} , the molar concentrations, M , of each absorbing species, n , in the solution and their molar absorptivity coefficients, ϵ , at wavelength, λ , so the familiar equation:

$$A = \epsilon cl$$

becomes:

$$A_{\lambda}^S = l_{\text{path}} \sum_{n=1}^{\text{NAS}} M_n^S \epsilon_{n,\lambda} \quad \text{Eq. 5.3}$$

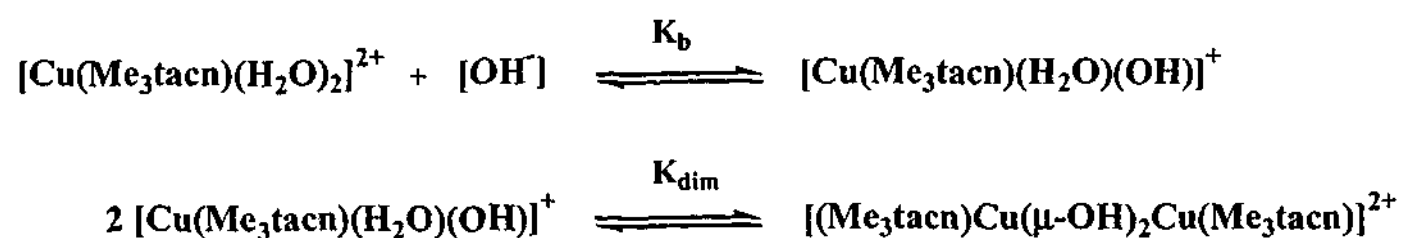
where NAS is the total number of absorbing species. The spectra of solutions of $[\text{Cu}(\text{Me}_3\text{tacn})(\text{H}_2\text{O})_2]^{2+}$ were measured at different concentrations under similar conditions, *i.e.* at constant pH and temperature. The resulting spectra can be put into a matrix \tilde{A} of total absorbances, where each column represents a different wavelength and the rows correspond to the different complex concentrations. Equation 5.3 can be written in the matrix form:

$$\tilde{A} = \mathbf{C} \times \mathbf{E} \quad \text{Eq. 5.4}$$

Where \mathbf{C} (number of solutions \times NAS) is the matrix of concentrations of the absorbing species and \mathbf{E} (NAS \times number of samples wavelengths) is the matrix of molar absorptivity coefficients. The aim of the analysis is to determine the concentration and

the molar absorptivity of each of the species in solution (1-3 Scheme 5.4), *i.e.* to find the matrices **C** and **E** that best reproduce the experimental data and produce the best fit between the measured and calculated spectra.

The data was fitted to the species model as shown in Scheme 5.6.



Scheme 5.6 Model for the determination of equilibrium constants

The calculation and optimisation of the formation constants (K_b and K_{dim}) and the matrix **E** includes two optimisation algorithms performed in an outer and inner programming loop. Inside the inner loop, the distribution of the three species was calculated for a given set of log K values, and the molar absorptivity for each species was optimised using a quadratic programming method.⁶⁵ In the outer loop of the program, the log K values varied using a simplex type algorithm⁶⁶ to reduce the residual function to a minimum. The residual function used in the calculations is the sum of the squares of the differences between measured and calculated values.

An example of the fit of the calculated spectra to the experimental data is shown in Figure 5.8, and an example of calculated spectra for the three species is shown in Figure 5.9.

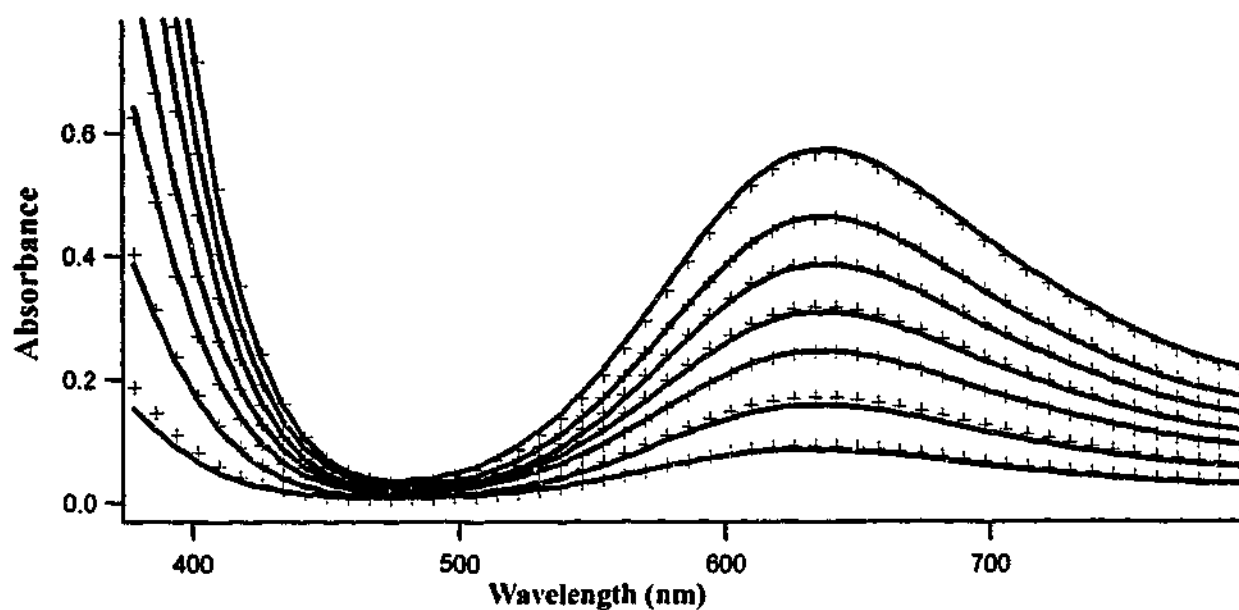


Figure 5.8 Electronic spectra of $[\text{Cu}(\text{Me}_3\text{tacn})(\text{H}_2\text{O})_2]^{2+}$ (lines) and the calculated data (crosses) at 65°C and $\text{pH } 9.1$

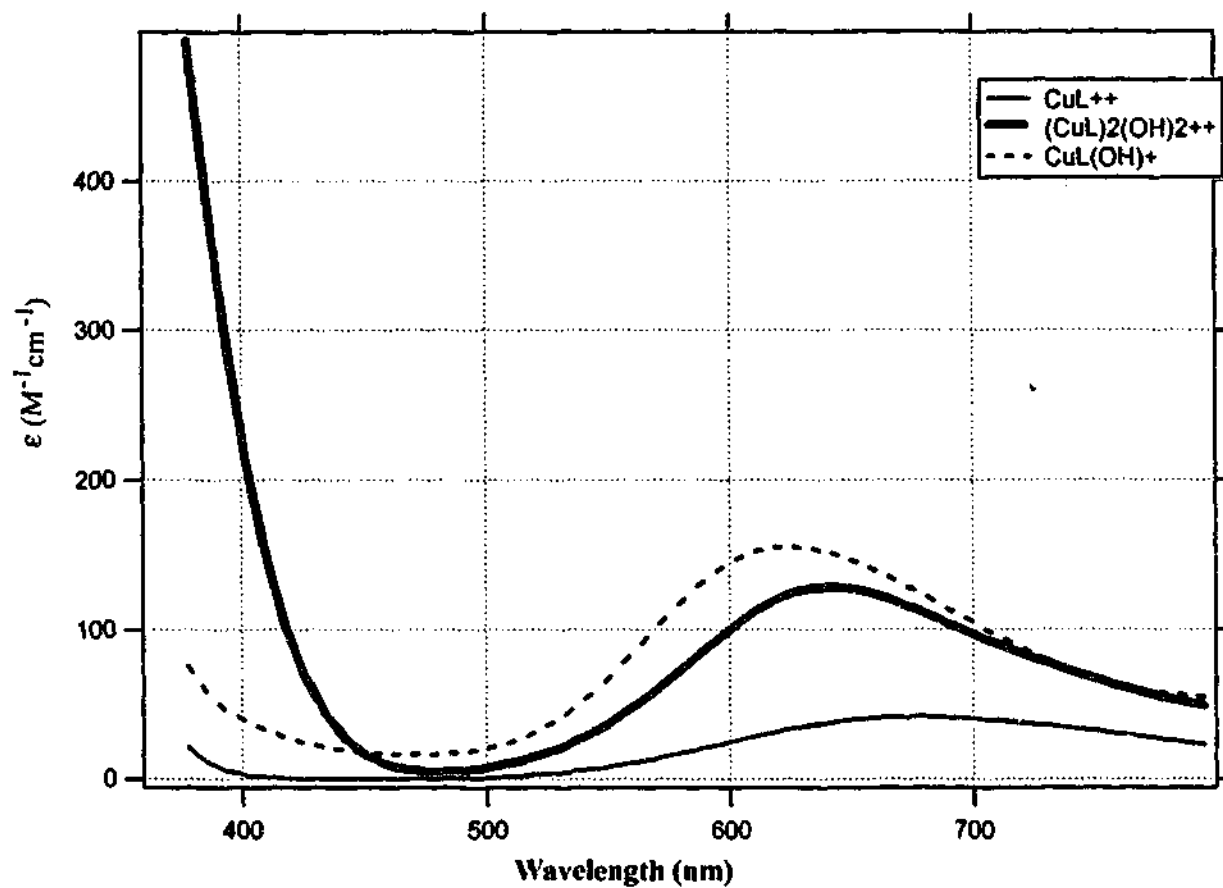


Figure 5.9 Calculated electronic spectra for the three species absorbing in solution (Temperature 50°C)

The formation constants K_a (derived from K_b using K_w) and K_{dim} are shown in Table 5.7.

Table 5.7 Equilibrium constants derived from modelling of absorbance spectra of $[\text{Cu}(\text{Me}_3\text{tacn})(\text{H}_2\text{O})_2](\text{ClO}_4)_2$

T (°C)	K_b (M)	K_a (M)	p K_a	K_{dim} (M ⁻¹)
42.5	5.13×10^{-6}	6.67×10^{-9}	8.18	20900
50.0	2.63×10^{-6}	2.07×10^{-8}	7.69	2630
57.5	1.32×10^{-6}	6.33×10^{-8}	7.20	251
65	1.00×10^{-6}	1.24×10^{-7}	6.91	50

K_w calculated at different temperatures using: $\log K_w = -\frac{4470.99}{T} + 6.0875 - 0.01716T$ ⁶⁷

5.3.5 Determination of Second Order Rate Constants

The analysis of the kinetic data was used to establish the species that are active in phosphate ester cleavage. The intention was that this analysis would be aided by the determined equilibrium constants, K_a and K_{dim} as these parameters allow the concentration of each form of the complex to be determined under each of the reaction conditions (pH, concentration and temperature), however, it will emerge later that a better fitting of the data was possible by allowing the parameters to float rather than be fixed at values determined by equilibrium measurements.

The mass balance equation for copper(II) is determined as follows, taking into account each of the species that the copper(II) complex forms in solution in the absence of the phosphate ester (see Scheme 5.4, page 255):

$$[Cu]_{total} = [Cu^{2+}]_{free} + [Cu - OH^+] + 2[Dimer] \quad \text{Eq. 5.5}$$

where $[Cu]_{total}$ is the concentration of copper complex put into the system; $[Cu^{2+}]_{free}$ is the diaquo species, $[Cu(Me_3tacn)(H_2O)_2]^{2+}$, $[Cu - OH^+]$ is the hydroxo-aquo species, $[Cu(Me_3tacn)(H_2O)(OH)]^+$, and $[Dimer]$ is $[(Me_3tacn)Cu(\mu-OH)_2Cu(Me_3tacn)]^{2+}$.

From Scheme 5.4 the equilibrium equations are written as:

$$K_a = \frac{[Cu - OH^+][H^+]}{[Cu^{2+}]_{free}} \quad \text{Eq. 5.6}$$

and

$$K_{dim} = \frac{[Dimer]}{[Cu - OH^+]^2} \quad \text{Eq. 5.7}$$

Equations 5.6 and 5.7 can be rearranged to the forms:

$$[Cu - OH^+] = K_a \frac{[Cu^{2+}]_{free}}{[H^+]} \quad \text{Eq. 5.8}$$

$$[Dimer] = K_{dim} [Cu - OH^+]^2 \quad \text{Eq. 5.9}$$

Substituting Equation 5.8 into Equation 5.9, the following equation for the concentration of the dimer species is derived:

$$[Dimer] = \frac{K_{dim} K_a^2 [Cu^{2+}]_{free}^2}{[H^+]^2} \quad \text{Eq. 5.10}$$

Substituting Equations 5.8 and 5.9 into Equation 5.5 gives:

$$[Cu]_{total} = [Cu^{2+}]_{free} + \frac{K_a [Cu^{2+}]_{free}}{[H^+]} + \frac{2K_{dim} K_a^2 [Cu^{2+}]_{free}^2}{[H^+]^2}$$

followed by rearrangement to:

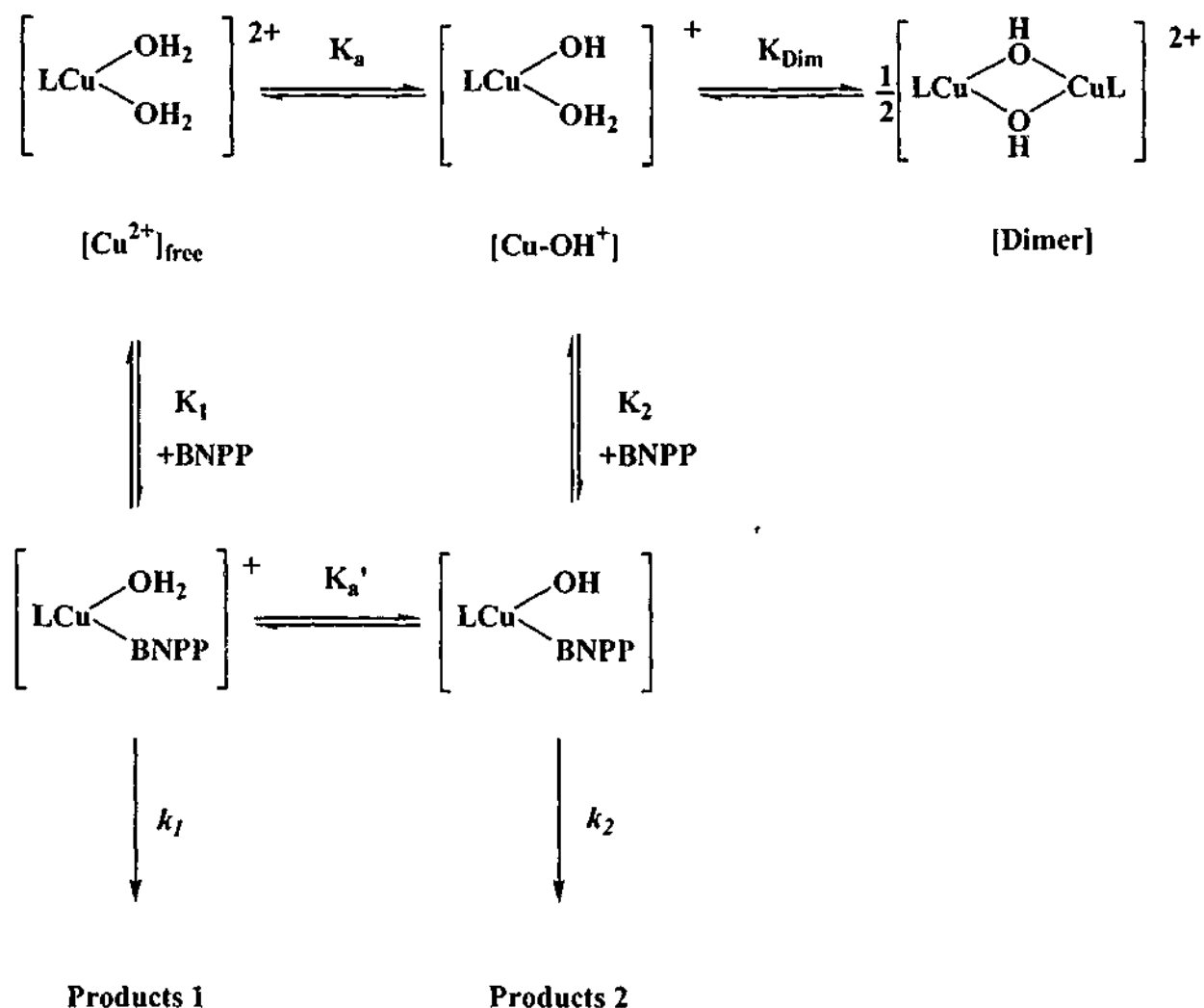
$$0 = [Cu^{2+}]_{free} \left(1 + \frac{K_a}{[H^+]} \right) + \frac{2K_{dim} K_a^2 [Cu^{2+}]_{free}^2}{[H^+]^2} - [Cu^{2+}]_{total}$$

This can be factorised to produce the equation in terms of $[Cu^{2+}]_{free}$:

$$[Cu^{2+}]_{free} = \frac{-\left(1 + \frac{K_a}{[H^+]}\right) + \sqrt{\left(1 + \frac{K_a}{[H^+]}\right)^2 + \frac{8K_{dim} K_a^2 [Cu]_{total}}{[H^+]^2}}}{\frac{4K_{dim} K_a^2}{[H^+]^2}} \quad \text{Eq. 5.11}$$

From Equation 5.11, the amount of $[Cu^{2+}]_{free}$ can be calculated at any $[H^+]$ and any $[Cu]_{total}$.

As seen from Scheme 5.4 (page 255), three species are available for binding of the phosphate and subsequent hydrolysis of BNPP, $[\text{Cu}(\text{Me}_3\text{tacn})(\text{H}_2\text{O})_2]^{2+}$, $[\text{Cu}(\text{Me}_3\text{tacn})(\text{H}_2\text{O})(\text{OH})]^+$ and $[(\text{Me}_3\text{tacn})\text{Cu}(\mu\text{-OH})\text{Cu}(\text{Me}_3\text{tacn})]^{2+}$. In the analysis of the kinetic data, we have assumed the dimer does not participate in the reaction. This assumption (see below) is in keeping with conclusions reached from the study of the tacn system.⁸ Scheme 5.7 proposes a mechanism for the equilibrium between the copper species and BNPP, followed by hydrolysis of BNPP.



Scheme 5.7 Schematic for the species in solution prior to the hydrolysis of BNPP

The dimer complex, [Dimer], has not been included in the rate calculations as it is presumed to be inactive in the hydrolysis of BNPP. This conclusion is based on previous studies¹⁹ as well as the requirement that there must be a free site for the coordination of the substrate, BNPP. A further stipulation for hydrolysis to occur is to have a water ligand *cis* to the coordinated phosphate ester for the generation of a nucleophile to attack the phosphorus centre. As is obvious from Scheme 5.7, the dimeric complex possesses neither of these important features.

From Scheme 5.7, the equilibrium constants are written as follows:

$$K_1 = \frac{[Cu^{2+}_{free} - BNPP]}{[Cu^{2+}]_{free}[BNPP]}$$

or

$$[Cu^{2+}_{free} - BNPP] = K_1[Cu^{2+}]_{free}[BNPP] \quad \text{Eq. 5.12}$$

and

$$K_2 = \frac{[Cu - OH - BNPP]}{[Cu - OH^+][BNPP]}$$

or

$$[Cu - OH - BNPP] = K_2[Cu - OH^+][BNPP] \quad \text{Eq. 5.13}$$

The expressions for each of the rate equations are:

$$\frac{d[\text{Products}]}{dt} = k_1[Cu^{2+}_{free} - BNPP] + k_2[Cu - OH - BNPP] \quad \text{Eq. 5.14}$$

Substituting Equation 5.12 and Equation 5.13 into Equation 5.14 yields Equation 5.15:

$$\frac{d[\text{Products}]}{dt} = k_1 K_1 [\text{Cu}^{2+}]_{\text{free}} [\text{BNPP}] + k_2 K_2 [\text{Cu-OH}^+] [\text{BNPP}] \quad \text{Eq. 5.15}$$

or

$$\frac{d[\text{Products}]}{dt} = (k_1 K_1 [\text{Cu}^{2+}]_{\text{free}} + k_2 K_2 [\text{Cu-OH}^+]) [\text{BNPP}]$$

Since the reaction is followed under pseudo first order conditions, and the concentration of BNPP is *ca.* 100 times less than $[\text{Cu}]_{\text{tot}}$, this reagent is consumed in the reaction and the $[\text{Cu}]_{\text{tot}}$ is essentially constant during the reaction.

$$\frac{d[\text{Products}]}{dt} = k_{\text{obs}} [\text{BNPP}]$$

Consequently, the expression for k_{obs} becomes:

$$k_{\text{obs}} = k_1 K_1 [\text{Cu}^{2+}]_{\text{free}} + k_2 K_2 [\text{Cu-OH}^+] \quad \text{Eq. 5.16}$$

Rearrangement of Equation 5.8 (page 261) into terms of $[\text{Cu}^{2+}]_{\text{free}}$ and then substitution into Equation 5.16 gives:

$$k_{\text{obs}} = k_1 K_1 \frac{[\text{H}^+]}{K_a} [\text{Cu-OH}^+] + k_2 K_2 [\text{Cu-OH}^+]$$

or

$$k_{obs} = \left(k_1 K_1 \frac{[H^+]}{K_a} + k_2 K_2 \right) [Cu-OH^+] \quad \text{Eq. 5.17}$$

In order to determine $k_1 K_1$ and $k_2 K_2$, the values of $[Cu]_{free}$ must be calculated from the thermodynamic data, or determined as part of a fitting procedure. Taking account of the pH dependent equilibrium of the complex, the expression for k_{obs} (Equation 5.17) can be written as:

$$k_{obs} = \left\{ k_1 K_1 \frac{[H^+]}{K_a} + k_2 K_2 \right\} \left\{ \frac{1}{4K_{dim}} \left[- \left(\frac{[H^+]}{K_a} + 1 \right) + \sqrt{\left(\frac{[H^+]}{K_a} + 1 \right)^2 + 8K_{dim} [Cu^{2+}]_{total}} \right] \right\}$$

$$\text{Eq. 5.18}$$

Fitting of the data to Equation 5.18 gave values to the 4 variables, namely $k_1 K_1$, $k_2 K_2$, K_a and K_{dim} . The MATLAB⁶⁸ programming environment was used to analyse the data. From initial calculations using the four parameters, it was observed that under the reaction conditions used in this study the value of $k_1 K_1$ is zero within experimental error, indicating that this pathway makes little contribution to the reaction rate. Consequently, the value of $k_1 K_1$ was assigned to zero, and the remaining three parameters fitted to the data, according to Equation 5.19. The data obtained from this analysis are given in Table 5.8.

$$k_{obs} = \frac{k_2 K_2}{4K_{dim}} \left\{ - \left(\frac{[H^+]}{K_a} + 1 \right) + \sqrt{\left(\frac{[H^+]}{K_a} + 1 \right)^2 + 8K_{dim} [Cu^{2+}]_{total}} \right\} \quad \text{Eq. 5.19}$$

Table 5.8 Constants derived from fitting the observed data to Equation 5.19

using MATLAB

T (°C)	$k_2 K_2$ ($M^{-1}s^{-1}$)	K_a (M)	pK _a	K_{dim} (M^{-1})
42.5	0.11	7.25×10^{-9}	8.14	1960
50.0	0.15	3.40×10^{-8}	7.47	2425
57.5	0.19	2.09×10^{-8}	7.71	297
65.0	0.28	2.98×10^{-8}	7.53	197

Residual plots have been calculated for the above data and those for 50°C and 57.5°C are presented in Figures 5.10 and 5.11 and the remaining plots are shown in Appendix 2. The inner three circles in each plot are the 90, 95 and 99% confidence limits (the values for the residuals are given in Appendix 2). It is obvious from these residual plots that the values obtained for K_{dim} have large ranges of values, within the constraints of the calculated $k_2 K_2$ and K_a . It is also apparent that the parameters are highly correlated, *i.e.* a small change in any of the values will alter all other values significantly. Interestingly, the data at 57.5°C seems better behaved, and the final parameters are better constrained. Despite having some limitation, the information obtained from this detailed study is valuable. Further analysis of this data is presented later in this chapter.

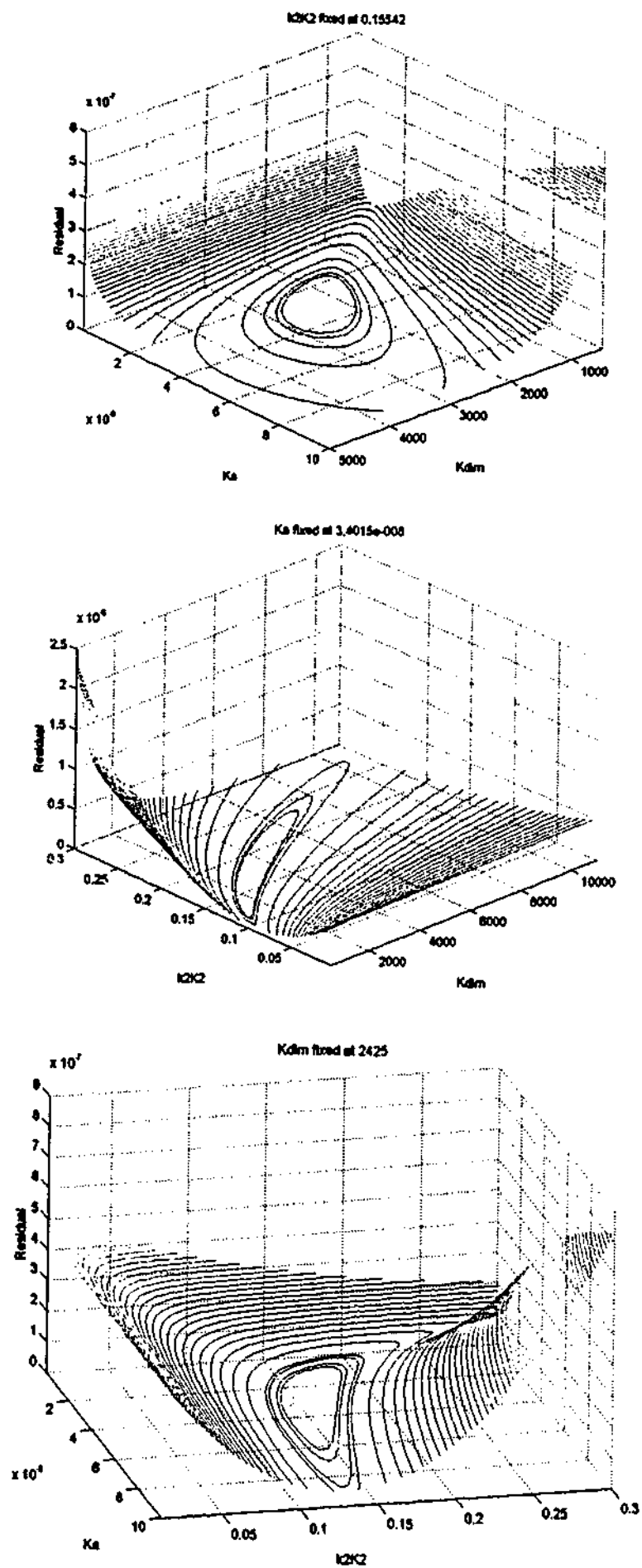


Figure 5.10 Residual Plots for the data calculated as shown in Table 5.8 at 50°C

Note the inner three rings represent the 90, 95 and 99% confidence limits

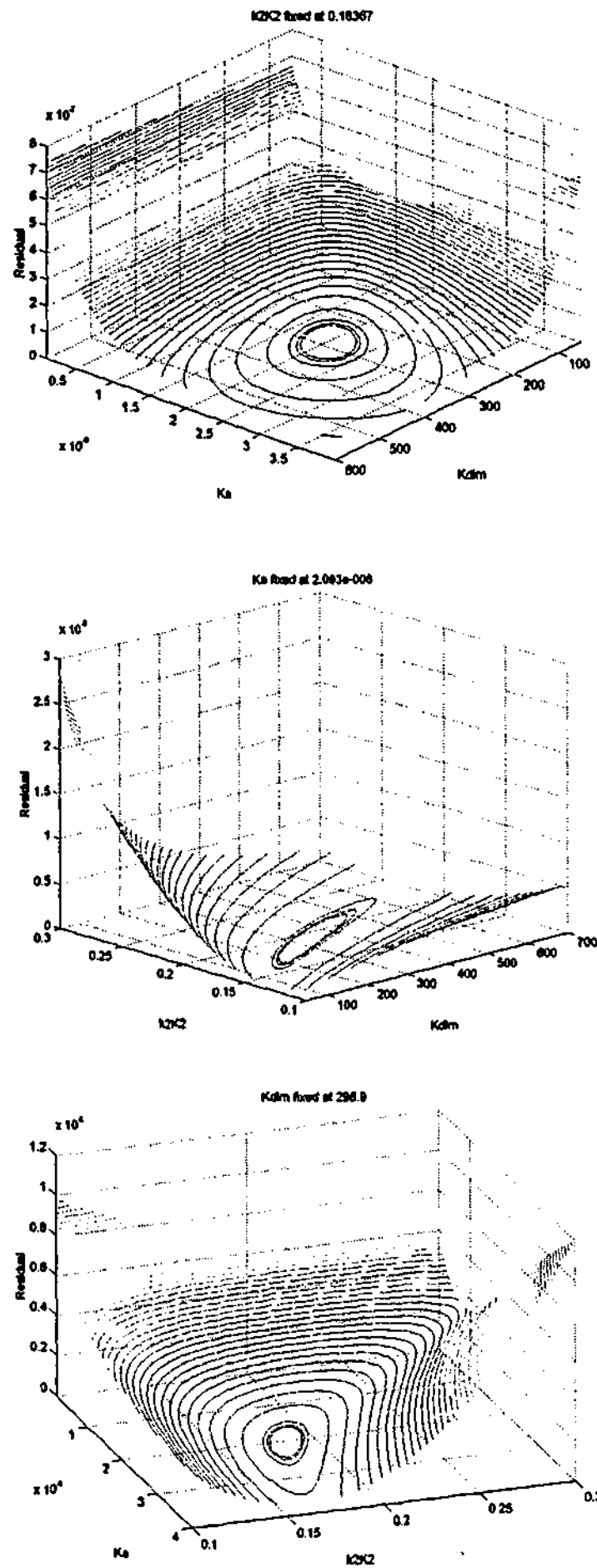
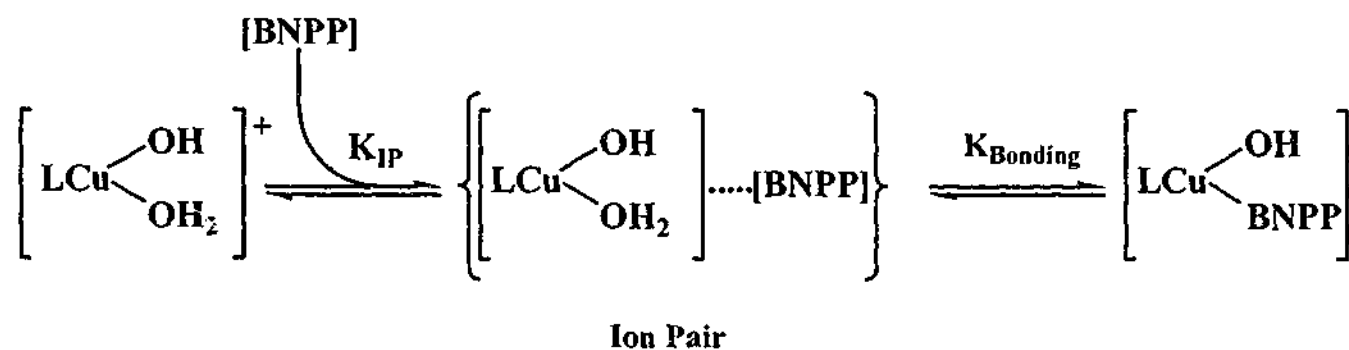


Figure 5.11 Residual Plots for the data calculated shown in Table 5.8 at 57.5°C

Note the inner three rings represent the 90, 95 and 99% confidence limits

5.3.6 Attempt at Determining the Equilibrium Constant for Attachment of BNPP to the Complex

The equilibrium constants K_1 and K_2 are the product of an ion pairing constant, K_{IP} , and an equilibrium constant for the bonding of BNPP to complex $[\text{Cu}(\text{Me}_3\text{tacn})(\text{H}_2\text{O})_2](\text{ClO}_4)_2$, K_{Bonding} , *i.e.* $K_1 \text{ or } 2 = K_{IP}K_{\text{Bonding}}$ (Scheme 5.8).



Scheme 5.8 Schematic of the two equilibria leading to the attachment of BNPP

The Fuoss-Davies Equation^{69,70} predicts an ion-pairing constant, K_{IP} , of approximately 1 M^{-1} between two species of charges +1 and -1, while that for a +2 and -1 species is predicted to be *ca.* 40 M^{-1} .⁷¹ From this value one can see the concentration of the ion pair is very small (*ca.* 10^{-8} M for +1/-1 and 10^{-7} M for +2/-1) and under the conditions used in our experiment, *i.e.* less than 1% of all BNPP would be complexed in solution.

To determine K_1 and K_2 , the rate constant was measured with constant $[\text{Cu}(\text{Me}_3\text{tacn})(\text{H}_2\text{O})_2]^{2+}$ concentration and increasing BNPP concentration. Ideally, at high concentrations of BNPP, the plot of k_{obs} versus $[\text{BNPP}]$ will show saturation enabling a Michaelis constant to be determined,¹⁹ but the experiment was limited due to the insolubility of BNPP above a concentration 10 mM. A plot of Rate versus $[\text{BNPP}]$

for a copper concentration of 0.3 mM showed a straight line, without saturation behaviour, and the value of the thermodynamic constants for bonding of BNPP to the Cu(II) complex could therefore not be separated from the rate constant k_2 . The plot of Rate versus [BNPP] is shown in Figure 5.12, with a computer generated line of best fit.

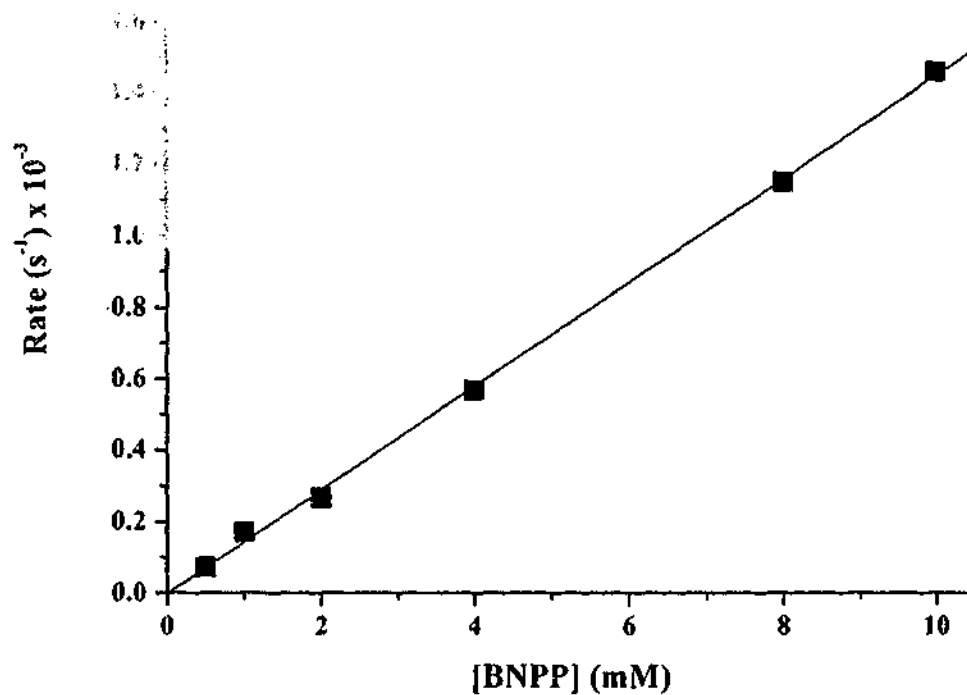


Figure 5.12 Plot of Rate vs. [BNPP] at 0.3 mM $[\text{Cu}(\text{Me}_3\text{tacn})(\text{H}_2\text{O})_2]^{2+}$, pH 7.2, Temperature 50°C and Ionic Strength at 150 mM. The line is a computer generated line of best fit with $R = 0.9995$. Points are an average of three experiments.

5.3.7 Thermodynamic Parameters

From the thermodynamic constants (Table 5.7, page 260, K_a and K_{dim}) calculated previously, and through the use of the Arrhenius equation (Equation 5.20), the thermodynamic parameters were determined.

$$K = e^{\frac{-\Delta H^\circ}{RT} + \frac{\Delta S^\circ}{R}} \quad \text{Eq. 5.20}$$

Plotting K_a versus $1/T$, and fitting an exponential curve to the data, yielded $\Delta H^\circ = 116 \pm 9 \text{ kJ mol}^{-1}$ and $\Delta S^\circ = 213 \pm 22 \text{ J mol}^{-1} \text{ K}^{-1}$. The plot of K_a versus $1/T$ is shown in Figure 5.4.1. The Gibbs free energy was calculated at 53 kJ mol^{-1} at 25°C (see also Table 5.9 below). The same method for determining the values from K_{dim} yielded values of $\Delta H^\circ = -245 \pm 20 \text{ kJ mol}^{-1}$ and $\Delta S^\circ = -694 \pm 40 \text{ J mol}^{-1} \text{ K}^{-1}$, and a value of ΔG° of -38 kJ mol^{-1} .

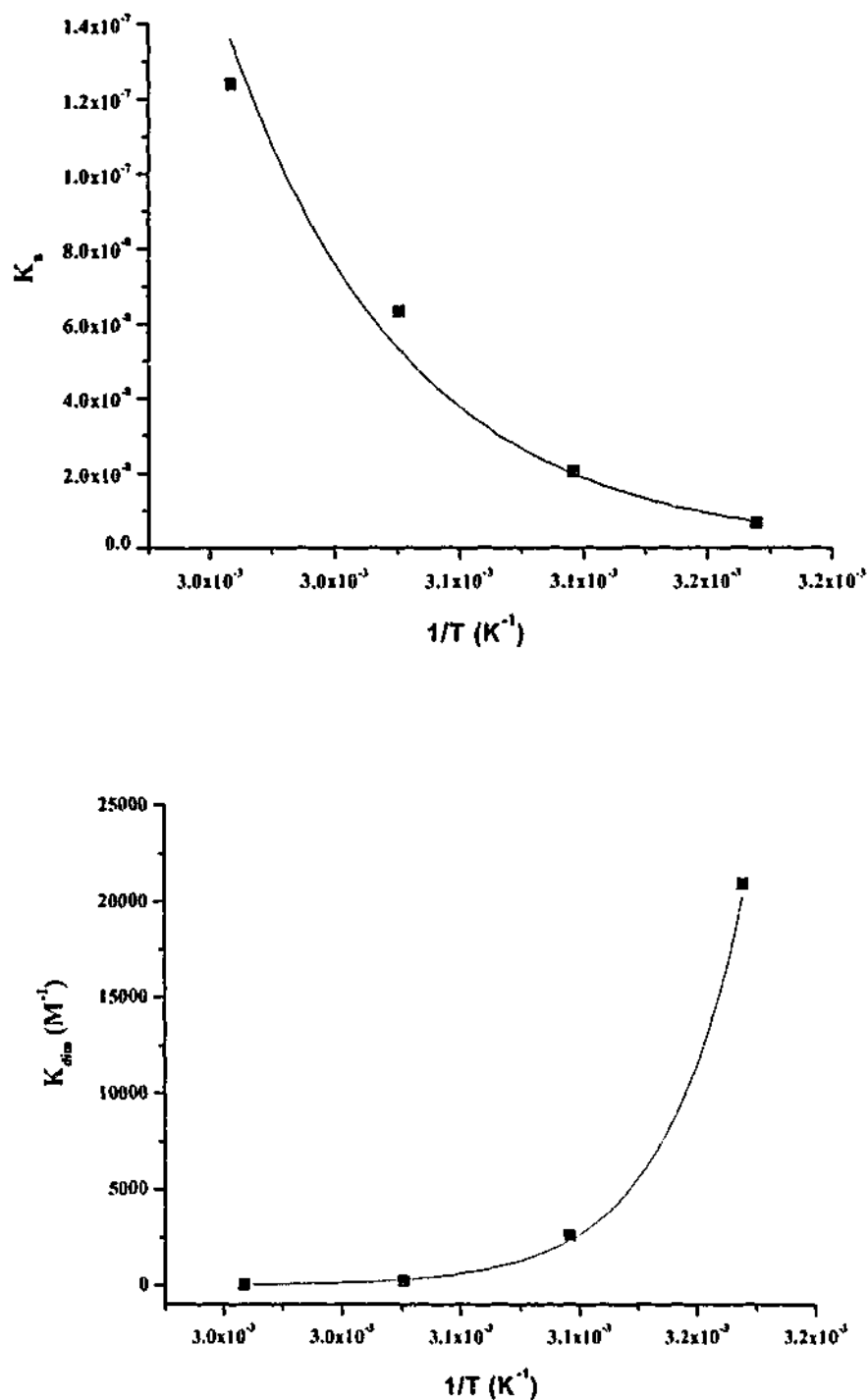


Figure 5.13 Plot of K_a versus $1/T$ (top) and K_{dim} versus $1/T$ (bottom) for the values obtained from Method 1. The solid line is a computer generated line of best-fit.

The values of K_a and K_{dim} used in calculating the thermodynamic parameters obtained from Method 1 (*i.e.* fitting K_a and K_{dim} using a spectrophotometric titration of $[\text{Cu}(\text{Me}_3\text{tacn})(\text{H}_2\text{O})_2]^{2+}$) are somewhat different from the values calculated by Method

2, *i.e.* using the rate data and fitting Equation 5.19. Values calculated by Method 1 are presented in Table 5.9. Thermodynamic parameters for K_a and K_{dim} determined using Method 2 (kinetic analysis) were not calculated due to inconsistencies in the values (see Table 5.8 page 267).

Table 5.9 Thermodynamic Parameters for K_a and K_{dim} from Method 1

	ΔH° kJ mol ⁻¹	ΔS° J mol ⁻¹ K ⁻¹	ΔG° kJ mol ⁻¹
K_a	116 ± 9	213 ± 22	53 ± 5
K_{dim}	-245 ± 30	-694 ± 40	-38 ± 3

5.3.8 Activation Parameters

The activation parameters for k_{obs} were determined at 2.0 mM at pH 7.4 and 9.1 were calculated using the Eyring rate equation (Equation 5.21) and the values obtained from Method 2. The graph is shown in Figure 5.14 with a computer generated line of fit to Equation 5.21, and the values for the activation parameters are given in Table 5.10.

$$k = \frac{RT}{Nh} e^{\left(\frac{\Delta S^\ddagger}{R} - \frac{\Delta H^\ddagger}{RT} \right)} \quad \text{Eq. 5.21}$$

where R is the universal gas constant, N is Avogadro's Number and h is Planck's constant.

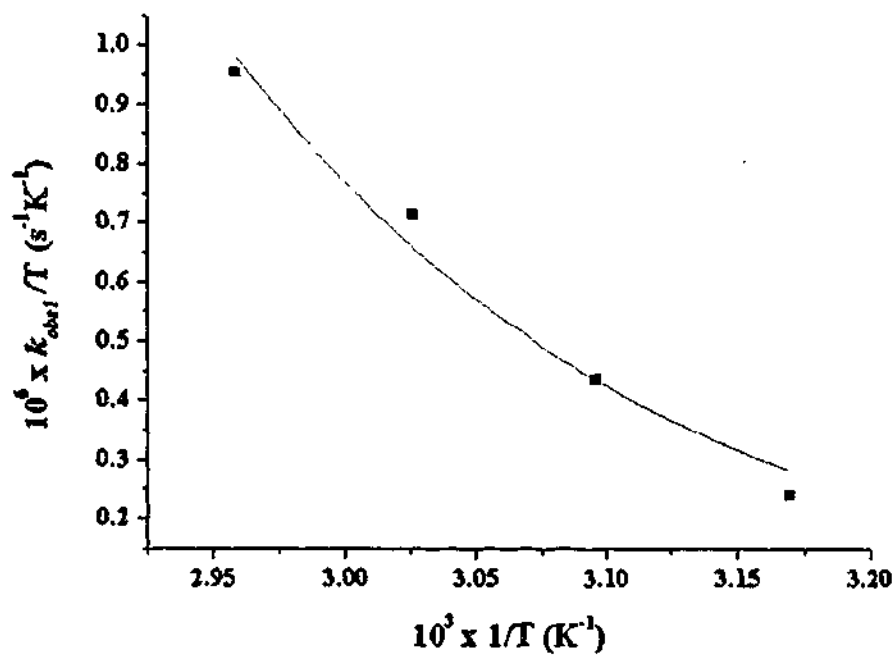
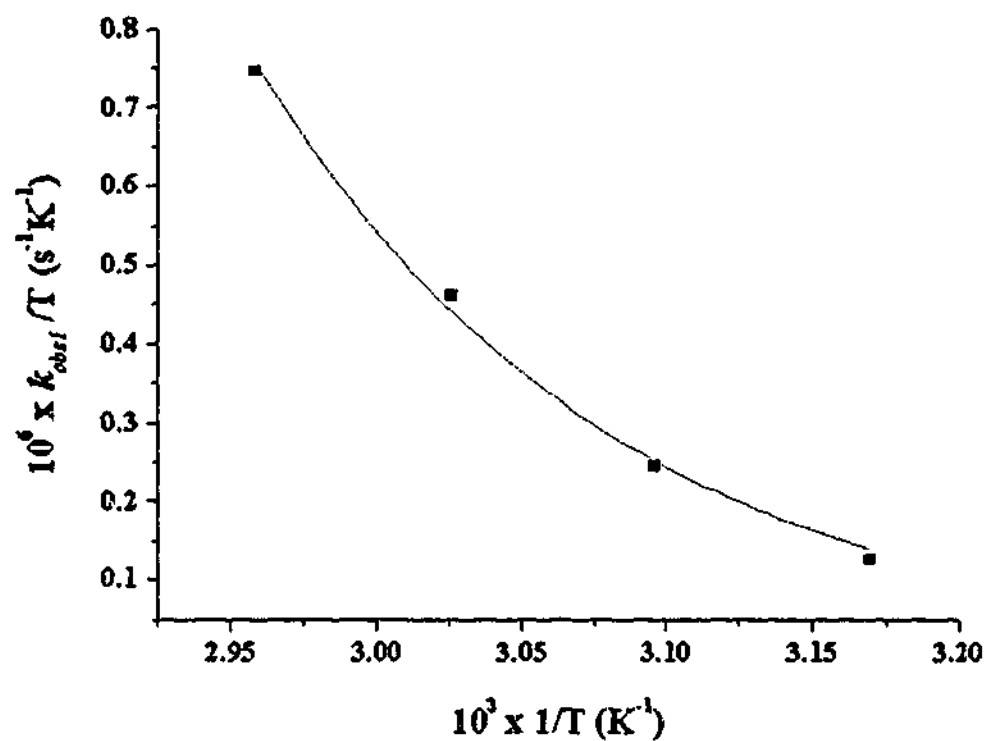


Figure 5.14 Plots of $\frac{k_{obs}}{T}$ vs. $\frac{1}{T}$ for pH 7.4 (top) and pH 9.1 (bottom).

ΔH^\ddagger and ΔS^\ddagger were obtained from the plot of $\frac{k_{obs}}{T}$ vs. $\frac{1}{T}$

Table 5.10 Activation parameters calculated for k_{obs1}

	ΔH^\ddagger (kJ mol ⁻¹)	ΔS^\ddagger (J mol ⁻¹ K ⁻¹)	ΔG^\ddagger (kJ mol ⁻¹)
pH 7.4	67 ± 4	-116 ± 10	101 ± 7
pH 9.1	49 ± 6	-166 ± 17	98 ± 11

ΔG^\ddagger was calculated from the equation $\Delta G^\ddagger = \Delta H^\ddagger - T\Delta S^\ddagger$ at 298 K

The activation parameters for the second order rate constant (k_2K_2) were calculated, again using the Eyring rate equation (Equation 5.21). The graph is shown in Figure 5.15, and the values of the activation parameters are given in Table 5.11.

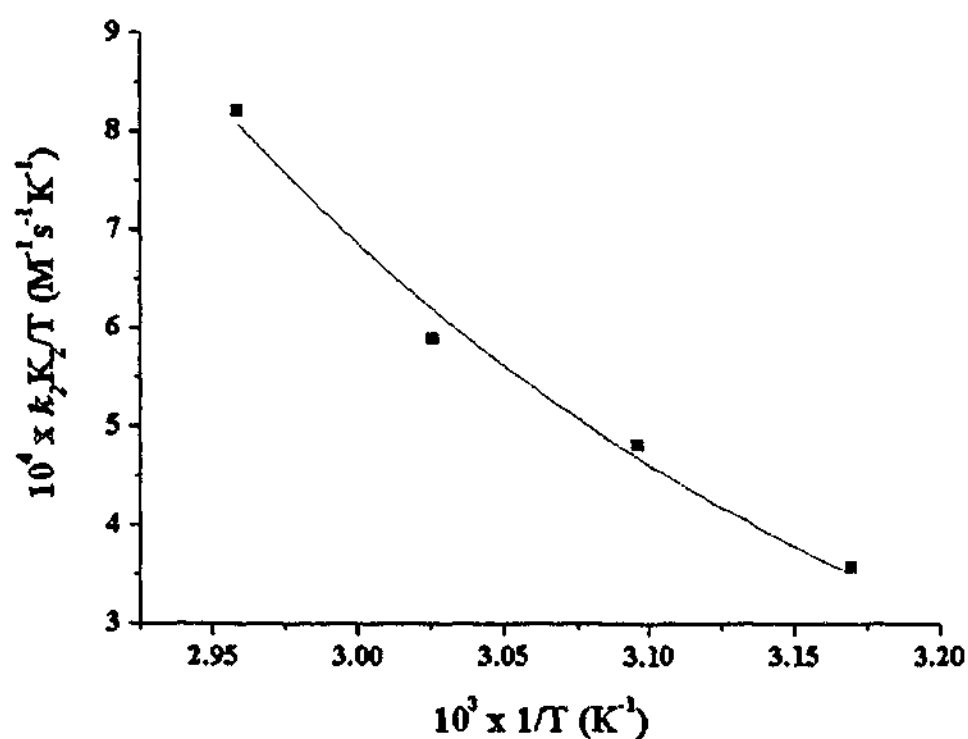


Figure 5.15 Plot of k_2K_2 versus $1/T$ for the values obtained MATLAB (Method 2).

ΔH^\ddagger and ΔS^\ddagger were obtained from the plot of $\frac{k_2 K_2}{T}$ vs. $\frac{1}{T}$

Table 5.11 Activation Parameters calculated for k_2K_2

	ΔH^\ddagger (kJ mol ⁻¹)	ΔS^\ddagger (J mol ⁻¹ K ⁻¹)	ΔG^\ddagger (kJ mol ⁻¹)
Method 2	33 ± 3	-159 ± 8	80 ± 5

ΔG^\ddagger was calculated from the equation $\Delta G^\ddagger = \Delta H^\ddagger - T\Delta S^\ddagger$ at 298 K

5.3.9 Catalytic Turnover

The definition of a catalyst not only includes rate enhancement, but also requires the “catalyst” to be regenerated. The regeneration of a catalyst is indicated in this experiment by the production of more than stoichiometric amount of 4-nitrophenylate.

The complex $[\text{Cu}(\text{Me}_3\text{tacn})(\text{H}_2\text{O})_2](\text{ClO}_4)_2$ was tested for the ability to act as a catalyst, and not merely just as a “rate enhancer”. The previous experiments can only show the latter as the amount of BNPP is less than that of the complex. The concentration of the substrate BNPP was kept constant at 1.0 mM, while the concentration of $[\text{Cu}(\text{Me}_3\text{tacn})(\text{H}_2\text{O})_2](\text{ClO}_4)_2$ was varied so that the BNPP concentration was in a 10, 40, 100 and 1000 times excess over that of $[\text{Cu}(\text{Me}_3\text{tacn})(\text{H}_2\text{O})_2](\text{ClO}_4)_2$. The reactions were performed at pH 5.9, 7.4 and 9.1, while maintaining the temperature at 50°C. The reaction was monitored over a period of weeks and the only spectral change observed was due to the release of NPP at 400nm (Scheme 5.1 page 237). The results of the experiment are shown in Figure 5.16.

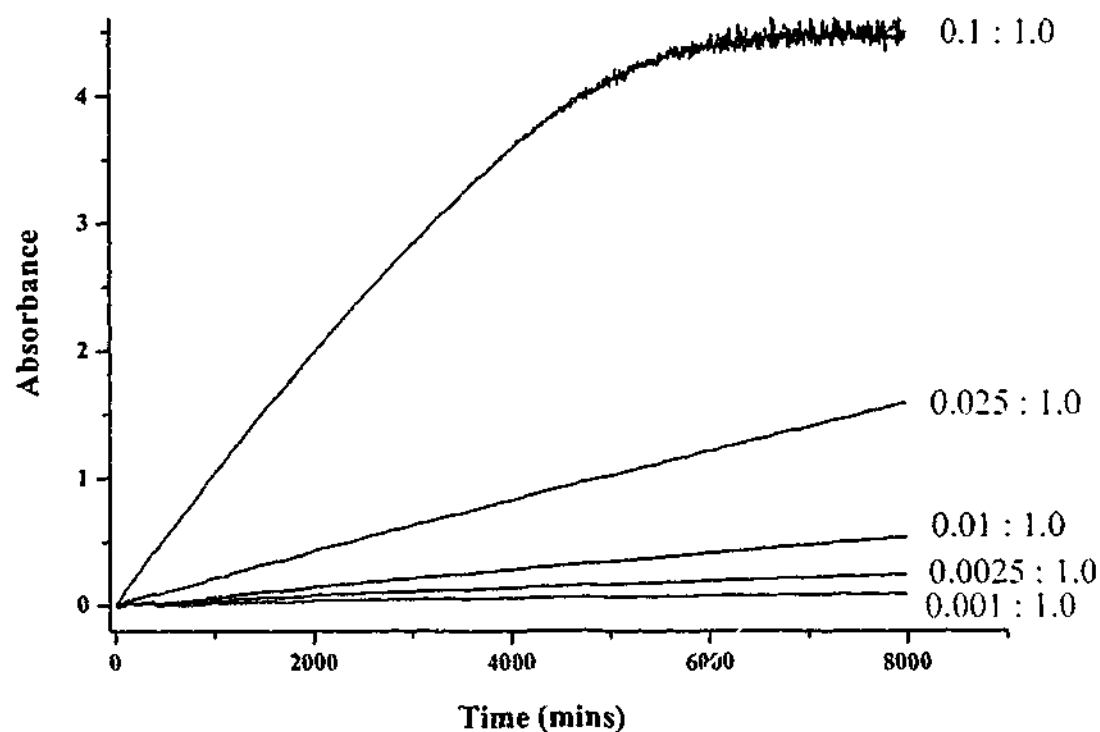


Figure 5.16 Plot of Absorbance change versus time for the first 8000 minutes of the catalytic experiment of $[\text{Cu}(\text{Me}_3\text{tacn})(\text{H}_2\text{O})_2](\text{ClO}_4)_2$ with $[\text{Complex}]$ (mM): $[\text{BNPP}]$ (1.0 mM) shown and at pH 7.4 and Temperature of 50°C . Note the high noise level of the curve for the top trace is due to the limitations of the instrument.

From the absorbance change and the molar extinction coefficient the amount, of NP produced is calculated, and therefore the number of turnovers determined. The pK_a of 4-nitrophenol is 7.15⁷², which has to be taken into account when calculating the turnovers. The molar extinction coefficients at the given pH's are shown in Table 5.12.

Table 5.12 Molar extinction coefficients for NP at 400 nm and at variable pH

pH	(M ⁻¹ cm ⁻¹)
5.9	1600
7.4	11800
9.1	20000

The initial turnover rate of the systems were calculated from the initial linear section of the graph. The turnover rate is given in Table 5.13 and the total number of turnovers are shown in Table 5.14.

Table 5.13 Turnover rate per moles of [Cu(Me₃tacn)(H₂O)₂]²⁺ for the first six days of the experiment. Quoted values are the number of turnovers per day

Ratio of [Cu] to [BNPP]	pH 5.9	pH 7.4	pH 9.1
0.1	0.015	0.860	0.877
0.025	0.016	0.790	0.203
0.01	0.014	0.448	0.618
0.001	-	0.205	0.542

Table 5.14 Total turnovers after 63 days

Ratio of [Cu] to [BNPP]	pH 5.9	pH 7.4	pH 9.1
0.1	11	13	10
0.025	14	21	19
0.01	6	13	17
0.001	18	21	15

5.4 Discussion of Results

5.4.1 General Observations

Kinetic screening experiments indicated that the copper(II) complexes exhibited a faster rate of hydrolysis than the Zn(II) or the Ni(II) complexes studied. It was also observed that the rate increased as the nuclearity of the complex increased *viz.* mononuclear Cu(II) tacn complex, $[\text{Cu}(\text{tacn})(\text{H}_2\text{O})_2]^{2+}$ ^{19,61,73} vs. binuclear Cu(II) tacn complexes, $[\text{Cu}_2(\text{T}_2\text{-}o\text{-X})\text{Cl}_4]$ and $[\text{Cu}_2(\text{T}_2\text{-}m\text{-X})(\text{H}_2\text{O})_4]^{4+}$, vs. the trinuclear Cu(II) complex $[\text{Cu}_3(\text{T}_3\text{mes})(\mu\text{-OH})_2(\text{H}_2\text{O})_2]^{4+}$. In particular, the trinuclear copper(II) complex with the T₃mes ligand exhibits the highest reactivity and warrants further investigation. Yashiro and coworkers studied the rate of hydrolysis of diribonucleotides by a trinuclear Zn(II) complex, and also found the rate enhancement of the trinuclear exceeds that of analogous mono- and binuclear complexes.⁴⁷ Lui *et al.*⁷⁴ compared the rate of hydrolysis of phosphate esters by related mono- and binuclear complexes and in this study it was also found that increasing the nuclearity of the complex resulted in an increase in the rate by up to 500 times. A binuclear complex reported by Young *et al.*³⁵ consisting of two copper(II) tacn units linked by a naphthalene bridge exhibited a 300-

500 fold increase in the rate of hydrolysis of ApA and cyclic 2',3'-cAMP over that of $[\text{Cu}(\text{tacn})(\text{H}_2\text{O})_2]^{2+}$.

For the complexes of the bis(tacn) ligands, reduction in the number of free sites on the Cu(II) centre led to a reduction in the rate of hydrolysis, *viz.* $\text{T}_2\text{-o-X}$ and $\text{T}_2\text{-m-X}$ ligands (bis(tridentate) ligands) are more efficient than $\text{T}_2\text{-o-X Ac}_2$ and $\text{T}_2\text{-m-X Ac}_2$ ligands (bis(tetradentate) ligands). It is interesting to note, however, that the Cu-tren complex is a better cleavage agent than all but two of the complexes. In this case, reduction of the number of free sites could be restricting the formation of an inactive dimer as was found in the tacn systems. It may be postulated that this reaction involves two complexes reacting with one BNPP, where the BNPP is attached to one Cu(II) centre and is attacked by a nucleophile from a second Cu(II) centre. The other major difference between Cu(II) tren complexes and the tacn complexes is the location of the phosphate ester binding site. Assuming the tacn-based complexes are square pyramidal (SP), the ester will attach at an equatorial site on the SP, while for the Cu(II)-tren complex, the geometry of the complex is assumed to be trigonal bipyramidal (TBP) and the BNPP would bind in the apical position. A search of the Cambridge Crystallographic Database showed copper(II) complexes with the ligand tren are all five-coordinate with TBP Cu(II) geometry. This change in coordination from SP to TBP geometry may have some influence on the rate of BNPP hydrolysis.

The Cu(II) complex of the alkylated tacn derivative, Me_3tacn , produced the fastest rate of phosphate ester bond cleavage of all complexes studied and as a result, this complex was subjected to a detailed study.

5.4.2 First Order Rate Constants

An exponential fit to the absorbance data yielded two first order rate constants for the two consecutive releases of 4-nitrophenylate (NP) from bis(4-nitrophenyl) phosphate (BNPP). The rate of the first cleavage was *ca.* 100 times faster than the second. The Rate-pH profile shown in Figure 5.5 (page 251) shows the characteristic S-shaped curve which is typical of a process where a deprotonation takes place. The fitting of the data, however, requires that allowance is made for the formation of the $[(\text{Me}_3\text{tacn})\text{Cu}(\mu\text{-OH})_2\text{Cu}(\text{Me}_3\text{tacn})]^{2+}$ species (see Scheme 5.4, page 255).

A comparison of the first order rate constants (k_{obs}) obtained in this study (Table 5.5) to those reported previously is limited due to the differing conditions used in the studies. Many groups use different phosphate esters, each with different reactivities. Other commonly used phosphate diesters include 2-hydroxypropyl 4-nitrophenyl phosphate (HPNP),²⁷ 2,4-dinitrophenyl ethyl phosphate (DNPEP)⁷⁵ and ethyl 4-nitrophenyl phosphate (ENPP).^{19,76} A comparison between the reactivities of these phosphate esters is only possible when the same conditions are used for the hydrolysis. For example, Planalp and coworkers⁷⁶ show the hydrolysis of BNPP *cf.* ENPP (ethyl 4-nitrophenyl phosphate) to be *ca.* 16 times faster by copper(II) *N,N',N''*-trimethyl-*cis,cis*-1,3,5-triaminocyclohexane ($[\text{Cu}(\text{tach-Me}_3)]^{2+}$), while Deal *et al.*¹⁹ use three different phosphate ester in the course of testing the hydrolytic activity of $[\text{Cu}(\text{tacn})(\text{H}_2\text{O})_2]^{2+}$ and show the hydrolysis of ENPP to be *ca.* 17 times slower than BNPP, and that of NPP to be *ca.* 46 times slower than BNPP. In addition, as the concentration of the substrate increases relative to the metal concentration, so does the rate.^{73,76}

The concentration of substrate used in the present study is comparatively low ($15 \mu\text{M}$), with many studies using a similar concentration of substrate compared with complex concentration (*ca.* 1 mM) and applying the initial rates method of analysis. Table 5.15 shows first order rate constants for various complexes including the conditions of the hydrolysis.

Table 5.15 Observed first-order rate constants for the hydrolysis of BNPP by various complexes at 50°C

Complex [†]	[Complex]	[Substrate]	pH	Rate (s ⁻¹)	Ref.
[Cu(Me ₃ tacn)(H ₂ O) ₂] ²⁺	1.0 mM	15 μM	7.4	3.7 × 10 ⁻⁵	TW
[Co(III)(cyclen)(H ₂ O) ₂] ²⁺	10 mM	10 μM	7.0	4.6 × 10 ⁻³	22
[Co(III)(tren)(H ₂ O) ₂] ²⁺	10 mM	10 μM	7.0	8.1 × 10 ⁻⁵	22
[Co(III)(trpn)(H ₂ O) ₂] ²⁺	10 mM	10 μM	7.0	2.5 × 10 ⁻²	22
[Cu(Me ₃ tacn)(H ₂ O) ₂] ²⁺	0.3 mM	4.0 mM	7.2	4.7 × 10 ⁻⁴	TW
[Cu(tacn)Cl ₂]	1 mM	5 mM	7.24	1.3 × 10 ⁻⁶	19
[Cu(Me ₃ tach)Cl ₂]	1.0 mM	5mM	7.2	1.1 × 10 ⁻⁵	76
[ZnL ¹ OH ₂] ²⁺	1.0 mM	20 μM	8.5	1.8 × 10 ⁻⁶	26
[ZnL ² OH ₂] ²⁺	1.0 mM	20 μM	8.5	1.0 × 10 ⁻⁵	26
[Cu(Me ₃ tacn)(H ₂ O) ₂] ²⁺	1.0 mM	15 μM	8.2	5.5 × 10 ⁻⁵	TW
[EuL ⁴] ^{3+ a}	5.0 mM	37.6 μM	7.0	3.1 × 10 ⁻⁴	28
[EuL ⁵] ^{3+ a}	5.0 mM	37.6 μM	7.0	1.1 × 10 ⁻³	28
[EuL ⁶] ³⁺	0.4 mM	40 μM	8.5	1.5 × 10 ⁻³	30
[Zn(tren)OH ₂] ²⁺	1.0 mM	20 μM	8.5	5.5 × 10 ⁻⁷	26
[ZnL ⁷ OH ₂] ²⁺	1.0 mM	20 μM	8.5	1.8 × 10 ⁻⁶	26
[Zn(H ₃ L ⁸)OH ₂] ³⁺	1.0 mM	20 μM	8.5	1.0 × 10 ⁻⁵	26

[†]Abbreviations: cyclen = 1,4,7,10-tetraazacyclododecane; tren = tris(2-aminoethyl)amine; trpn = tris(3-aminopropyl)amine; L¹ = *N,N',N''*-tris(2-benzylaminoethyl)amine; L² = *N,N',N''*-tris(im-benzyl-L-histylethylaminoethyl)amine; L³ = 2,6-bis[*bis*(2-pyridylmethyl)amino]methyl-4-methoxyphenolate; L⁴ = *N*-(propylcarboxylic acid)benoaza-15-crown-5 ether; L⁵ = *N*-(butylcarboxylic acid)benoaza-15-crown-5 ether; L⁶ = 4,7,13,16,21-pentaoxo-1,10-diazabocyclo[8.8.5]tricosane; L⁷ = *N,N',N'*-tris(2-benzylaminoethyl)amine; L⁸ = *N,N',N'*-tris(imbenzyl-L-histidylethylaminoethyl)amine.

^aComplex made *in situ* and additional ligands not specified.

As can be seen from a comparison of the data in the above table, the k_{obs} for $[\text{Cu}(\text{Me}_3\text{tacn})(\text{H}_2\text{O})_2]^{2+}$ is larger than for the other 2+ transition metals presented. Comparison with the related system, $[\text{Cu}(\text{tacn})(\text{H}_2\text{O})_2]^{2+}$, shows the alkylation of the tacn ring with methyl group increases the rate significantly. The rate of hydrolysis of BNPP by $[\text{Cu}(\text{tacn})(\text{H}_2\text{O})_2]^{2+}$ is $1.3 \times 10^{-6} \text{ s}^{-1}$ at pH 7.24, 1 mM [complex] and 5 mM [substrate], whereas $[\text{Cu}(\text{Me}_3\text{tacn})(\text{H}_2\text{O})_2]^{2+}$ is *ca.* 400 times faster ($4.7 \times 10^{-4} \text{ s}^{-1}$) at the same temperature with a [complex] of 0.3 mM and [BNPP] slightly lower at 4 mM. The recently reported complex $[\text{Cu}(\text{tachMe}_3)\text{Cl}_2]$ cleaves BNPP with a rate of $1.1 \times 10^{-5} \text{ s}^{-1}$ for a 1 mM complex concentration,⁷⁶ which is again slower (*ca.* 50 times) than that of $[\text{Cu}(\text{Me}_3\text{tacn})(\text{H}_2\text{O})_2]^{2+}$ ($4.7 \times 10^{-4} \text{ s}^{-1}$) at pH 7.2. The Zn(II) complex of the ligand *N,N',N''*-tris(im-benzyl-L-histylethylaminoethyl)amine (L^2) has a rate of $1.0 \times 10^{-5} \text{ s}^{-1}$ for a 1 mM solution pH 8.4 and a comparable BNPP concentration to that used in this study, which is about 5 times less than the rate of hydrolysis of BNPP by $[\text{Cu}(\text{Me}_3\text{tacn})(\text{H}_2\text{O})_2]^{2+}$ ($5.5 \times 10^{-5} \text{ s}^{-1}$). The effect of ligands can be seen by comparing the Zn(II) complex of L^2 , with a related Zn(II) complex of ligand L^1 , *N,N',N''*-tris(2-benzylaminoethyl)amine (see Figure 5.17 for structures). This latter complex exhibits a rate of *ca.* 5 times less than the complex of L^2 , and about 30 times less than $[\text{Cu}(\text{Me}_3\text{tacn})(\text{H}_2\text{O})_2]^{2+}$. Although only a limited amount of data is available for alkylated complexes, it indicates that this speeds up the hydrolysis reaction. The complexes with trivalent metal ions, such as Co(III) and Eu(III), react considerably faster than the divalent metal complexes, probably due to the higher charge on the metal atom, and therefore a greater electrostatic attraction.¹⁹ These metal ions are also harder Lewis acids than Cu(II) due to the increased charge-to-radius ratio. It has been previously pointed out, however, that due to their kinetic inertness these complexes do

not function as catalysts because of slow rates of product release or substrate attachment.⁷³

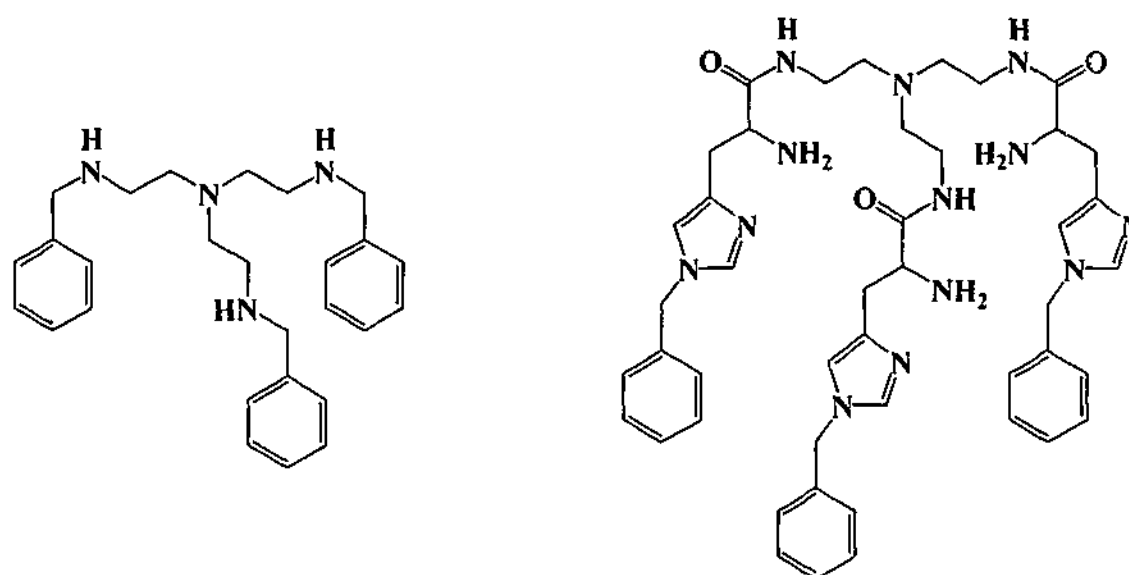


Figure 5.17 Ligands *N,N',N''*-tris(2-benzylaminoethyl)amine (left) (L^1 Table 5.15) and *N,N',N''*-tris(im-benzyl-L-histylethylaminoethyl)amine (right) (L^2 Table 5.15)

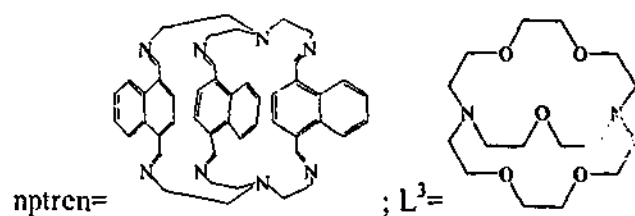
Comparison of k_{obs2} with literature values are mainly confined to studies with NPP, as reports of the biphasic hydrolysis of BNPP are limited. As the rate of hydrolysis of the phosphate diesters by such complexes is often faster than for the monoester for these types of systems, there are fewer studies using NPP. The rate of hydrolysis of the monoester, NPP, by $[Cu(Me_3tacn)(H_2O)_2]^{2+}$ is similar to that of many other previously reported complexes, however its greater ability to cleave the diester, BNPP, is an exciting finding. Table 5.16 shows the rate constants for a number of reported complexes that hydrolyse NPP. In particular the complex $[EuL^3]^{3+}$ showed biphasic kinetics and the data was used to determine rate constants for the sequential hydrolysis of BNPP producing two moles of NP (see Scheme 5.1 page 237, k_1 and k_2). The two

rate constants were quite similar (first release NP (k_1) = $4.3(5) \times 10^{-5} \text{ s}^{-1}$ and for the second production (k_2) = $4.78 \times 10^{-5} \text{ s}^{-1}$ at pH 7.5, 50°C, [BNPP] = $4.0 \times 10^{-5} \text{ M}$ and [Complex] = 1.0 mM).³⁰ The similarities in the two rates, however, lead us to question whether setting of two rate constants is appropriate. If the release of the first NP is rate determining then mono-phase kinetics would be observed, and the data cannot be compared with that for NP release from NPP.

Table 5.16 First order rate constants for the hydrolysis of NPP

Complex ^a	[Complex]	[Substrate]	pH	T (°C)	Rate (s ⁻¹)	Ref.
[Cu(iMe ₃ tacn)(H ₂ O) ₂] ²⁺	3.0 mM	15 μM	7.4	50	1.93 × 10 ⁻⁶	TW
[Cu ₂ (tdciH ₃)(OH ⁻) ₂] ^b	3 mM	3 mM	8.4	25	1.98 × 10 ⁻⁶	75
<i>cis</i> -[Co(en) ₂ (OH ₂)NPP]	75 μM	0.5 mM	9-11.8	25	7.8 × 10 ⁻⁴	77
[Zn ₂ L ¹] ³⁺	5 mM	10 mM	5.9	35	7.5 × 10 ^{-6c}	78
[Zn ₂ L ²] ^{4+ d}	0.23	0.23	7.6	55	2.8 × 10 ^{-6c}	51
[EuL ³] ³⁺	1.0 mM	40 μM	7.5	50	4.78 × 10 ⁻⁵	30
[Cu(I)(nptren)] ⁺	0.1 mM	0.5 mM	8.0	75	3.8 × 10 ⁻⁶	79
[Cu(I) ₂ (nptren)] ²⁺	0.1 mM	0.5 mM	8.0	75	1.14 × 10 ⁻⁵	79
[Ni(nptren)] ²⁺	0.1 mM	0.5 mM	8.0	75	1.34 × 10 ⁻⁵	79
[Co(nptren)] ²⁺	0.1 mM	0.5 mM	8.0	75	8.2 × 10 ⁻⁶	79
[Cu(tren)] ⁺	0.1 mM	0.5 mM	8.0	75	5.2 × 10 ⁻⁶	79
[Ni(tren)] ²⁺	0.1 mM	0.5 mM	8.0	75	5.6 × 10 ⁻⁶	79
H ₂ O	-	-	-	25	2 × 10 ⁻⁹	80

^aL¹H=(26-hydroxy-1,4,7,10,13,16,19,22-octaazabicyclo[11.11.3]heptacosane; L²=S, S'-bis(10-(1,4,7-triazacyclodidecyl))-1',3'-dithiobenzene; tren=tris(2-aminoethyl)amine; tdci=1,3,5-trideoxy-1,3,5-tris(dimethylamino)-*cis*-inositol;



^b proposed structure

^c values estimated from rate vs. pH plot

^d Complex not isolated and additional ligands present in water.

As can be seen from Table 5.16, (and Table 5.6) the hydrolysis of NPP is faster for the Co(III) complex, as has been seen with BNPP, and, again, is probably due to the higher charge on the metal ion. Comparison of the behaviour of the complexes listed in Table 5.16 is also limited due to the different temperatures used. It is evident, however, from both Cu(I) complexes of the nptren ligand⁷⁹ that dinuclear complexes react faster than mononuclear complexes. These complexes also showed selectivity for the monoester over the diester, BNPP, with no hydrolytic activity for the latter.

The activation parameters were calculated from the k_{obs} data at pH 7.4 and 9.1 by fitting the data to Equation 5.21 (see Table 5.10, page 276). From these values it can be seen that ΔG^\ddagger is slightly lower for the reaction at pH 9.1 *cf.* 7.4, as would be expected from the observed increases in rate. Other groups have reported the activation parameters for complex-promoted phosphate ester hydrolysis, using the first order rate constant⁷³ and a list of the activation parameters of these complexes is given in Table 5.17. The free energy of activation, ΔG^\ddagger , for the unassisted cleavage of BNPP was estimated to be 120 kJ mol⁻¹ by Burstyn and coworkers from the rate of alkaline hydrolysis of BNPP measured at 25°C (10^{-9} s⁻¹) by Sargeson *et al.* This value is included in Table 5.16 for comparison.

Table 5.17 Activation parameters[§] for phosphate ester hydrolysis and calculated values of first order rate constants (k_{calcd}) for BNPP hydrolysis at 25°C using activation parameters .

Nucleophile ^{†‡}	Substrate [†]	ΔH^\ddagger (kJ mol ⁻¹)	ΔS^\ddagger (J mol ⁻¹ K ⁻¹)	ΔG^\ddagger (kJ mol ⁻¹)	$10^6 \times k_{calcd}$ (s ⁻¹)	Ref.
[(Me ₃ tacn)Cu-OH] ⁺ pH 9.1	BNPP	49	-166	98	34	TW
[(tacn)Cu-OH] ⁺ ^a	BNPP	85	-79	108	0.58	73
[(en) ₂ Ir-OH] ²⁺ ^b	BNPP	69	-93	97	70	23
[(en) ₂ Co-OH] ²⁺ ^c	NPP	71	-65	90	900	77
OH ⁻	BDNPP	80	-107	111	0.15	20
OH ^d	BNPP	-	-	120	0.001	73

ΔG^\ddagger was calculated from the equation $\Delta G^\ddagger = \Delta H^\ddagger - T\Delta S^\ddagger$ at 298 K

[§]Values calculated from the first order rate constant (k_{obs}).

[†]Abbreviations: tacn=1,4,7-triazacyclononane; en=ethylenediamine; NPP=4-nitrophenyl phosphate; BDNPP=bis(2,4-dinitrophenyl) phosphate)

[‡]Addition aquo ligands are not specified.

^a k_{obs} calculated over temperature range 30-90°C and pH > 9.

^b k_{obs} calculated over temperature range 15-35°C and pH range 5.94-10.43.

^c k_{obs} calculated over temperature range 25-45°C and pH 10.

^d ΔG^\ddagger was estimated by Burstyn and coworkers from the measured rate of alkaline hydrolysis of BNPP.⁷³

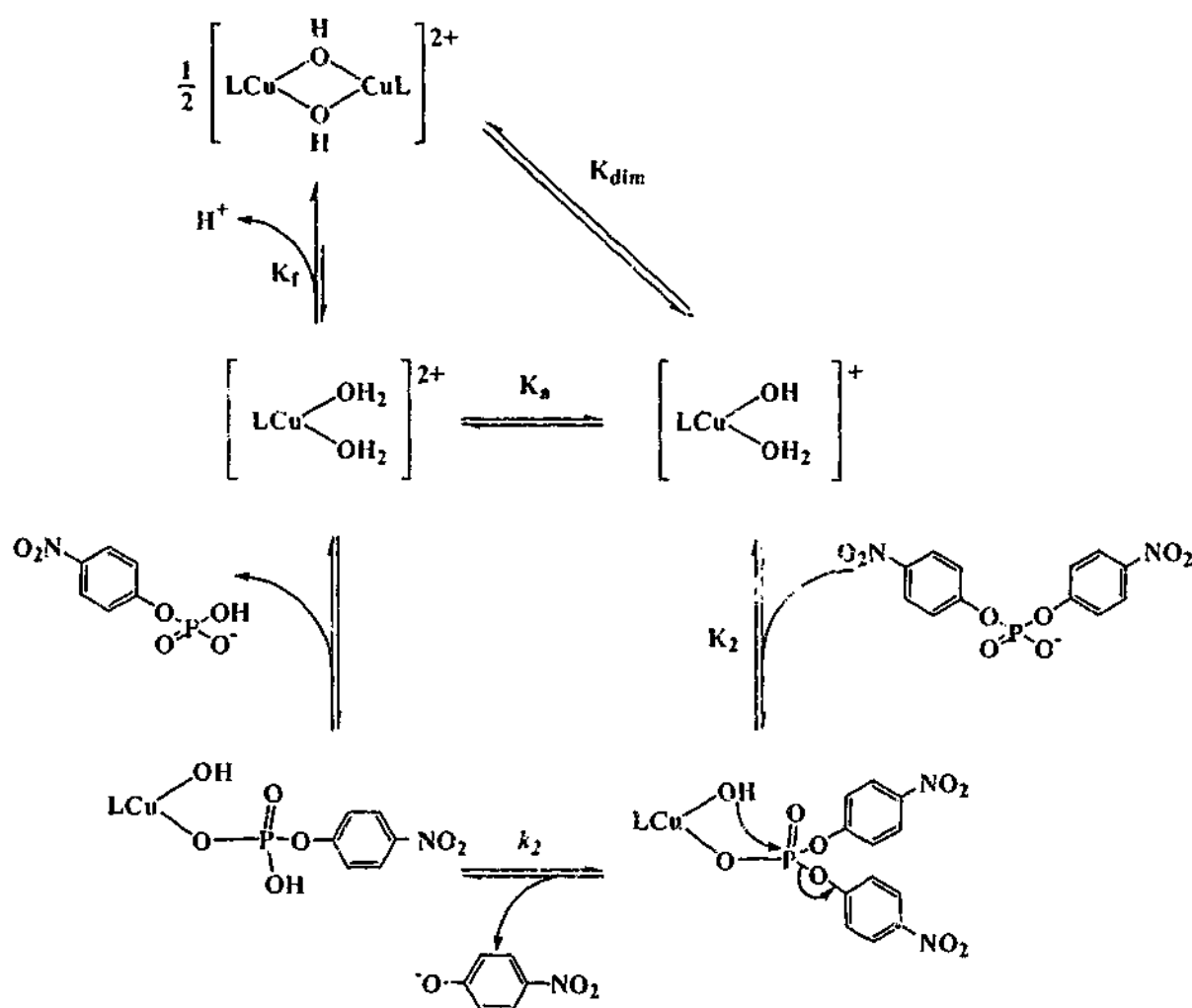
It is clearly seen from Table 5.17 that a lower ΔG^\ddagger is associated with an increase in the rate constant. A decrease in value of ΔG^\ddagger of 10 kJ mol⁻¹ was observed when comparing

the complexes $[\text{Cu}(\text{Me}_3\text{tacn})(\text{H}_2\text{O})_2]^{2+}$ and $[\text{Cu}(\text{tacn})(\text{H}_2\text{O})_2]^{2+}$, coupled with a 60-fold increase in the rate. Similarly, a decrease in ΔG^\ddagger for the complex $[(\text{en})_2\text{Ir}-\text{OH}_2]^{3+}$ *cf.* $[\text{Cu}(\text{tacn})(\text{H}_2\text{O})_2]^{2+}$ of 11 kJ mol^{-1} increases the rate by 120 fold.

From the data presented in the Table 5.17, it can be seen the Cu(II)- Me_3tacn complex exhibits quite different activation parameters, but there is insufficient data reported which allow trends to be established and the factors contributing to these parameters to be elucidated. It is noted, however, that the parameters obtained for the $[\text{Cu}(\text{Me}_3\text{tacn})(\text{H}_2\text{O})_2]^{2+}$ are somewhat different from those of the other complexes presented, with a lower ΔH^\ddagger value and a higher negative ΔS^\ddagger value. It has been noted in the literature^{81,82} that a negative value of ΔS^\ddagger is related to an increase in bond order going from the reactants to the transition state. The increase in the ΔS^\ddagger seen for $[\text{Cu}(\text{Me}_3\text{tacn})(\text{H}_2\text{O})_2]^{2+}$ may correspond to an increase in the bonding at the phosphorus centre, going from free BNPP to the complex-BNPP adduct, followed by intramolecular attack to form to a 5-coordinate intermediate (or activated state), where the number of bonds to the phosphorus has increased by one. The increase in rate for this system relative to the Cu-tacn system seems to be associated with a considerable difference in ΔH^\ddagger , which is partly compensated by the increase in ΔS^\ddagger . At this stage it is difficult to ascertain whether the activation parameters reflect a change in the energetics of the transition state or the initial state. A cursory look at the rate constants in the table again highlights the effectiveness of the Cu- $\text{Me}_3\text{-tacn}$ complex to cleave BNPP relative to the other complexes.

5.4.3 Second Order Rate Constants

$[\text{Cu}(\text{Me}_3\text{tacn})(\text{H}_2\text{O})]^{2+}$ has a similar structure to $[\text{Cu}(\text{tacn})(\text{H}_2\text{O})]^{2+}$, and since the kinetic analysis paralleled that of the tacn complex, although variation in the parameters are apparent, and the analysis returned identical behaviour in terms of the rate the law, the mechanism of hydrolysis can be assumed to be the same as that determined by Burstyn and coworkers for the Cu(II)-tacn system.¹⁹ The mechanism as applies to the system described in this work is shown in Scheme 5.9.



Scheme 5.9 Adapted mechanism as determined by Burstyn and coworkers¹⁹

Note: L = (Me₃tacn)

The mechanism in Scheme 5.9 shows the monomer-dimer equilibrium, and the formation of the catalytically active species, the aquo-hydroxo complex as previously established. Once the phosphate diester has coordinated, attack by the coordinated hydroxide on the phosphorus centre cleaves the first mole of NP from the substrate. Release of the second mole of is achieved by a second catalytic cycle.

Comparison of second order rate constants determined in this work with those reported previously again shows that this system exhibits faster rates of cleavage of BNPP than do many other Cu(II) systems studied (Table 5.18). The Co(III) systems are faster than $[\text{Cu}(\text{Me}_3\text{tacn})(\text{H}_2\text{O})_2]^{2+}$ system, probably because of the larger charge on the Co(III) *cf.* M(II), which better activates the phosphorus centre for nucleophilic attack.⁸

Table 5.18 Second order rate constants for the hydrolysis of BNPP

Complex [†]	$10^3 \times k$ (M ⁻¹ s ⁻¹)	T (°C)	pH	Ref. [‡]
[Cu(Me ₃ tacn)(H ₂ O) ₂] ^{2+†a}	110	42.5	-	TW
[Cu(Me ₃ tacn)(H ₂ O) ₂] ^{2+a}	150	50.0	-	TW
[Cu(Me ₃ tacn)(H ₂ O) ₂] ^{2+a}	190	57.5	-	TW
[Cu(Me ₃ tacn)(H ₂ O) ₂] ^{2+a}	280	65.0	-	TW
[Cu ₂ (tdciH ₃)(OH) ₂] [§]	950	25	8.5	75
[Cu(tacn)(H ₂ O) ₂] ²⁺	1.3	50	7.2	19
[Cu(bpy)(H ₂ O) ₂] ²⁺	20	75	8.0	21
[ZnL ¹ -O] ⁺	0.3	35	7.2	10
[Zn ₂ L ² (OH) ₂] ²⁺	0.115	35.1	10.5	24
[Zn ₂ L ³ (OH) ₂] ²⁺	0.09	35.1	10.9	25
[Co(cyclen)(H ₂ O) ₂] ²⁺	440	50	7.0	22
[Co(tren)(H ₂ O) ₂] ²⁺	8	50	7.0	22
[Co(trpn)(H ₂ O) ₂] ²⁺	3000	50	7.0	22

[†]Abbreviations: tdci= 1,3,5-trideoxy-1,3,5-tris(dimethylamino)-*cis*-inositol; L¹= (S)-1-(2-hydroxy-2-phenylethyl)-1,4,7,10-tetraazacyclododecane; L²= [12]aneN₃; L³= [12]andN₄; tdci=1,3,5-trideoxy-1,3,5-tris(dimethylamino)-*cis*-inositol.

[§] Proposed structure

[‡] = This Work

^aThe active species is the hydroxo aqua species.

As can be seen from Table 5.18, the only Cu(II) complex which exhibits a larger rate constant than [Cu(Me₃tacn)(H₂O)₂]²⁺ is [Cu₂(tdciH₃)(OH)₂][§], reported by Gajda *et al.*⁷⁵ with the proposed structure is shown in Figure 5.18, A. Using the activation parameters calculated in Section 5.3.8 (see Table 5.11, page 277), the second order rate constant for

$[\text{Cu}(\text{Me}_3\text{tacn})(\text{H}_2\text{O})_2]^{2+}$ at 25°C is $0.05 \text{ M}^{-1}\text{s}^{-1}$. The binuclear complex displays a 19-fold increase in the hydrolytic rate compared with $[\text{Cu}(\text{Me}_3\text{tacn})(\text{H}_2\text{O})_2]^{2+}$. The reaction mechanism for the binuclear complex proposes cooperative effects of both copper(II) centres, working together to stabilise the complex-phosphate ester intermediate (Figure 5.18 B).

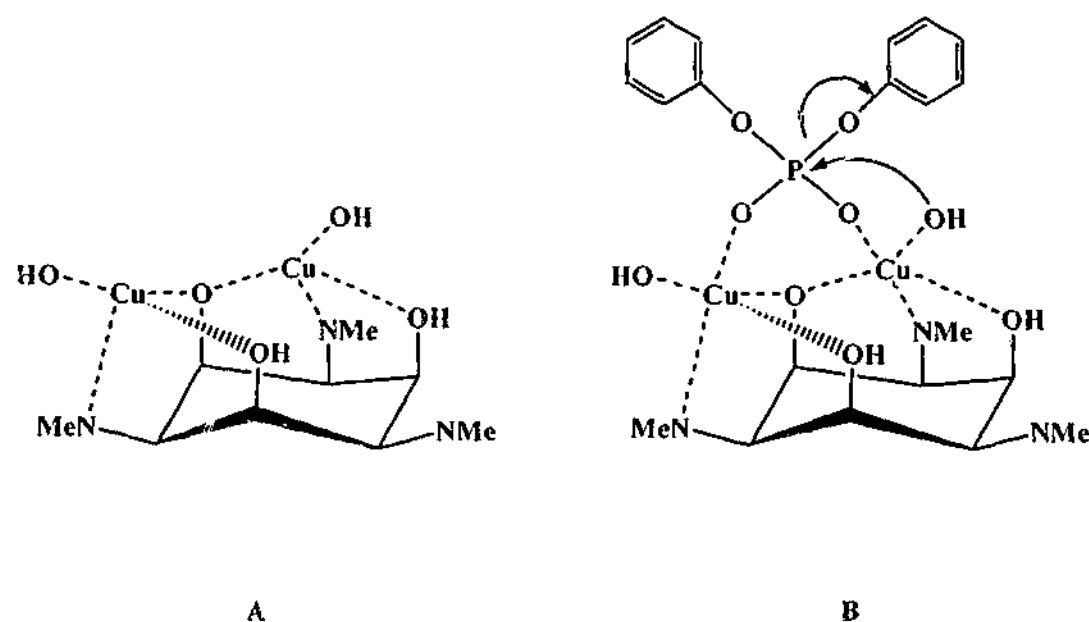


Figure 5.18 A: Proposed structure of $[\text{Cu}_2(\text{tdcH}_3)(\text{OH})_2]$ reported by Gajda *et al.*⁷⁵

It was noted by the authors that additional water ligands are possible.

B: Proposed mechanism for the hydrolysis of BNPP

The values calculated for K_a and K_{dim} , by each of the methods (spectrophotometric titration and rate constant analysis using MATLAB) are somewhat different (see Tables 5.7, page 260 and 5.8 page 267). The high dependency of one parameter on the other has made determining the absolute values of K_a and K_{dim} difficult. The values of K_a and K_{dim} extracted from each of the two methods are within an order of magnitude, however the data are not sufficiently reliable for further detailed comparisons to be made.

Suffice to say the values obtained in this study ($pK_a = 7.5$; $K_{dim} = 2425 \text{ M}^{-1}$ at 50°C) are similar to those reported for the complex $[\text{Cu}(\text{tacn})(\text{H}_2\text{O})_2]^{2+}$ by Burstyn,¹⁹ (pK_a 7.3) while Hay reports it at 7.5 at 35°C .³ K_{dim} was quoted as 1220 M^{-1} by Burstyn.¹⁹

Few studies have a detailed kinetic study to determine the activation parameters for second order rate constants. In comparing the activation parameters between different systems, the order of the rate constant from which they were determined must be taken into account. Direct comparison of the ΔH^\ddagger values is valid as ΔH^\ddagger does not change with a change in rate order, however, the value of ΔS^\ddagger is dependent on the rate order. It is seen from the values presented in Tables 5.11 (page 277) and 5.17 (page 289) that the enthalpy for the reaction of BNPP with $[\text{Cu}(\text{Me}_3\text{tacn})(\text{H}_2\text{O})_2]^{2+}$ is lower than that for the other systems studied.^{73, 23, 77}

Burstyn and coworkers⁷³ also calculated the activation parameters for the $[\text{Cu}(\text{tacn})\text{Cl}_2]$ system, using the second order rate constant and obtained values of $\Delta H^\ddagger = 85 \pm 2 \text{ kJ mol}^{-1}$ and $\Delta S^\ddagger = -40 \pm 5 \text{ J mol}^{-1}$, and therefore $\Delta G^\ddagger = 97 \text{ kJ mol}^{-1}$ at 298 K. The value for ΔG^\ddagger ($\Delta G^\ddagger = 80 \text{ kJ mol}^{-1}$ at 298 K) presented in this work is lower than that determined by Burstyn and coworkers¹⁹ (see Table 5.19), as expected with a faster rate of reaction.

Table 5.19 Activation parameters for phosphate ester hydrolysis and calculated values of second order rate constants (k_{calcd}) for BNPP hydrolysis at 25°C.

Nucleophile ^{†‡}	Substrate [†]	ΔH^\ddagger (kJ mol ⁻¹)	ΔS^\ddagger (J mol ⁻¹ K ⁻¹)	ΔG^\ddagger (kJ mol ⁻¹)	k_{calcd} (M ⁻¹ s ⁻¹)	Ref.
[(Me ₃ tacn)Cu-OH] ⁺	BNPP	33	-159	80	0.05	TW
[(tacn)Cu-OH] ^{+a}	BNPP	85	-40	98	6 × 10 ⁻⁵	73

ΔG^\ddagger was calculated from the equation $\Delta G^\ddagger = \Delta H^\ddagger - T\Delta S^\ddagger$ at 298 K

[§]Values calculated from the second order rate constants

It is again observed that the value of ΔH^\ddagger is lower for the [Cu(Me₃tacn)(H₂O)₂]²⁺ than for the [Cu(tacn)(H₂O)₂]²⁺ complex, and that the value of ΔS^\ddagger is larger. As has been previously mentioned, a negative ΔS^\ddagger is indicative of an increase in bond order and the larger value may correspond an increased number of bonds to the phosphorus centre in the complex-BNPP intermediate *cf.* free BNPP.

Although very similar, the two complexes [Cu(tacn)(H₂O)₂]²⁺ and [Cu(Me₃tacn)(H₂O)₂]²⁺ display markedly different rates for the hydrolysis of BNPP. This faster rate exhibited by [Cu(Me₃tacn)(H₂O)₂]²⁺ may be due to a number of factors. The internal nucleophile (Cu-OH) may be more efficient in the Me₃tacn complex, the affinity for this complex for BNPP may be higher or the alkylation of the tacn macrocycle may stabilise the complex-BNPP intermediate. Any or all of these factors will contribute to an increase in the rate of hydrolysis.

5.4.4 Catalytic Turnover Experiment

It is clearly demonstrated from the data shown in Table 5.14 that the hydrolysis of BNPP by $[\text{Cu}(\text{Me}_3\text{tacn})(\text{H}_2\text{O})_2]^{2+}$ is truly catalytic. The greater than stoichiometric production of the 4-nitrophenylate anion (*cf.* [complex]) is indicative of this. The complex showed a turnover rate of up to 0.9 turnovers per day at 50°C when the substrate was in a 10 fold excess. The number of turnovers achieved over the 63 day period of the experiment was up to a total 21.

Catalytic turnover of BNPP by the complex $[\text{Cu}(\text{tacn})\text{Cl}_2]$ has also been confirmed by Burstyn and coworkers.⁶¹ The reaction were carried out at pH 7.24 (HEPES) and a concentration of BNPP of 5 mM. The actual rate of turnover was not reported, only that a greater than stoichiometric amount of NP was produced from the reaction. Hay *et al.*³ reports catalytic turnover for the reaction of $[\text{Cu}(\text{tacn})\text{Cl}_2]$ with the substrate 2,4-dinitrophenyldiethyl phosphate (a phosphate triester). The rate of turnover with this substrate was found to be much higher, at 2.2 turnovers hr^{-1} at pH 7.0 at 25°C. Catalytic turnover was also reported by Gajda *et al.*⁷⁵ with the complex $[\text{Cu}_2(\text{tdciH}_3)(\text{OH})_2]$ (tdci=1,3,5-trideoxy-1,3,5-tris(dimethylamino)-*cis*-inositol). The reaction was monitored for 400 minutes, during which time 9 turnovers were observed. The [complex] was 0.255 mM and the substrate was in a 10.5 fold excess. The rate of turnover for this system equates to *ca.* 32 turnovers per day, which is faster than the system studied in this work, which has a rate of 0.9 turnovers per day.

5.5 Concluding Remarks and Future Directions

Second order rate constants for the hydrolysis of bis(4-nitrophenyl)phosphate by the complex $[\text{Cu}(\text{Me}_3\text{tacn})(\text{H}_2\text{O})_2]^{2+}$ were determined for 4 temperatures, ranging between 42.5°C and 65°C. The activation parameters were calculated from the determined rate constants.

It has been shown here that complex $[\text{Cu}(\text{Me}_3\text{tacn})(\text{H}_2\text{O})_2]^{2+}$ enhances phosphodiester hydrolysis, with the second order rate constant calculated to be $0.15 \text{ M}^{-1}\text{s}^{-1}$ at 50°C. This rate constant is significantly larger than for other mononuclear copper(II) complexes reported in the literature to date. Other complexes which exhibit larger rate constants are either polynuclear in nature or contain harder Lewis acids, such as Co(III) and Ln(III). The complex also shows catalytic turnover, with a rate of up to 0.9 turnovers per day at pH 9.1 and 50°C, and up to a total of 21 turnovers achieved during the 63 day period for which the reaction was measured.

From previous studies (see Section 1.5 of the Introduction) and those conducted in this work, the number of available sites for the coordination of a phosphate ester can increase the rate of substrate hydrolysis. As it was observed that the copper(II) complex of the alkylated tacn, Me_3tacn , increases the rate, it would be of interest to investigate the effect on the rate of hydrolysis of complexes of other *N*-alkylated tacn derivatives. It would also be interesting to synthesise bi- and tri-nuclear complexes of $\text{Me}_2\text{tacn-R}$, and compare the rates of hydrolysis. Future work may also involve the testing of $[\text{Cu}(\text{Me}_3\text{tacn})(\text{H}_2\text{O})_2]^{2+}$ for the ability to hydrolyse both DNA and RNA. Modification of the ligand in such a way as to prevent the formation of the dimeric complex, which is inactive in the hydrolysis of phosphate esters, would be expected to yield even greater

rate enhancements. Further kinetic investigations are also warranted for the copper complex of the tris(tacn) ligand, which also showed a large increase in the observed rate over that of the uncatalysed reaction.

Relating the system studied in this work to enzymes such as alkaline phosphatase shows that although this complex is one of the most efficient studied for a divalent metal complex, its rate enhancement of the hydrolysis of the phosphodiester is by no means close to that exhibited by nature. These enzymes show rates many orders of magnitude higher than those achieved here. Nevertheless, two complexes, namely $[\text{Cu}(\text{Me}_3\text{tacn})(\text{H}_2\text{O})_2]^{2+}$ and $[\text{Cu}_3(\text{T}_3\text{mes})(\mu\text{-OH})_6](\text{ClO}_4)_6 \cdot 6\text{H}_2\text{O}$, show promising rate enhancements for the hydrolysis of 4-bis(nitrophenyl) phosphate.

5.6 Experimental

Materials, reagents and Instruments

Materials and Reagents: 1,4,7-trimethyl-1,4,7-triazacyclononane was obtained from Unilever and was distilled prior to use. The buffers CHES (2-(*N*-cyclohexylamino)ethanesulfonic acid), HEPES (*N*-(2-hydroxyethyl)piperazine-*N'*-ethanesulfonic acid), MES (2-(*N*-morpholino)ethanesulfonic acid), MOPS (3-(*N*-morpholino)propanesulfonic acid), and TAPS (*N*-tris(hydroxymethyl)methyl-3-aminopropanesulfonic acid) were purchased from Sigma Chemical Co. All other chemicals were purchased from Aldrich Chemical Co. Sodium perchlorate solution was made from standardised sodium hydroxide solution neutralised with perchloric acid. All water was distilled prior to use.

Instruments: Kinetic measurements and catalytic turnover spectra were made on a Varian Cary 5G spectrophotometer, equipped with a water-jacketed cell holder. The temperature was regulated ($\pm 0.1^\circ\text{C}$) by an external circulating water bath (Varian Cary). pH was measured with an Orion electrode. Elemental analysis was performed by Otago University, Otago, New Zealand.

Buffers

Buffers were made up in 100 ml volumes using the methods as described on the WWW site at <http://www.bi.umist.ac.uk/users/mjfrbn/Buffers/Makebuf.asp>. The free acid was used at a concentration of 0.150 M and ionic strength of 0.382 M, so that a 1:3 dilution with BNPP and $[\text{Cu}(\text{Me}_3\text{tacn})(\text{H}_2\text{O})_2]^{2+}$ solutions gave the desired final concentrations. The solutions were made up to *ca.* 90 ml, and then titrated to the desired pH with 1 M NaOH and a pH meter.

[Cu(Me₃tacn)(H₂O)₂]²⁺ Solutions

Solutions of [Cu(Me₃tacn)(H₂O)₂]²⁺ were made to three times the desired final concentration so that 1:3 dilution with buffer and BNPP solutions gave the desired final concentrations for the kinetic experiments. Solutions were made up at concentrations of 3.0 mM, 4.5 mM, 6.0 mM, 7.5 mM, 9.0 mM, 10.5 mM, 12.0 mM, 13.5 mM, 15.0 mM and 22.5 mM. Standardised NaClO₄ solution (1.044 M) was added so that the solutions each had an ionic strength of 22.5 mM. The solutions were stored at 4°C.

BNPP solutions

Solutions of BNPP used for the kinetic experiments were made at thirty times the desired final concentration using BNPP (0.0155 g) in water (100 ml) and diluted 1:10. The final solution of BNPP was then three times the concentration to be used for the hydrolysis kinetics.

Solutions of BNPP used in the saturation experiment were made in two ways. The solutions which had a final concentrations of 4.0 mM or less, were diluted from a stock solution of 12.0 mM of BNPP (0.0121 g, 0.0356 mmol, 25 ml). Due to the limited solubility of BNPP in aqueous solution, the experimental solutions with higher concentrations of BNPP (*i.e.* final concentrations of >4 mM) were made with 0.0136 g (0.0400 mmol) and 0.0170 g (0.0509 mmol), the copper(II) and NaClO₄ solutions added in the appropriate volumes and made up to a final volume of 5 ml.

A 3.0 mM solution of BNPP (0.0511 g, 0.0444 mol, 50 ml) was made up for use in the catalytic turnover experiments, and diluted 1:3 so that the final concentration of BNPP in the solution was 1.0 mM.

Kinetic Studies

The rate of production of 4-nitrophenylate was monitored spectrophotometrically at 400 nm. Reactions were performed in either quartz or glass 1 cm cuvettes, fitted with teflon stoppers, with a final volume of 4.02 ml.

In a typical experiment, stock solutions of $[\text{Cu}(\text{Me}_3\text{tacn})(\text{H}_2\text{O})_2](\text{ClO}_4)_2$ in water (3.0 mM, 4.5 mM, 6.0 mM, 7.5 mM, 9.0 mM, 10.5 mM, 12.0 mM, 13.5 mM, 15.0 mM and 22.5 mM) with added NaClO_4 so that the ionic strength of each solution was 22.5 mM, were added to an equal volume of buffer solution (CHES, HEPES, MES, MOPS, or TAPS) (150 mM) containing sodium perchlorate to maintain the ionic strength, and the temperature allowed to equilibrate for approximately 10 minutes. An equal volume of stock solution of BNPP (0.045 mM) was added and the cuvettes inverted to mix the solutions. The temperature was then allowed to equilibrate for a further 2 minutes before readings commenced. The stock solutions were made three times the final desired concentration so that the final concentrations in the cuvettes were those required, *i.e.* complex final concentration of 1.0 – 7.5 mM, buffer final concentration of 50 mM, a final ionic strength of 150 mM, and BNPP final concentration of 0.015 mM. Four different temperatures were used in most cases, 42.5, 50.0, 57.5 and 65.0°C ($\pm 0.1^\circ\text{C}$). Reactions were generally followed for 8000 minutes, with an absorbance reading taken every 5 minutes.

Catalytic Turnover

Solutions of BNPP (1 mM), $[\text{Cu}(\text{Me}_3\text{tacn})(\text{H}_2\text{O})_2](\text{ClO}_4)_2$ (1000 μM , 25 μM , 10 μM and 1 μM) and NaClO_4 (to maintain the ionic strength at 150 mM) in 50 mM of buffer

(MOPS, pH 5.9; MES, pH 7.0; CHES, pH 9.1), as well as a control for each pH, identical to the other solutions except containing no $[\text{Cu}(\text{Me}_3\text{tacn})(\text{H}_2\text{O})_2](\text{ClO}_4)_2$, were incubated in an oven at 50°C for 63 days. Samples were removed at intervals and the electronic spectra measured between 1200 nm and 200 nm at 50°C . The aliquots were returned to the stock solution. In the cases where the absorbance of the original solution exceeded the limits of the instrument, a 1.0 cm^3 aliquot was removed from the stock solution and diluted appropriately. These solutions were discarded after measurements. To determine the catalytic turnover, the absorbance at 400 nm was recorded and plotted against time, with the appropriate dilution factors taken into account. The catalytic turnover was corrected for the uncatalysed reactions at each pH, by subtracting the blank absorbance from that of the sample. To determine the concentration of BNPP in solution, and hence the number of turnovers, molar extinction coefficients of 1600, 11800 and $20000\text{ M}^{-1}\text{cm}^{-1}$ were used for pH 5.9, 7.4 and 9.1, respectively.

Synthesis of Complexes

The complexes used in the screening studies for the hydrolysis of BNPP were synthesised as described in the preceding chapters or below.

$[\text{Cu}(\text{tren})\text{H}_2\text{O}](\text{ClO}_4)_2$

Tren (2.40 g, 0.016 mol) was dissolved in ethanol (20 ml) and added to a solution of $\text{Cu}(\text{ClO}_4)_2 \cdot 6\text{H}_2\text{O}$ (6.09 g, 0.016 mol) in ethanol (40 ml). A solid formed immediately and the mixture was stirred for 10 minutes. The solid was filtered under vacuum filtration, washed with ethanol and dried at 90°C for one hour.

Yield: 5.17 g (76 %). Microanalytical data: Found (%): C 17.5; H 4.6; N 13.2.
Calculated for $\text{CuC}_6\text{H}_{20}\text{N}_4\text{O}_9\text{Cl}_2$ (%): C 16.9; H 4.7; N 13.1.

$[\text{Zn}(\text{tren})\text{H}_2\text{O}](\text{ClO}_4)_2$

$[\text{Zn}(\text{tren})\text{H}_2\text{O}](\text{ClO}_4)_2$ was synthesised in an analogous way to the copper complex, using tren (2.17 g, 0.015 mol) was dissolved in ethanol (20 ml) and added to a solution of $\text{Zn}(\text{ClO}_4)_2 \cdot 6\text{H}_2\text{O}$ (5.53 g, 0.015 mol) in ethanol (40 ml). A solid formed immediately and the mixture was stirred for 10 minutes. The solid was filtered under vacuum filtration, washed with ethanol and dried at 90°C for one hour.

Yield: 4.97 g (77 %). Microanalytical data: Found (%): C 17.0; H 4.6; N 12.9;
Calculated for $\text{ZnC}_6\text{H}_{20}\text{N}_4\text{O}_9\text{Cl}_2$ (%): C 16.8; H 4.7; N 13.1.

$[\text{Ni}(\text{Me}_3\text{tacn})(\text{H}_2\text{O})_3](\text{ClO}_4)_2$ and $[\text{Ni}(\text{Me}_3\text{tacn})(\text{H}_2\text{O})_3] \cdot 2\text{CH}_3\text{CN}$

Me_3tacn (1.00 g, 5.84 mmol) was dissolved in ethanol (20 ml) and a solution of $\text{Ni}(\text{ClO}_4)_2 \cdot 6\text{H}_2\text{O}$ (4.27 g, 11.7 mmol, in excess), also in ethanol (20 ml). The solution was filtered to remove any precipitate of $\text{Ni}(\text{OH})_2$ that formed and the solution was left to evaporate slowly. Blue crystals formed overnight, the bulk of which were collected by vacuum filtration, washed with acetone and air dried. The remaining crystals were kept for X-ray crystallographic analysis (see Appendix 1.10).

Yield: 0.64 g, (23 %). Microanalytical data: Found (%): C 22.3; H 5.2; N 8.7;
Calculated for $\text{NiC}_9\text{H}_{27}\text{N}_3\text{O}_{11}\text{Cl}_2$ (%): C 22.4; H 5.6; N 8.7.

After addition of acetonitrile to the above solution, a different product formed. The purple crystals was collected by vacuum filtration, washed with ether and air dried.

Yield: 1.27 g, (38 %). Microanalytical data: Found (%): C 27.4; H 5.4; N 11.9;
Calculated for $\text{NiC}_{13}\text{H}_{33}\text{N}_5\text{O}_{11}\text{Cl}_2$ (%): C 27.6; H 5.9; N 12.4.

[Cu(tacn)Cl₂]

The copper(II) complex of tacn was synthesised according to published methods,⁸³ using CuCl₂.2H₂O (1.32 g, 7.7 mmol) and tacn.3HCl (0.92 g, 3.9 mmol).

Yield: 0.96 g, (94 %). Microanalytical data: Found (%): C 27.2; H 5.9; N 16.0; Calculated for CuC₉H₁₅N₃Cl₂ (%): C 27.3; H 5.7; N 15.9.

[(Me₃tacn)Cu(μ-OH)₂Cu(Me₃tacn)](ClO₄)₂

Crystals which formed from the kinetic solutions were analysed by X-ray crystallography, and the unit cell found to be the same as that as for the complex reported by Chaudhuri *et al.*⁶² Unit cell: a = 8.1519 Å; b = 8.571 Å; c = 20.309 Å; α = 88.932°; β = 90.071°; γ = 90.03°. Lit.⁶² : a = 20.410 Å; b = 8.257 Å; c = 20.410 Å; α = 90°; β = 94.44°; γ = 90°.

5.7 References

- (1) Yun, J. W., Tanase, T., Lippard, S.J. *Inorg. Chem.* **1996**, *35*, 7590.
- (2) Gómez-Tagle, P., Yatsimirsky, A. K. *J. Chem. Soc., Dalton Trans.* **2001**, 2663.
- (3) Hay, R. W., Govan, N. *Polyhedron* **1998**, *17*, 463.
- (4) Hegg, E. L., Burstyn, J. N. *J. Am. Chem. Soc.* **1995**, *117*, 7015.
- (5) Hegg, E. L., Burstyn, J. N. *Inorg. Chem.* **1996**, *35*, 7474.
- (6) Hegg, E. L., Deal, K. A., Kiessling, L. L., Burstyn, J. N. *Inorg. Chem.* **1997**, *36*, 1715.
- (7) Hegg, E. L., Burstyn, J. N. *Coord. Chem. Rev.* **1998**, *173*, 133.
- (8) Hegg, E. L., Mortimore, S. H., Cheung, C. L., Huyett, J. E., Powell, D. R., Burstyn, J. N. *Inorg. Chem.* **1999**, *38*, 2961.
- (9) Kimura, E. *Prog. Inorg. Chem* **1994**, 443.
- (10) Kimura, E., Kodama, Y., Koike, T., Shiro, M. *J. Am. Chem. Soc.* **1995**, *117*, 8304.
- (11) Kimura, E., Aoki, S., Koike, T., Shiro, M. *J. Am. Chem. Soc.* **1997**, *119*, 3068.
- (12) Kimura, E., Koike, T. *Adv. Inorg. Chem.* **1997**, *44*, 229.
- (13) Kimura, E., Koike, T., Shionoya, M. *Structure and Bonding* **1997**, *89*, 1.
- (14) Koike, T., Kimura, E. *J. Am. Chem. Soc.* **1991**, *113*, 8935.
- (15) Hendry, P., Sargeson, A.M. *Prog. Inorg. Chem.* **1990**, *38*, 201.
- (16) Kövári, E., Krämer, R. *J. Am. Chem. Soc.* **1996**, *118*, 12704.
- (17) Berg, T., Simeonov, A., Janda, K. D. *J. Comb. Chem.* **1999**, *1*, 96.
- (18) Radzicka, A., Wolfenden, R. *Science* **1995**, *267*, 90.
- (19) Deal, K., Burstyn, J. *Inorg. Chem.* **1996**, *35*, 2792.
- (20) Kirby, A. J., Younas, M. *J. Chem. Soc. B* **1970**, 510.
- (21) Morrow, J. R., Trogler, W. C. *Inorg. Chem.* **1988**, *27*, 3387.

-
- (22) Chin, J., Banzsczyk, M., Jubian, V., Zou, X. *J. Am. Chem. Soc.* **1989**, *111*, 186.
- (23) Hendry, P., Sargeson, A.M. *J. Am. Chem. Soc.* **1989**, *111*, 2521.
- (24) Bazzicalupi, C., Bencini, A., Bianchi, A., Fusi, V., Giorgi, C., Paoletti, P., Valtancoli, B., Zanchi, D. *Inorg. Chem.* **1997**, *36*, 2784.
- (25) Bencini, A., Berni, E., Bianchi, A., Fedi, V., Giorgi, C., Paoletti, P., Valtancoli, B. *Inorg. Chem.* **1999**, *38*, 6323.
- (26) Ibrahim, M. M., Shimomura, N., Ichikawa, K., Shiro, *Inorg. Chim. Acta* **2001**, *313*, 125.
- (27) Albedyhl, S., Averbuch-Pouchot, M. T., Belle, C., Krebs, B., Pierre, J. L., Saint-Aman, E., Torelli, S. *Eur. J. Inorg. Chem.* **2001**, 1457.
- (28) Roigk, A., Yescheulova, O. V., Federov, Y. V., Fedorova, O. A., Gromov, S. P., Schneider, H-J. *Org. Lett.* **1999**, *1*, 833.
- (29) Takeda, N., Irisawa, M., Komiyama, M. *J. Chem. Soc., Chem. Commun.* **1994**, 2773.
- (30) Oh, S. J., Song, K. H., Whang, D., Kim, K., Yoon, T. H., Moon, H., Park, J. W. *Inorg. Chem.* **1996**, *35*, 3780.
- (31) Rammo, J., Schneider, H-J. *Inorg. Chim. Acta* **1996**, *251*, 125.
- (32) Bazzicalupi, C., Bencini, A., Berni, A., Fedi, V., Fusi, V., Giorgi, C., Pailletti, P., Valtancoli, B. *Inorg. Chem.* **1999**, *38*, 4115.
- (33) Morrow, J. R., Buttrey, L. A., Shelton, V. M., Berback, K. A. *J. Am. Chem. Soc.* **1992**, *114*, 1903.
- (34) Chu, F., Smith, J., Lynch, V.M., Anslyn, E. V. *Inorg. Chem.* **1995**, *34*, 5689.
- (35) Young, M. J., Chin, J. *J. Am. Chem. Soc.* **1995**, *117*, 10577.
- (36) Chin, K. O. A., Morrow, J. R. *Inorg. Chem.* **1994**, *33*, 5036.
- (37) Komiyama, M., Yoshinari, K. *J. Org. Chem.* **1997**, *62*, 2155.

-
- (38) Hurst, P., Takasaki, B.K., Chin, J. *J. Am. Chem. Soc.* **1996**, *118*, 9982.
- (39) Molenveld, P., Engbersen, J.F.J., Reinhoudt, D.N. *Angew. Chem. Int. Ed.* **1999**, *38*, 3189.
- (40) Jenkins Autry, L. A., Bashkin, J.K. *Inorg. Chim. Acta* **1997**, *263*, 49.
- (41) Detmer, C. A., Pamatong, F. V., Bocarsly, J. R. *Inorg. Chem.* **1997**, *36*, 3676.
- (42) Detmer, C. A., Pamatong, F.V., Bocarsly, J.R. *Inorg. Chem.* **1996**, *35*, 6292.
- (43) Silver, G. C., Trogler, W. C. *J. Am. Chem. Soc.* **1995**, *117*, 3983.
- (44) Rangunathan, K. G., Schneider, H-J. *Angew. Chem. Int. Ed. Engl.* **1996**, *35*, 1219.
- (45) Hettich, R., Schneider, H.-J. *J. Chem. Soc., Perkin Trans.* **1997**, 2069.
- (46) Gómez-Tagle, P., Yatsimirsky, A. K. *J. Chem. Soc., Dalton Trans.* **1998**, 2957.
- (47) Yashiro, M., Ishikubo, A., Komiyama, M. *Chem. Commun.* **1997**, 83.
- (48) Irisawa, M., Takeda, N., Komiyama, M. *J. Chem. Soc., Chem. Commun.* **1995**, 1221.
- (49) Yashiro, M., Ishikubo, A., Komiyama, M. *Chem. Commun.* **1995**, 1793.
- (50) Miyama, S., Asanuma, H., Komiyama, M. *J. Chem. Soc., Perkins Trans. 2* **1997**, 1685.
- (51) Chapman, W. H., Breslow, R. *J. Am. Chem. Soc.* **1995**, *117*, 5462.
- (52) Wang, C., Choudhary, S., Vink, C. B., Secord, E. A., Morrow, J. R. *Chem. Commun.* **2000**, 2509.
- (53) Shelton, V. M., Morrow, J. R. *Inorg. Chem.* **1991**, *30*, 4295.
- (54) Bruice, T. C., Tsubouchi, A., Dempcy, R.O., Olson, L.P. *J. Am. Chem. Soc.* **1996**, *118*, 9867.
- (55) McCue, K. P., Morrow, J. R. *Inorg. Chem.* **1999**, *38*, 6136.
- (56) McCue, K. P., Voss, D. A., Jr, Marks, C., Morrow, J. R. *J. Chem. Soc., Dalton Trans.* **1998**, 2961.

-
- (57) Itoh, T., Hisada, H., Sumiya, T., Hosono, M., Usui, Y., Fujii, Y. *Chem. Commun.* **1997**, 677.
- (58) Jenkins, L. A., Bashkin, J.K., Autry, M. E. *J. Am. Chem. Soc.* **1996**, *118*, 6822.
- (59) Parand, A., Royer, A. C., Cantrell, T. L., Meitzel, M., Memon, N., Vincent, J. B., Crowder, M. W. *Inorg. Chim. Acta* **1998**, 211.
- (60) Kimura, E., Hashimoto, H., Koike, T. *J. Am. Chem. Soc.* **1996**, *118*, 10963.
- (61) Burstyn, J., Deal K. *Inorg. Chem.* **1993**, *32*, 3585.
- (62) Chaudhuri, P., Ventur, D., Weighardt, K., Peters, E-M., Peters, K., Simon, A. *Angew. Chem., Int. Ed. Engl.* **1985**, *24*, 57.
- (63) The spectra were modelled by Dr Joël Brugger from The South Australian Museum, Adelaide., South Australia, Australia and Department of Geology and Geophysics, University of Adelaide, South Australia, Australia .
- (64) Brugger, J., McPhail, D. C., Black, J., Spiccia, L. *Geochimica Cosmochimica Acta* **2001**, *65*, 2691.
- (65) Neumaier, A. **1998**, MINQ -General definite and bound constrained indefinite quadratic programming. WWW document, <http://solon.com.univie.ac.at/~neum/software/minq/>.
- (66) Nelder, J. A., Mead, R. *The Comp. J.* **1965**, *7*, 308.
- (67) Whitfield, M., in *Chemical Oceanography*; 2nd ed.: New York, 1975.
- (68) MATLAB Version 5.3.1.29215a (R11.1) (1999); The Maths Works Inc.
- (69) Fuoss, R. M. *J. Am. Chem. Soc.* **1958**, *80*, 5059.
- (70) Davies, C. W. *Ionic Association*; Butterworths: London, 1965.
- (71) Burgess, J. *Metal Ions In Solution*; Ellis Horwood Limited: Sussex, England, 1978.

-
- (72) *Handbook of Chemistry and Physics*; 57th ed.; CRC Press, Inc.: Cleveland, Ohio, 1976-1977.
- (73) Deal, K., Hengge, A. C., Burstyn, J. N. *J. Am. Chem. Soc.* **1996**, *118*, 1713.
- (74) Lui, S., Luo, Z., Hamilton, A. D. *Angew. Chem. Int. Ed. Engl.* **1997**, *36*, 2678.
- (75) Gajda, T., Düpre, Y., Török, I., Harmer, J., Schweiger, A., Sander, J., Kuppert, D., Hegetschweiler, K. *Inorg. Chem.* **2001**, *40*, 4981.
- (76) Deal, K. A., Park, G., Shao, J., Chasteen, N. D., Brechbiel, M. W., Planalp, R. P. *Inorg. Chem.* **2001**, *40*, 4176.
- (77) Jones, D. R., Lindoy, L. F., Sargeson, A. M. *J. Am. Chem. Soc.* **1983**, *105*, 7327.
- (78) Koike, T., Inoue, M., Kimura, E., Shiro, M., *J. Am. Chem. Soc.* **1996**, *118*, 3091.
- (79) Tsubomura, T., Ezawa, M., Sato, T., Sakai, K. *Inorg. Chim. Acta* **2000**, *310*, 265.
- (80) Kirby, A. J., Jenks, W. P. *J. Am. Chem. Soc.* **1965**, *87*, 3209.
- (81) Langford, C. H., Gray, H. B. *Ligand Substitution Processes*; W. A. Benjamin Inc.: New York, 1966.
- (82) Atwood, J. D. *Inorganic and Organometallic Reaction Mechanisms*; Cole Publishing Co.: Monterey, California, 1985.
- (83) Schwindinger, W. F., Fawcett, T. G., Lalancette, R. A., Potenza, J. A., Schugar, H. J. *Inorg. Chem.* **1980**, *19*, 1379.

Appendix One

Crystallography Data

The X-ray crystal structure determination of **3** was carried out by Dr E. R. T. Tiekink of the University of Adelaide. The structure of **4** was solved by Prof. A. White of the University of Western Australia. Structure determinations of **8** and **10** were carried out by Paul Jensen of Monash University. Crystal structures of **9** and **19** were performed by Dr C. Kepert of Monash University and those of **12** and **14** were carried out by Dr G. D. Fallon of Monash University. The crystal structure of $[\text{Ni}(\text{Me}_3\text{tacn})(\text{H}_2\text{O})_3](\text{ClO}_4)_2$ was solved by Mr A. Warden of Monash University.

Appendix One

1.1 [Cu₂(T₂-p-X)Cl₄] (3)

diffractometer	Rigaku AFC6R
radiation type	Mo-K α
radiation wavelength	0.7107
radiation monochromator	graphite
2 θ (°)	55.4
temperature (K)	293
crystal description	dark blue needle
chemical formula	C ₂₀ H ₃₆ Cu ₂ N ₆ Cl ₄
fw, g mol ⁻¹	629.45
crystal system	orthorhombic
space group	Pbca
a, Å	13.11(2)
b, Å	30.14(1)
c, Å	7.28(1)
α , deg	90
β , deg	90
γ , deg	90
V, Å ³	2879(5)
Z	4
D _c , g cm ⁻³	1.452
F(000)	1296
μ (MoK α), cm ⁻¹	1.867
No. data measured	3850
No. unique data	3849
No. Observed data ($I \geq 3\sigma$)	1088
R	0.059
R _w	0.054

Appendix One

1.2 [Cu₂(T₂-PrO)Br₂]Br·2H₂O (4)

diffractometer	Enraf-Nonius CAD-4
radiation type	Mo-K α
radiation wavelength	0.7107
radiation monochromator	graphite
2 θ (°)	58°
temperature (K)	300
crystal description	dark blue needle (0.55 × 0.30 × 0.16)
chemical formula	C ₃₆ H ₄₆ CuN ₁₀ O ₁₆ P ₂
fw, g mol ⁻¹	716.30
crystal system	triclinic
space group	$P\bar{1}$ (#2)
a, Å	7.438(1)
b, Å	13.326(2)
c, Å	13.812(3)
α , deg	64.635(2)
β , deg	78.858(3)
γ , deg	89.469(3)
V, Å ³	1209.6(7)
Z	2
D _c , g cm ⁻³	1.966
F(000)	712
μ (MoK α), cm ⁻¹	67.4
No. data measured	13565
No. unique data	5844
No. Observed data ($I \geq 3\sigma$)	4201
R	0.054
R _w	0.061

Appendix One

1.2 [Cu(tacn)₂](BNPP) (8)

diffractometer	Nonius Kappa CCD
radiation type	Mo-K α
radiation wavelength	0.71073
radiation monochromator	graphite
chemical formula	C ₃₆ H ₄₆ Cu ₁₀ O ₁₆ P ₂
fw, g mol ⁻¹	1000.30
crystal system	Monoclinic
space group	C2/c (#15)
2 θ (°)	59.1
temperature (K)	123
crystal description	Dark blue needle (0.33 × 0.22 × 0.025 mm)
a, Å	24.7105(5)
b, Å	12.8627(3)
c, Å	14.0079(3)
α , deg	90
β , deg	106.600(1)
γ , deg	90
V, Å ³	4266.76(16)
Z	4
D _c , g cm ⁻³	1.557
F(000)	2076
μ (MoK α), cm ⁻¹	6.71
No. data measured	30443
No. unique data	6249
No. Observed data ($I \geq 3\sigma$)	3683
R	0.047
R _w	0.050

Appendix One

1.4 $[\text{Cu}_3(\text{Me}_3\text{tacn})_3(\text{PhP})_2](\text{ClO}_4)_2 \cdot \frac{1}{2}\text{H}_2\text{O}$ (9)

diffractometer	Nonius Kappa CCD
radiation type	Mo-K α
radiation wavelength	0.71073
radiation monochromator	graphite
2 θ (°)	60
temperature (K)	173
crystal description	dark blue needle
chemical formula	$\text{C}_{39}\text{H}_{74}\text{Cu}_3\text{N}_9\text{O}_{16.5}\text{Cl}_2\text{P}_2$
fw, g mol ⁻¹	1188.34
crystal system	triclinic
space group	$P\bar{1}$ (#2)
a, Å	9.8053(2)
b, Å	12.9068(2)
c, Å	22.1132(3)
α , deg	98.636(1)
β , deg	99.546(1)
γ , deg	101.1733(8)
V, Å ³	2658.98(8)
Z	2
D _c , g cm ⁻³	1.569
F(000)	1308.0
$\mu(\text{MoK}\alpha)$, cm ⁻¹	14.13
No. data measured	12379
No. unique data	12379
No. Observed data ($I \geq 3\sigma$)	9559
R	0.038
R _w	0.040

Appendix One

1.5 $[\text{Cu}_2(\text{T}_2\text{-}m\text{-X})(\text{NPP})(\mu\text{-OH})](\text{ClO}_4)\cdot\frac{1}{2}\text{H}_2\text{O}$ (10)

diffractometer	Nonius Kappa CCD
radiation type	Mo-K α
radiation wavelength	0.7107
radiation monochromator	graphite
2 θ (°)	60
temperature (K)	173
crystal description	blue crystal (0.2 × 0.2 × 0.2 mm)
chemical formula	$\text{C}_{52}\text{H}_{86}\text{Cu}_4\text{N}_{14}\text{O}_{24}\text{Cl}_2\text{P}_2$
fw, g mol ⁻¹	1678.35
crystal system	monoclinic
space group	P2/c
a, Å	22.9936(7)
b, Å	14.1919(5)
c, Å	20.8331(7)
α , deg	90
β , deg	90.13
γ , deg	90
V, Å ³	6798.3(4)
Z	4
D _c , g cm ⁻³	1.640
F(000)	3472
$\mu(\text{MoK}\alpha)$, cm ⁻¹	14.48
No. data measured	62384
No. unique data	18851
R	0.0708
R _w	0.1290

Appendix One

1.6 $[\text{Zn}(\text{T}_2\text{-}o\text{-X})](\text{ClO}_4)_2 \cdot \text{H}_2\text{O}$ (12)

diffractometer	Nonius Kappa CCD
radiation type	Mo-K α
radiation wavelength	0.71073
radiation monochromator	graphite
2θ ($^\circ$)	59.6
temperature (K)	173
crystal description	colourless needle
chemical formula	$\text{C}_{20}\text{H}_{38}\text{N}_6\text{ZnO}_9\text{Cl}_{12}$
fw, g mol^{-1}	642.81
crystal system	monoclinic
space group	$\text{P}2_1/\text{c}$ (#14)
a, Å	9.2186(1)
b, Å	18.1297(4)
c, Å	16.4532(3)
β , deg	102.764(1)
V, Å^3	2681.88(7)
Z	4
D_c , g cm^{-3}	1.582
F(000)	1328.00
$\mu(\text{MoK}\alpha)$, cm^{-1}	11.75
No. data measured	36310
No. unique data	6830
No. Observed data ($I \geq 3\sigma$)	3667
R	0.059
R_w	0.057

Appendix One

1.7 $[\text{Zn}_2(\text{T}_2\text{-}p\text{-X})(\text{H}_2\text{O})_4(\text{DMF})_2][\text{ZnCl}_4]$ (14)

diffractometer	Nicolet R3m
radiation type	Mo-K α
radiation wavelength	0.71069
radiation monochromator	graphite
2 θ (°)	50.0
temperature (K)	173
crystal description	colourless acicular (0.30 \times 0.10 \times 0.10 mm)
chemical formula	$\text{Zn}_4\text{C}_{26}\text{H}_{58}\text{N}_8\text{C}_{18}\text{O}_6$
fw, g mol ⁻¹	1123.94
crystal system	monoclinic
space group	P2 ₁ /n (#14)
a, Å	8.157(4)
b, Å	24.62(1)
c, Å	11.032(6)
β , deg	93.96(4)
V, Å ³	2209(1)
Z	4
D _c , g cm ⁻³	1.689
F(000)	1148.00
$\mu(\text{MoK}\alpha)$, cm ⁻¹	29.75
No. data measured	4243
No. unique data	3958
No. Observed data ($I \geq 3\sigma$)	2552
R	0.048
R _w	0.044

Appendix One

1.8 $[\text{Zn}_2(\text{Me}_3\text{tacn})_2(\text{H}_2\text{O})_4(\text{PhP})](\text{ClO}_4)_2 \cdot \text{H}_2\text{O}$ (19)

diffractometer	Nonius Kappa CCD
radiation type	Mo-K α
radiation wavelength	0.71073
radiation monochromator	graphite
2 θ (°)	55
temperature (K)	173
crystal description	colourless needle
chemical formula	$\text{C}_{24}\text{H}_{57}\text{Cl}_2\text{N}_6\text{O}_{17}\text{Zn}_2\text{P}$
fw, g mol ⁻¹	934.38
crystal system	monoclinic
space group	$\text{F}2_1/\text{c}$ (#14)
a, Å	13.6248(2)
b, Å	11.6002(2)
c, Å	25.9681(4)
β , deg	102.0072(9)
V, Å ³	4014.5(1)
Z	4
D_c , g cm ⁻³	1.546
F(000)	1952.00
$\mu(\text{MoK}\alpha)$, cm ⁻¹	14.12
No. data measured	7565
No. unique data	935
No. Observed data ($I \geq 3\sigma$)	6841
R	0.039
R_w	0.041

Appendix One

1.9 [Ni(Me₃tacn)(H₂O)₃](ClO₄)₂

diffractometer	Nonius Kappa CCD
radiation type	Mo-K α
radiation wavelength	0.71073
radiation monochromator	graphite
2 θ (°)	56.6
temperature (K)	123(2)
crystal description	Purple needle 1.00 x 0.80 x 0.40 mm
chemical formula	C ₉ H ₂₇ N ₄ O ₁₁ Cl ₂ Ni
fw, g mol ⁻¹	643.93
crystal system	Orthorhombic
space group	P21/c
a, Å	a = 8.6483(17) Å
b, Å	b = 15.101(3) Å
c, Å	c = 14.042(3) Å
β , deg	90.40(3)
V, Å ³	1833.8(6)
Z	3
D _c , g cm ⁻³	1.749
F(000)	1008
μ (MoK α), cm ⁻¹	14.10
No. data measured	15128
No. unique data	4457
No. Observed data ($I \geq 3\sigma$)	3342
R	0.0389
R _w	0.0917

Appendix One

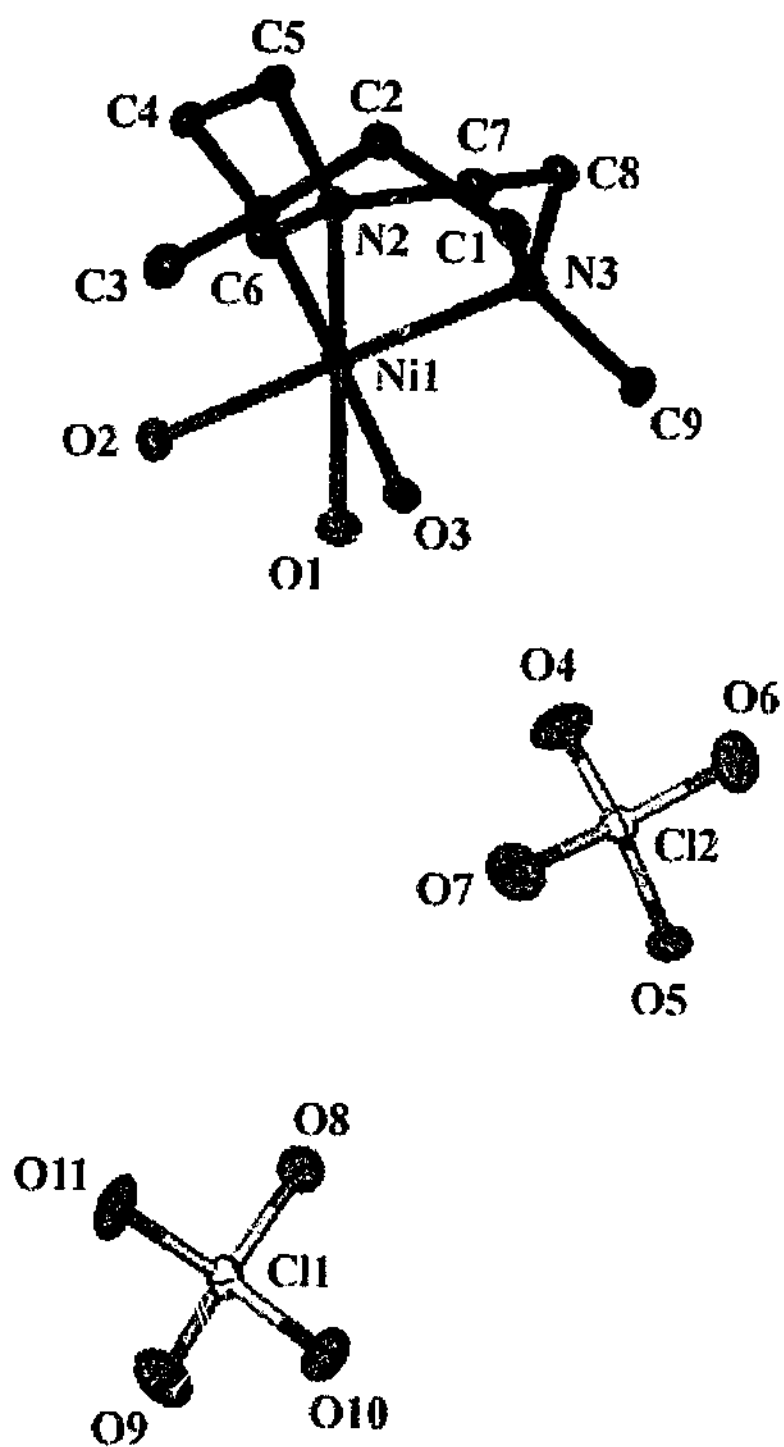


Figure 1.1 ORTEP plot of [Ni(Me₃tacn)(H₂O)₃](ClO₄)₂

Appendix One

Table 1.10 Bond lengths (Å) and angles (°) for [Ni(Me₃tacn)(H₂O)₃](ClO₄)₂.

Ni(1)-O(2)	2.0848(19)	Ni(1)-O(3)	2.0887(19)
Ni(1)-N(1)	2.097(2)	Ni(1)-N(2)	2.099(2)
Ni(1)-N(3)	2.1015(19)	Ni(1)-O(1)	2.128(2)
Cl(1)-O(9)	1.4283(18)	Cl(1)-O(11)	1.4366(19)
Cl(1)-O(8)	1.4444(18)	Cl(1)-O(10)	1.4475(18)
N(1)-C(3)	1.478(3)	N(1)-C(4)	1.495(3)
N(1)-C(2)	1.502(3)	C(1)-N(3)	1.488(3)
C(1)-C(2)	1.518(4)	Cl(2)-O(7)	1.427(2)
Cl(2)-O(4)	1.428(2)	Cl(2)-O(6)	1.4376(18)
Cl(2)-O(5)	1.4564(18)	N(2)-C(6)	1.483(3)
N(2)-C(7)	1.490(3)	N(2)-C(5)	1.494(3)
N(3)-C(9)	1.479(3)	N(3)-C(8)	1.497(3)
C(4)-C(5)	1.521(4)	C(7)-C(8)	1.518(3)
O(2)-Ni(1)-O(3)	81.75(8)	O(2)-Ni(1)-N(1)	95.89(8)
O(3)-Ni(1)-N(1)	175.63(8)	O(2)-Ni(1)-N(2)	95.91(8)
O(3)-Ni(1)-N(2)	91.79(8)	N(1)-Ni(1)-N(2)	84.77(8)
O(2)-Ni(1)-N(3)	178.83(8)	O(3)-Ni(1)-N(3)	97.41(8)
N(1)-Ni(1)-N(3)	85.00(8)	N(2)-Ni(1)-N(3)	84.91(8)
O(2)-Ni(1)-O(1)	83.19(8)	O(3)-Ni(1)-O(1)	87.83(8)
N(1)-Ni(1)-O(1)	95.57(8)	N(2)-Ni(1)-O(1)	179.07(7)
N(3)-Ni(1)-O(1)	95.97(8)	O(9)-Cl(1)-O(11)	110.89(12)
O(9)-Cl(1)-O(8)	109.44(12)	O(11)-Cl(1)-O(8)	109.09(11)
O(9)-Cl(1)-O(10)	109.40(11)	O(11)-Cl(1)-O(10)	109.03(11)
O(8)-Cl(1)-O(10)	108.96(11)	C(3)-N(1)-C(4)	108.7(2)
C(3)-N(1)-C(2)	110.1(2)	C(4)-N(1)-C(2)	111.67(19)
C(3)-N(1)-Ni(1)	114.96(16)	C(4)-N(1)-Ni(1)	102.82(14)
C(2)-N(1)-Ni(1)	108.47(15)	N(3)-C(1)-C(2)	111.6(2)
O(7)-Cl(2)-O(4)	110.96(13)	O(7)-Cl(2)-O(6)	110.92(13)
O(4)-Cl(2)-O(6)	108.87(12)	O(7)-Cl(2)-O(5)	109.23(11)
O(4)-Cl(2)-O(5)	108.97(11)	O(6)-Cl(2)-O(5)	107.82(11)
C(6)-N(2)-C(7)	109.1(2)	C(6)-N(2)-C(5)	109.8(2)
C(7)-N(2)-C(5)	111.95(19)	C(6)-N(2)-Ni(1)	114.69(15)
C(7)-N(2)-Ni(1)	102.63(14)	C(5)-N(2)-Ni(1)	108.65(15)
N(1)-C(2)-C(1)	111.2(2)	C(9)-N(3)-C(1)	109.3(2)
C(9)-N(3)-C(8)	109.8(2)	C(1)-N(3)-C(8)	111.6(2)
C(9)-N(3)-Ni(1)	114.63(15)	C(1)-N(3)-Ni(1)	103.12(15)
C(8)-N(3)-Ni(1)	108.22(14)	N(1)-C(4)-C(5)	110.7(2)
N(2)-C(5)-C(4)	110.6(2)	N(2)-C(7)-C(8)	111.1(2)
N(3)-C(8)-C(7)	111.22(19)		

Appendix Two

Kinetic Data

2.1 Calculated k_{obs} Values

Table 2.1 Calculated values of $10^5 \times k_{obs1}$ (s^{-1}) determined at 42.5°C

	pH 6.3	pH 7.0	pH 7.4	pH 9.1
1.0mM			1.638±0.004	2.4±0.1
1.5mM			2.421±0.004	2.7±0.1
2.0mM			3.41±0.05	6.17±0.01
2.5mM			3.942±0.004	7.52±0.02
3.0mM			4.677±0.007	
3.5mM			5.251±0.007	
4.0mM	0.4±0.1	2.07±0.05	4.80±0.02	
4.5mM			6.50±0.01	
5.0mM	0.87±0.05	2.67±0.02	7.15±0.02	
6.0mM			7.67±0.02	
7.5mM	1.37±0.03	4.63±0.03		

Appendix Two

Table 2.2 Calculated values of $10^6 \times k_{obs2}$ (s^{-1}) determined at 42.5°C

	pH 7.4	pH 9.1
1.0mM	0.97±0.04	-
1.5mM	1.00±0.02	24.3±0.5
2.0mM	1.50±0.04	2.0±0.3
2.5mM	1.23±0.01	2.5±0.3
3.0mM	1.44±0.02	-
3.5mM	1.41±0.01	-
4.0mM	1.53±0.02	-
4.5mM	1.68±0.01	-
5.0mM	0.98±0.02	-
6.0mM	2.14±0.02	-
7.5mM	-	-

Appendix Two

Table 2.3 Calculated values of $10^5 \times k_{obs1}$ (s^{-1}) determined at 50°C

	pH 5.9	pH 6.3	pH 6.7	pH 7.0	pH 7.4	pH 7.8	pH 8.2	pH 9.1
1.0mM	0.36±0.01	1.115±0.007	2.02±0.02		3.67±0.01		5.50±0.03	-
1.5mM	0.90±0.09	1.50±0.01	3.02±0.02		5.06±0.07		9.22±0.04	8.61±0.01
2.0mM	1.02±0.04	2.04±0.01	4.12±0.03		6.26±0.01		10.60±0.05	11.20±0.01
2.5mM	1.23±0.03	2.541±0.007	5.27±0.02		8±0.02		12.56±0.06	14.0±0.2
3.0mM	1.80±0.05	3.22±0.001	7.17±0.02		10±0.02	3.1±0.4		16.0±0.5
3.5mM	1.98±0.05	3.74±0.04	8.02±0.02		10.25±0.02	7.44±0.07		17.1±0.3
4.0mM	2.10±0.05	4.17±0.04	9.0±0.8		11.16±0.02	5.03±0.06		
4.5mM	2.45±0.05	4.70±0.04	8.85±0.07		12.55±0.05	10.1±0.1		
5.0mM	2.92±0.07	5.18±0.05	9.73±0.08	8.18±0.05	12.77±0.04	12.3±0.1		
6.0mM	3.32±0.05	6.61±0.08	10.77±0.03	10.41±0.07	15.17±0.07	15.9±0.2		
7.5mM	4.08±0.07	7.50±0.08	12.7±0.1	13.0±0.1	17.28±0.09	19.9±0.2		

Appendix Two

Table 2.4 Calculated values of $10^6 \times k_{obs2}$ (s^{-1}) determined at 50°C

	pH 5.9	pH 6.3	pH 6.7	pH 7.0	pH 7.4	pH 7.8	pH 9.1
1.0mM		0.2±0.1			0.21±0.09		0.42±0.03
1.5mM	2.2±0.5	1.82±0.07	0.09±0.06		1.18±0.02		0.83±0.01
2.0mM	0.77±0.4	1.92±0.08	0.67±0.05		1.57±0.02		1.10±0.06
2.5mM	0.76±0.4	2.01±0.03	1.33±0.04		1.89±0.03		1.30±0.01
3.0mM	2.3±0.2	2.19±0.05	1.67±0.04		1.93±0.03	1.1±0.8	1.71±0.01
3.5mM	0.9±.2	2.3±0.1	2.00±0.03		2.24±0.02	1.2±0.1	1.67±.01
4.0mM	2.2±0.2	2.70±0.08	2.17±0.04		2.50±0.01	1.1±0.5	
4.5mM	1.7±0.2	2.76±0.08	2.50±0.04		2.44±0.02	1.4±0.3	
5.0mM	2.1±0.2	2.83±0.07	2.50±0.03	1.46±0.07	2.84±0.02	1.3±0.2	
6.0mM	1.7±0.1	5.71±0.09	2.67±0.03	1.81±0.07	2.51±0.02	2.0±0.2	
7.5mM	2.0±0.1	3.24±0.07	3.00±0.03	2.59±0.07	3.71±0.02	2.5±0.1	

Appendix Two

Table 2.5 Calculated values of $10^5 \times k_{obs}$ (s^{-1}) determined at 57.5°C

	pH 5.9	pH 6.3	pH 6.7	pH 7.0	pH 7.4	pH 8.2	pH 9.1
1.0mM	1.13±0.07		4.73±0.07		6.42±0.02	10.50±0.05	4.8±0.9
1.5mM	1.55±0.05	0.4±0.3	7.8±0.1	6.03±0.7	9.78±0.02	15.82±0.6	15.21±0.02
2.0mM	1.87±0.05		10.0±0.1		12.66±0.01	21.0±0.2	18.81±0.03
2.5mM	2.33±0.05	1.2±0.1	12.2±0.2	2.04±0.08	15.23±0.02	23.6±0.2	23.55±0.04
3.0mM	2.50±0.05		12.0±0.2		17.97±0.03	28.3±0.2	27.85±0.06
3.5mM	2.82±0.05	1.78±0.05	13.5±0.2	5.07±0.04	20.59±0.02	31.1±0.4	30.78±0.05
4.0mM	3.33±0.05		6.10±0.03		21.73±0.04		33.81±0.08
4.5mM	2.58±0.03	4.5±0.1	5.93±0.06	10.3±0.2	24.24±0.05		36.2±0.1
5.0mM	4.17±0.07		4.50±0.05		22.5±0.2		39.9±0.07
6.0mM	5.6±0.1	7.1±0.2	2.03±0.08	16.1±0.1	29.66±0.05		
7.5mM	7.2±0.1	9.5±0.2	1.60±0.07	22.6±0.2	34.63±0.09		

Appendix Two

Table 5.6 Calculated values of $10^6 \times k_{obs2}$ (s^{-1}) determined at 57.5°C

	pH 6.7	pH 7.4	pH 8.2	pH 9.1
1.0mM		1.65±0.05	3.00±0.03	1.8±0.1
1.5mM		2.96±0.03	2.33±0.02	1.91±0.02
2.0mM	3.3±0.1	3.07±0.01	2.67±0.02	2.46±0.02
2.5mM	4.0±0.1	4.12±0.01	2.67±0.02	2.86±0.02
3.0mM	5.8±0.1	4.65±0.01	3.33±0.02	3.32±0.02
3.5mM	5.83±0.05	5.17±0.01	3.50±0.02	2.57±0.01
4.0mM	0.15±0.03	5.59±0.01		3.97±0.01
4.5mM	6.33±0.03	6.19±0.01		4.30±0.02
5.0mM		7.24±0.06		4.55±0.01
6.0mM		7.67±0.01		
7.5mM		9.23±0.01		

Appendix Two

Table 2.7 Calculated values of $10^5 \times k_{obs1}$ (s^{-1}) determined at 65°C

	pH 6.3	pH 7.0	pH 7.4	pH 8.2	pH 9.1
1.0mM			14.44±0.08	16.21±0.05	11.96±0.01
1.5mM	2.80±0.04	2.63±0.02	20.9±0.3	24.00±0.09	25.55±0.06
2.0mM			25.2±0.3	32.5±0.1	32.19±0.03
2.5mM	3.46±0.09	8.67±0.07	29.7±0.6	38.1±0.2	36.9±0.1
3.0mM			35±1	45.3±0.2	49.6±0.2
3.5mM	7.04±0.08	8.70±0.07	37.6	50.9±0.3	55.9±0.2
4.0mM			46±1	54.0±0.3	61.0±0.3
4.5mM	7.52±0.09	19.6±0.3	41±2	58.7±0.4	68.0±0.3
5.0mM			56±3	64.0±0.8	69.5±0.3
6.0mM	10.2±0.2	26.2±0.5			78.0±0.3
7.5mM	4.7±0.1	37±1			

Appendix Two

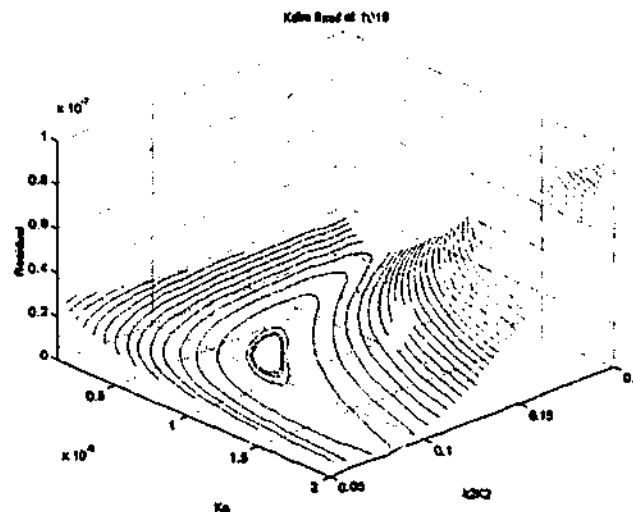
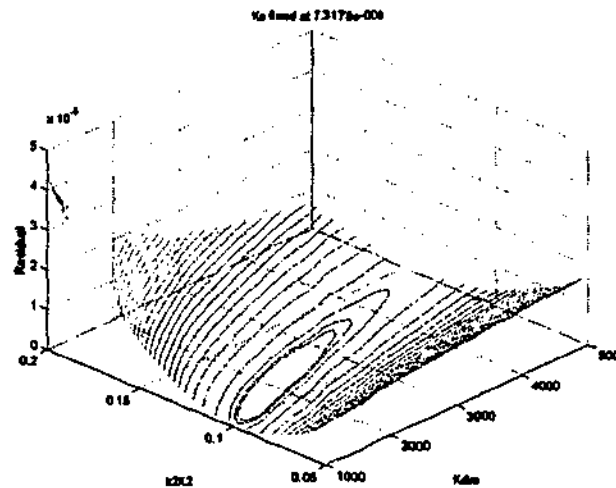
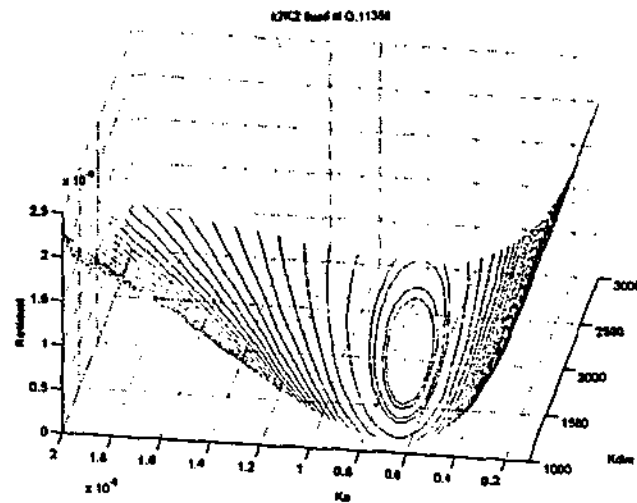
Table 5.8 Calculated values of $10^6 \times k_{obs2}$ (s^{-1}) determined at 65°C

	pH 6.3	pH 7.0	pH 7.4	pH 8.2	pH 9.1
1.0mM			5.35±0.02	2.49±0.02	1.97±0.01
1.5mM	5.79±0.08	5.22±0.03	6.71±0.04	3.15±0.01	3.80±0.01
2.0mM			8.75±0.03	4.31±0.01	5.45±0.02
2.5mM	3.5±0.1	3.21±0.02	10.00±0.04	5.07±0.01	6.30±0.01
3.0mM			11.62±0.07	5.96±0.01	6.43±0.01
3.5mM	4.69±0.05	2.8±0.1	13.39±0.04	6.57±0.01	8.05±0.01
4.0mM			14.95±0.06	7.27±0.01	8.74±0.01
4.5mM	5.17±0.04	7.65±0.04	17.60±0.07	8.10±0.01	9.63±0.01
5.0mM				7.51±0.02	10.22±0.01
6.0mM	6.81±0.05	8.67±0.05			11.75±0.01
7.5mM	4.9±0.1	12.3±0.1			

Appendix Two

2.2 Residual Maps for k_2K_2 , K_a and K_{dim} determined at 42.5°C using MATLAB

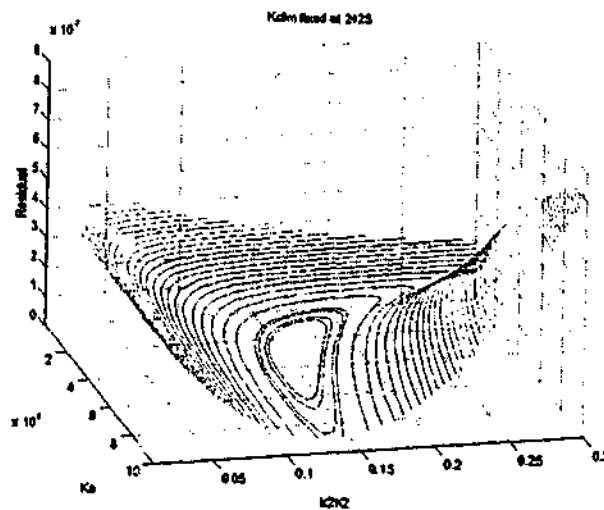
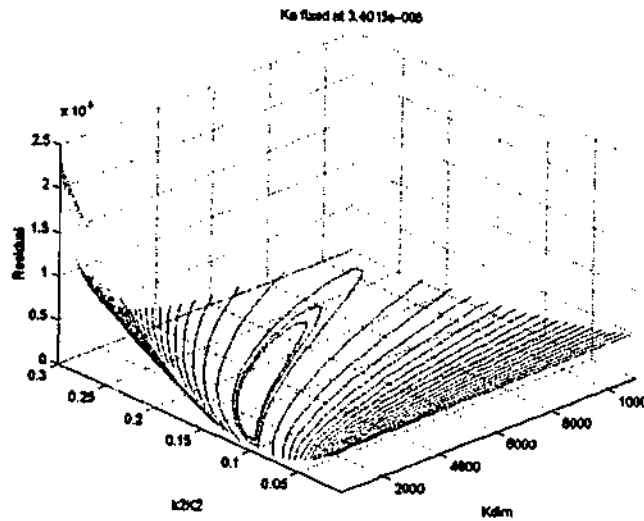
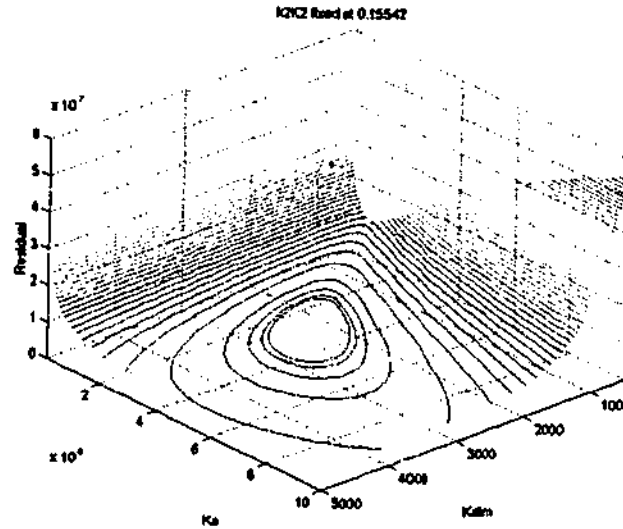
Inner three circles correspond to the 90, 95 and 99% confidence limits. The values for the residuals are: Solution = 3.169×10^{-10} ; 90% = 4.826×10^{-10} ; 95% = 5.342×10^{-10} ; 99% = 6.686×10^{-10} .



Appendix Two

2.3 Residual Maps for k_2K_2 , K_a and K_{dim} determined at 50°C using MATLAB

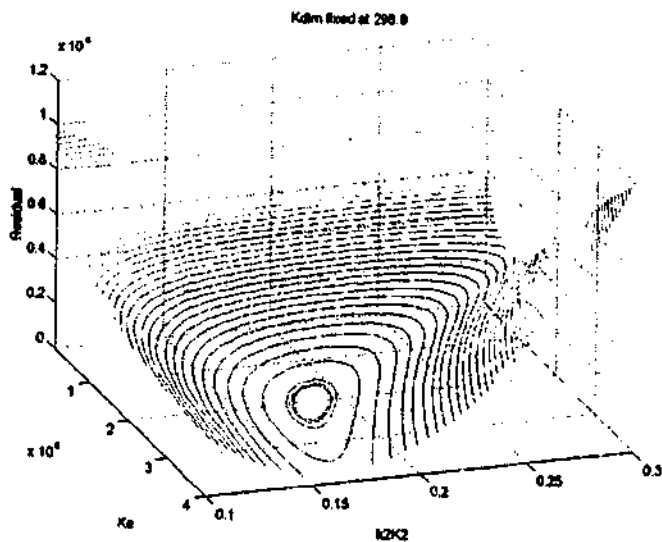
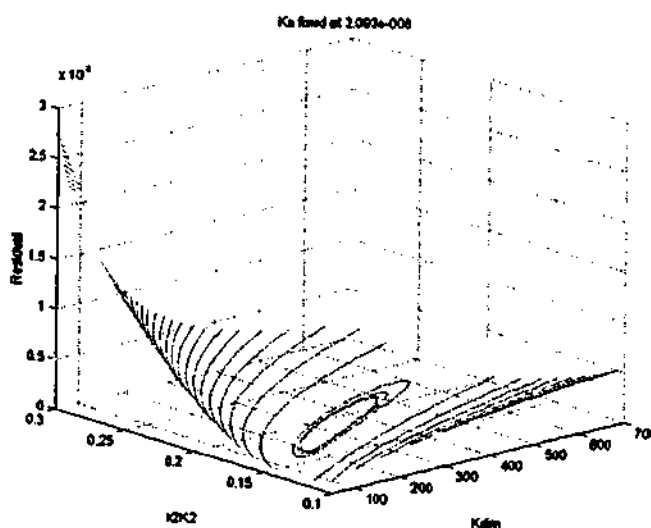
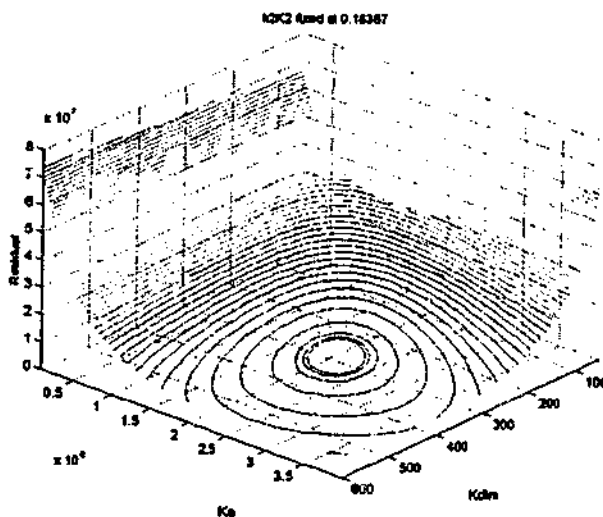
Inner three circles correspond to the 90, 95 and 99% confidence limits. The values for the residuals are: Solution = 3.546×10^{-8} ; 90% = 3.865×10^{-8} ; 95% = 3.943×10^{-8} ; 99% = 4.146×10^{-8} .



Appendix Two

2.4 Residual Maps for k_2K_2 , K_a and K_{dim} determined at 57.5°C using MATLAB

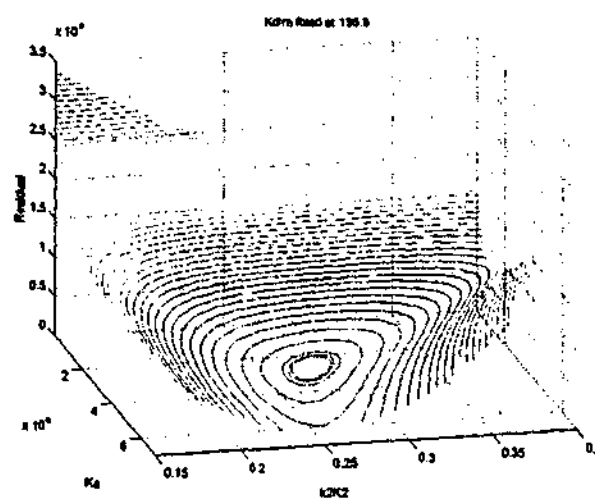
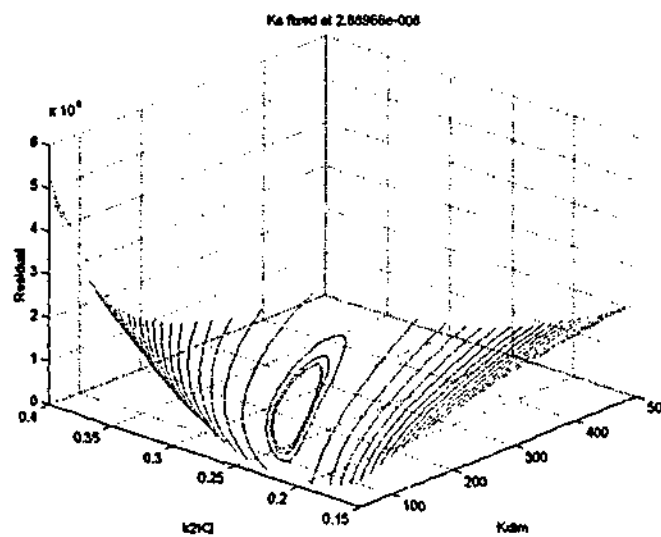
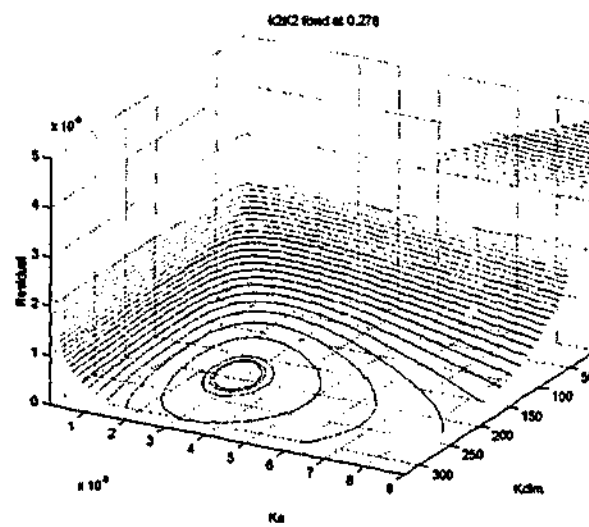
Inner three circles correspond to the 90, 95 and 99% confidence limits. The values for the residuals are: Solution = 1.741×10^{-8} ; 90% = 2.076×10^{-8} ; 95% = 2.169×10^{-8} ; 99% = 2.391×10^{-8} .



Appendix Two

2.5 Residual Maps for k_2K_2 , K_a and K_{dim} determined at 65°C using MATLAB

Inner three circles correspond to the 90, 95 and 99% confidence limits. The values for the residuals are: Solution = 4.989×10^{-8} ; 90% = 4.133×10^{-8} ; 95% = 4.336×10^{-8} ; 99% = 4.884×10^{-8} .

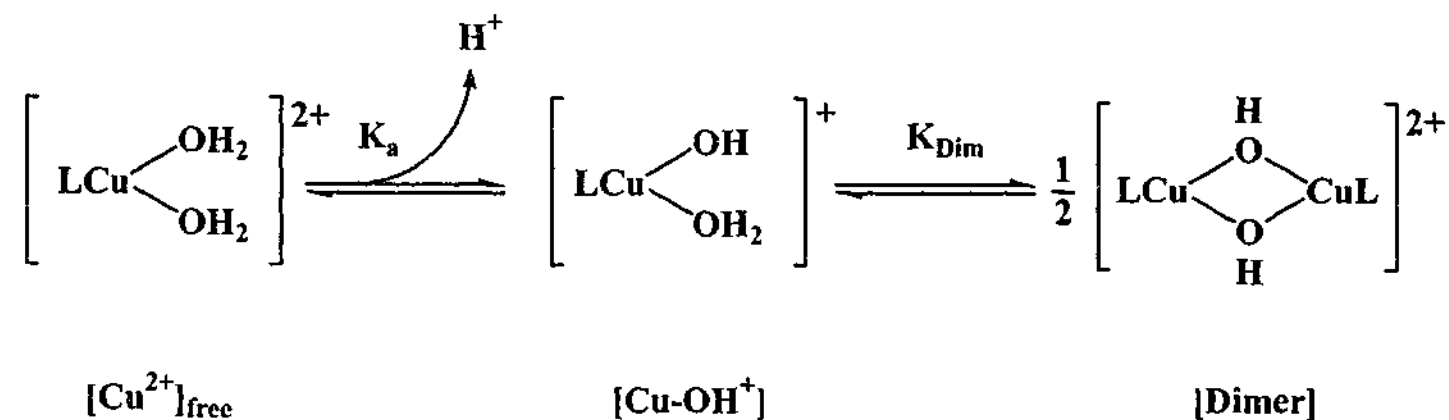


Appendix Two

2.6 Derivation of Equation used in the MATLAB fitting procedure

Presented below is the derivation of Equation 5.19.

The reaction scheme for the equilibrium between the copper species found in solution is presented below.



The mass balance equation for copper(II) in solution for the above reaction scheme is:

$$[\text{Cu}]_{\text{total}} = [\text{Cu}^{2+}]_{\text{free}} + [\text{Cu-OH}^+] + 2[\text{Dimer}] \quad \text{Eq. 1}$$

and the equilibrium constants are written as:

$$K_a = \frac{[\text{Cu-OH}^+][\text{H}^+]}{[\text{Cu}^{2+}]_{\text{free}}} \quad \text{Eq. 2}$$

and

$$K_{\text{dim}} = \frac{[\text{Dimer}]}{[\text{Cu-OH}^+]^2} \quad \text{Eq. 3}$$

Appendix Two

where $[Cu]_{total}$ is the amount of copper put into the system, ; $[Cu^{2+}]_{free}$ is the diaquo species, $[Cu(Me_3tacn)(H_2O)_2]^{2+}$, $[Cu-OH^+]$ is the hydroxo-aquo species, $[Cu(Me_3tacn)(H_2O)(OH)]^+$, and $[Dimer]$ is $[(Me_3tacn)Cu(\mu-OH)_2Cu(Me_3tacn)]^{2+}$.

Equations 5.2 and 5.3 can be rearranged to the forms:

$$[Cu^{2+}]_{free} = \frac{[Cu-OH^+][H^+]}{K_a} \quad \text{Eq. 4}$$

$$[Dimer] = K_{dim}[Cu-OH^+]^2 \quad \text{Eq. 5}$$

Substituting Equation 4 and Equation 5 into the mass balance equation (Equation 1) the following equation is derived:

$$[Cu]_{total} = \frac{[Cu-OH^+][H^+]}{K_a} + [Cu-OH^+] + 2K_{dim}[Cu-OH^+]$$

which can be written in terms of:

$$0 = \frac{[Cu-OH^+][H^+]}{K_a} + [Cu-OH^+] + 2K_{dim}[Cu-OH^+] - [Cu^{2+}]_{total} \quad \text{Eq. 6}$$

This can be factorised to produce the equation in terms of $[Cu-OH^+]$:

$$[Cu-OH^+] = \frac{-\left(\frac{[H^+]}{K_a} + 1\right) + \sqrt{\left(\frac{[H^+]}{K_a} + 1\right)^2 + 8K_{dim}[Cu^{2+}]_{total}}}{4K_{dim}} \quad \text{Eq. 7}$$

Appendix Two

The observe rate constant is equal to:

$$k_{obs} = k_1 K_1 [Cu^{2+}]_{free} + k_2 K_2 [Cu - OH^+] \quad \text{Eq. 8}$$

Substituting Equation 7 into Equation 8 derives the expression of k_{obs} :

$$k_{obs} = k_1 K_1 \frac{[Cu - OH^+][H^+]}{K_a} + k_2 K_2 [Cu - OH^+] \quad \text{Eq. 9}$$

$$k_{obs} = k_1 K_1 \frac{[Cu - OH^+][H^+]}{K_a} + \frac{k_2 K_2}{4K_{dim}} \left\{ - \left(\frac{[H^+]}{K_a} + 1 \right) + \sqrt{\left(\frac{[H^+]}{K_a} + 1 \right)^2 + 8K_{dim} [Cu^{2+}]_{total}} \right\}$$

Eq. 10

As has been determined previously (see Chapter 5), $k_1 K_1$ was determined to be zero, so the final equation used in the fitting of the data was:

$$k_{obs} = \frac{k_2 K_2}{4K_{dim}} - \left(\frac{[H^+]}{K_a} + 1 \right) + \sqrt{\left(\frac{[H^+]}{K_a} + 1 \right)^2 + 8K_{dim} [Cu^{2+}]_{total}} \quad \text{Eq. 11}$$